

Characterising the Mechanical Properties of Large Intestine

Zahra Ehteshami

Submitted in accordance with the requirements for the degree of
Doctor of Philosophy

The University of Leeds
Mechanical Engineering
Leeds, UK

August, 2015

The candidate confirms that the work submitted is his/her own and that appropriate credit has been given where reference has been made to the work of others.

This copy has been supplied on the understanding that it is copyright material and that no quotation from the thesis may be published without proper acknowledgement.

© 2015 The University of Leeds and Zahra Ehteshami

Acknowledgements

Firstly, I would like to express my gratitude to my primary supervisor, Prof. Anne Neville, whose expertise and understanding made my postgraduate experience very enjoyable and valuable. I appreciate her vast knowledge and her assistance and support in every stage of my research. Her great personality and attitude towards work, students, fellow staff and life in general have made her an idol to me as a researcher, as a woman, and above all, as a person.

I would also like to thank my secondary supervisor, Dr. Pete Culmer, for all the motivation and assistance he has provided me at all levels of the research project. He was always happy to provide me with direction, technical support and eventually became more of a mentor and friend than just my supervisor.

Appreciation also goes to my colleagues Dr. Ali Alazmani, William Mayfield, Earle Jamieson and James Chandler for their suggestions and help with various aspects of my research. I must acknowledge David Reedman, a member of technical engineering staff, for all his advice and technical assistance with developing the acoustic impedance method in this research and throughout my graduate/postgraduate program. Gratitude also goes to all the technical staff especially Graham Brown, Ron Cellier, and Robert Ingham for all the times they assisted me along the way.

Above all, I would like to thank my family for the immense moral and financial support they provided me throughout this seemingly eternal chapter of my life. I must also acknowledge my dear friends Pariya, Negar, Simin, Earle, James, Evan, Doris, Nazrana and Ali who have turned into family throughout this journey and whose encouragement and kindness at the best and worse of times I would not have reached this stage without.

Abstract

This research was carried out to characterise mechanical properties of the large intestine. Assessing the mechanical properties of tissue plays an important role in understanding the links between histological structure and physical properties, physical functioning and normal anatomy. The mechanical properties of large intestine are poorly understood but essential for more accurate characterisation of their behaviour, for example during interaction with surgical instrumentation or devices.

This project was set in the context of designing a new robotic colonoscopy device. The aim of this study was to develop and evaluate a robust methodology to characterise the ex-vivo mechanical properties of porcine large intestine tissue and create a database of these properties. In order to study the unique and complex physical properties of the large intestine two common techniques were employed: indentation and tensile stretching. A series of indentation and tensile tests were conducted and the time, strain-rate and strain history dependent responses of porcine large intestine during loading and stress relaxation were observed. Linear and non-linear models were used to analyse the tissue response. The results identified strong dependency of the large intestine mechanical properties to strain-rate and loading history. Tissue preconditioning was also found to be an effective way to stabilise the tissue response in air. Tissue hydration was also found to better preserve the natural state of tissue similar to the in-vivo environment. One of the most important observations was the necessity to produce an appropriate testing protocol for such investigations. Guidelines are proposed to set the requirements for mechanical tissue characterisation.

For in-vivo investigation of tissue properties, a system based on measuring acoustic impedance properties of the tissue was successfully designed. Stiffness and tissue relaxation properties of the large intestine were examined using this probe and the results were linked back to the indentation outcomes. This system has the capability to be miniaturised and deployed during conventional colonoscopy or robotic hydro-colonoscopy.

Table of contents

Acknowledgements	ii
Abstract	iii
Chapter 1. Introduction	1
Chapter 2. Literature review	3
2.1 Mechanical properties of soft tissue	3
2.2 Large intestine characterisation	6
2.2.1 Existing literature on ex-vivo characterisation of the large intestine.....	10
2.2.2 Existing literature on in-vivo characterisation of the large intestine	15
2.3 Biological tissue testing	20
2.3.1 Imaging techniques	21
2.3.1.1 Optical imaging	22
2.3.1.2 Mechanical Imaging (MI)	22
2.3.1.3 Ultrasound imaging	23
2.3.2 Non-imaging techniques	23
2.3.2.1 Indentation	24
2.3.2.2 Tensile extension	29
2.3.2.3 Vibration	30
2.4 Biological tissue modelling	35
2.5 Experimental variables	47
2.5.1 In-vivo versus ex-vivo effect	47
2.5.2 Hydration effect	48
2.5.3 Preconditioning effect	48
2.5.4 Varying strain-rate effect	49
2.5.5 Strain history effect	49
2.6 Conclusions	51
2.6.1 Aims	51
2.6.2 Objectives	52

Chapter 3. Materials and methods	53
3.1 Introduction	53
3.2 Specimen preparation	53
3.2.1 Rectum	53
3.2.2 Large intestine.....	54
3.3 Instrumentation.....	55
3.3.1 MUST rig	55
3.3.2 MMC rig	56
3.3.3 In-vivo tissue characterisation rig-Acoustic impedance measurement.....	61
3.4 Mechanical properties measurement	64
3.5 Experimental protocols.....	66
3.5.1 Method I: Indentation characterisation using the MUST rig	66
3.5.2 Method II: Combined indentation plus tensile characterisation using the MMC rig	67
3.5.3 Method III: Acoustic impedance tissue characterisation	69
3.6 Data analysis.....	71
3.6.1 Linear modulus.....	71
3.6.2 Stress relaxation model fitting	73
3.6.2.1 Method 1: Wiechert 5-element modelling	73
3.6.2.2 Method 2: AQLV modelling.....	76
3.6.3 Model fitting	76
3.6.4 Viscoelastic ratio.....	76
3.6.5 Data normalising	77
3.6.6 Statistical analysis and data representation	77
3.6.7 Acoustic impedance response noise reduction.....	77
Chapter 4. Mechanical characterisation of the rectum under indentation using the MUST rig	79
4.1 Introduction	79

4.2	Test objectives	79
4.3	Methods	79
4.4	Results	80
4.4.1	Repeated interaction test	80
4.4.2	Strain-rate variation test	83
4.4.3	Intra-rectal tissue variation test	85
4.5	Chapter summary	86
Chapter 5.	Mechanical characterisation of the large intestine under indentation	88
5.1	Introduction	88
5.2	Test objectives	88
5.3	Method	89
5.4	Results	90
5.4.1	Length, circumference and thickness measurements	90
5.4.2	Intra-large intestine variation test	90
5.4.3	Repeated interaction test	96
5.4.4	Varying strain level dependency examination	101
5.5	Chapter summary	105
Chapter 6.	Mechanical characterisation of large intestine under tensile stretch	106
6.1	Introduction	106
6.2	Test objectives	106
6.3	Methods	106
6.4	Results	107
6.4.1	Intra-large intestine variation	107
6.4.2	Repeated interaction test	111
6.5	Strain level dependency examination	118
6.6	Chapter summary	121
Chapter 7.	Acoustic impedance characterisation of large intestine	122

7.1	Introduction	122
7.2	Method.....	122
7.3	Results	123
7.3.1	Validation of the method.....	123
7.3.2	Ex-vivo tissue testing	126
7.4	Chapter summary.....	130
Chapter 8.	Discussion	132
8.1	Mechanical characterisation of the large intestine	132
8.1.1	Repeated interaction effect.....	133
8.1.1.1	Stress- strain response.....	133
8.1.1.2	Stress relaxation response	134
8.1.2	Strain-rate variation effect.....	137
8.1.2.1	Stress-strain response	137
8.1.2.2	Stress relaxation response	138
8.1.3	Strain history dependency	139
8.1.4	Testing protocol design for tissue characterisation experiments	139
8.2	Tissue modelling	140
8.2.1	Linear modulus.....	141
8.2.2	Non-linear modelling	143
8.2.2.1	Wiechert 5-element model.....	143
8.2.2.2	Adaptive Quasi-Linear Viscoelastic (AQLV) model.....	145
8.3	Acoustic impedance tissue characterisation	148
Chapter 9.	Conclusions	150
Chapter 10.	Future work	153
References	154

List of tables

Table 2-1: A comparison of studies conducted on mechanical properties of large intestine in the ex-vivo and the in-vivo conditions	9
Table 2-2: Values of results comparing five equally spaced colonic segment sites, A-E, progressing distally	12
Table 3-1: Testing protocol for MMC rig validation.....	60
Table 3-2: Testing protocol set for characterising mechanical properties of rectum.....	67
Table 3-3: Testing procedure for characterising indentation/tensile properties of large intestine	69
Table 3-4: Testing procedure for in-vivo characterisation of impedance properties of tissue.....	71
Table 4-1: Summary of the experimental set-up for each experiment.....	80
Table 4-2: Typical shift of linear modulus and strain for every five cycles. The negative strain shift means the shift of cycles to the left direction (i.e. lower strain) on the strain-stress graph.....	82
Table 4-3: The Wiechert coefficients at 0.5 mm/s strain-rate in section E.....	82
Table 4-4: The Wiechert model coefficients of the 5 th cycles at three strain-rates from the repeated interaction test in section G	85
Table 4-5: An overview of Chapter 4 aims and results.....	87
Table 5-1: Illustration of the main features of the experimental set-up.....	89
Table 5-2: The average value of length and circumference of 9 porcine large intestines for five segments	90
Table 5-3: AQLV parameters of the model fitting to the relaxation data for the two specimens in Figure 5-5	94
Table 5-4: Optimum time constants and coefficients of the AQLV fit to the stress relaxation data for three samples, each sample includes three indentations at each segments.....	96
Table 5-5: The shift of strain and linear modulus between each cycle for the samples in PBS solution corresponding to Figure 5-8-a.....	97

Also confirmed by Lista *et al.* [115] and Provenzano *et al.* [90] this trend indicates that the stiffness of the large intestine is significantly affected with the strain level. In order to investigate the effect of varying strain level on the stress relaxation response the

stress relaxation drop $\Delta\sigma$ at each strain step was obtained. The results show full $\Delta\sigma$ of 100% for both 20% and 35% strain steps, 96% $\Delta\sigma$ for 50% strain step and 74% $\Delta\sigma$ for the highest strain steps 65%, indicating that the average equilibrium value increases with increasing strain level. Also, as shown in Table 5-6, the average stress at 50 s decreases with increasing strain level which signifies that the lower the strain level, the greater the relaxation/decaying rate. 102

Table 5-7: Typical mean reduced relaxation function +/- SD for all the four strain levels obtained at several points in time along the relaxation process 103

Table 5-8: An overview of the key points in this chapter 105

Table 6-1: Summary of the experimental set-up..... 107

Table 6-2: AQLV parameters of the model fitting to the relaxation data for the two specimens in Figure 6-3 109

Table 6-3: Optimum time constants and coefficients of the AQLV fit to the stress relaxation data for three samples, each sample includes three longitudinal stretches at each segments..... 110

Table 6-4: Optimum time constants and coefficients of the AQLV fit to the stress relaxation data for three samples, each sample includes three circumferential stretches at each segments..... 111

Table 6-5: The shift of strain and its corresponding linear modulus shift for every two consecutive cycles under tensile stretch..... 113

Table 6-6: The Wiechert model coefficients of the loading viscoelastic response occurred in viscoelastic region corresponding to the responses in Figure 6-10 under longitudinal stretch..... 117

Table 6-7: The Wiechert model coefficients of the loading viscoelastic response occurred in the viscoelastic region corresponding to the responses in Figure 10 under circumferential stretch..... 117

Table 6-8: Typical mean reduced relaxation function +/- SD for all the four strain levels obtained at several points in time along the relaxation process..... 119

Table 6-9: The outline of the objectives addressed in Chapter 5 121

Table 7-1: Summary of the experimental set-up for each stage of the concept development 123

Table 7-2: An overview of the key points in this chapter 131

List of figures

Figure 2-1: Schematic diagram of typical stress-strain curve [21]	4
Figure 2-2: A typical a) load-elongation and b) load-time diagram for anterior cruciate ligament of rabbit knee [18]	6
Figure 2-3: Structure of the human large intestine [30]	7
Figure 2-4: Schematic diagram of colonic wall structure, a) four layers of colonic wall. Muscular fibres are distributed in b) axial directions within taenia coli layer, c) circumferential direction within muscularis externa layer, d) clockwise and anti-clockwise helices within submucosa layer and d) isotropic for mucosa layer [29]	7
Figure 2-5: Stress relaxation of sigmoid colon for African and European group. Africans are closed circles and upper regression line. Europeans are the open circles and lower regression line [12]	11
Figure 2-6: Rat colon stress-strain response. L values (L_0 , L_1 & L_2) are measured after drawing the tangent to the steep section of the stress-strain response. E is the strain at burst strength. A & B are the two points on the stress-strain curve specify the most straight relationship between strain and stress just before the point of burst strength [13]	11
Figure 2-7: Colon segment at distended, no-load and zero-stress states [7]	13
Figure 2-8: Schematic diagram of Sokolis device allows for simultaneous inflation and extension of tissue [11]	15
Figure 2-9: In-vivo and in-vitro stress-strain curve of goat colon [8]	16
Figure 2-10: Stress-strain graph of the abdominal organs (1 st and 5 th cycles), BL-bladder, GB-gallbladder, LI-large intestine, LV-liver, SI-small intestine, SP –spleen and ST-stomach [10]	17
Figure 2-11: Balloon catheter probe for measurement of cross sectional area and pressure	19
Figure 2-12: Elasticity imaging approaches [44]	21
Figure 2-13: 3D MI reconstruction of a phantom which contains hard nodules [51]	22
Figure 2-14: a) Hand-held compliance probe to indent tissue in-vivo, and b) Stress-strain graph of in-vivo indentation test. Broken lines show normal liver and solid line is for an obstructive liver diseased [60]	25
Figure 2-15: Schematic diagram of Araghi's indenter [63]	26
Figure 2-16: TeMPeST indenter sensor/actuator assembly	26

Figure 2-17: Swine brain indentation, a) in-vivo experiment configuration, and b) schematic diagram of the device [67] 27

Figure 2-18: Samur et al. robotic indenter and its schematic diagram [69]..... 28

Figure 2-19: a) A finger mounted device suitable for the in-vivo assessment of prostate tissue properties, & b) An example of stiffness map obtained from the dynamic compression of ex-vivo prostate tissue containing tumour [70] 29

Figure 2-20: Concept diagram explains the frequency response of electrical impedance as a function of stiffness change. Here $k_{t1}=5.0 \times 10^9$ (Ns/m) and $k_{t1}=1.1 \times 10^{10}$ (Ns/m) [80] 32

Figure 2-21: illustration of a) a tactile sensor element consists of a driving and pick up PZT ceramic elements and b) 64-element tactile sensor probe [84]..... 33

Figure 2-22: Schematic diagram of a resonance circuit linked to a PZT probe [76]..... 33

Figure 2-23: The PZT transducer detection of frequency shift against a) depth for various tumour nodes implanted in a Gelatin sheet [84] and b) Young's Modulus for various materials of different hardness levels [86] 35

Figure 2-24: Frequency shift and amplitude change versus Young's Modulus of silicon rubber at different density levels [76] 35

Figure 2-25: Fundamental viscoelastic elements – from left to right: damper (Newton element) and spring (Hooke element) [18] 36

Figure 2-26: Linear Viscoelastic models a) Maxwell body, b) Voigt body and c) Kelvin body [18]..... 37

Figure 2-27: Stress relaxation of a Maxwell model [92] 38

Figure 2-28: Creep of Voigt model [92] 38

Figure 2-29: Creep functions of a) Maxwell, b) Voigt and c) Kelvin [18]..... 39

Figure 2-30: Relaxation functions of a) Maxwell, b) Voigt and c) Kelvin [18] 40

Figure 2-31: Wiechert model showing physical representation of colonic tissue [97]... 42

Figure 2-32: Schematic block diagram of Fung's QLV model [99] 43

Figure 2-33: Schematic diagram of the AQLV model. The red box stands for the non-linear process $\mathbf{E}t$ of converting the elongation into the force. The blue box represents a step response $\mathbf{g}(\boldsymbol{\epsilon})$ induced by a linear process [99] 46

Figure 2-34: Prediction of the AQLV fit (solid lines) for four strain incremental stress relaxation data (grey dots) for the 2nd, 3rd and 4th ramp and hold data..... 47

Figure 2-35: Stress relaxation of tissue at various levels of strain [114]..... 50

Figure 2-36: Strain history effect on viscoelastic response of a) human ligament and b) rat ligament 51

Figure 3-1: A porcine large intestine [94]..... 54

Figure 3-2: A porcine rectum divided into 10 equally cut segments for tissue mechanical properties variation test..... 54

Figure 3-3: (a) Photograph of the entire large intestine, laid out and marked into five segments - Rectum, descending, transverse, ascending, and cecum, (b) The circumference of rectum was measured at three equally spaced locations..... 55

Figure 3-4: a) MUST rig, b) Indenter schematic..... 56

Figure 3-5: a) 3D design and b) the built model of MMC rig. The annotations represent 1-linear stage actuator, 2-load cell, 3-indenter & 4-sample holder..... 57

Figure 3-6: Schematic of the Modular Mechanical Characterisation (MMC) rig 58

Figure 3-7: Software flowchart adapted for indentation testing protocol in Table 3-3 .. 59

Figure 3-8: Cross section view of a)the indentation sample holder, and b) the tensile test sample holder in the sample bath. The annotations represent 1-indenter-load cell connector, 2-indenter, 3- specimen, 4-sample holder top plate, 5-sample holder bottom plate, 6-sample holder top clamp, 7-sample holder bottom clamp & 8-Sample bath..... 59

Figure 3-9: Stress versus strain response of the sorbothane sample with the linear regression fits 60

Figure 3-10: Strain versus stress data of the sorbothane sample under varying load and strain-rate 60

Figure 3-11: The components of the impedance measurement probe attached to the MMC rig for stationery movement. The annotations represent 1-Linear stage actuator, 2-load cell $100 \times 10 \times 30$ mm, 3-stack PZT element $5 \times 5 \times 7$ mm & 4-sample holder $100 \times 70 \times 40$ mm..... 61

Figure 3-12: Schematic of impedance measurement using Agilent Network Analyser E5061B with adaption of an external power amplifier and potential dividers [120]..... 62

Figure 3-13: Schematic of PZT probe III comprises a portable impedance acquisition system consists of a HP 3310 function generator and a NI USB-5133 acquisition board 63

Figure 3-14: Software flowchart adapted for acoustic impedance measurement of the tissue. The flowchart is set in accordance with the testing protocol in Table 3-4 64

Figure 3-15: Typical a) stress-strain and b) stress-time responses of tissue to indentation/tension in 3 phases. Phases are defined as loading (1), stress relaxation (2),

unloading (3). The red line in figure ‘a’ represents a linear regression fit used to determine the linear modulus. The regression fit starts from the point of maximum stress/strain threshold and a variable start point. The start point is progressively moved back until $R^2 > 0.99$ 65

Figure 3-16: Schematic diagram of thickness measurement technique..... 69

Figure 3-17: An example of frequency sweep starting from 20 Hz to 1 MHz. The yellow and blue signals represent the impedance magnitude and impedance phase respectively 70

Figure 3-18: Viscoelastic models a) Maxwell, b) Standard Linear (Kelvin model), c) Wiechert 5-element, d) Wiechert 7-element, and e) Wiechert 9-element [12]..... 74

Figure 3-19: Typical stress relaxation response of soft tissue fitted to a series of viscoelastic models presented in Figure 3-18 . The models are a) Maxwell, b) Standard Linear (Kelvin model), c) Wiechert 5-element, d) Wiechert 7-element, and e) Wiechert 9-element..... 74

Figure 3-20: Mean error \pm SD of the viscoelastic models. From left to right: Maxwell Model, Kelvin Model, Wiechert Model 5, 7, and 9 elements..... 75

Figure 3-21: An example of the noise in the detected excitation signal (blue lines) and the polynomial fit for peak detection 78

Figure 4-1: MUST Tester stress-strain relationship measurement capability to other colon mechanics studies [7, 8, 10-14, 41]..... 80

Figure 4-2: Typical loading stress-strain curves of porcine rectum where the value of strain is normalised to the first point of contact. Red arrow shows the direction of cyclic progression..... 81

Figure 4-3: Typical stress relaxation curves (coloured lines) and Wiechert 5-element fits (black lines) for 20 consecutive indentations at 0.5mm/s strain-rate in segment E. Red arrow shows the direction of cyclic progression..... 81

Figure 4-4: Repeatability effect on linear modulus obtained from the loading phase at 0.5mm/s strain-rate in segment E..... 83

Figure 4-5: Typical trend of viscoelastic ratio obtained from the indentation test 83

Figure 4-6: Typical a) stress versus strain response of the large intestine at varying strain rate, b) the strain was normalised to compare the gradients of the curves..... 84

Figure 4-7: The typical trend of normalised stress relaxation response at three strain-rates of 0.05mm/s (red), 0.2mm/s (green) and 0.5mm/s (blue) for the 5th cycle of

repeated interaction test in section G. The black line represents the Wiechert fit for the curves 85

Figure 4-8: Linear modulus versus thickness measurements for three spatial indentations in segments A at 0.5mm/s strain-rate. This pattern is consistent for all the other segments..... 86

Figure 5-1: Box plot of the tissue thickness obtained in the indentation test for five segments..... 91

Figure 5-2: Linear modulus variation at five segments 92

Figure 5-3: The plot of linear modulus versus tissue thickness at various segments of the large intestine. This correlation is consistent across all the data..... 92

Figure 5-4: Viscoelastic ratio obtained from the indentation test 93

Figure 5-5: Typical AQLV fit to the stress versus time data of a) a rectum sample and b) an ascending sample during intra large intestinal indentation test. The black dash line separates the loading phase from the relaxation phase 94

Figure 5-6: Exponential fit of the AQLV model (black lines) to the stress relaxation data. Optimum time constants are 3, 30 and 300 s 95

Figure 5-7: Stress versus strain response of transverse colon under 10 repetitive loading in a) PBS and b) air. Red arrow on b) indicates the progression of cycles..... 97

Table 5-5: The shift of strain and linear modulus between each cycle for the samples in PBS solution corresponding to Figure 5-8-a..... 97

Figure 5-9: Effect of hydration level on linear modulus of transverse colon during the repeated interaction test..... 98

Figure 5-10: Effect of hydration level on viscoelastic ratio of transverse colon during the repeated interaction test..... 99

Figure 5-11: Fitted values of σ_0 & k_i for the AQLV model under repeated interaction test for both hydration conditions, in PBS and in air 100

Figure 5-12: Typical curve of stress versus time for 4 incremental strain steps. The peak and final stresses are identified as $\sigma^i(0)$ and $\sigma^i(\text{end})$, respectively..... 101

Figure 5-13: Linear modulus distribution at four strain levels 20%, 35%, 50% and 65%. 101

Figure 5-14: Normalised stress versus time for four strain increments. The curves represent the AQLV model fit of the normalised experimental data 103

Figure 5-15: Measured (red curves) and predicted (black curves) stress relaxation for the large intestine using the AQLV model under stepwise strain test. The initial strains are a) 35%, b) 50%, & c) 65% 104

Figure 6-1: The distribution of linear modulus in various segments of the large intestine for a) longitudinal and b) circumferential samples 108

Figure 6-2: The distribution of viscoelastic ratio in various segments of the large intestine for a) longitudinal and b) circumferential samples..... 108

Figure 6-3: Typical AQLV fit (black line) to the stress relaxation data of both longitudinal and circumferential samples. The black dash line separates the loading phase from the relaxation phase 109

Figure 6-4: Exponential fit of the AQLV model (black lines) to the averaged relaxation data under longitudinal tensile stretch. Optimum time constants are 3, 30 and 300 s.. 110

Figure 6-5: Exponential fit of the AQLV model (black lines) to the averaged stress relaxation data under circumferential tensile stretch. Optimum time constants are 3, 30 and 300 s 111

Figure 6-6: Typical stress-strain response of the large intestine to repeated interaction under tensile stretch. Red arrow on the magnified view shows the direction of cyclic progression 112

Figure 6-7: The stress-strain response of the large intestine during the loading phase for longitudinal and circumferential samples 113

Figure 6-8: Effect of fibre orientation on a) linear modulus and b) viscoelastic ratio of transverse colon during the repeated interaction test 114

Figure 6-9: Fitted values of σ_0 & k_i for the AQLV model under repeated interaction test for both fibre directions, longitudinal and circumferential alignments..... 116

Figure 6-10: An example of the Wiechert fit to the loading viscoelastic region for 10 consecutive cycles..... 117

Figure 6-11: Normalised stress versus time for four strain increments for two fibre alignments; longitudinal and circumferential directions..... 119

Figure 6-12: Measured (red curves), fitted/predicted (black curves) stress relaxation for the large intestine using the AQLV model under stepwise strain tensile test. The initial strains are a) 20%, b) 35%, c) 50%, & d) 65%. The AQLV model parameter from a) 20% strain level is used to predict the response of tissue for the rest of steps..... 121

Figure 7-1: Change in resonance frequency and impedance magnitude upon contact on silicon samples with different hardness 125

Figure 7-2: The spread of frequency and impedance magnitude shifts	125
Figure 7-3: Change in resonance frequency upon contact on silicon samples with different hardness	126
Figure 7-4: Change in impedance magnitude upon contact on silicon samples with different hardness	127
Figure 7-5: The change of a) frequency and b) impedance amplitude for two segments of the large intestine under varying applied load	129
Figure 7-6: Acoustic impedance response of the tissue during stress relaxation. The red curve parted from the rest represents the frequency sweep under no load and all the other curves demonstrate the frequency sweep at 1 N loaded tissue	129
Figure 7-7: a) Frequency shifts and b) impedance magnitude shifts of the tissue to the PZT probe II oscillation under 1 N contact pressure during 300 s relaxation phase. ...	130
Figure 8-1: The effect preconditioning and hydration on the linear modulus values in this study and the literature. All the samples are obtained from pig large intestine except Meghezi et al. study on collagen gel	134
Figure 8-2: The effect of preconditioning and hydration on viscoelastic ratio of the large intestine. Rectum samples were used for the MUST-Indentation whilst transverse colon samples were obtained for all the other of data	136
Figure 8-3: The effect of preconditioning and hydration on the equilibrium modulus of Wiechert model (MUST-Indentation) and AQLV model (MMC-Indentation/Tensile). Rectum samples were used for the MUST-Indentation whilst transverse colon samples were obtained for the rest of data	137
Figure 8-4: Comparison of linear modulus values between different techniques used in this study and the literature on the large intestine. All the reported studies were performed on pig samples except stated otherwise	143
Figure 8-5: The equilibrium modulus obtained from different viscoelastic model to indentation and tensile experimental data	146
Figure 8-6: Comparison between the RMSE values obtained from different models used in this research and in the literature	147

List of abbreviations

CSA: **Cross section area** (mm)

F: **Force** (N)

A: **Area** of the indenter tip (mm)

ΔL : **Deformation** (mm)

L_0 : **Initial length** (mm)

σ : **Stress** load per unit area; $\sigma = F/A$ (N/m²)

ε : **Strain** is the amount of elongation which the material undergoes under applied load;

$$\varepsilon = \Delta L/L_0$$

YM: **Young's Modulus** or stiffness is the applied stress per unit strain; $E = \sigma/\varepsilon$ (N/m²)

E: **Elasticity constant** (N/m²)

η : **Viscosity constant** (N^{-s}/m²)

VR: **Viscoelastic ratio**

$E(t)$: **Relaxation modulus** (N/m²)

E_i : **Elastic modulus** (N/m²)

η_i : **Viscous coefficients** (N^{-s}/m²)

τ_i : **Time constant** (s)

$R(t)$: **Reduced relaxation function**

$\Delta\sigma$: **Stress relaxation drop** (N/m²)

Δf : **Frequency change** (Hz)

f: **Loaded resonance frequency** (Hz)

f_0 : **Unloaded resonance frequency** (Hz)

Chapter 1. Introduction

Colorectal cancer is reported to be the fourth most common cause of cancer deaths worldwide [1]. Colonoscopy aims to evaluate abnormalities, unexpected sources of bleeding, surveillance for colonic cancer growths and other colorectal complications [1]. The current colonoscopy devices are equipped with an optical camera, illumination and biopsy tools to visually examine the colon and extract samples. Evaluating mechanical properties of the large intestine can help for generic design of colonoscopy instruments. It also can be used as a diagnostic tool since one of the drawbacks to colonoscopy devices is that they rely only on the visual ability of the practitioner, and therefore suspicious abnormalities cannot be assessed accurately in real-time. Performing elastic property examination of the large intestine during colonoscopy procedures may be a potential way to avoid complications such as unnecessary biopsy, which is a source of trauma [2]. Also, it may aid to detect the hidden tumours (tumours hidden under different layers) and spontaneously state on the nature of the detected abnormalities such as normal lumps, inflammatory lumps, benign tumours and malignant tumours. In this regard, a thorough investigation must be conducted to measure and characterise the mechanical properties of the large intestine in a controlled laboratory environment.

The emergence of laparoscopic surgery has initiated a new culture towards more efficient abdominal surgery. It offers less complications and trauma in comparison with conventional open surgeries [3]. Since the first laparoscopic surgery in 1901 by Kelling [4] there have been increasing efforts to enhance the design and functionality of laparoscopic tools for minimally invasive surgery. One of the main requirements for designing these tools is to understand the behaviour of tissue under manipulation by the surgical instruments such as tissue palpation for detecting tumours and abnormalities. Also, creating tissue-like phantoms which exhibit realistic mechanical properties is crucial for the evaluation of new surgical tools. Similarly, in robotic endoscopy it is essential to be fully aware of the robot's surrounding environment and the response of tissues to any possible physical interaction with the robot (i.e. collisions).

Previous studies show that the large intestine is a soft biological tissue which exhibits a complex mechanical response including viscoelastic, non-linear, anisotropic and inhomogeneous behaviours [5-14]. These properties are all time, strain history and strain-rate dependent and are affected by factors including age, disease, sex and diet.

Therefore, changes in viscoelastic properties may correlate to the influence of disease. Mechanical behaviour of tissues differs extensively among various organs and pathologies. Physiological changes in living soft tissue affect mechanical characteristics of tissue and may indicate the existence of abnormal pathologies. Accurate knowledge on these properties has been proven to greatly benefit medical assessment of tissue in physiological and diseased states. For instance, in the case of breast and prostate cancer, detection of a relatively stiffer tissue is associated with pathology and it is possibly a sign of tumour [15, 16]. It is found out that the stiffness difference between the breast tumour and healthy tissue can vary by a factor of 90 [17].

In this context, one of the main complications in characterising soft tissue properties is the extensive number of approaches upon which these measurements have been obtained. Choosing the appropriate method can be really challenging since beside the choice of the technique, i.e. whether it be a compression, stretch or expansion types of interaction, there are various environmental conditions (such as the hydration and temperature levels), boundary conditions (the size and shape of the samples) and the experimental protocols (such as the strain-rate and strain or stress threshold levels) that can be utilised in which directly influence the result of the tissue properties examination. Measurements of mechanical properties should often be performed with the end application being considered. It can still be confusing what direction to take to establish parameters to describe the tissue. Therefore, this thesis has facilitated a design of an appropriate testing protocol to include all the right elements.

Chapter 2. Literature review

In this chapter, an overview of the main published work concerning characterisation of the mechanical properties of the large intestine is provided. It begins with providing a broad review of the mechanical properties of soft tissues. Then, it highlights the existing research on ex-vivo and in-vivo properties of the large intestine. Following that, an insight into the current techniques developed to measure these properties is given. Then, the common methods that have been employed to analyse these measured data were investigated. Lastly, the effects of various factors in testing protocols which may influence the response of the tissue are explored. A brief summary of the main discussion points in the literature review is presented in the final part of this chapter.

2.1 Mechanical properties of soft tissue

Soft tissues can be uniquely characterised by the following physical features under applied stress: non-linear stress-strain relationship, viscoelasticity, time and rate dependency and preconditioning. In this chapter, soft tissue mechanical characteristics, which have been greatly investigated by Fung [18], Holzapfel et al. [19] and Brown et al. [20], are described.

Figure 2-1 shows the fibre structure of the stress-strain relationship obtained from tensile testing on human skin. The curve is divided into three regions and the collagen fibres morphology associated with each region is drawn. Before any stress is applied to collagen fibres in 'Region I' or 'toe-region' the collagen fibres are randomly oriented and relaxed. As the smallest amount of stress is applied to them, a very high deformation is generated. Elastin fibres are mainly in charge of the stretch pattern. At this stage the tissue behaves isotropic. This part of the graph is nearly linear with a very low gradient or Young's Modulus [20, 21].

At 'region II' (the so-called 'heel region'), as the stress increases, the collagen fibres start to line up in the direction of the stretch and the tissue gradually stiffens. At this point, the linear curve of 'region I' turns to an exponential curve. In the last region, 'region III' or linear-region, as the stiffness of the tissue rapidly increases a perfect aligned collagen fibres are formed in the direction of the load. The friction generated between the collagen fibres is responsible for observing a viscous response in this region. A linear trend is observed in this portion of the curve [20-22]. At this point, if the deformation/strain is kept constant at the peak force/stress, the two main

characteristic lengths of the collagen fibres ‘shorter chains’ and ‘longer chains’ generate two different relaxation processes. Each of these relaxation processes has its own amplitude and relaxation time. The viscous process induced by the friction between the shorter chains is rapidly negligible compare to those of longer chains; therefore, higher elasticity in shorter time is induced by the shorter chains [22].

Under cyclic or lengthy loading, deformation recovery happens slowly. This implies that under these loading types the tissue deformation does not reverse at the same speed as it stretched. This causes the tissue to stay deformed temporarily. Passing the third region, the tissue reaches the ultimate tensile strength and ruptures. This state is marked as plastic phase where tissue completely loses its flexibility and it starts to deform permanently in the direction of the applied load.

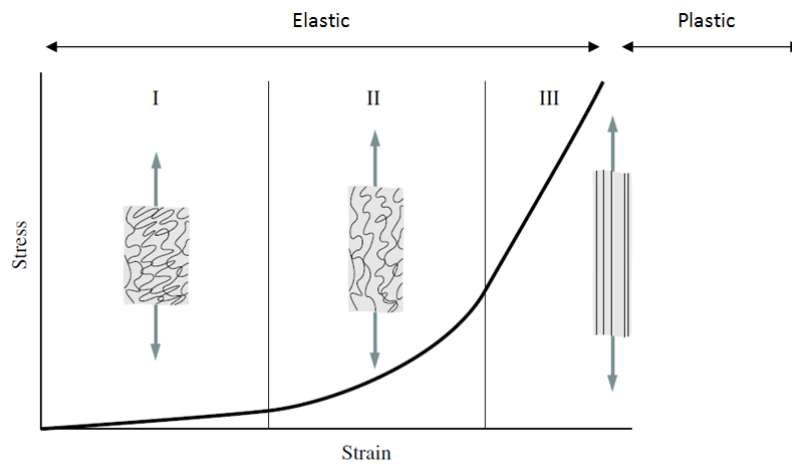


Figure 2-1: Schematic diagram of typical stress-strain curve [21]

Previous studies [7, 8, 10, 12-14] show that colon as a soft biological tissue exhibits very complex mechanical characteristics such as viscoelastic, non-linear, anisotropic and inhomogeneous behaviour. Viscoelasticity is a product of fluid flow resistance (viscosity) and solid behaviour (elasticity) within the cellular level of soft tissues. The known features of viscoelasticity are time-dependent load relaxation and creep, rate dependence, and hysteresis. Non-linearity refers to stress-strain relationship where deformation rate varies under constant loading steps. One of the indications of non-linearity is when the viscoelastic force response to an elongation of $\Delta L_1 + \Delta L_2$ is different from the sum of viscoelastic force response to elongation $\Delta L_1 + \Delta L_2$ [23]. Anisotropic properties are described as when tissue delineates different properties along longitudinal and transversal axis, and inhomogeneous behaviour is the lack of

uniformity in composition. These properties are time and load history dependent and are affected by age, disease, sex, diet, heritage and etc. Any change in these properties can correlate to the influence of diseases.

Viscoelasticity in soft tissues is the study of elasticity and viscosity, a combined solid-like and liquid-like characteristic. There are three features that explain viscoelasticity in materials: Stress relaxation, creep and hysteresis. 'Stress relaxation' happens when a tissue goes through a sudden extension and then the strain is maintained constant. At this point the stress induced in the tissue falls with time. In other hand, if the tissue is suddenly stressed and then the stress is maintained constant at the new value, the tissue continues to deform with time until equilibrium. This phenomenon is known as 'creep'. Now if the tissue undergoes a cyclic loading, the loading part of the stress-strain curve exhibits a different path to the unloading portion. This behaviour is named 'hysteresis'. Hysteresis is determined by the dashed area between loading and unloading curve. In soft tissues, the unloading curve is usually steeper than the loading curve. This area presents an energy loss when the tissue fails to rapidly deform back to its original shape in the removal of applied stress [24]. This behaviour opposes the behaviour of pure elastic solid organs, such as bones, where the unloading curves match the loading curves of force-displacement graph. This implies that no energy loss is induced after removal of an applied load. Hence, the viscous nature of viscoelastic material causes the unloading portion of the curve to show some energy dissipation.

All the above properties of viscoelasticity are counted as passive properties of tissue and depend on time-history of load. There is also a 'preconditioning' property which depends on maximum load history, and used to be categorised as part of the viscoelastic characteristics (Figure 2-2). Preconditioning is related to a loss of stiffness when the internal structure of the tissue changes under cyclic loading. Mullins [25] established that maximum previous load history in rubber significantly affects the stress-strain relationship. He realised that after rubber is stretched to a certain level, it permanently softens [26]. As Figure 2-2 demonstrates the deformation of the tissue changes with each consecutive loading. The loading-deformation curves shift to the right (Figure 2-2-a), and the load relaxation curves move upwards (Figure 2-2-b). The upward movement of force relaxation curves is due to a decrease in the load relaxation at each sequential cycle.

As can be observed, after a series of loading, the behaviour of the tissue reaches a steady-state level and the hysteresis is stabilised. At this point tissue is said to become conditioned. Preconditioning or stress softening is performed to attain repeatable results, independent of previous manipulation [25, 27].

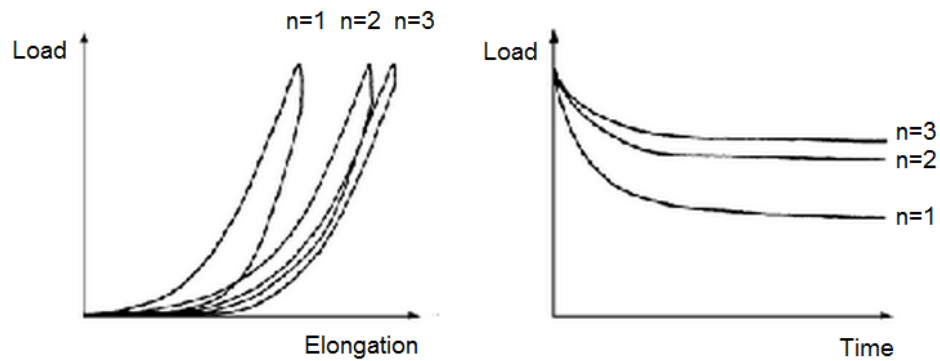


Figure 2-2: A typical a) load-elongation and b) load-time diagram for anterior cruciate ligament of rabbit knee [18]

2.2 Large intestine characterisation

Soft tissues embrace a wide range of biological living materials which can be easily differentiated from hard material (e.g. bones) by their level of flexibility and mechanical properties. Soft tissues, including tendon, ligament, large intestine, and skins and so on, have their own particular composition of cells and extracellular matrix. The features which dominate the specific mechanical response of soft tissues are the embedded cells within extracellular matrix of the tissues. Elastin and collagen fibres are the main two protein fibre elements of extracellular matrix. Elastin is responsible for the great flexible behaviour and collagen is the source of the stiffness and the tensile load bearing in the tissues [21, 28].

Large intestine functionality is to receive the indigestible food from the small intestine and after absorbing the water and vitamins from it, it passes the more solid faeces to the rectum [7]. Human colon can be conventionally divided into four functionally distinct segments, ascending colon, transverse colon, descending colon and sigmoid colon (Figure 2-3).

As shown in Figure 2-4 the colonic wall consists of four main layers, mucosa, submucosa, muscularis externa and serosa [29]. The mucosa and serosa layers are composed of loose arrangement of collagen fibrils (Figure 2-4-e). Mucosa is surrounded

by clockwise and anti-clockwise helix network of collagen fibres of submucosa layer. Muscularis externa, contains two smooth muscle layers one in longitudinal direction forming three thick bands known as taenia coli (Figure 2-4-b) and one in circumferential direction (Figure 2-4-c) [29].

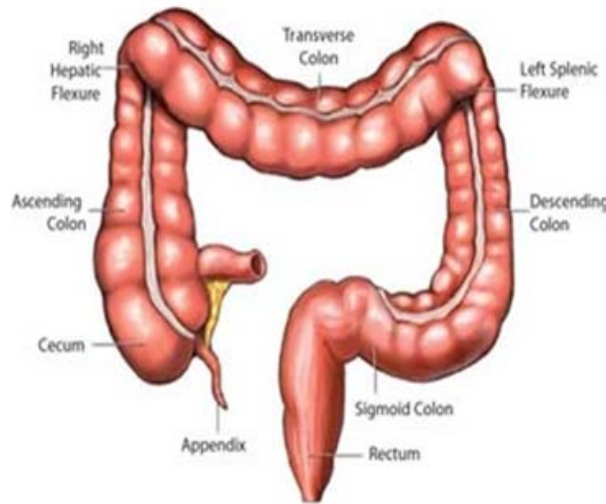


Figure 2-3: Structure of the human large intestine [30]

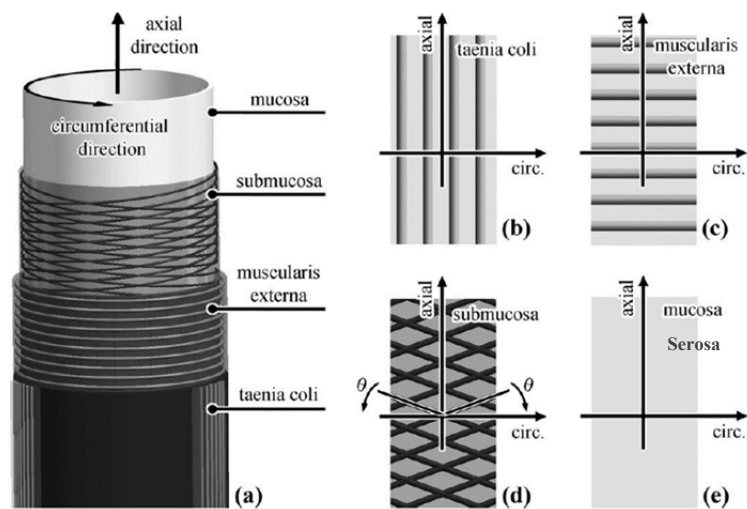


Figure 2-4: Schematic diagram of colonic wall structure, a) four layers of colonic wall. Muscular fibres are distributed in b) axial directions within taenia coli layer, c) circumferential direction within muscularis externa layer, d) clockwise and anti-clockwise helices within submucosa layer and d) isotropic for mucosa layer [29]

Table 2-1 summarises the existing studies that have been conducted on the ex-vivo and the in-vivo mechanical properties of the large intestine. The table captures each study’s selected tissue type, experimental method, testing protocol and outcomes. This

	Study	Tissue Type	Experimental Methods	Testing protocol	Research Outcomes
In-vivo	Dall <i>et al.</i> 1991 [31]	Porcine rectum	Distension Test (using impedance planimetry)	$P_{max}=80$ cmH ₂ O	Pressure vs. CSA, volume, cross section area, stiffness and compliance
	Dall <i>et al.</i> 1993 [32]	Human rectum	Distension Test (using impedance planimetry)	$P_{max}=40$ cmH ₂ O	Pressure vs. CSA, volume, cross section area, stiffness and compliance
	Lundby <i>et al.</i> 1998 [33]	Mouse rectum	Distension Test (using impedance planimetry)	$P_{max}=2.5$ kPa	Pressure vs. CSA, volume, cross section area, stiffness and compliance
	Petersone <i>et al.</i> 2000 [34]	Human rectum and sigmoid	Distension Test (using impedance planimetry)	$P_{max}=6$ kPa	Pressure vs. CSA, volume, cross section area, stiffness and compliance as a function of rectal pain threshold to distension for healthy
	Kern <i>et al.</i> 2001 [35]	Human rectum	Distension Test (using MRI technique)	P_{max} = at moderate pain level	Tension and stress as a function of infused volume and circumferential strain using 3D MRI technique
	Bharucha 2001 [5]	Human Descending colon	Distension Test	Intraluminal pressure range =0-44mmHg rate=0.16,0.5, 1 & 10 ml/s	Pressure vs. volume relation at Quasi-static vs. dynamic distensions
	Drewes <i>et al.</i> 2001 [36]	Human rectum and sigmoid colon	Distension Test (using impedance planimetry)	$P_{max}=6$ kPa	Pressure vs. CSA, volume, cross section area, stiffness and compliance as a function of rectal pain threshold to electrical stimuli for healthy vs. patients with irritable bowel syndrome.
	Petersone <i>et al.</i> 2003 [37]	Human rectum and sigmoid	Distension Test (using impedance planimetry)	Rate=50, 100 and 200 ml/min P_{max} = at moderate pain level	Pressure vs. CSA, volume, cross section area, stiffness and compliance as a function of rectal pain threshold to distension
	FRØKJÆR <i>et al.</i> 2005 [38]	Human rectum	Distension Test (using MRI technique)	P_{max} = at moderate pain level	Tension and stress as a function of infused volume and circumferential strain using 3D MRI technique
	Higa <i>et al.</i> 2006 [8]	Goat large intestine	Compression test	Tests in air at RT $\epsilon_{max}=80\%$, rate=0.02, 0.5 & 5 mm/s	Strain-stress relation and stiffness at different rate and strain levels
	Drewes <i>et al.</i> 2006 [39]	Human rectum and sigmoid	Distension Test (using impedance planimetry)	rate=1.6 ml/s P_{max} = at moderate pain level 3xpreconditioning cycle until a moderate pain detection	Pressure vs. CSA, volume, cross section area, stiffness and compliance as a function of rectal pain threshold to distension for healthy vs. patients with ulcerative colitis.

	Rosen and Brown 2007 [10]	Pig large intestine	Endoscopic rasping test	Stress relaxation time=60 s $\epsilon_{max}=42-60\%$	Tensile strength, stiffness, strain-stress relation, stress relaxation response and model fitting analysis
Ex-vivo	Yamada 1970 [14]	Human & animal large intestine	Uniaxial tensile, expansion and bursting tests	-	Tensile, Expansive & burst Properties at various ages
	Watters et al. [12] 1985	Human large intestine	Tissue elongation test (Instron Tensiometer)	Tests in PBS, preconditioning at 30% strain Stress relaxation time=180 s rate=300 mm/s	Burst Strength, Tensile Strength, % elongation & Stress relaxation in varying age, race and health groups
	Watters et al. 1985 [13]	Rat colon and rectum	Tissue elongation test (Instron Tensiometer)	Tests in PBS, preconditioning at 100% strain Stress relaxation time=180 s rate=300 mm/s YM=135 kN/m ² at stress 0.25-1 N	Burst Strength, Tensile Strength, elongation, Stress relaxation & Young's Modulus in varying age and sex groups
	Itasaka et al. 1992 [9]	Rat distal colon	Distension Test	Tests in serosal solution Distension time=15 s Intraluminal balloon pressure=15 cmH ₂ O	Pressure vs. volume relation at various tissue conditions
	Gao and Gregersen 2000 [7]	Rat large intestine	Uniaxial distension Test (pressure vs. volume test)	Tests in Krebs solution Intraluminal pressure range=0-2 kPa	Morphological data at no load and zero states. Diameter and longitudinal extension as functions of pressure
	Egorov et al. 2002 [6]	Human large bowel	Uniaxial tissue elongation test (Instron Tensiometer)	Tests in air at RT, preconditioning at 30% strain rate=0.83 mm/s	Maximum tensile strength and destructive strain
	Qiao et al. 2005 [40]	Pig rectum	Uniaxial tensile, compression, shear tests	Tests in air at RT, preconditioning at 40% strain rate=0.1 mm/s	Stress vs. strain and Linear modulus
	Higa et al. 2006 [8]	Goat large intestine	Compression test	Tests in air at RT $\epsilon_{max}=80\%$, rate=0.02, 0.5 & 5 mm/s	Strain-stress relation and stiffness at different rate and strain levels
	Sokolis et al. 2011 [11]	Rat large intestine	Uniaxial 3D Inflation/ Extension test	Tests in Krebs solution, preconditioning at pressure=0-15 mmHg Stretch of $\epsilon_{max}=100-130\%$, Intraluminal $P_{max}=15$ mmHg at rate=0.15 mmHgs ⁻¹	Thickness and stiffness comparison at Zero state, no load state & pressurized state.

Table 2-1: A comparison of studies conducted on mechanical properties of large intestine in the ex-vivo and the in-vivo conditions

summary helps to understand and analyse the background research, reveals the gaps in this field, and provides evidence for explaining the current study's findings.

2.2.1 Existing literature on ex-vivo characterisation of the large intestine

The earliest attempt to collect a comprehensive database on mechanical properties of a wide variety of organs and tissues was performed by Yamada [14]. The work includes the tests on animal in-vitro and human cadavers. The group of soft tissues under test included small and large intestine, lung, stomach, liver, gallbladder and esophagus, and so on. For large intestine, Yamada carried out a series of human cadavers and animals experiments on four sections of colon; ascending, transverse, descending & rectum segments, in longitudinal and transverse directions. As the above table illustrates, Yamada quantitatively characterised tensile, expansive and bursting properties of colon at various ages. However, his study did not consider characterising the viscoelastic properties of the large intestine [14].

Watters *et al.* [12], in his work on post-mortem human large intestine, focused on the influence of age and particularly race on the mechanical properties of large intestine. He employed an Instron tensiometer to elongate the tissue in longitudinal direction. Concerning the influence of age factor, his experiments show that the tensile strength deteriorates with advancing age. Comparing African and European samples, he concluded that since African colons are stronger, wider and thinner than European ones, their mechanical functionalities are more efficient. This presumably is due to the different environmental factors such as diet. Viscoelastic properties were said to be similar in both groups and independent of age factor. Figure 2-5 depicts the stress relaxation of sigmoid with respect to the age and race factors. The measured parameters were burst strength, tensile strength, % elongation & stress relaxation. Just like Yamada, Watters *et al.* found that these parameters decline from ascending to sigmoid; proving that sigmoid has weaker mechanical properties [12].

As already mentioned, Figure 2-5 plots the results of stress relaxation testing of colon for both races. In this experiment, the tissue was stretched 10 times to 30% strain and then the stress relaxation was measured for 3 minutes. In Figure 2-5, the linear regression lines against age of the two groups (African and European) are fitted to stress relaxation values.

Watters and his group [13] in another paper, investigated the same mechanical properties and employed the same strategies but in rat colon. The two extra features measured in this study were hysteresis and Young's Modulus. The following curve, Figure 2-6, is the stress-strain response of rat colon that suggested by Watters *et al.* [13].

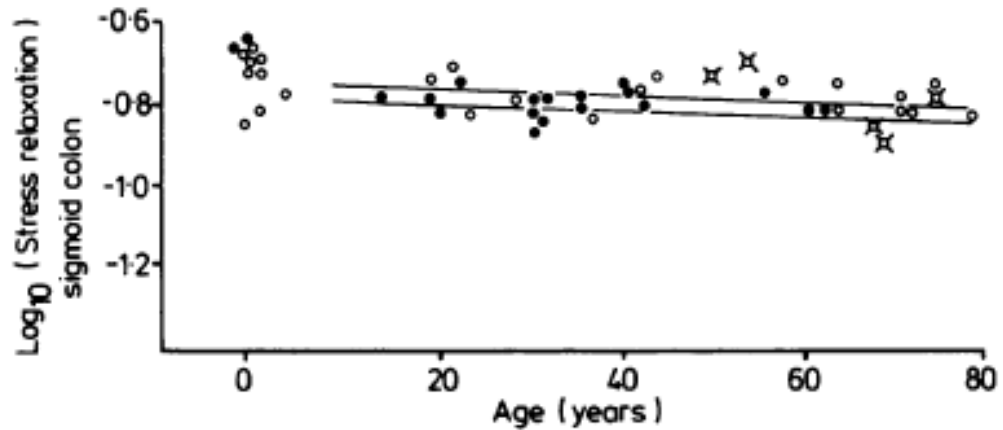


Figure 2-5: Stress relaxation of sigmoid colon for African and European group. Africans are closed circles and upper regression line. Europeans are the open circles and lower regression line [12]

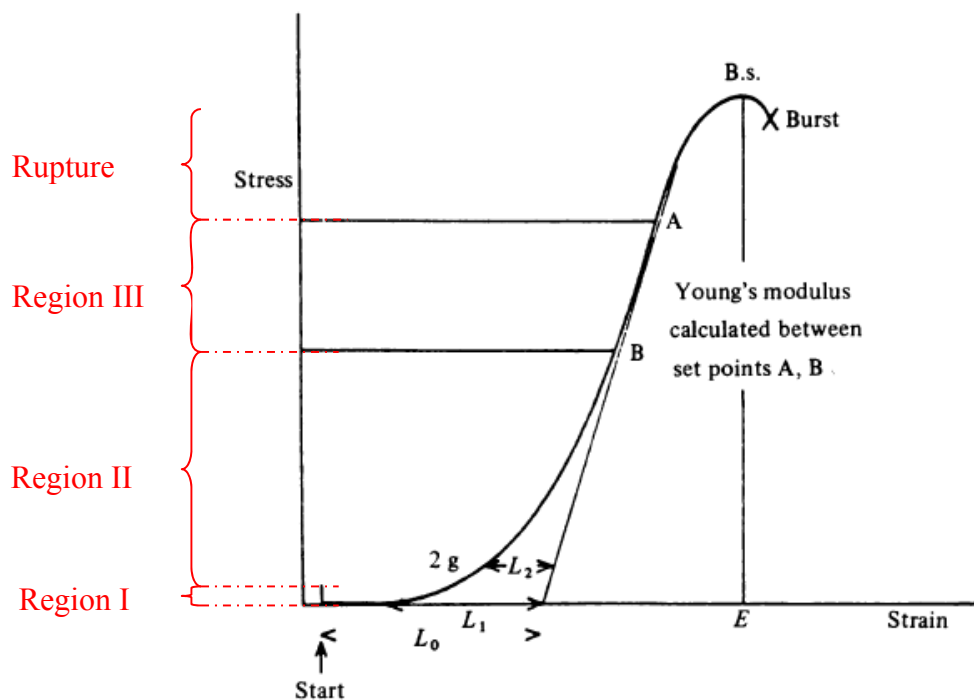


Figure 2-6: Rat colon stress-strain response. L values (L_0 , L_1 & L_2) are measured after drawing the tangent to the steep section of the stress-strain response. E is the strain at burst strength. A & B are the two points on the stress-strain curve specify the most straight relationship between strain and stress just before the point of burst strength [13]

This graph ties well to the configuration of collagen fibre morphology for a typical stress-strain curve in Chapter 2.1.1. Similar regions to those of Figure 2-2 are marked on this graph. It is noticeable that the straight line in ‘Region III’, between points A and B, where the most linear response is observed was taken for Young’s Modulus calculations. The quantitative outcomes of the experiments on the rat colon are given in the Table 2-2. Five equally spaced segments were tested. Young’s Modulus was reported for two sites, 25-100 gram and 125-200 gram of applied stresses.

Parameter	A	B	C	D	E
Burst strength (g)	251.0±55.0	251.0±43.0	250.0±39.0	268.0±37.0	270.0±50.0*
Percentage elongation	81.0±23.0	89.0±18.0	97.0±16.0	120.0±30.0	118.0±31.0
L_0 (mm)	40.2±12.2	37.2±6.6	33.0±2.9	37.2±7.9	32.2±1.6
L_1 (mm)	21.2±9.1	21.6±8.0	19.4±8.0	25.0±7.1	27.6±5.0
L_2 (mm)	11.6±5.3	10.8±3.7	16.6±6.5	18.0±7.8	16.9±4.3*
Stress relaxation	0.2029±0.0221	0.1717±0.0176	0.1905±0.0205	0.2215±0.0278	0.2177±0.321
Hysteresis	0.77±0.04	0.83±0.06	0.74±0.10	0.78±0.08	0.76±0.05
Energy under curve (kJ)	55.0±21.0	45.0±15.0	55.0±84.0	73.0±14.0	82.0±38.0*
Young’s modulus (25–100 g) (g/mm ²)	327.0±109.0	374.0±239.0	303.0±116.0	206.0±63.0	325.0±135.0
Young’s modulus (125–200 g) (g/mm ²)	754.0±320.0	802.0±359.0	832.0±403.0	638.0±388.0	729.0±623.0

Table 2-2: Values of results comparing five equally spaced colonic segment sites, A-E, progressing distally

The result for the tensile strength of the rat colon was similar to those of cat and domestic fowl measured by Yamada [14]. The effect of age on all the measured parameters shared the same trend in rat and human cadaver, a result in line with the outcome of Yamada’s work [13].

Various storage techniques were also discussed in this paper. Watters *et al.* [13] stated that Young’s Modulus declines with each day of storage. He found out that saline was the best option to preserve mechanical properties of colon up to 1 week; whereas deep freezing and liquid nitrogen weakened the tissue properties. For longer storage, salt is a simple and cheap option to preserve the tissues for up to 25 days [13]. No viscoelastic properties of the large intestine were reported in any of these two papers.

Gao and Gregersen [7] in 2000, examined mechanical properties of the large intestine in three different states: pressurized, no-load and zero-stress states. For hollow organs, the no-load state is referred to a closed ring of the organ with no external force applied to it. Zero stress state is when an open ring of the organ is under absolutely no applied stress, as shown in Figure 2-7.

In this study, at pressurised states four segments of colon were distended from one end while the other end was blocked. At no-load state, each segment was cut into five short rings. And finally at zero-stress state, the short rings were cut radially to release the existing circumferential stress. The tissue was photographed at each step for morphometric data measurements. They also calculated the ‘residual strain’ that exists between the zero-stress state and no-load state [7].

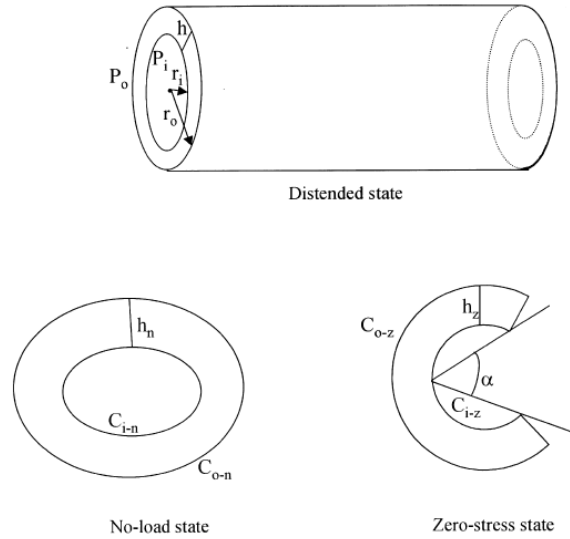


Figure 2-7: Colon segment at distended, no-load and zero-stress states [7]

Stress and strain in longitudinal and circumferential directions were calculated as follow:

$$\text{Circumferential Kirchhoff stress: } \sigma_{\theta} = \frac{\Delta P r_i}{h \lambda_{\theta}^2} \quad 2.1$$

$$\text{Longitudinal Kirchhoff stress: } \sigma_l = \frac{\Delta P r_i^2}{h \lambda_l^2 (r_o + r_i)} \quad 2.2$$

$$\text{Circumferential mid-wall Green strain: } E_{\theta} = \frac{1}{2} \frac{(C_{m-p}^2 - C_{m-z}^2)}{C_{m-z}^2} = \frac{\lambda_{\theta}^2 - 1}{2} \quad 2.3$$

$$\text{Longitudinal Green strain: } E_l = \frac{1}{2} \frac{(L_p^2 - L_n^2)}{L_n^2} = \frac{\lambda_l^2 - 1}{2} \quad 2.4$$

Where ΔP , h , r_i and r_o are the transmural pressure difference, wall thickness, luminal radius and outer radius, respectively. The length of the mucosal and serosal circumferences is C_i and C_o . L_p and L_n are the length of the pressurised and no-load

states. The longitudinal mid-wall stretch ratio λ_l is defined as (L_p / L_n) and circumferential stretch ratio is $\lambda_\theta = (C_{m-p} / C_{m-z})$ where subscripts 'p' signifies pressurized state and 'm' denotes the mid-wall.

The longitudinal and circumferential stresses versus strain curves were then analysed with regards to the stiffness of the colonic wall. It was found that all the segments of colon are stiffer in longitudinal than circumferential directions, from which the transverse colon is the stiffest segment in both directions. They also suggested that the exponential nature of the stress-strain curve helps to protect soft tissue from over expanding under high applied pressure inside the lumen [7].

Egorov *et al.* [41] also used Instron tensiometer to quasi-statically measure cadaveric and surgically removed large intestine mechanical properties. In his study the large intestine wall was modelled as a multi-layered construction rather than one-layer membrane. His data indicated that different layers of the bowel wall have different mechanical properties in axial and transversal directions. This was due to the different adhesive connectivity between the layers at different directions. The tensile tests were conducted both along and transverse to the fibre direction. The results of the ultimate tensile strength were 0.7MPa and 0.9MPa for longitudinal and transversal specimens, very similar to the works of Yamada [14] and Watters [12].

The mechanical behaviour of pig rectum under tensile (longitudinal and circumferential directions), compressive and shear stresses were evaluated in [40]. The results showed a significant difference in the linear modulus at different orientations. The tensile resistance was found to be higher for circumferential than the longitudinal direction possibly due to high number density of horizontal folds in the rectal wall [40].

Sokolis *et al.* [11] examined a 3D constitutive model to mechanically analyse multi-axial behaviour of the large intestine. He developed a device, depicted in Figure 2-8, which allowed simultaneous inflation and extension of the tissue, as an effort to understand the food transport function of the large intestine. A stress and strain model was produced to suit the multi-axial distension/expansion testing of the tissue [11].

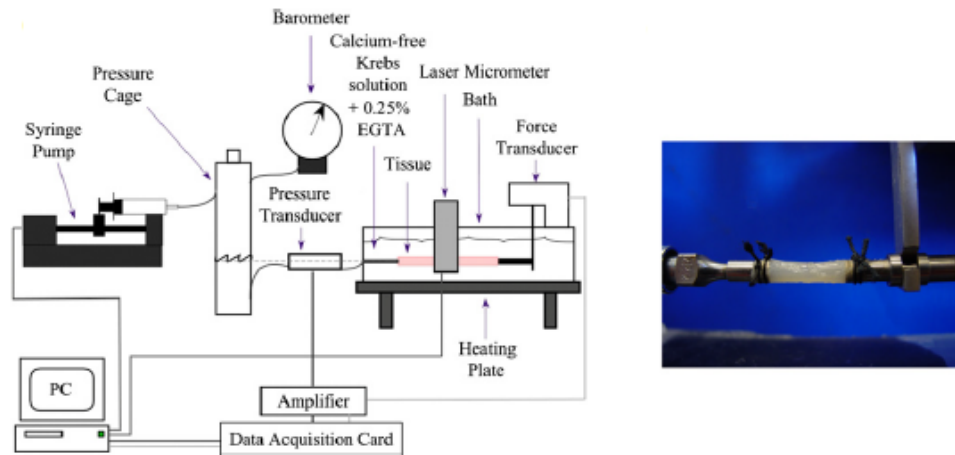


Figure 2-8: Schematic diagram of Sokolis device allows for simultaneous inflation and extension of tissue [11]

Sokoli's choice for constitutive model was Fung-type exponential strain energy function (SEF), also known as pseudo-elastic constitutive formulation, in which is a function of circumferential and axial strains. This function is built to achieve through thickness stress distributions [11]. His results from inflation/expansion experiment strongly correlate to those of Gao and Gregersen, stating that all segments of colon are stiffer in longitudinal direction than circumferential direction, in which transverse colon is the stiffest segments among all in both directions [7, 11].

2.2.2 Existing literature on in-vivo characterisation of the large intestine

In an attempt to develop an artificial anal sphincter, in-vivo and in-vitro mechanical properties of goat colon were evaluated by Higa et al. in 2006 [8]. The stress-strain graphs of uniaxial compression tests at varying strain-rates are displayed in Figure 2-9. A strain of 0.8 was given to all the specimens under the test. As it can be seen, at in-vitro condition higher stress values were required to deform the tissue to a certain amount compare to in-vivo condition. This indicates that the colon is stiffer in-vitro than in-vivo [8]. One of the draw backs to Higa's technique was that under in-vivo condition, the bodies were invasively cut open and the colon segments were examined from the outside wall. In addition, in this study no viscoelastic response of the tissue was reported.

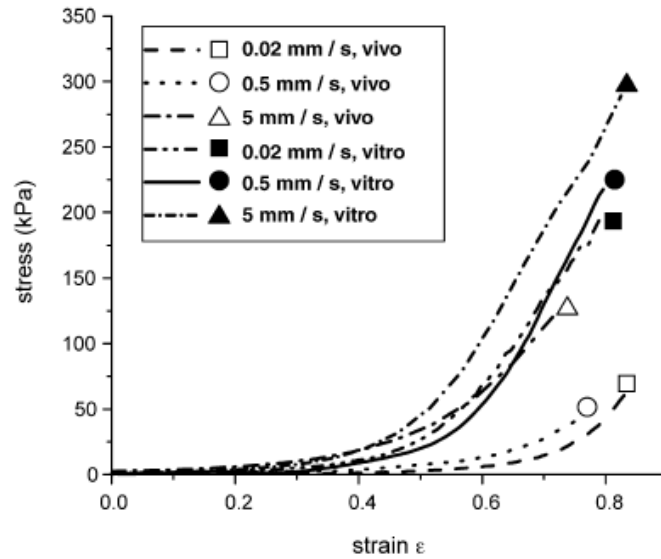


Figure 2-9: In-vivo and in-vitro stress-strain curve of goat colon [8]

Rosen and Brown [10] examined stress-strain relationship and stress relaxation of abdominal organs using a motorised endoscopic grasper, under three testing conditions: in-vivo, in-situ and ex-corpore. The Large intestine was only examined in-vivo from its outside wall under minimally invasive surgical procedure. As shown in Figure 2-10, the large intestine appears to have the highest stiffness among all the other organs as it underwent less deformation to achieve the same level of force compare to the others. Also, the response of the large intestine in the fifth cycle (a typical loading condition represents the mechanical characterisation of the biomechanical soft tissue) seems to be stiffer than the first cycle (in which represents the typical loading conditions during surgery) [10]. This difference was assumed to be due to the movements of the stool inside the lumen during the grasp and most importantly the slow recovery of the initial tissue thickness after the first cycle [10]. An important limitation of the grasping techniques can be attributed to the fact that it only represents the clinical relevant behaviour of the organ rather than the generic response of the tissue to compression. This is because when a hollow organ is grasped the walls start to approach each other and compress the contents. Therefore, the true response of the tissue to compression is obtained when the walls contact each other, and so each stress-strain curve contains two different tissue responses which need to be recognised.

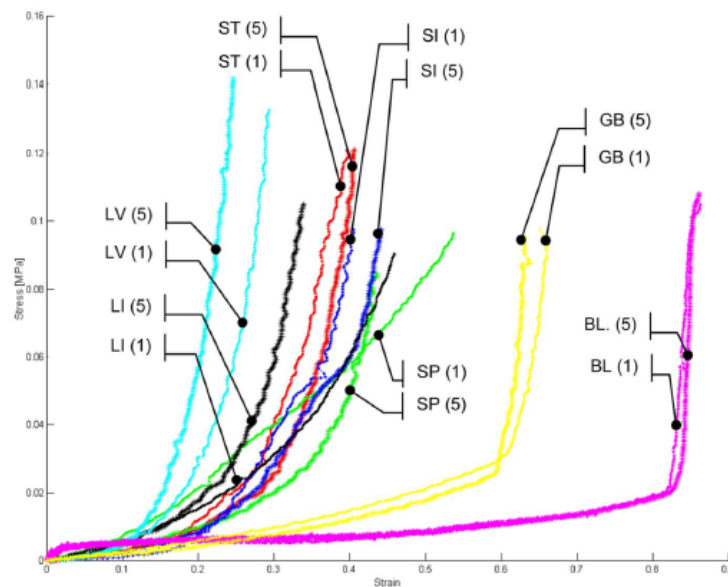
Various phenomenological curve fitting models for these organs were explored in this study. Many nominal uniaxial exponential models were introduced and examined to find the most suitable fit to the in-vivo experimental data. The best curve fitting model

for large intestine found to be EXP2 and REXP2 for elasticity and stress relaxation respectively:

$$EXP2: \quad \sigma = \beta (e^{\alpha \varepsilon^2} - 1) + \gamma \varepsilon \quad 2.5$$

$$REXP2: \quad \sigma(t) = \exp\left(\frac{-t}{\tau}\right)^\beta \quad 2.6$$

where α, β and γ are coefficients determined by curve fitting the experimental data. EXP2 is the basic exponential function $\beta (e^{\alpha \varepsilon} - 1)$ which increased the strain order to ε^2 , plus a linear term ' $\gamma \varepsilon$ '. REXP2, for modelling stress relaxation, comprises of a decaying



exponential function raised to a power, and a single time constant.

Figure 2-10: Stress-strain graph of the abdominal organs (1st and 5th cycles), BL-bladder, GB-gallbladder, LI-large intestine, LV-liver, SI-small intestine, SP –spleen and ST-stomach [10]

The derivative stress-strain function with respect to strain is called stiffness or Young's Modulus. Taking the derivative of exponential stress-strain function EXP2, results in:

$$\frac{d\sigma}{d\varepsilon} = 2\alpha(\beta e^{\alpha \varepsilon^2})\varepsilon + \gamma \quad 2.7$$

Altering the derivative, the overall stiffness indicator scalar ($\beta\alpha + \gamma$) was obtained to compare between stiffness of materials. Small and large intestine were found to have similar stiffness indicator scalar at high strains [10].

Bharucha *et al.* [5] explored two balloon distension methods to characterise viscoelastic properties of the human large intestine. In the first method the large intestinal lumen was quasi-statically pressurised, where the tissue was inflated to maximum pressure in even steps. The second method utilised a dynamic distension modality in which tissue was inflated all the way to the maximum pressure. By plotting pressure against volume and comparing the two methods, the paper concluded that rapid distension and deflation activates the neural reflex of colon muscles. This in turn reduces the compliance of colon, and increases the risk of permanent tissue deformation. Therefore, to model viscoelasticity, quasi-static distension is favoured over dynamic distension [5]. However, one of the recognised complexities of balloon distension technique is related to the unreliability of the volume and pressure measurements as firstly the rectum lumen is not perfectly tubular and secondly the balloon at some degree of distension tends to expand in the longitudinal direction where resistance is less. A good estimation of circumferential tension can only be driven from accurate measurement of balloon diameter at all time and the balloon's pressure and so the use of impedance planimetry is essential to obtain accurate CSA during balloon distension [39].

Several studies [31-34, 36, 37, 39] have been reporting the use of electrical impedance measurement technique for biomechanical characterisation of the walls in luminal organs under distension. Proposed by Harris *et al.* in 1971 [42] a series of electrodes located inside a balloon were used to measure the cross sectional area (CSA) of any hollow organs. This idea was developed further by Gregersen *et al.* [43] in 1988 and resulted in a design of a four electrodes balloon catheter probe as shown in Figure 2-11. The excitation electrodes are placed either side of the detecting electrodes [43]. The electrical field gradient between the electrodes determines the CSA measurements [42]. In principle, When a current I is induced in the excitation electrodes, the voltage difference V between the detecting electrodes is expressed as $V=IR$, where R is the resistance of the fluid inside the balloon and is $1/CSA$ [43]. Using this technique the biomechanical characterisation of various large intestines were investigated including porcine rectum [31], mouse rectum [33] human rectum/sigmoid colon [32, 34, 37],

human rectum and sigmoid colon in patients with irritable bowel syndrome [36] and ulcerative colitic [39]. Although, since the thickness of the lumen wall during distension cannot be measured in this technique, the biomedical characterisation is in terms of circumferential wall tension, compliance and the pressure elastic modulus rather than stress and Young's Modulus [32].

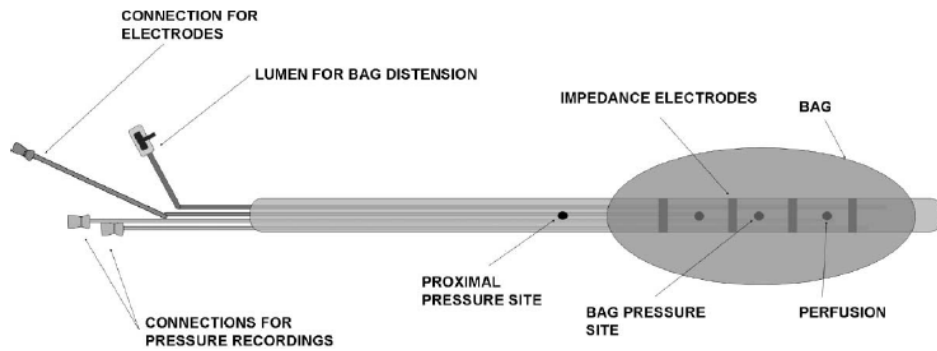


Figure 2-11: Balloon catheter probe for measurement of cross sectional area and pressure

The results of biomechanical characterisation of healthy human rectum [32] under balloon distension probe showed a linear increase of rectal wall tension with the increase of distension pressure and a non-linear relationship with the decrease of rectal compliance. The pressure elastic modulus increases with distension pressure until 35 cmH₂O [32]. These results were similar to the results obtained in an early study by the same group on porcine rectum, however, higher distension pressure threshold of 80 cmH₂O was selected for the pig study [31]. The impedance planimetric method was also employed by Lundby *et al.* [33] on different aged mice rectums where the samples were subjected to repeated distensions for four weeks. The results of pressure-CSA relations showed no change in CSA and no long term effect of repeated measurements in the samples [33].

Pain studies using balloon distension have been utilised for diagnosis and organ dysfunction [37]. In these studies the degree of pain associated with the expansion of the rectum wall was measured in order to find any relation between tissue stiffness and pain level in healthy/diseased tissue. The CSA, volume, pressure, tension, and strain were also recorded at each pain level. Using this approach in conjunction with the impedance planimetric method, Petersen *et al.* [34, 37] observed that human rectum and sigmoid colon have very similar biomechanical properties [34]. Also the CSA and volume of human rectum wall shows no strain-rate dependency and they were not

affected by muscle relaxation [37]. Drewes *et al.* [36, 39] performed two studies to compare the biomechanical behaviour of healthy human rectum/sigmoid colon to patients with irritable bowel syndrome [36] and ulcerative colitis [39]. In case of the ulcerative colitis patients the slope of the CSA-pressure curves between the healthy and patient subjects shows no difference in compliance of rectum. However, hypersensitivity and increased tone of the smooth muscle were observed for the patients compare to the healthy subjects [39]. For the study on patients with irritable bowel syndrome higher pressure at the pain detection threshold was found for the healthy subject than the patients. No difference was found in strain, tension and the sensation rating between the two groups [36].

Measurements taken using impedance planimetric method are only valid with assumption of circularity of the luminal wall and so it only applies to thin wall structures and as mentioned earlier the results are in terms of circumferential wall tension [38]. To assess the complex geometry of the rectum luminal wall FRØKJÆR *et al.* [38] utilised the cross sectional magnetic resonance imaging to characterise the three dimensional biomechanical properties of the human rectum during balloon distension. This approach allows for obtaining extra geometrical information on the luminal wall such as the spatial distribution of the curvatures and bends, radii of curvature, wall thickness, tension and stress [38]. Large variation of the tension and stress was observed throughout the rectal lumen wall during distension which implies strong in-homogeneity of the rectal tissue. Similar study was conducted by Kern *et al.* [35] in which substantial difference were found between cortical activity caused by various levels of rectal distension between healthy human male and female subjects.

2.3 Biological tissue testing

For physicians, hand palpation has become a time-tested diagnosis method to examine the tissue and detect pathology. Although, palpation is commonly practiced in open surgeries, in non-surgical levels, it is limited to superficial organs and pathologies, and the outcome depends on the skill and experience of the consultant [17, 44].

Beside palpation, many other medical devices and techniques have been considered to have great potentials for testing tissue mechanics, including imaging techniques: optical, mechanical and ultrasound elastography, and so on; and non-imaging techniques: laparoscopic indentation, tissue elongation and vibration. Employing an

appropriate technique to characterise soft tissue response relates directly to factors such as under what environmental condition the tissue is assessed, the tissue's fluid content, the boundary conditions, shape and the typical loading strategy [45]. In this light, a short review on some of these approaches is given next.

2.3.1 Imaging techniques

Enhancements in imaging technologies have been very desirable for medical sector in the last four decades. Elastic imaging, known as 'Elastography' is a technique to visually display the elastic properties of biological tissue in form of colour contrasted images. High contrast in the images determines a large deviation in elasticity of tissue and vice versa. Few numbers of elastography methods are rather capable of quantitatively measuring the hardness or elastic modulus of the tissue. The significant advantage of mapping elasticity is the ease of detailed observation and interpretation for the practitioner; something that is not taken into account in the normal imaging. Elastographic contrast shows promising outcomes to distinguish healthy from diseased tissues, and also benign from malignant lesions [17, 44].

Various approaches are developed to performed elastography. Figure 2-12 categorises elasticity imaging on three bases: excitation, response detection and estimation methods. The main criteria that makes each technique distinct is the method employed to detect the tissue strain response from the applied load. Divided into four modalities, the response measurement techniques are: Optical, mechanical, ultrasound and magnetic resonance elasticity imaging.

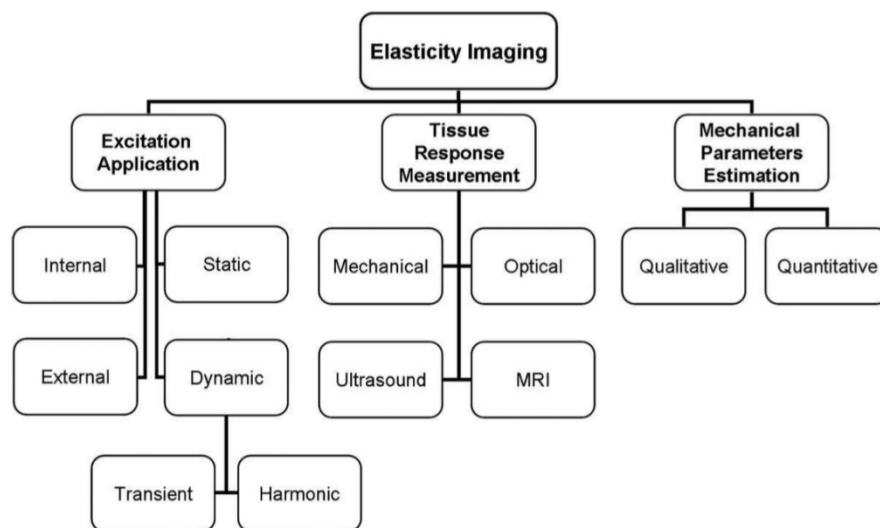


Figure 2-12: Elasticity imaging approaches [44]

2.3.1.1 Optical imaging

Optical imaging is one of the earliest techniques discovered by Gierke et al. [46] in 1952 to image the surface of tissue by stroboscopic photography using visible light. The excitation of tissue (thigh and upper arm) was carried out by a sound source or vibrating piston and mechanical wave propagation was observed to measure elastic and viscous properties of soft tissue. Advances in this technique led to the emergence of Optical Coherence Elastography (OCE), the next generation of optical imaging reported in 1998, utilising Optical Coherence Tomography (OCT) imaging technique. OCT is based on the same principle as Gierke et al. photography, except the fact that it has higher probing depth and transversal resolutions in the scattering media, in the range of 1-15 μm . To create contrasts in the images, OCE non-invasively excite the tissue using various frequency domains and extract the vibration amplitude and micro-strain excitation on the surface of the tissue [46-48].

2.3.1.2 Mechanical Imaging (MI)

This technique employs inexpensive mechanical sensors to reconstruct visual anatomy in 3D and mechanical properties of tissue. Unlike other elastography techniques, MI applies some kind of compression to the tissue and measures the stress using a sensor such as pressure, tactile or accelerometer sensors. The displacement of the device penetrating into the organ is measured by a position sensor. Sarvazyan and his group [49] are the pioneers of MI technology in the late 80s. Inherently low cost, ease-of-use, portability, and minimal required are among the advantages of MI. Figure 16, illustrates 3D MI reconstruction of a phantom which contains hard nodules. It is reported that MI has mostly been utilised for diagnosing breast and prostate cancer where palpation is accounted to be the most effective way to detect diseases [6, 49, 50].

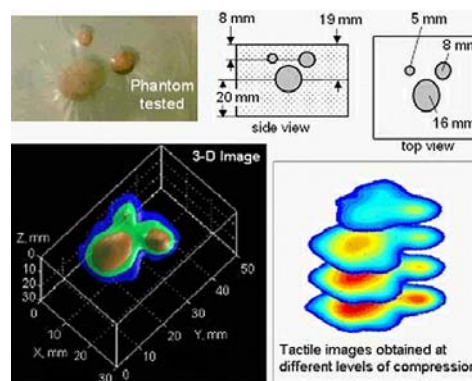


Figure 2-13: 3D MI reconstruction of a phantom which contains hard nodules [51]

2.3.1.3 Ultrasound imaging

Ultrasound imaging, similar to OCE technique, uses an external (applied vibration or pressure) or internal (nearby pulsatile organ) means to displace the organ and detect the motion utilising ultrasound. The resulting image of the elastography presents hard area as darker objects and soft area as lighter objects. The use of ultrasound to image the tissue elasticity was first investigated by Dickinson & Hill [16] in 1982. In their work, they measured the deformation of the tissue near blood vessel which was internally stimulated by cardiac impulse in order to acquire elastic parameters of tissue. They measured the amplitude and frequency of tissue motion between successive ultrasonic images (A-scanning) of the organ [16].

Fundamentally, ultrasound elastic imaging falls into three categories: compression elastography or strain imaging, transient elastography, and vibration sonoelastography. Compression elastography compares ultrasound echoes observed before and after a static compression is applied to the tissue. This technique was first performed by Ophir *et al.* [52] in 1991, who suggested the word of elastography for elastic imaging. The result of static elastography is map of strain with no quantitative elastic data [16, 44].

The second class, transient elastography, low frequency transient vibration is adopted to stimulate the tissue and the resulting movement is detected by pulse-echo ultrasound. Catheline *et al.* [53] employed this technique to extract the elasticity and viscosity parameters from the observed propagation [53].

In other hand, Vibration sonoelastography applies low frequency (>1 kHz) shear waves driven through deep tissue by an external device such as piston shaker or audio speaker. It then detects the vibration pattern using real-time ultrasound Doppler. It is observed that the pick vibration amplitude decreases where the lesion is located. Krouskop *et al.* [54], Lerner *et al.* [55] and Yamakoshi *et al.* [56] used this technique to map the tissue elastic data [16, 44, 57].

2.3.2 Non-imaging techniques

Imaging techniques seem to be the best solution to measure elastic properties of live tissue since they do not cause any trauma and complication. However, they are very costly, bulky, non-portable and cause large errors on the test results due to producing ambient noise [58]. Therefore, non-imaging techniques are developed as cheap alternatives to the imaging techniques [59].

Non-imaging techniques such as tissue indentation, elongation and vibration are employed to measure mechanical properties of soft organs. Generally speaking, these devices are usually equipped with force and displacement sensors to monitor the applied load and the tissue deformation according to the applied displacement. The testing organ can be under intact live body (in-vivo), intact dead body (in-situ) or excised from the dead body (in-vitro) conditions.

Using these approaches, assessing the intact live/dead specimen is performed either invasively or minimally invasively. Invasive measurements are the most common method in which a large incision is made on the body surface and the testing device is inserted into the body. Although this method allows for easy access to the organ, it causes significant skin damage. To minimise the possible damage, minimal invasive approaches are developed in order to allow small opening on the body.

Non-imaging methods can be divided into two groups in terms of the way they are operated; human-operated devices and machine-operated devices. Human-operated devices, as the name suggests, use the manual force of an operator to indent the tissue and the on board sensors to record displacement and force response e.g. Carter *et al.* [60], Vuskovic [61], Mazza *et al.* [62], Jia *et al.* [58], and Araghi *et al.* [63].

2.3.2.1 Indentation

To replicate palpation, indentation techniques are employed for mapping the local properties in inhomogeneous tissues [56]. As shown in Table 2-1 most studies focus on tensile and expansion properties of the large intestine and less has been focused on characterising tissues properties using indentation techniques which are typical of tissue palpation assessment and the tool-tissue interface during surgical manipulation. Indentation techniques eliminate the complications with tight tissue gripping and machining dog bone specimens which exist with tensile tests. It also allows for mapping the local properties in inhomogeneous tissues [64]. Unlike other tissue characterisation technique such as tensile tests, indentation can be performed both in-vivo and ex-vivo, for example, Carter *et al.* conducted the same indentation technique in ex-vivo pig spleen and kidney prior to in-vivo human liver [44]. Examples of several indentation devices which successfully served their purpose have been given as follows.

Carter *et al.* [60] developed the first hand-held indenter, Figure 2-14-a, to quantitatively measure mechanical property of human healthy and diseased liver, in open surgery. A load-cell capable of measuring up to 5N was connected mechanically to the indenter tip.

Since the device is hand-held, the error caused by the vibration of surgeon's hand is inevitable. To minimise the error, the displacement of the indenter tip is measured relative to the reference ring, in which is connected to the displacement transducer (Linear Variable Differential Transformer LVDT). The estimated elastic modulus of human liver was 0.27 MPa, while diseased liver has twice the stiffness value of healthy one of around 0.74 MPa, as illustrated in Figure 2-14-b [60]. However, Carter's device is not used to measure viscoelastic properties of tissue.

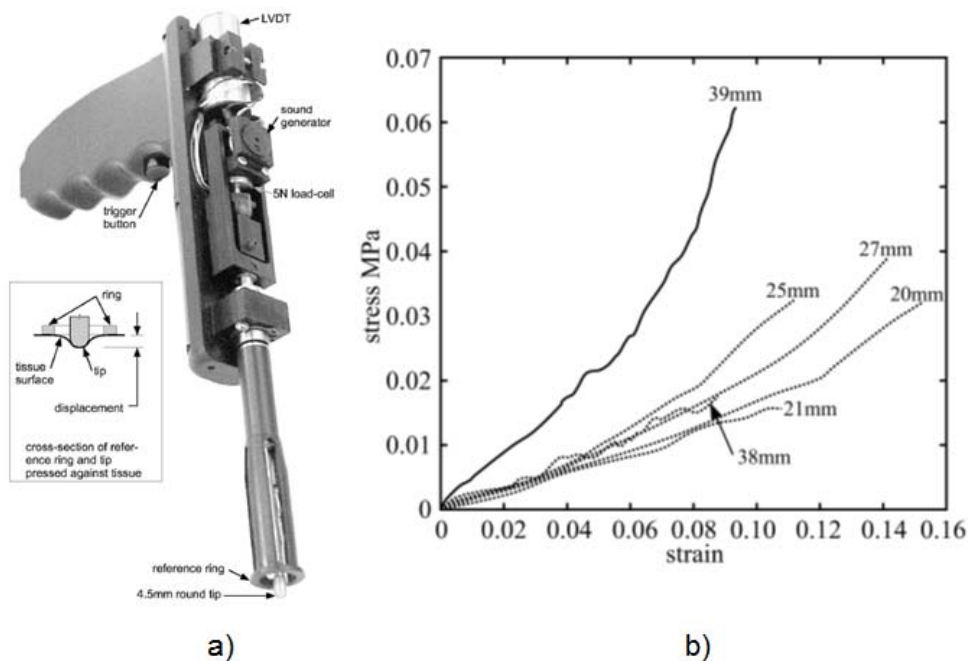


Figure 2-14: a) Hand-held compliance probe to indent tissue in-vivo, and b) Stress-strain graph of in-vivo indentation test. Broken lines show normal liver and solid line is for an obstructive liver diseased [60]

Based on a similar principle, Araghi *et al.* [63] developed a resonance based instrument to measure the stiffness, damping and effective mass of the soft tissues. He deployed a piezoelectric actuator, a more efficient way to excite the tissue. The schematic diagram of the device is illustrated in Figure 2-15.

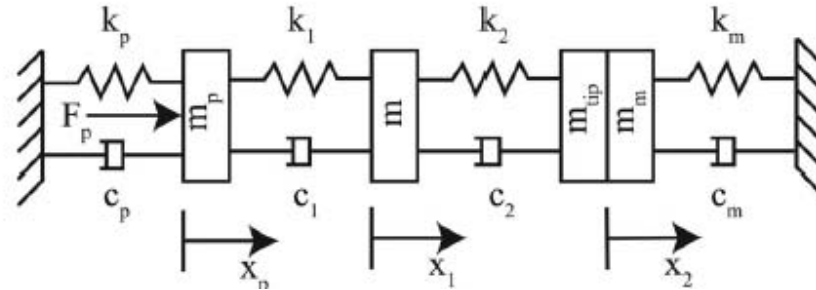


Figure 2-15: Schematic diagram of Araghi's indenter [63]

A Tissue Material Properties Sampling Tool TeMPeST 1-D, was developed by Ottensmeyer [59] to explicitly measure the response of tissue to dynamic motion for very small indentation of $\pm 500 \mu\text{m}$, applied force of $< 300 \text{ mN}$, and high frequency of $< 80 \text{ Hz}$, as shown in Figure 2-16 [59]. The device measures the dynamic applied force and tissue displacement and by extracting the amplitude and phase of the force over the displacement transfer function it analyses the elastic and viscous part of the tissue response [58]. Using this technique a series of in-vivo measurements on porcine liver were conducted and it was found that liver can be approximately counted as an elastic material with a Young's Modulus of $10\text{-}15 \text{ kPa}$ [59, 65]. A number of drawbacks to these type of devices are known to be the effect of breathing and natural respiration on the measure of force responses and the lengthy procedure as high number of data point at each frequency are required for data validation [58].

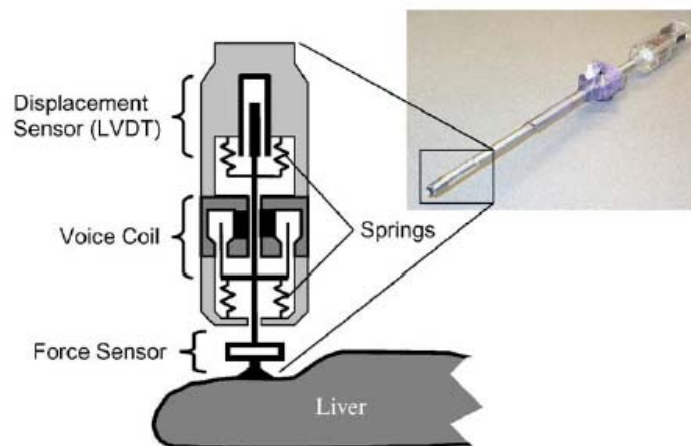


Figure 2-16: TeMPeST indenter sensor/actuator assembly

Hand-held devices are portable and easy to use; nevertheless they are subjected to some disturbances such as hand tremor and undefined boundary condition for the experiment during in-vivo measurements [61, 63]. In order to rectify these issues, the second group, machine-operated devices, are presented where a robotic device is employed to hold and control the measuring device (Rosen *et al.* [66], Miller *et al.* [67], Ottensmeyer [59], Brown and Rosen [68], Samur [69]).

Figure 2-17 depicts a robust two-linear degree of freedom robotic indenter, by Miller *et al.* [67]. The depth of the indentation was recorded by a robot which drives the indenter. The system was also equipped with a strain gauge load cell. The force-deformation curves were achieved for tissue properties analysis. Straight after the indentation experiments, the swine was sacralised and the brain was imaged using magnetic resonance imaging (MRI) in order to assess the geometry of the brain [67].

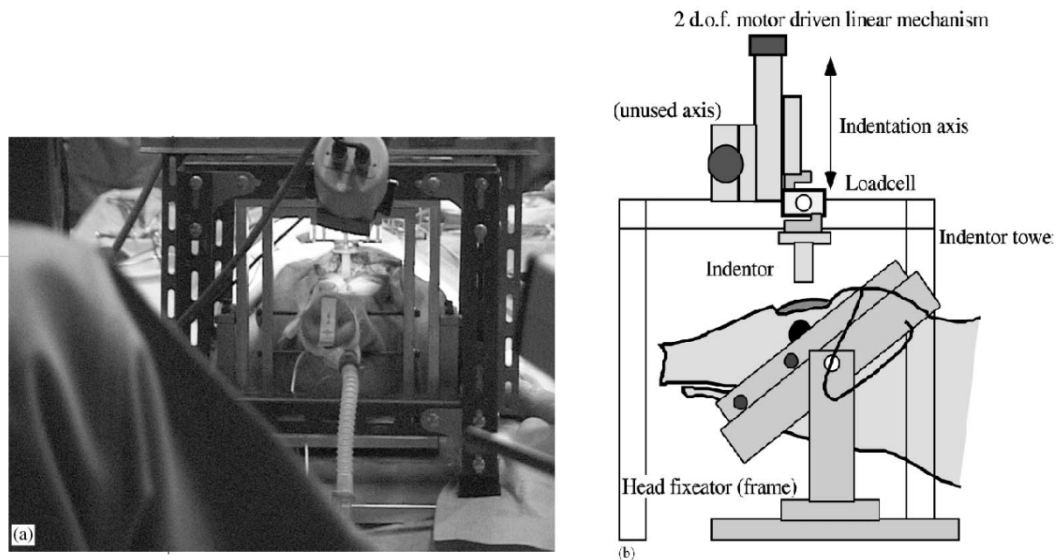


Figure 2-17: Swine brain indentation, a) in-vivo experiment configuration, and b) schematic diagram of the device [67]

Samur and his group in 2005 [69] performed in-vivo experiments on pig liver during a minimally invasive surgery. The device they introduced, as shown in Figure 2-18, included a robotic arm controlling a laparoscopic indenter with a probe size of 2mm radius. The load cell is mounted on the proximal section of the probe.

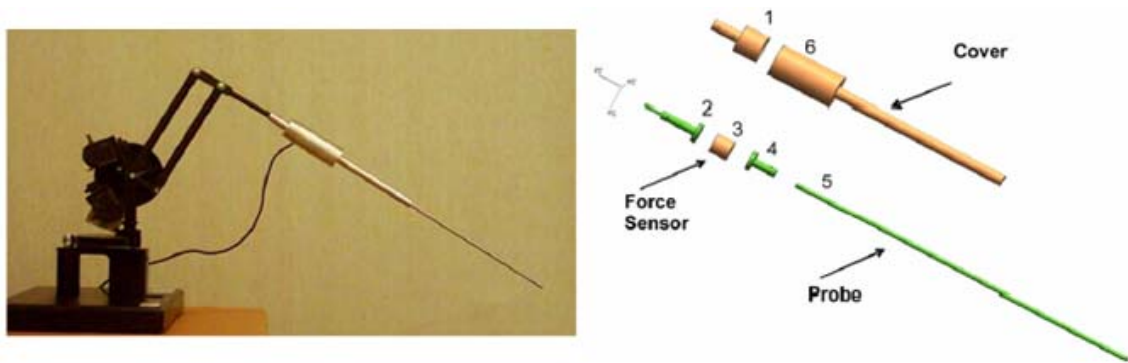


Figure 2-18: Samur et al. robotic indenter and its schematic diagram [69]

A more advanced palpation device that avoids any complications with regard to the bulky, expensive and complex structure of the existing robotic probes has recently been introduced by Scanlan *et al.* [70]. In this method which is based on dynamic compression of the tissue the complex stiffness of tissue is calculated by measuring the dynamic force-displacement relationship. As shown in Figure 2-19-a, the device is mounted on the index finger and comprises of a piezoelectric pressure sensor, a strain gauge as a displacement sensor, and a pneumatic actuator for dynamic expansion/contraction motions of the probe head. The results are in form of stiffness maps, Figure 2-19-b, produced from the amplitude/phase of the pressure and strain signals. The ex-vivo examination of the prostate using this device demonstrates a good correlation between the actual location of the tumour and the perceived stiffness points on the stiffness map. When compared with the traditional digital rectal examination technique, the dynamic stiffness measurement was found not only as a good indicator of tissue stiffness but more accurate technique in defining the shape and size of tumours [70].

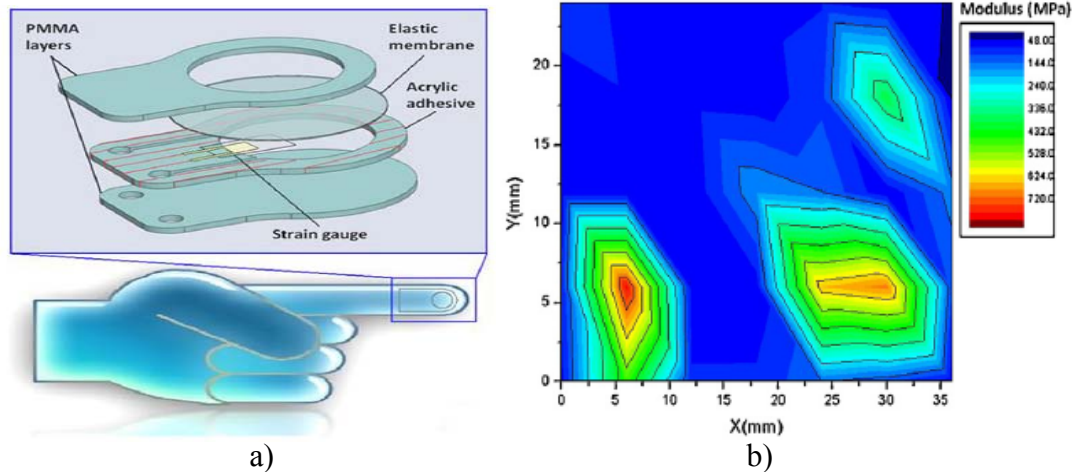


Figure 2-19: a) A finger mounted device suitable for the in-vivo assessment of prostate tissue properties, & b) An example of stiffness map obtained from the dynamic compression of ex-vivo prostate tissue containing tumour [70]

2.3.2.2 Tensile extension

Most studies reported in Table 2-1 employ tensile technique for tissue characterisation. The distinctive feature of the tensile examinations compared to all the other mechanical characterisation technique is the possibility of measuring the true Young's Modulus/elastic modulus. Young's Modulus can only be calculated from the linear-region of a stress versus strain curve just before the plastic region as shown in Figure 2-1. Ultimate tensile strength is also another useful mechanical properties measure which defines the maximum stress that a material can withstand before rupture.

There has been a limited amount of research into the tensile properties of large intestine [6, 11-13], where reports of varying mechanical and viscoelastic properties of large intestine in different fibre orientations have only been reported by Yamada [14] and Egorov *et al.* [6]. Both attempts are limited in finding the multi-axial tensile strength and tissue modulus quantification whilst no investigation on the viscoelastic response of the large intestine was undertaken.

Testing tensile properties of various biological tissues is commonly studied in samples aligned with the fibre direction. Although this is justified for isotropic tissues, other soft biological tissue which are largely known to be anisotropic show differences in the mechanical and viscoelastic properties dependent on the orientation of the loading direction. For example, the linear modulus of human collateral ligament and sheep tendon was found one to two orders of magnitude greater in the longitudinal direction than in transversal fibre direction [71, 72]. Lee and Boughner [73] also observed significantly higher tissue modulus and ultimate tensile strength for dog pericardium cut

in vertical over horizontal alignments. Moreover, their data indicated that the stress relaxation and creep responses are independent of the fibre orientation. The variation in the multi-layer structure (haustra and tenia layers) and multi-axial properties of the large intestine were investigated by Egorove *et al.*[6]. The results of the tensile tests showed approximately 30% greater ultimate tensile strength in the axial compare with the transversal specimens in both tenia and haustra layers. However, the location where the specimens were taken from was not stated.

In terms of the testing equipment, the typical example of a commercialised tensile machine is Instron tensile testers (Instron Corp., MA, USA), which can handle variety of specimen geometries [22, 74, 75]. The typical strain-rate for tensile testing protocols was suggested to be 10 mm/min (or 1.6 mm/s) however, depending on the test requirements there are a variety of strain-rates as low as 0.08 mm/s recorded in various studies. The same is applied to the maximum strain and stress threshold values.

2.3.2.3 Vibration

This method has been used by a number of groups [76-82], there is a slight variation in their approach but here the fundamental principle is described. This method is based on measuring the mechanical contact interaction between a resonant system and a material of interest as the most fundamental feature of any physical system [83]. The interaction is formed by a resonant system containing tactile transducers/sensors and works based on the principle of change in the transducer resonance frequency with the applied pressure [83]. The characteristics of the resonant system vary with the temperature, body surface, the transducer weight and base area. Measuring the contact resonance provides information on the characteristics of the contact compliance (i.e. softness or hardness). The contact compliance depends on the elastic modulus and the area of real contact [81]. In this method, an external resonance oscillation is induced to a body, and the resonance frequency and impedance magnitude of the system before and after the contact is monitored [76]. The tissue-resonator contact is commonly in the form of small deformations and forces. The shift of frequency and impedance due to the pressure change is calculated as:

$$\Delta f = f \text{ (loaded resonance frequency)} - f_0 \text{ (unloaded resonance frequency)}$$

$$\Delta z = z \text{ (loaded impedance at resonance frequency)} - z_0 \text{ (unloaded impedance at resonance frequency)}$$

The objects with different stiffness values can be distinguished by analysing the Δf and Δz at the resonant (the lowest peak of the impedance in the frequency response graph) or anti-resonant frequencies (the highest peak of the impedance in the frequency response graph). An example of frequency shift as a function of stiffness is given in Figure 2-20 [80]. In this figure as the stiffness of the object increases ($k_{t1}=5.0\times 10^9$ (Ns/m) and $k_{t2}=1.1\times 10^{10}$ (Ns/m)) the peak value at the resonance and anti-resonance frequency increases where both resonance and anti-resonance change an equal amount [80]. It is stated that the shift of frequency in a piezoelectric transducer depends on the mass loading effect and elastic properties of the samples whilst the Δz corresponds to the density and acoustic velocity or in other terms the damping properties of the samples [79, 80].

This technique has already been used in medicine for applications such as breast cancer stiffness and follow-up therapy evaluations [84], measuring stiffness of liver tissue to evaluate the stage of chronic liver diseases and function [85], and tactile sensing for detecting tissue properties in real-time [76-82]. The disadvantages of this technique are the common high natural frequency range selected to run the actuators which are not relevant to surgical applications and the fact that these devices can only measure the elastic properties of the tissue [58].

Previously, tactile transducers/sensors were typically used to measure the applied pressure or force to a body employing strain gauges, conductive elastomers and piezoelectric polymer films [86]. However, nowadays they are deployed for more complex tasks such as detection of hardness and/or softness of an object over a predetermined sensing area. For such applications, the transducers are commonly made of piezoelectric ceramic material lead zirconate titanate [84]. The excitation frequencies for these transducers are ranged in the lower end of ultrasound spectrum. This technique has been reported to be a very safe and reliable method for medical applications which allows for in-vivo non-invasive examinations of soft tissue [84, 85].

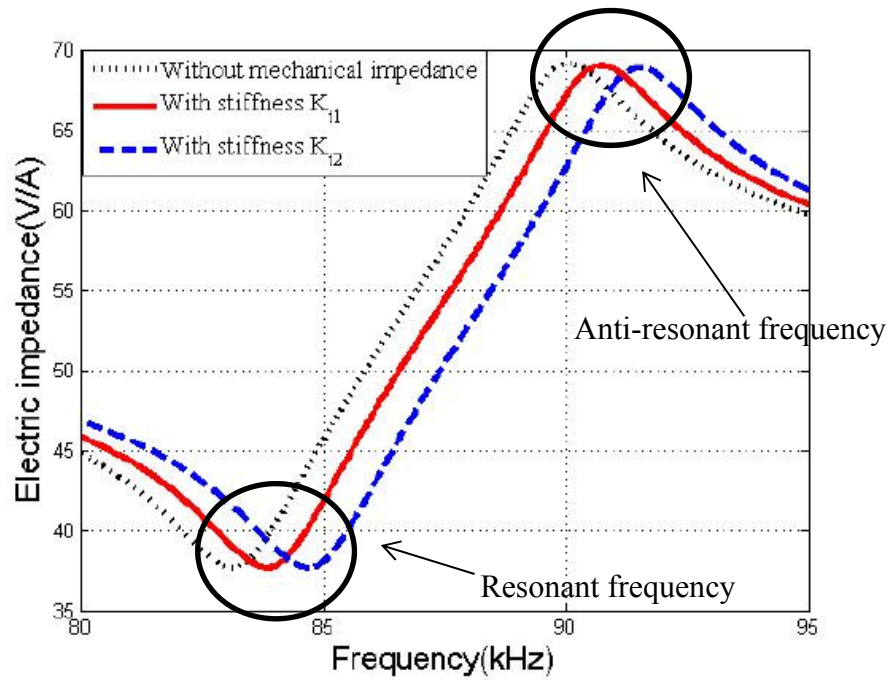


Figure 2-20: Concept diagram explains the frequency response of electrical impedance as a function of stiffness change. Here $k_{t1}=5.0 \times 10^9$ (Ns/m) and $k_{t1}=1.1 \times 10^{10}$ (Ns/m) [80]

An example of an acoustic impedance probe is shown in Figure 2-21. Using haptic technology, Murayama *et al.* [84] designed a compact palpation probe to check for lumps/hardness of breast cancer. One of the main impressive features of the device is the 64-element tactile sensor array which examines an area of 45 x 45 mm of breast tissue within 0.45 s. Attached to the end of each tactile sensor element in Figure 2-21-a, a spring is deployed to control the contact pressure. The spring stiffness is specified so to allow for an optimised detection sensitivity. The sensors utilise a driving PZT to vibrate the system at its own resonance frequency. The resonance frequency shifts are detected by the pickup PZT which triggers the amplifier to vibrate the piezoelectric transducer at the new frequency. Knowing the Young's Modulus of the object, a relationship between the frequency shift and stiffness is calculated [84].

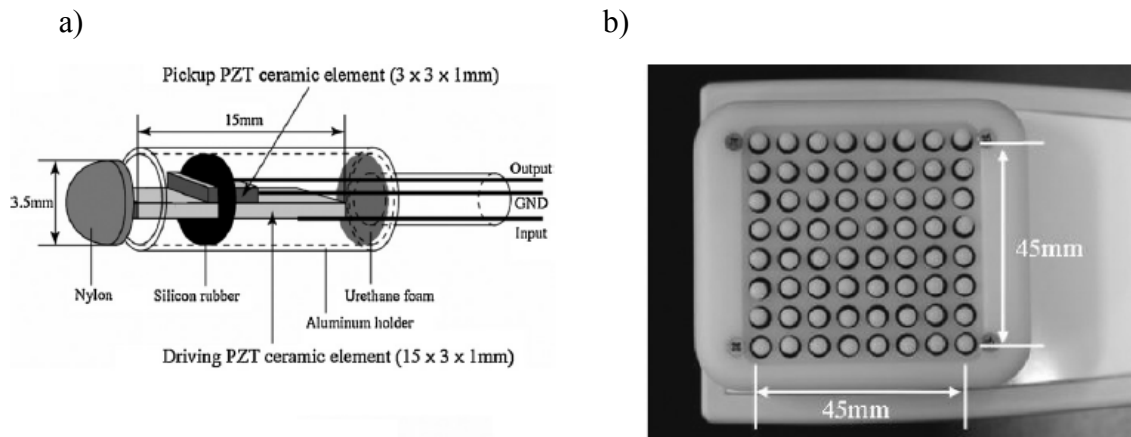


Figure 2-21: illustration of a) a tactile sensor element consists of a driving and pick up PZT ceramic elements and b) 64-element tactile sensor probe [84]

The other important feature of acoustic impedance technique is the design of the resonance circuit and data acquisition system. A schematic diagram of a typical resonance circuit is shown in Figure 2-22 [76]. The resonance circuit supports the resonance of the driving PZT through a feedback loop containing filters, an amplifier and a phase shift. The circuit generates periodic sine waves for the driving PZT and detects the new signal from the sensor. For continuous resonance, the detected signal is filtered to only extract the resonance frequency component and then amplified to boost the power of the signal. Since amplification distorts the signal phase, a phase shift circuit is also deployed to induce the resonance of the detected signal at the same phase as the generating signal [76].

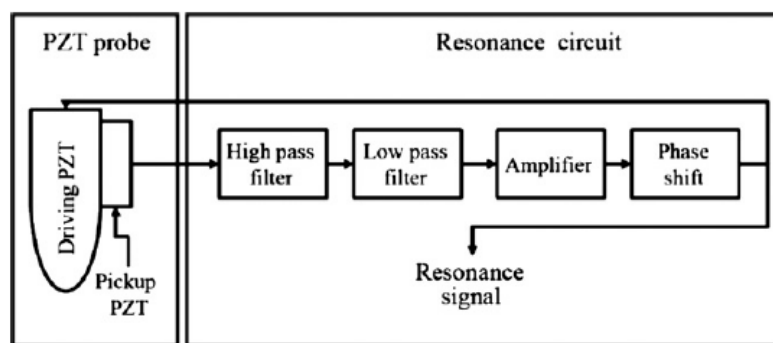
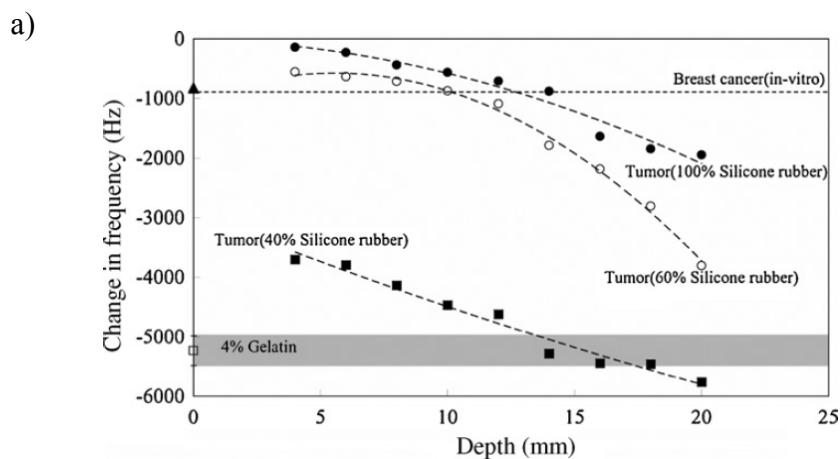


Figure 2-22: Schematic diagram of a resonance circuit linked to a PZT probe [76]

A resonance sensor system, Venustron (Axiom Co., Ltd, Koriyama Fukushima, Japan) is one of the only commercialised acoustic impedance measuring devices which has been applied for medical use. The stiffness of an object is detected based on the response of pressure force, depression and frequency of the system. This device was employed to

relate the frequency shift and measured force to the material properties, density and elasticity [78]. The simulation result showed that the Δf is dependent upon density (ρ) and contact area (S) as $\Delta f \propto \rho S^{3/2}$. The contact force was modelled as $F \propto E S^{3/2}$ where E is the elastic modulus. Finally, the force and frequency shift are related through contact area and the following model was found: $\Delta f \propto \rho E^{-1} F$ [78].

Figure 2-23-a shows the results of palpation examination on phantom breast cancer models using the proposed tactile sensor probe in Figure 2-21 by Murayama *et al.* [84]. The grey zone represents a gelatin sample with no tumour nodes. The results indicate high sensitivity of the frequency shift to contact pressure and stiffness of the objects. It can be seen from the figure that as the object stiffness increases lower negative shift in frequency is observed. In similar studies [82, 86], shown in Figure 2-23-b, this shift becomes positive with further increase in the hardness of the material. It was suggested that for soft objects the negative Δf tend to increase with reduction of stiffness due to the larger contact area between the transducer and the object. Regarding the trend in impedance magnitude shift, studies [76, 79] have reported an increase of positive Δz as a function of object stiffness. Figure 2-24, demonstrates an increase of Δf and impedance magnitude Δz as a function of Young's Modulus for a series of silicon rubbers with different degrees of density [76]. The trend of impedance shift was observed differently in a study on optimizing the quantity of crystal of polyester resin where the impedance magnitude decreases with an increase of resin percentage of hardener [87]. Additionally, an increase in contact pressure results in an increase of negative frequency shift [78, 82, 84]. All the above trends are in accordance with the actual tactile sensor function of the human finger [82, 86].



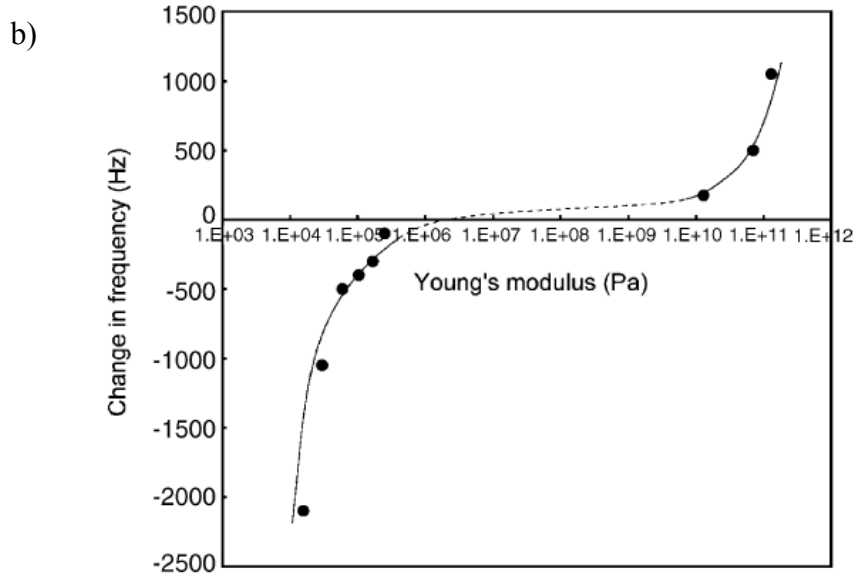


Figure 2-23: The PZT transducer detection of frequency shift against a) depth for various tumour nodes implanted in a Gelatin sheet [84] and b) Young's Modulus for various materials of different hardness levels [86]

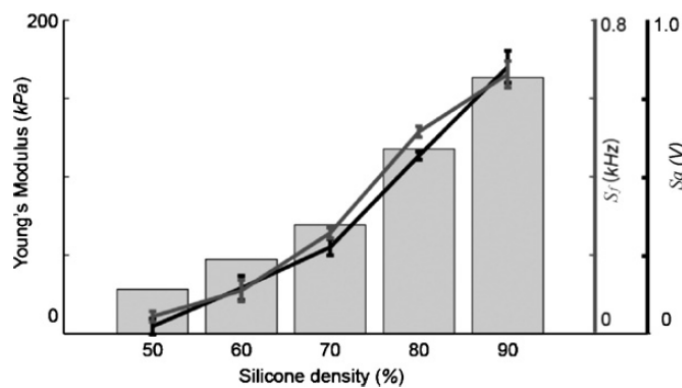


Figure 2-24: Frequency shift and amplitude change versus Young's Modulus of silicon rubber at different density levels [76]

2.4 Biological tissue modelling

Modelling behaviour of tissue in forms of mathematical expressions for predicting elastic and viscoelastic properties is essential and complementary to experimental data obtained from soft tissues. Fundamentally, there are two approaches for determining the functional nature of the constitutive equations: Physics-based and phenomenological approaches. Physics based models use physical laws to drive strain energy function whereas phenomenological models have very little significance to the physical laws but they are better fit with the experimental data. In physics-based approaches the influence of various factors on the mechanical behaviour of the tissue, such as viscosity and elasticity, is observed, so to extract the more meaningful parameters. [27, 65, 88]

However, phenomenological models are much better in terms of simplicity. They rather identify the physical features of data in one specific experiment, sufficient enough to describe the response of the tissue, ignoring the actual properties of the tissue. These physical features could be the non-linear response of force-displacement, the initial slope of the curve, amount of hysteresis and rate of stress relaxation. These equations are in forms of polynomials or exponentials [27, 65, 88].

The main phenomenological models used to quantify viscoelastic behaviour of tissue include linear, quasi-linear and non-linear [23, 89, 90]. The **linear viscoelastic model** depends on the time t and the unit step relaxation function $E(t)$ which is explained as the stress obtained from a unit step elongation of the tissue. The model follows linear convolution/Boltzmann integral:

$$\sigma(t) = \int_0^t E(t - \tau) \frac{d\varepsilon(\tau)}{d\tau} d\tau \quad 2.8$$

$\sigma(t)$ is stress, $\varepsilon(t)$ is strain and τ is a time variable of integration. In principle, $E(t - \tau)$ represents the decaying effect of strain at a time τ before the current time t on the current stress $\sigma(t)$.

Linear viscoelastic properties of soft tissue are explained by combination of a spring and dashpot in physics-based models, where springs represent the elastic solid-like and dashpots exhibit viscous fluid behaviour cause by fluid movement within the tissue, as shown in Figure 2-25. The advantage of using this model as oppose to Fung's model lies on the simplicity of solving the convolutional integral for the stress response to a stretch input [23].

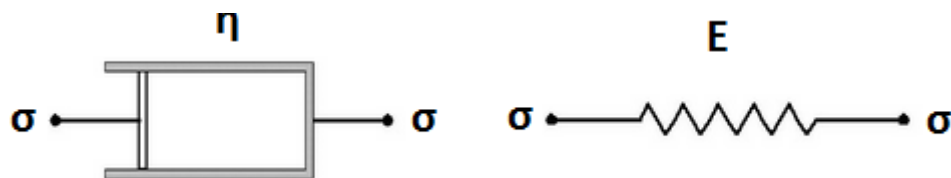


Figure 2-25: Fundamental viscoelastic elements – from left to right: damper (Newton element) and spring (Hooke element) [18]

As was mentioned previously, the behaviour of soft tissues is strain and strain-rate dependant. The concept of springs and dampers are explained by these dependencies. In the elastic element, strain (or deformation) is solely dependent on the stress (or applied

load). In Newton's model of the hydraulic piston (dashpot), the viscous stress depends on the rate of strain. The following equations are designed to explain these concepts [91]:

$$\text{Spring : } \sigma_E = E \cdot \varepsilon \quad 2.9$$

$$\text{Damper : } \sigma_\eta = \eta \cdot \dot{\varepsilon} \quad 2.10$$

where σ_E and σ_η are the stress of spring and damper, and E and η are the elasticity (N/m^2) and viscosity ($\text{N}^{\cdot}\text{s}/\text{m}^2$) constants, respectively. ε is the strain of spring and $\dot{\varepsilon}$ or $\frac{d\varepsilon}{dt}$ represents strain-rate of damper. Equation 1 for spring is known as Hooke's element and represents pure elastic. The damper expression, Equation 2, is a Newton element and characterises pure viscous.

The biomechanical models are represented as various combinations of spring and dashpot. The three commonly used linear viscoelastic models are Maxwell body, Figure 2-26-a, Voigt body, Figure 2-26-b, and Kelvin body (standard linear solid), Figure 2-26-c.

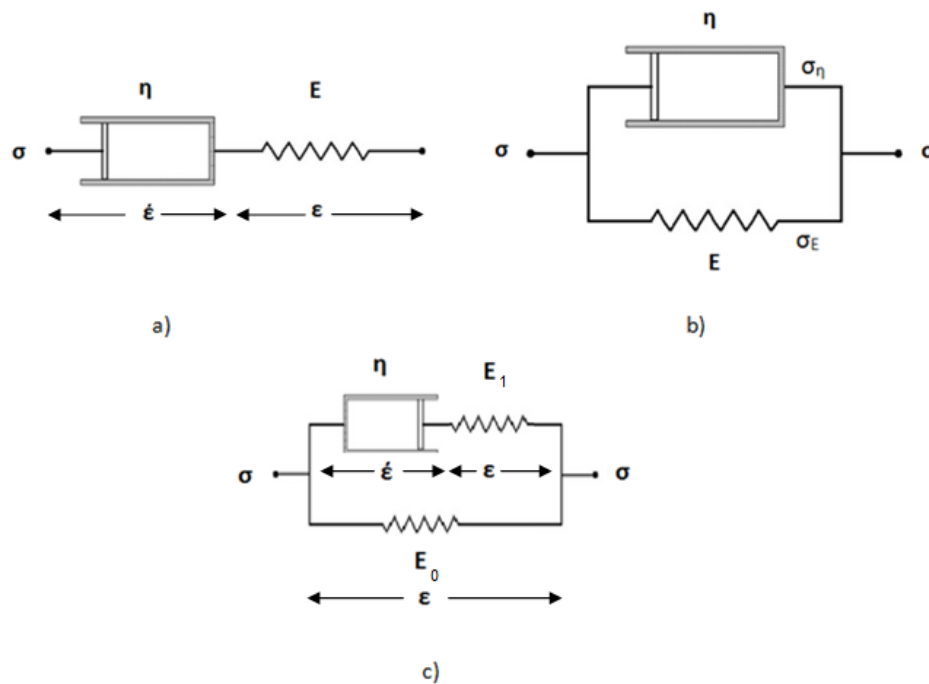


Figure 2-26: Linear Viscoelastic models a) Maxwell body, b) Voigt body and c) Kelvin body [18]

Maxwell model allows for an instantaneous deformation, where both spring and dashpot are subjected to the same stress. As shown in Figure 2-27, at $t=+0$ the spring is strained

to ϵ and dashpot stays unmoved, so the stress respond is $\sigma_0 = E \cdot \epsilon$. Keeping the strain constant, at $t=t$ the dashpot starts flowing, causing the strain and stress of the spring to gradually fall. The time it takes to reduce the stress to $1/e$ times its original value (about 37%) is called relaxation time [92].

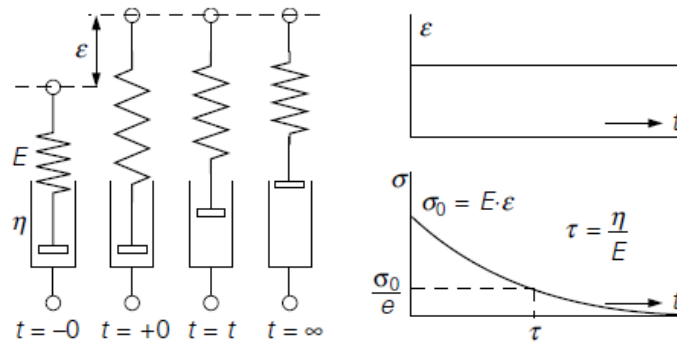


Figure 2-27: Stress relaxation of a Maxwell model [92]

In contrast, Voigt model can't allow for instantaneous deformation, since the dashpot is in parallel with the spring and the strain responses should be equal. Therefore Voigt model does not exhibit stress relaxation. However, the model shows creep. As in Figure 2-28, the stress is kept constant after a sudden applied stress. At time t , the total stress is the summation of the stress of both elements: spring $\sigma = E \cdot \epsilon(t)$ plus dashpot $\sigma = \eta \dot{\epsilon}$.

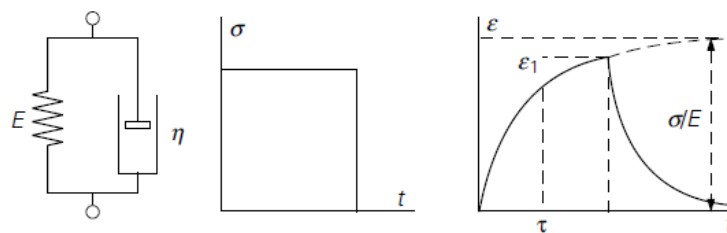


Figure 2-28: Creep of Voigt model [92]

As explained earlier, Maxwell and Voigt have limitations in explaining the behaviour of a real viscoelastic model. As $t \rightarrow \infty$, the Maxwell model behaves fully viscous while Voigt fully elastic. Maxwell can't exhibit the time-dependent feature of creep and Voigt can't describe stress relaxation. Also these two elements models, Maxwell and Voigt, represent materials in which their stress decays to zero. Kelvin model with an extra spring can solve this limitation. This three-element model can explain both creep and

stress relaxation. It also can represent the materials with which the stress does not decay to zero in their stress relaxation curve [93].

The governing equations of these three models are given as follows:

$$\text{Maxwell body: } \dot{\varepsilon} = \frac{\dot{\sigma}}{E} + \frac{\sigma}{\eta} \quad 2.11$$

$$\text{Voigt body: } \sigma = E \cdot \varepsilon + \eta \cdot \dot{\varepsilon} \quad 2.12$$

$$\text{Kelvin body: } \sigma + \frac{\eta_1}{E_1} \dot{\sigma} = E_0 \varepsilon + \eta_1 \left(1 + \frac{E_0}{E_1}\right) \dot{\varepsilon} \quad 2.13$$

where subscript '0' is the element of spring and '1' is the element of Maxwell model. These equations can be used when $\sigma(t)$ is a unit-step function $\mathbf{1}(t)$, in which case the results are called creep functions $c(t)$ (Figure 2-29). This happens when a constant force of magnitude 1 is applied to the tissue and produce deformation at $t = 0$. So the equations turn to the followings [18, 94]:

$$\text{Maxwell body: } \left(\frac{1}{E} + \frac{1}{\eta} t\right) \mathbf{1}(t) \quad 2.14$$

$$\text{Voigt body: } c(t) = \frac{1}{E} \left(1 - e^{-\left(\frac{E}{\eta}\right) t}\right) \mathbf{1}(t) \quad 2.15$$

$$\text{Kelvin body: } c(t) = \frac{1}{E} \left[1 - \left(1 - \frac{\tau_\varepsilon}{\tau_\sigma}\right) e^{-t/\tau}\right] \mathbf{1}(t) \quad 2.16$$

where $\tau_\varepsilon = \frac{\eta_1}{E_1}$ and $\tau_\sigma = \frac{\eta_1}{E_0} \left(1 + \frac{E_0}{E_1}\right)$

$$\text{Unit - step function is defined as: } \begin{cases} 1 & \text{when } t > 0 \\ \mathbf{1}(t) = 0.5 & \text{when } t = 0 \\ 0 & \text{when } t < 0 \end{cases} \quad 2.17$$

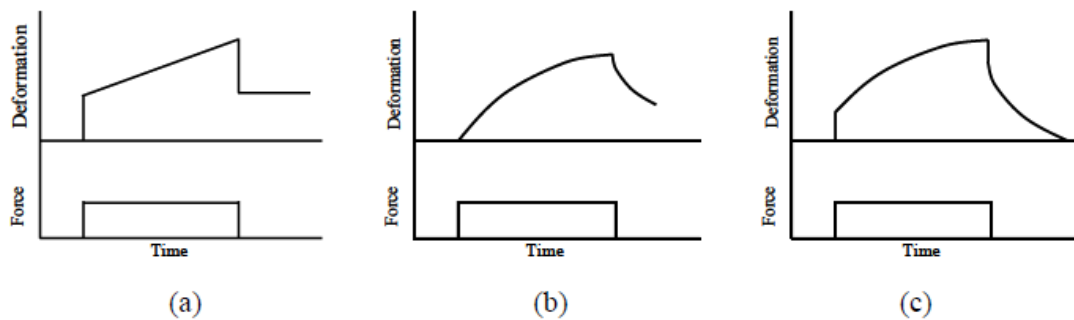


Figure 2-29: Creep functions of a) Maxwell, b) Voigt and c) Kelvin [18]

Interchanging the function of σ and ϵ , the relaxation function is obtained as a response $\sigma(t) = K(t)$ when elongation goes to unity $\epsilon(t) = \mathbf{1}(t)$ (Figure 2-30). Relaxation function $K(t)$ implies to the amount of force has to be applied to the tissue so then the elongation changes at $t=0$ to unity and remains constant. This will form the viscoelastic equations as [18, 94]:

$$\text{Maxwell body: } K(t) = E e^{-(E/\eta)t} \mathbf{1}(t) \quad 2.18$$

$$\text{Voigt body: } K(t) = \eta \delta(t) + E \mathbf{1}(t) \quad 2.19$$

$$\text{Kelvin body: } K(t) = (E_0 + E_1 e^{-t/\tau}) \mathbf{1}(t) \quad 2.20$$

where $\tau = \frac{\eta}{E_1}$ is the relaxation time.

Unit impulse function $\delta(t)$ is expressed as:

$$\delta(t) = 0 \quad (\text{for } t < 0 \text{ and } t > 1) \quad 2.21$$

$$\int_{-\epsilon}^{\epsilon} f(t) \delta(t) dt = f(0) \quad (\epsilon > 1) \quad 2.22$$

Where $f(t)$ is an arbitrary function, continuous at $t=0$.

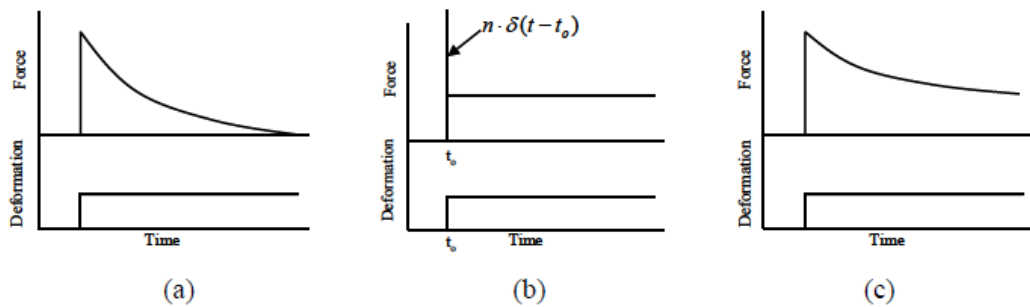


Figure 2-30: Relaxation functions of a) Maxwell, b) Voigt and c) Kelvin [18]

Wiechert 5-element model: The Wiechert 5-element model has been employed to model tissue response by many studies [22, 95, 96] as it results in a good representation of soft tissue behaviour in a simple form. The model includes two relaxation processes, as defined in the relaxation modulus formula:

$$E(t) = E_1 e^{-t/\tau_1} + E_2 e^{-t/\tau_2} + E_3 \quad 2.23$$

where E_1 and E_2 are elastic moduli (or elastic coefficients) of relaxation processes 1 and 2, E_3 is time-independent elastic modulus (or equilibrium modulus), and τ_1 and τ_2 are the corresponding relaxation durations for each relaxation process. Viscous coefficients η_1 and η_2 are calculated as $\tau = \eta_i/E_i$ where 'i' is the number of parallel Maxwell bodies.

The sum of the three moduli is the instantaneous modulus E_0 which essentially represents the stress value at the beginning of the stress relaxation process and where the peak stress is attained [22].

Initial values were estimated for the model coefficients by using the 3-element Kelvin model. The Kelvin model is expressed as:

$$N = N_0 \exp^{-\lambda t} + N_1 \quad 2.24$$

Where $N(t)$ is the decaying substance value, N_1 is the final value of decay substance, N_0 the initial decaying substance value minus N_1 , and λ is the rate of decay which is defined as $\lambda = 1/\tau$. N_1 is obtained from the last value of stress relaxation. For the remaining parameters a method is employed where the value of τ and N_0 are found by evaluating the stress at half its peak. Assuming $N(t_{1/2}) = \frac{1}{2}N_0$, τ is calculated as:

$$N(t_{1/2}) = N_0 \exp^{-\lambda t_{1/2}} \quad 2.25$$

Thus:

$$t_{1/2} = \frac{-\ln(2)}{\lambda} \quad 2.26$$

And N_0 is obtained by rearranging:

$$N(t_{1/2}) = N_1 + N_0 \exp^{-\lambda t_{1/2}} \quad 2.27$$

Using this method the components of the Kelvin model are obtained. These values are subsequently fed into the 5-element model as $N_1 = E_3$, $\frac{1}{2}N_0 = E_1 = E_2$ and $\frac{1}{2}\tau = \tau_1 = \tau_2$.

The elements of Wiechert model can physically represent various layers of the colonic tissue as shown in Figure 2-31. The two parallel Maxwell models represents the thick, muscular serosa (1 and 2) corresponding to longitudinal and circular muscle. Additionally, the submucosa (3), muscularis (4) and mucosal layers (5) are characterised by the single parallel spring [97].

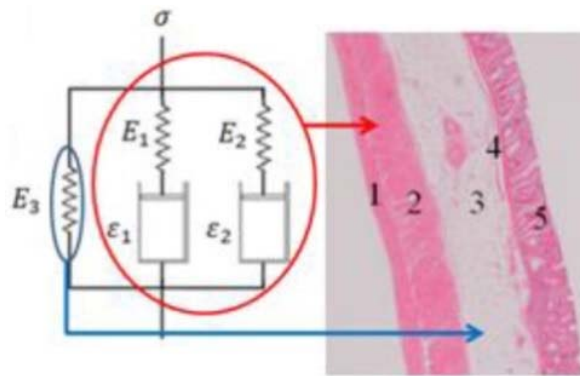


Figure 2-31: Wiechert model showing physical representation of colonic tissue [97].

These linear models have been used widely to represent the viscoelastic behaviour of various tissues as they are didactically useful for comparisons across various datasets. However, these types of representations have no predictive value as they are unable to simulate the non-linear tissues response to generic elongation [98, 99].

In general in viscoelastic models all the E_i and τ_i are independent of the strain, whilst the Fung models have all the τ_i constant and all the E_i proportional to the same function of the strain $\frac{d\sigma^{(e)}(\epsilon)}{d\epsilon}$ [100].

The Quasi-Linear Viscoelastic (QLV) model proposed by Fung [18], incorporates a non-linear function of strain into Eq. (1) and results in the following integral [23, 89, 90]:

$$\sigma(\epsilon, t) = \int_0^t E(t - \tau) \frac{d\sigma^{(e)}(\epsilon(\tau))}{d\tau} d\tau = \int_0^t E(t - \tau) \frac{d\sigma^{(e)}(\epsilon)}{d\epsilon} \frac{d\epsilon(\tau)}{d\tau} d\tau \quad 2.28$$

Here non-linearity is included within the elastic tangent stiffness $d\sigma^{(e)}(\varepsilon)/d\varepsilon$. The instantaneous elastic stress function σ^e explains the non-linear stress-strain response of soft tissue and is given by:

$$\sigma^e = A(e^{B\varepsilon} - 1) \tag{2.29}$$

where A and B are the elastic stress (N/m²) and elastic power (unitless) constants. As explained before, the relaxation modulus is the diminishing stress following an instantaneous strain. It depends on the strain history and is separable into the production of a function of time and a function of strain [23, 89, 90]:

$$E(t, \varepsilon) = E(t)g(\varepsilon) \tag{2.30}$$

This assumes that the non-linear behaviour is imposed by the elastic response $g(\varepsilon)$ and a linear viscoelastic process generates the reduce relaxation function $E(t)$ [99]. The reduced relaxation function explains a time course of force generated by an instantaneous step in the elastic response. A schematic block diagram of this model is presented in Figure 2-32. The red box stands for the non-linear process $E(t)$ converts the elongation into the force followed by a step response $g(\varepsilon)$ (blue box) induced by a linear process [99].

In this diagram, there is a non-linear relationship $E(L)$ between the peak force and the step size where Fung posited that the stress is dependent on the strain level whilst its time dependent portion is independent of the strain level [99].

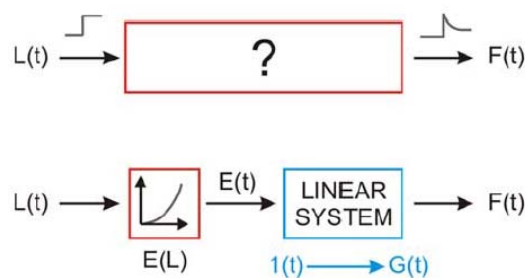


Figure 2-32: Schematic block diagram of Fung's QLV model [99]

According to this assumption the time dependent relaxation response must be the same for any levels of strain ε . However, this assumption has come under scrutiny by several studies as the shape of the relaxation curve for many biological tissues found to be different at various levels of strain [23, 90, 101]. To lift this limitation the **Generalised**

Fung QLV also known as the **non-linear model** has been proposed in which the relaxation response is altered so it can be a function of the strain history.

$$\sigma(t) = \int_0^t E(t - \tau, \varepsilon(\tau)) \frac{d\varepsilon(\tau)}{d\tau} d\tau \quad 2.31$$

The common forms of the reduced relaxation function has been defined by Fung [18] and spring and damper theory. The reduced relaxation function yields:

$$E(t) = \frac{1 + C[E_1\left(\frac{t}{\tau_2}\right) - E_1\left(\frac{t}{\tau_1}\right)]}{1 + C \ln\left(\frac{\tau_2}{\tau_1}\right)} \quad 2.32$$

where E_1 is the exponential integral function and expressed as:

$$E_1 = \int_{y=x}^{\infty} \left(\frac{\exp(-y)}{y} \right) dy \quad 2.33$$

The constant C defines the degree of viscous effect and the τ_1 and τ_2 are the fast and slow time constants.

The limitation of General Fung QLV model is that since the model assumes an instantaneous step in the strain the numerical calculation of the stretch input using a convolution integral is very complex. Also the reduced relaxation model function is designed to be fixed over small stretches [99]. A simpler model inspired by the generalised QLV model is proposed by Nekouzadeh *et al.* [23] which is based on a different principle to the QLV model. In the Fung QLV model the stress at any instant of time is influenced by the previous strain and the non-linear function. In the Nekouzadeh's model called Adaptive QLV (AQLV), only the history of strain is required [23]. The model essentially embeds the non-linearity in the linear elastic response. A more detailed description of this model is given in [23]. In this model the stress-strain relationship is expressed through a 'viscoelastic strain $V^{(\varepsilon)}(t)$ using a linear convolution integral:

$$\sigma(t) = k(\varepsilon(t)) V^{(\varepsilon)}(t) \quad 2.34$$

$$V^{(\varepsilon)}(t) = \int_{-\infty}^t g(t - \tau) \frac{d\varepsilon(\tau)}{d\tau} d\tau \quad 2.35$$

where $k(\varepsilon)$ is a pure non-linear function of strain, and $g(t)$ is a reduced relaxation function. $V^{(\varepsilon)}(t)$ represents the stress that is dependent on the history of strain. Here $k(\varepsilon)$ represents the non-linearity of the model through converting the strain history to stress by a simple multiplication. The generalised form which allows for different non-linear behaviour for different shape function is given as:

$$\sigma(t) = \sigma_0(\varepsilon(t)) + \sum_i k(\varepsilon(t)) V_i^{(\varepsilon)}(t), \quad i = 1, 2, \dots \quad 2.36$$

$$V_i^{(\varepsilon)}(t) = \int_{-\infty}^t g(t - \tau) \frac{d\varepsilon(\tau)}{d\tau} d\tau, \quad i = 1, 2, \dots \quad 2.37$$

here $\sigma_0(\varepsilon)$ is a pure function of strain indicating the long-term elastic part of the response which is equivalent to the equilibrium modulus E_3 in Wiechert model. Each $g(t)$ could be any relaxation function (exponentials with different time constant) such that $g(0) = 1$ and $g(\infty) = 0$. Wiechert model has been selected to describe the shape function by exponential terms as:

$$g_i(t) = e^{-t/\tau_i} \quad 2.38$$

where $\tau_i(\varepsilon) = \frac{\mu_i(\varepsilon)}{k_i(\varepsilon)}$. This way the model can be interpreted physically through different Maxwell elements with different relaxation time scales as:

$$\dot{V}^{(\varepsilon)}_i + \frac{V_i}{\tau_i(\varepsilon)} = \dot{\varepsilon}, \quad i = 1, 2, \dots \quad 2.39$$

$$\sigma_i = k_i(\varepsilon(t)) V_i^{(\varepsilon)}(t), \quad i = 1, 2, \dots \quad 2.40$$

The block diagram of this model is presented in Figure 2-33.

Finally, as explained in [23], the stress at any instant of time can be written:

$$\sigma(t) = \begin{cases} \sigma_0 \left((n-1)\Delta\varepsilon + \frac{\Delta\varepsilon}{T} t \right) + \frac{\Delta\varepsilon}{T} \sum_i k_i \left((n-1)\Delta\varepsilon + \frac{\Delta\varepsilon}{T} t \right) e^{-t/\tau_i}, & 0 < t < T \\ \sigma_0(n\Delta\varepsilon) + \frac{\Delta\varepsilon}{T} \sum_i k_i(n\Delta\varepsilon) \tau_i \left(e^{-\frac{T}{\tau_i}} - 1 \right) e^{-t/\tau_i} & t > T \end{cases} \quad 2.1$$

where n is the number of multi ramp-and-hold test in a stepwise strain test ($n=1$ in case of a single ramp-and-hold test). T is the duration of the loading and $\Delta\varepsilon$ is the loading

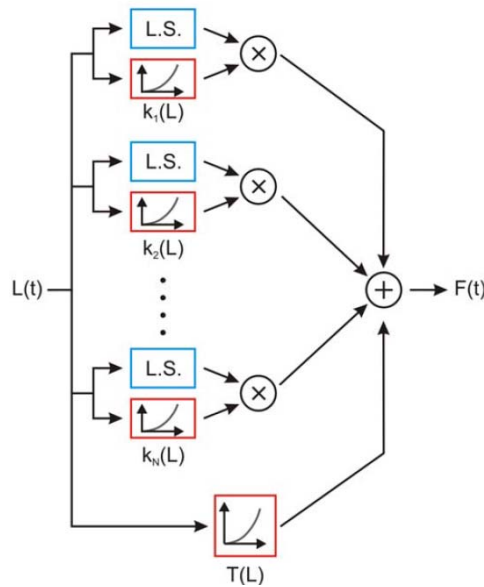


Figure 2-33: Schematic diagram of the AQLV model. The red box stands for the non-linear process $E(t)$ of converting the elongation into the force. The blue box represents a step response $g(\varepsilon)$ induced by a linear process [99]

strain as $\frac{\Delta \text{ length}}{\text{Sample length}}$. σ_0 is the equilibrium modulus. τ_i and k_i are the time constants of the shape function and stiffness of the tissue corresponding to each parallel Maxwell element [23]. Using this model Nekouzade *et al.* [23, 102] investigated the strain dependency of collagen gels synthesised from rat-tail under four consecutive tensile ramp and hold. Each ramp underwent 2 mm of stretch over 20 s which gives 0.1 mm/s strain rate. The specimens were allowed to relax for 200 s. The experimental data were fitted to the first relaxation increment and then using the model parameters calibrated to the first stretch the model prediction for the rest of increments (second to fourth increments) were calculated and plotted against the experimental data. As shown in Figure 2-34, the AQLV model is well suited to fit the calibrated data.

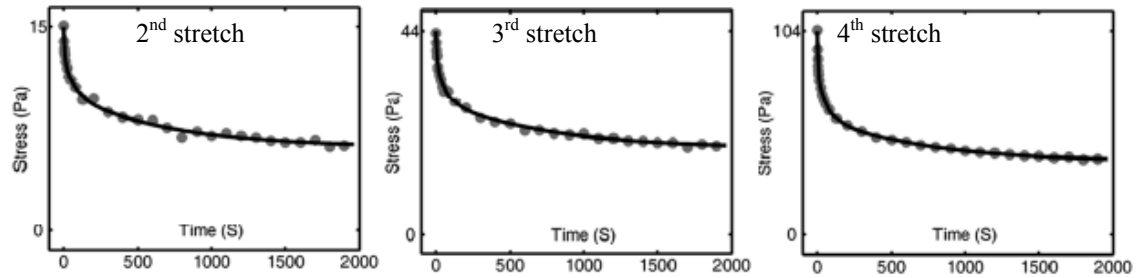


Figure 2-34: Prediction of the AQLV fit (solid lines) for four strain incremental stress relaxation data (grey dots) for the 2nd, 3rd and 4th ramp and hold data

2.5 Experimental variables

Development of advanced medical instruments such as computer aided surgery, robotic endoscopy/colonoscopy and artificial organs have been hindered by the lack of knowledge in mechanical properties of soft tissue [8, 22, 103]. Depending on the type of organ, various modalities have been used to characterise these properties. The mechanical response of biological tissue is influenced directly by many factors such as testing conditions, the type of tissue and species, experimental set up and protocol, and whether tissue is tested in-vivo or ex-vivo [8, 22, 103]. Some of these factors are touched on in this section.

2.5.1 In-vivo versus ex-vivo effect

Although the environmental conditions (such as temperature and hydration) and boundary conditions (such as the change in the tension and size of tissue) are changed post mortem, most of the published literature [12-14] have performed mechanical testing in the ex-vivo environment [45, 104]. The in-vivo and ex-vivo properties of tissue can be considerably different due to various factors including the change in the temperature, boundary conditions, hydration and loss of blood. However, ex-vivo tissue characterisation is commonly used to obtain a good approximation of tissue mechanical behaviour and to help determine the appropriate testing protocol for future in-vivo experiments. Comparing the results of in-vivo and post-mortem on different organs reveals that the stiffness increases in post-mortem conditions and tissue recovery between the cycles is greater for in-vivo than post-mortem [8, 10]. In-vivo tissue testing can impose limitations on tissue thickness measurements and disruption in data acquisition (due to cardiac and respiratory noise) [45]. The main benefit of ex-vivo when compared to in-vivo testing is the ease of control on testing conditions, various

issues raised around ethics of animal/human testing and when there is small samples of the tissue is available [45].

2.5.2 Hydration effect

Hydration effect on mechanical and viscoelastic properties in ex-vivo conditions has been investigated for various biological tissues such as trabecular bones [104], jaw cartilage [105], collagen gels [22], liver [45] and brain [106]. From these studies it is found that during the ex-vivo mechanical characterisation experiments, tissue gradually loses its capability to maintain its natural hydrated state and dries out. According to studies [104, 107, 108] the results of hydration effect on mechanical properties of bone under indentation test shows that dried tissue is significantly stiffer than hydrated tissue. Similarly, the tensile test performed by Meghazi et al. [22] on rat tail collagen gel presented 18% of increase in linear modulus for dehydrated conditions. Other examples are given by Kerdok et al. [45] and Mazza et al. [109] where an increase of stiffness is reported for dehydrated liver post mortem. The same trend was observed for the swine brain by Miller et al. [106].

The hydration effect on mechanical properties of large intestine is poorly known. To date the most relevant study by Higa et al. [8] examined the compressive mechanical properties of the large intestine was investigated in both the in-vivo and the in-vitro conditions. In this study the tissue was found to be stiffer when tested in the in-vitro than the in-vivo state. However, the tissue samples in-vitro were kept moist throughout the entire test [8], and so the deterioration of the mechanical properties of the tissue due to dryness was not observed. Hence, in Chapter 5 an experiment is designed to examine the hydration effect between the tissues kept in air and in PBS on the mechanical properties of the large intestine.

2.5.3 Preconditioning effect

Tissue preconditioning is reported to be a necessary step to stabilise tissue response through orientating the molecular structure of soft tissues similar to its natural in-vivo state [50]. Essentially, preconditioning is used to eliminate the strain history effect produced during repeatable interaction with soft tissues. Many studies have characterised the effect of repeatable loading and relaxation on biomechanical response of various tissues [22, 50, 96]. However, only Rosen *et al.* [10] characterised this effect for the large intestine with a focus on the effect of preconditioning on the stiffness

properties of the large intestine. Therefore, there is a need to investigate the influence of this effect on the viscoelastic response of the large intestine.

2.5.4 Varying strain-rate effect

Varying loading rate has been found to be one of the loading conditions that affect the mechanical and viscoelastic behaviours of biological tissues [8, 110-112]. According to a study by Vogel *et al.* [113], the rat skin tissue stiffens with an increase of loading rate during an uniaxial tensile testing. The viscoelastic properties of ligament is also found to be strain-rate sensitive as higher the strain-rate, the larger the magnitude of the stress relaxation [112]. In an study conducted by Hu *et al.* [110] the effect of varying loading speed on hardness of pig liver was investigated. This study was aimed to develop a real model of soft tissue for minimally invasive surgical training and simulation. The local effective elastic modulus of liver was derived experimentally at three different strain-rates. The results observed lower resistance to deformation at higher strain-rates and vice versa, which is opposing the results obtained by Vogel *et al.* [113] on rat skin tissue. Higa *et al.* [8] investigated the effect of varying compressive rates on goat large intestine. A larger deviation in the results of in-vivo experiments points out a strong rate dependency of mechanical properties of colon in-vivo. Additionally, under low loading rate the intestine was stiffer in the in-vitro test than in the in-vivo test. Also at higher rates the living tissue attests stiffer response to the applied stress than at the lower rates. However, this effect was only investigated on the loading response and needs to be examined further for stress relaxation response of the large intestine. It is notable from Figure 2-9 that in vitro results are less dependent on the rate of compression

2.5.5 Strain history effect

Using the Fung's quasilinear viscoelastic (QLV) model, several studies investigated the history effect on tissue such as swine skin [50], esophagus [74], canine vocalis muscle [114], and human and rat ligaments [90, 115]. Liu *et al.* found an inconsistency of strain history dependency of tissue viscoelastic behaviour to different strain level. In his study swine skin was stretched to 5%, 10% and 15% strains and the result showed that the relaxation rate of the skin samples are independent of strain history only at low levels of strain i.e. for 5% and 10% strains [50]. Performing incremental strain on porcine esophageal tissue, Yang *et al.* employed the separable QLV model to describe the separability of time and strain history during tissue stress relaxation. His results indicated that the viscoelastic behaviour during the stress relaxation process did not

differ at various strain levels [74]. Using the same model similar results, Figure 2-35, were found for canine vocalis muscle at strain increments of 13% to 33% [114].

However, the viscoelastic response of human and rat ligaments were found strongly dependent on the strain level as found by Lista *et al.* [90] and Provenzano *et al.* [115]. Human ligament was stretched between 4%- 45% strains and the normalised reduced relaxation results show that the tissue stiffness and the rate/magnitude of stress relaxation were strongly dependent upon strain level (Figure 2-36-a) [115].

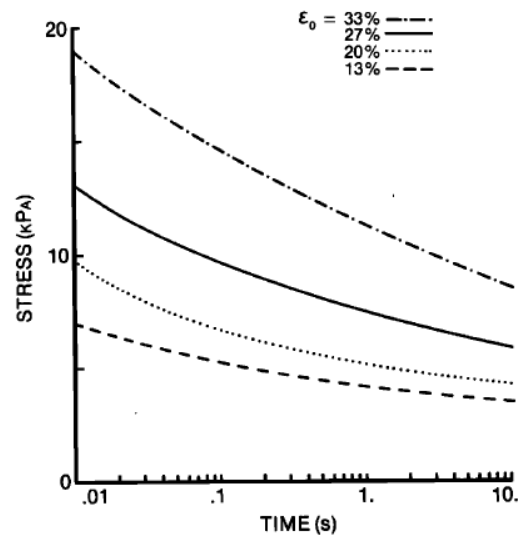


Figure 2-35: Stress relaxation of tissue at various levels of strain [114]

The same pattern was found for the rat ligament in Figure 2-36-b where higher strain level resulted in lower relaxation rate (incremental strains of 0.82% to 3.74%) [90]. However, to date the effect of strain history on stress-strain and stress relaxation responses of the large intestine is left undetermined.

Lynch *et al.* [71] conducted a series of incremental stress-relaxation tests and constant strain-rate ramp tests to calculate the elastic anisotropic and non-linear material properties in multi-axial fibre orientations. According to his findings, the linear modulus value obtained from constant strain-rate tests was greater than the incremental stress-relaxation tests. This was assumed to be due to dissipation of the viscoelastic effect in the incremental stress-relaxation tests which results in observing pure elastic material properties. He also agrees with Lista *et al.* [115] and Provenzano *et al.* [90] in the strain history dependency of the viscoelastic properties of the soft tissue.

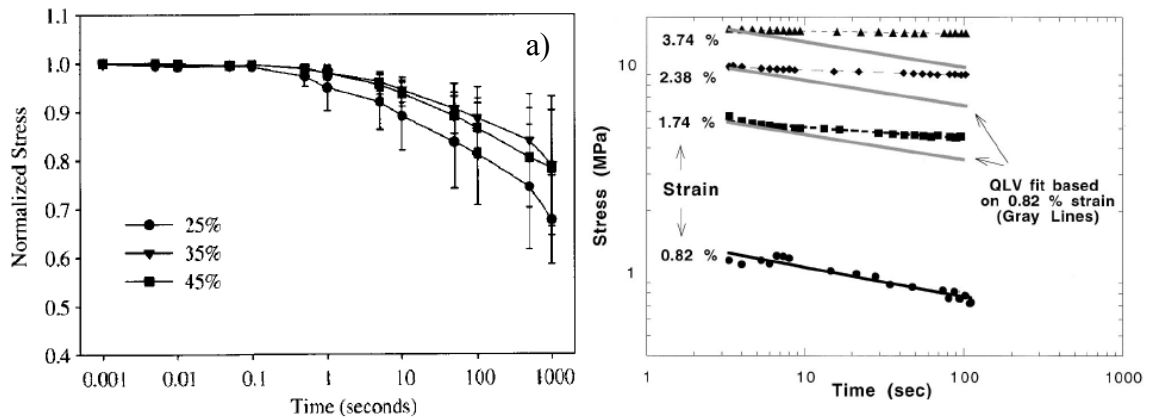


Figure 2-36: Strain history effect on viscoelastic response of a) human ligament and b) rat ligament

2.6 Conclusions

The large intestine exhibits very complex mechanical behavior and so in comparison to other tissues it is difficult to measure these properties and control the experimental conditions. Therefore, there is a big gap in the literature on the stiffness and viscoelastic properties of the large intestine subjected to various stretch modalities. Influence of testing variables including hydration level, preconditioning, strain rate variation and strain history on the large intestine need to be investigated. Both indentation and tensile modalities provide appropriate measurements on generic mechanical properties of soft tissue. However, the large degree of variability in the testing protocols employed in these studies has created a great deal of confusion when it comes to comparing the results between the studies and validating the outcomes.

Because the large intestine is a tubular organ, non-invasively accessing the inner wall of the lumen has been one of the main concerns for the in-vivo tissue characterisation. According to the reviewed literature, elastography techniques appear to be the most enhanced methods to map elasticity of the tissue and provide the ease of detailed observation and interpretation for the practitioner. However these techniques are complex and expensive. Acoustic impedance technique appears to be a relatively simple technique with the possibility of adapting with the design requirements of conventional colonoscopy tubes or the new coming robotic colonoscopy system such as stability, scalability and accuracy.

2.6.1 Aims

There are three aims in this project. The first aim is characterizing the generic properties of the large intestine in ex-vivo condition. The two reasons behind this are 1- there is a

gap of information in existing literature for mechanical response of the large intestine due to its complex mechanical behavior; and 2- this project is part of a bigger project called CoDIR which is set to design a robotic hydrocolonoscopy and so understanding the behavior of the tissue under manipulation by the robot is important. To achieve this, the second aim is set to design a robust methodology to measure these properties and ultimately provide a guideline for other researcher in this field to measure these properties. Lastly this project aims to develop a technique to assess in-vivo mechanical properties of tissue.

2.6.2 Objectives

The objectives defined for the presented work are:

- To identify an appropriate experimental protocol to measure mechanical properties of the large intestine
- To explore different testing techniques for examining various ex-vivo mechanical properties of the large intestine
- To extract and analyse ex-vivo mechanical properties of the large intestine using an appropriate data analysis method
- To develop and evaluate a suitable technique for assessing the in-vivo mechanical properties of the large intestine

Chapter 3. Materials and methods

3.1 Introduction

The following chapter contains a description of the three methods employed to measure mechanical, viscoelastic and acoustic impedance properties of the large intestine. The stress versus strain relationship as well as time, strain history and strain-rate dependency of the tissue properties in the ex-vivo condition are examined through a series of indentation and tensile tests. Furthermore, an in-vivo tissue characterisation technique based on measuring acoustic impedance properties of the tissue is investigated as a potential concept for evaluating the tissue properties during a hydro-colonoscopy procedure. To achieve the objectives of this study several techniques have been used. This chapter presents the sample preparation, instrumentation, testing protocol and the data analysis methods associated with each technique.

3.2 Specimen preparation

Animals used were bred and sacrificed in accordance with UK Home Office regulations (Animals [Scientific Procedures] Act 1986). In this research pig rectum is used as it is similar to human large intestine in terms of digestive and metabolic functionality [3]. Freshly excised porcine abdomens were obtained from a local abattoir. The large intestine was then separated from the rest of the abdominal organs and cut into the desired size and shape and finally stored in saline (PBS) solution.

3.2.1 Rectum

Figure 3-1 demonstrates the proposed conformation of pig large intestine. For this test 10 freshly excised porcine rectums were obtained. To observe the behaviour of porcine rectum along its length, the specimens were cut circumferentially into 10 equally sized segments each measuring 4x4cm and stored in saline (PBS) solution. Each segment was assigned a letter between A-J, where A is the most distal end of rectum starting from anus and J is the most proximal end of rectum as shown in Figure 3-2. The segments were then cut radially and freed from the mesocolon by dissection at the time of testing. All the tests were conducted at controlled room temperature (22°) within 24 hours of dissection.

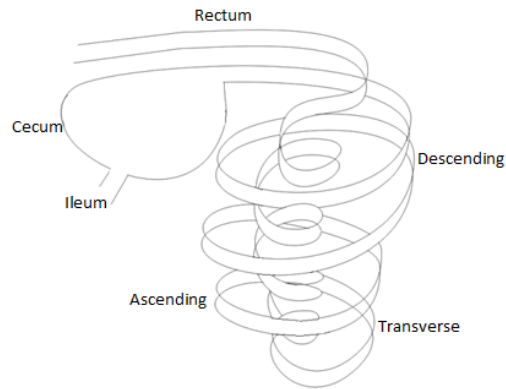


Figure 3-1: A porcine large intestine [94]

Tissues was left in air during testing to replicate the conditions in open surgery or CO₂ insufflated colonoscopy procedures [73, 116]. The effect of osmotic swelling and tissue deterioration were considered negligible during the experimental period and are no considered in the following discussion.

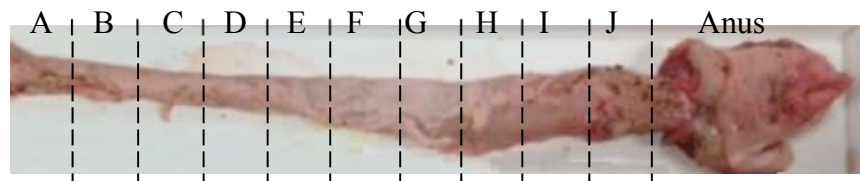


Figure 3-2: A porcine rectum divided into 10 equally cut segments for tissue mechanical properties variation test

3.2.2 Large intestine

Six freshly excised porcine large intestines were obtained for this experiment. In Figure 3-3-a full length of large intestine is laid out and the five segments were marked. Unlike human large intestine the division between cecum, ascending colon, transverse colon, descending colon and rectum in pig large intestine are not clearly delineated. Therefore, having rectum and cecum separated easily, the area between the rectum and cecum borders was divided into three equally spaced segments as descending colon, transverse colon and ascending colon. The length and circumference of all segments were measured prior to the tests.

For the indentation test, the specimens were cut into pieces of 8x4cm, and placed flat on a sample holder filled with saline solution to several millimetres above the sample surface so to maintain the tissue in its hydrated state during the entire testing process, as shown in Figure 3-8.

In the tensile experiments each segment was cut circumferentially into three equally spaced sections, cut along the longitudinal axis and straightened. The flattened specimen was then cut into a rectangular specimen of 30x90mm align or transverse to the fibre direction and stored in saline (PBS) solution.



Figure 3-3: (a) Photograph of the entire large intestine, laid out and marked into five segments - Rectum, descending, transverse, ascending, and cecum, (b) The circumference of rectum was measured at three equally spaced locations

3.3 Instrumentation

The first set of tests was performed using a commercial ‘Modular Universal Surface Tester’ (MUST) rig as the rig’s specifications matched the testing requirements. The findings obtained from the first batch of experiments were used to set new objectives for the next set of tests. However, due to several limitations of the MUST rig (which will be explained later) a new rig was designed and built in house to suit the modified testing protocol and run in various modes for multiple use.

3.3.1 MUST rig

A Modular Universal Surface Tester (Falex Tribology) was used to apply a controlled load to the tissue and monitor the resultant indentation depth. Force measurement, in mN, is achieved by employing a parallel spring set in contact with the indenter. A micro mirror is attached to the tip of each spring. As the indenter presses on the material, the springs and so the mirrors are deflected. Springs with different stiffness are available so that various range of force can be applied in an experiment. A fibre optic sensor, placed on the cantilever unit, detects the motion of the springs by emitting light to the mirrors and capturing the reflection. The reflected light is then converted to electrical signal. The signal represents the distance between the deflected spring and the optical sensor. The embedded data acquisition and control unit uses an algorithm to translate the reflection into force measurement. MUST tester main components including a

cantilever unit, sliding stage, indenter and sample holder are presented in Figure 3-4-a. Displacement data are measured at a resolution of $1\mu\text{m}$ and force data at $1\mu\text{N}$. The instrument allows for the applied force and indentation velocity to vary between 10-1000 mN, and 0.05-0.5 mm/s, respectively. A fine cylindrical indenter of diameter 5mm was attached to cantilever unit. Despite creating complication such as tissue cutting or stress concentration at the edge [117], a flat end cylindrical indenter is preferred as it maintains the net section stress under the indenter constant with time [118]. Specimens were mounted on the tissue holder as shown in Figure 3-4-b. Force and displacement data were recorded at 100 Hz for subsequent analysis.

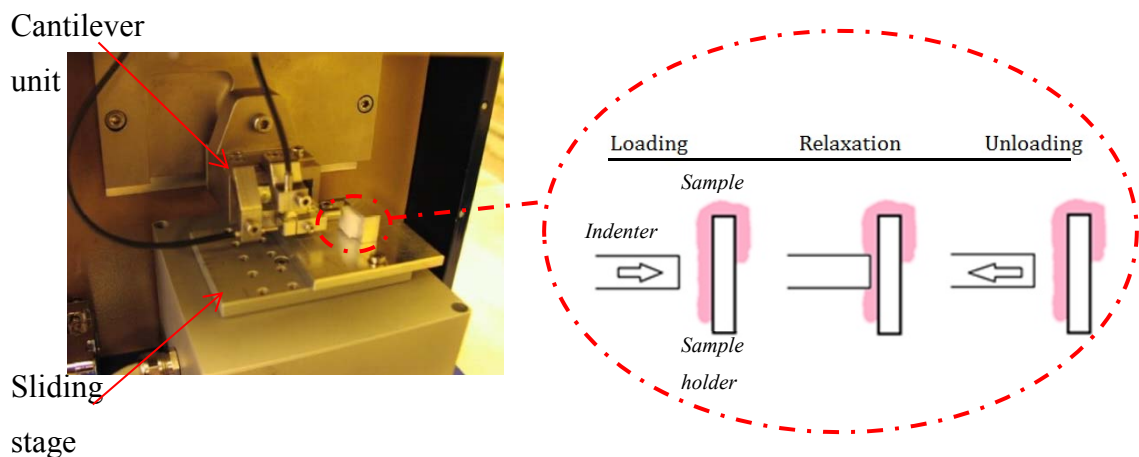


Figure 3-4: a) MUST rig, b) Indenter schematic

The device parameters have to be reset in every use, at least once a day. Resetting includes locating the fibre optic sensor in a suitable position so the spring unit at maximum deflection does not hit the sensor. Moreover, the spring constant value has to be checked. The Tare must be reset.

3.3.2 MMC rig

A 'Modular Mechanical Characterisation (MMC)' rig was designed based on the result of the indentation of the MUST rig. The MMC rig was designed and built as a bespoke piece of equipment as shown in Figure 3-5. A compression load cell (single point load cell, Vishay, model: 4001) with a force range of 0-6N and resolution of $6.7\mu\text{N}$ was mounted at the interface between the sample holder and a linear stage actuator (VT-80 motor and controller, Physik Instrumente, Germany) with a step resolution of 1nm. The actuator is fixed vertically to a rexroth aluminium frame. An amplifier was employed to amplify the voltage obtained from the load cell. A national instrument data acquisition card myDAQ was used at the interface of the amplifier and the PC. The control and data

acquisition were programmed using LabVIEW. A schematic diagram of all these components and the relevant connections are given in Figure 3-6.

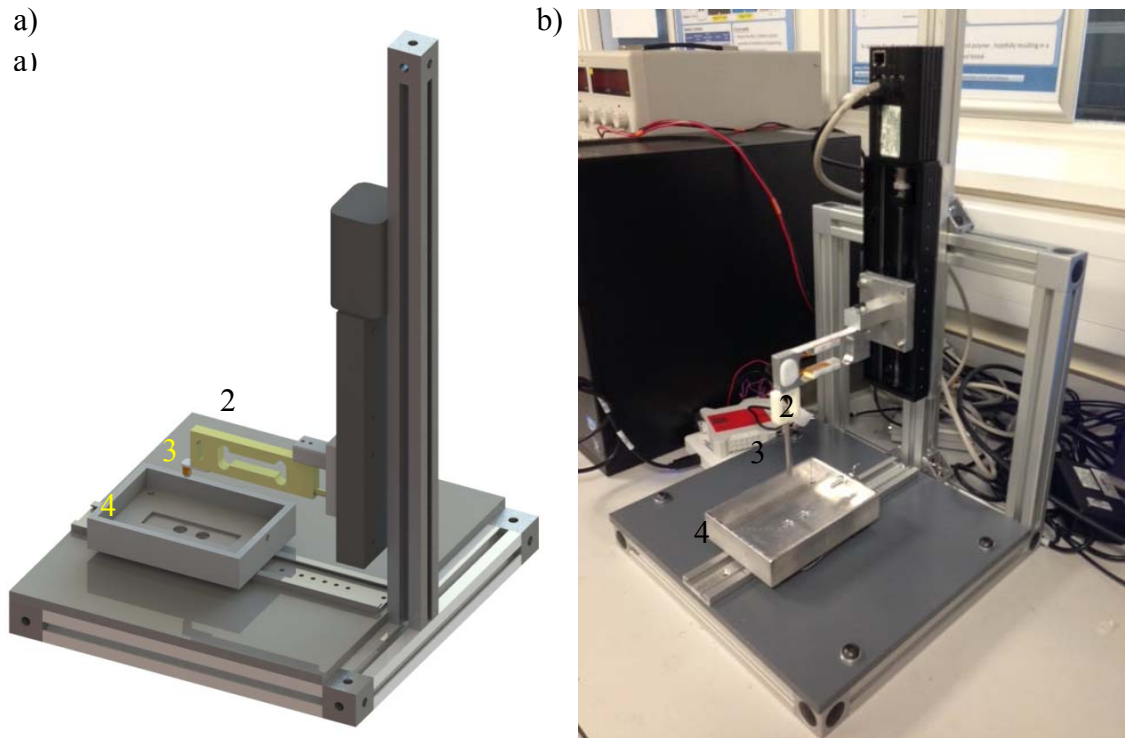


Figure 3-5: a) 3D design and b) the built model of MMC rig. The annotations represent 1-linear stage actuator, 2-load cell, 3-indenter & 4-sample holder

Force and displacement data were recorded at 60 Hz for subsequent analysis. All the experimental data were exported in form of time-displacement-force for analysis in MATLAB. Figure 3-7 illustrates the software flowchart adapted for the testing protocol in Table 3-3 which is designed for characterising mechanical properties of the large intestine. MMC rig was designed to perform mechanical properties testing in indentation and tensile modes. As shown in Figure 3-8, suitable tissue fixtures were designed for these two modes. For indentation tests a fine cylindrical indenter of diameter 5mm was attached to the load cell. The sample holder base comprises two plates with a rectangular opening in the middle Figure 3-8-a. The tissue is placed and squeezed lightly between the two plates for ultimate hold. For the tensile tests a new gripping technique was employed to avoid using the traditional technique of clamping the tissue in which causes a bulge at the gripped ends and creates uneven distribution of load.

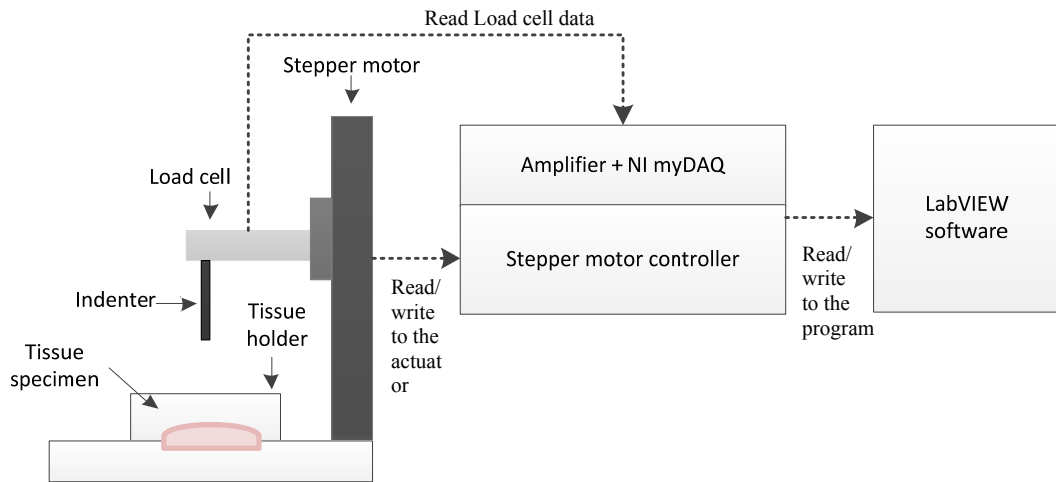


Figure 3-6: Schematic of the Modular Mechanical Characterisation (MMC) rig

The sample holder comprises two main frames holding in place three rods through which tissue is folded Figure 3-8-b. The tissue is clamped between the rods using small elastic bands which go around the three rods at each side. The specimens were fixed between the two sample holders in such a way that the distance between the sample holders was 30mm. The sample holder is designed such that to apply minimal damage to the tissue while allowing an equal distribution of tension along the exposed length of the sample. The sample holder is then placed inside a bath of saline to keep the tissue hydrated throughout the experiment.

A series of indentation tests Table 3-1 were conducted as part of the rig validation to ensure the rig accuracy and reproducibility. The test procedure includes a cyclic test and nine single indentations at varying load and strain-rate. Sorbothane samples with shore hardness of 30 were employed for this test.

The sorbothane sample was cut into a 40x40x10mm section. Since it was a small piece some of the locations on the sample might have been indented twice. Also, as the sample holder on MMC device is comprises of two plates (the top and bottom in order to sandwich the tissue for better hold) some of the indentations were taken place at the sections which were sandwiched by the two plates previously. So residual strain caused by the compression of sample holder might have slightly affected the results.

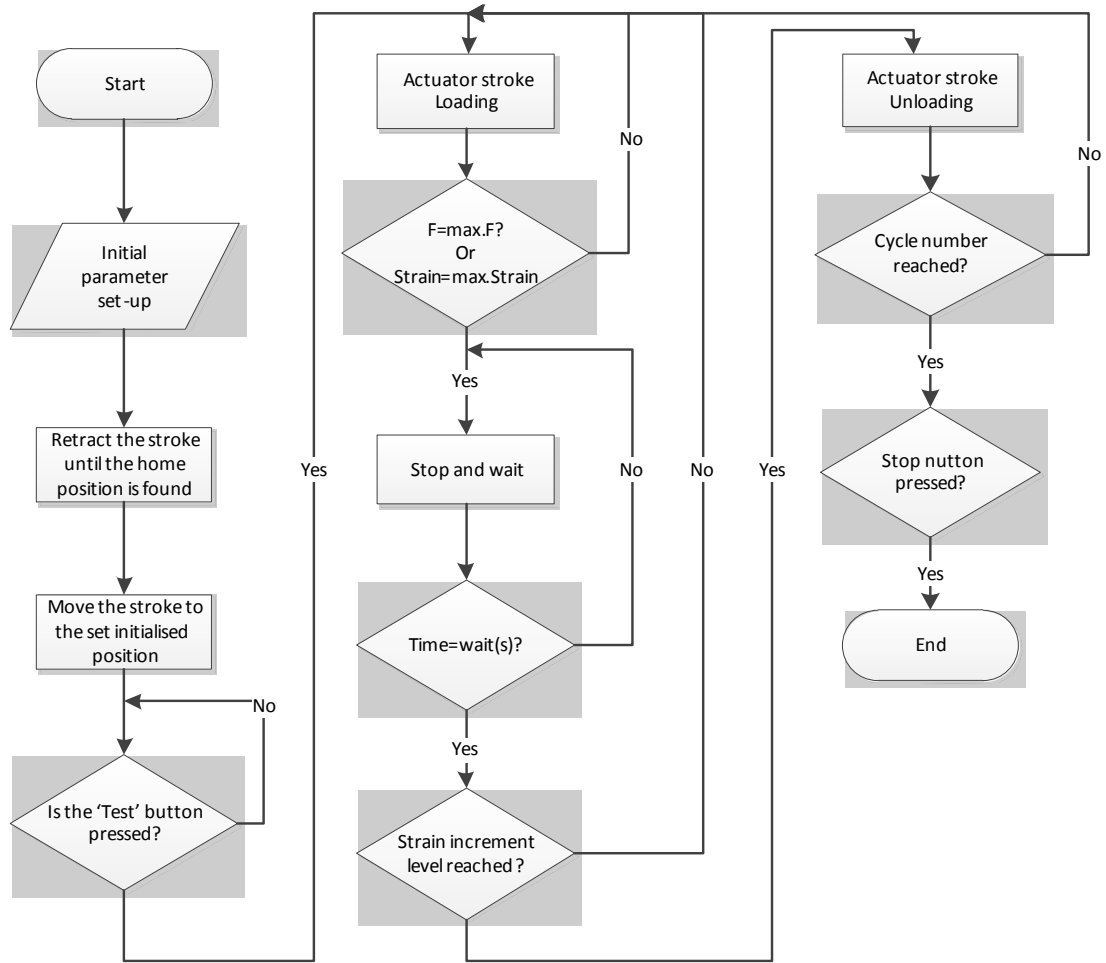


Figure 3-7: Software flowchart adapted for indentation testing protocol in Table 3-3

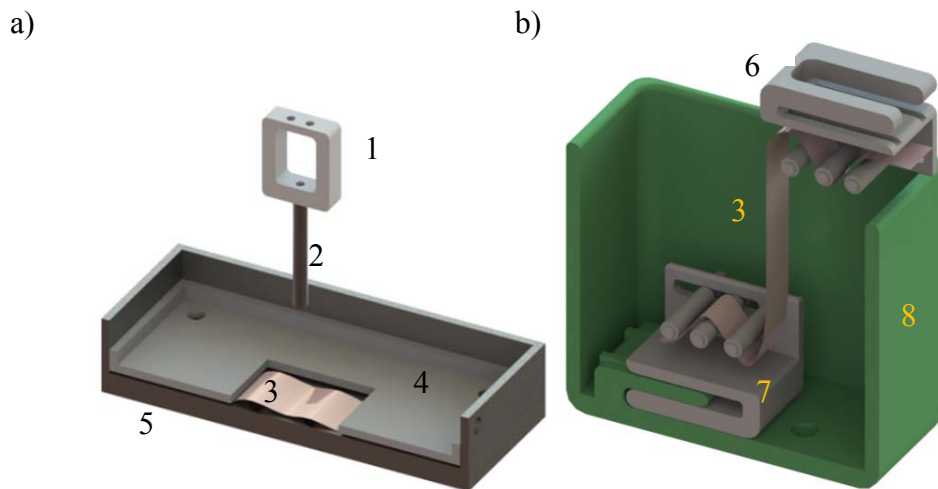


Figure 3-8: Cross section view of a)the indentation sample holder, and b) the tensile test sample holder in the sample bath. The annotations represent 1-indenter-load cell connector, 2-indenter, 3-specimen, 4-sample holder top plate, 5-sample holder bottom plate, 6-sample holder top clamp, 7-sample holder bottom clamp & 8-Sample bath

Test	Threshold force	Strain-rate	Repeat
Single spatial test	2.5 N	2.5 mm/s	10
Strain-rate variation test	0.1, 2.5 & 5 N	0.1, 2.5 & 5mm/s	1

Table 3-1: Testing protocol for MMC rig validation

Figure 3-9 demonstrates the stress versus strain response of tissue under single spatial indentation test. The linear modulus does not vary significantly. Figure 3-10 reveals the mechanical response of sorbothane sample under varying load and strain-rate. Overshoots of about 600mN for 5 mm/s, 200mN for 2.5 mm/s, and 14mN for 0.1 mm/s were observed.

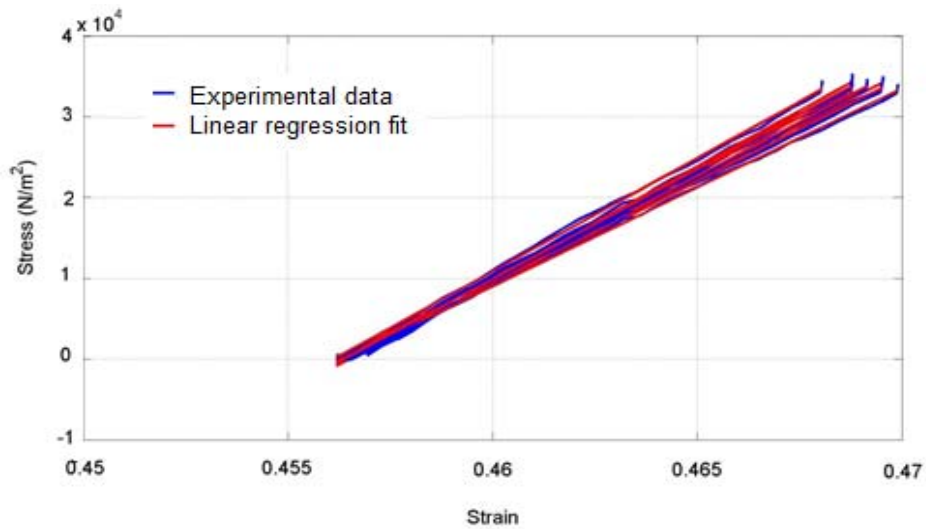


Figure 3-9: Stress versus strain response of the sorbothane sample with the linear regression fits

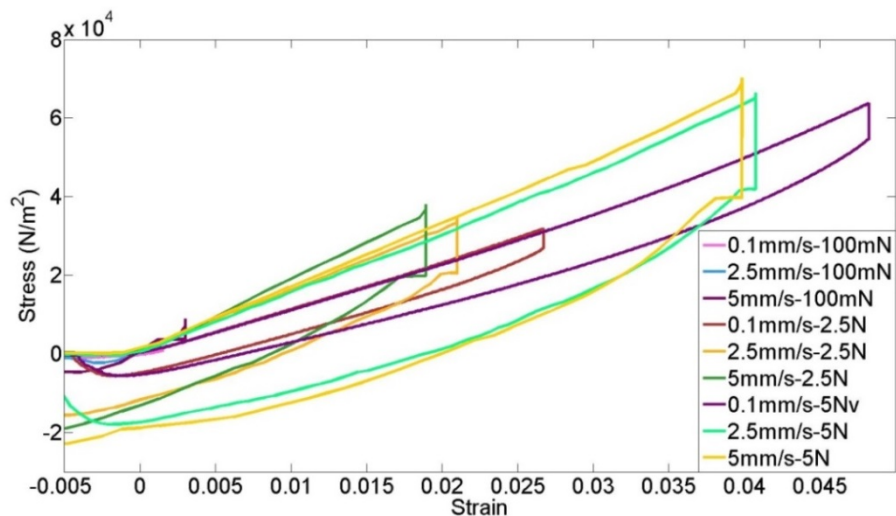


Figure 3-10: Strain versus stress data of the sorbothane sample under varying load and strain-rate

3.3.3 In-vivo tissue characterisation rig-Acoustic impedance measurement

The acoustic impedance technique was selected for its potential to be miniaturised and embedded within the body of an intra-corporal robot. The main component of this technique is the selection of the tactile sensor or the piezoelectric element. A variety of piezoelectric transducers have been employed to drive/pickup frequency/impedance shifts for this method. Based on a probe designed by [76] a stack actuator (PSt 150/5×5/7 by Piezomechanic, DE) was selected. Unlike [76] where a second PZT element was also employed in conjunction with the driving PZT to pick up the oscillation, here a more simplified technique was used where the one actuator which induces the mechanical oscillation is also used as a sensor. Stack actuators are favoured for their relatively high stress and large strain in comparison to bulk single element PZT actuators) [119] and are used for applications such as ultrasound drills and ultrasound transducers. The stack actuators consist of piezoelectric layers connected mechanically in series and electrically in parallel [119].

Figure 3-11 illustrates the set up for the acoustic impedance measurement. The stack PZT transducer is bonded to the load cell and contact tip of 5x3mm.

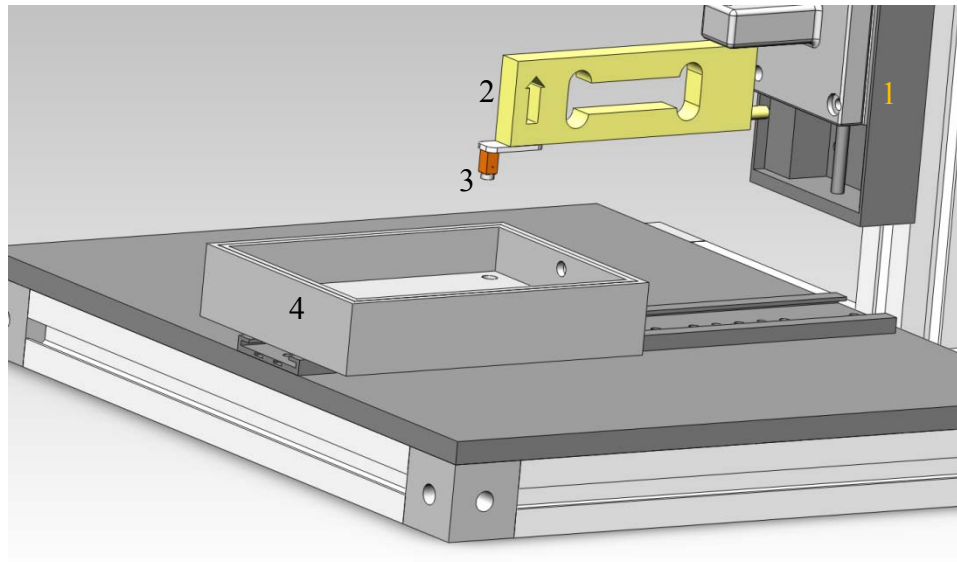


Figure 3-11: The components of the impedance measurement probe attached to the MMC rig for stationary movement. The annotations represent 1-Linear stage actuator, 2-load cell 100 ×10× 30 mm, 3-stack PZT element 5 × 5 ×7 mm & 4-sample holder 100 × 70 × 40 mm

The second part in developing this system is the design of a resonance circuit (refer to Chapter 2.3.2.3) and the data acquisition measuring system. This involves generating periodic sine wave signals for oscillating the PZT transducer at its resonance frequency

and reading the frequency and impedance shifts of the detected signal coming back from the PZT transducer. As explained in Chapter 2.3.2 the signal that is detected from the transducer is shifted in frequency and amplitude from the driving frequency. This signal is filtered, amplified and phase shifted and then fed back to drive the transducer. Designing the feedback loop is a complex task. Hence, this work was concerned with assessing the feasibility of the technique and for this reason the feedback stage was omitted. The resultant system retains the same functionality although the signal/noise ratio will be compromised in comparison to a system with feedback stage.

A Network Analyser (Agilent, model: E5061B) was deployed with a frequency range of 50 to 400 kHz. The results from testing silicon samples with differing compliances showed clear and consistent responses to the samples stiffness. This system will be referred to as (PZT probe I). The optimised loading force determined by trial and error for this set of experiment was 4 N. The number of points for the sweep frequency was 1601. The PZT transducer was induced with 400 mv. For validation purposes a series of test were conducted results are depicted in the results chapter.

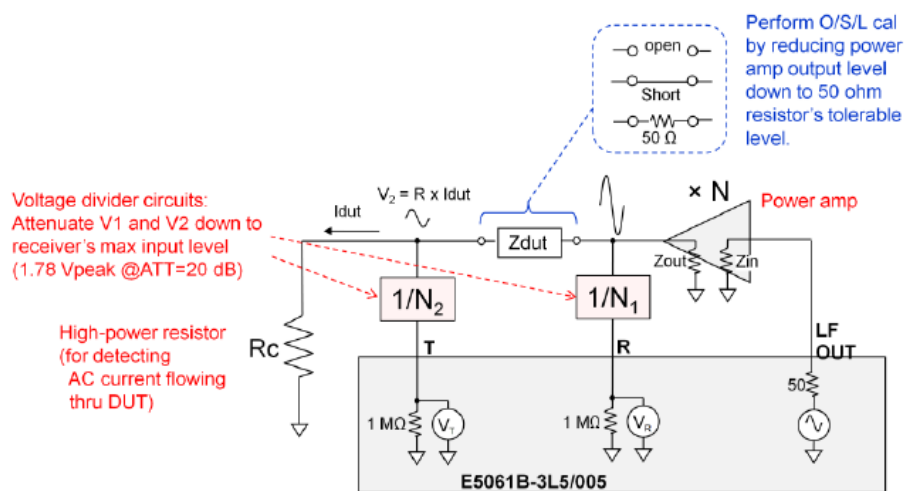


Figure 3-12: Schematic of impedance measurement using Agilent Network Analyser E5061B with adaption of an external power amplifier and potential dividers [120]

A new acquisitions system (PZT probe II) was developed to make a more bespoke system of lower cost. In this set up, an acquisition digital board National Instrument PCI-6110 was chosen with 5 MHz sampling rate per channel. A HP3310 signal generator was employed to drive the PZT transducer. The voltage output level was set to 400 mV on the signal generator to set the amplitude of the signal to the PZT transducer. The natural frequency of the PZT was 70-80 kHz and the anti-resonance frequency was 175-185 kHz. The range and oscillation of the frequency sweep was

controlled by the voltage control oscillation (VCO) input to the signal generator. The frequency range dial on the signal generator was set to the starting frequency and the desired frequency range and the sweep speed was controlled by a voltage from the data acquisition system (using a bespoke LabVIEW program).

The data acquisition board NI PCI-6110 is only compatible with desktop PCs. In order to make the system portable it was decided to use a laptop and hence a NI USB-5130 with 5 MHz sampling rate and two acquisition channels was selected. Despite the different acquisition boards the new system is designed based on the previous version and is referred to as (PZT probe III) as shown in Figure 3-13. Figure 3-14 demonstrates the flowchart of the LabVIEW software designed according to the testing protocol set in Table 3-4.

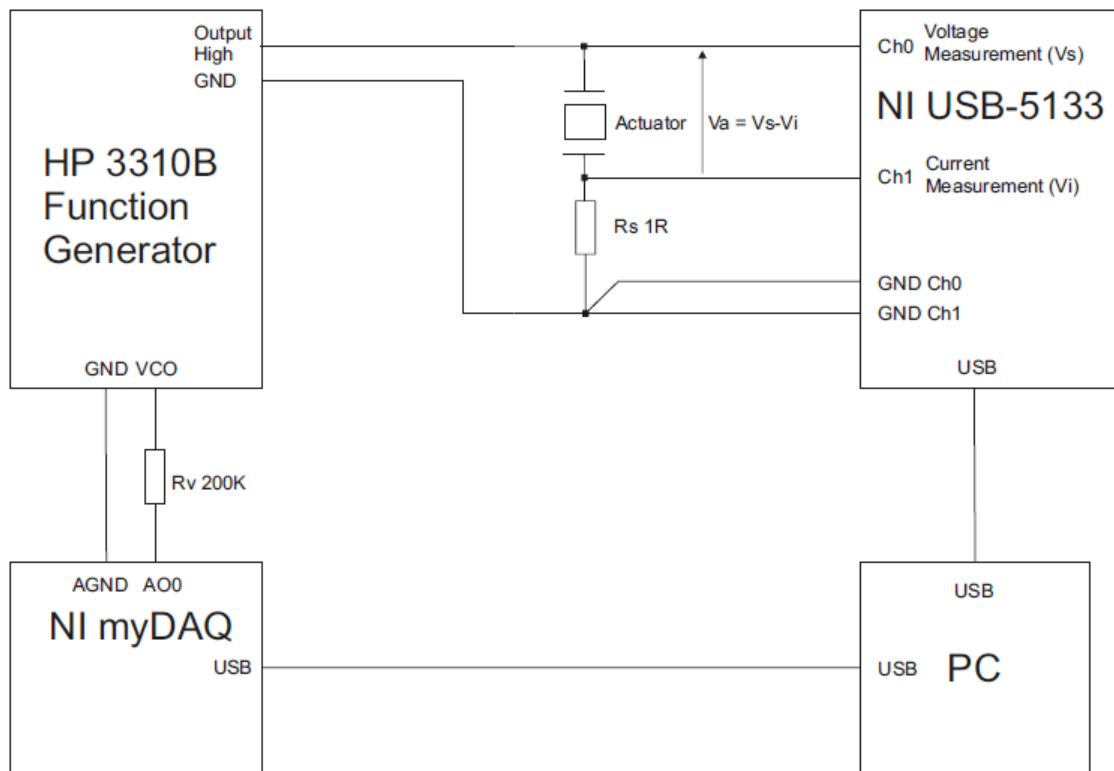


Figure 3-13: Schematic of PZT probe III comprises a portable impedance acquisition system consists of a HP 3310 function generator and a NI USB-5133 acquisition board

As seen in Figure 3-13, the voltage and current signals detected from the transducer are both used to measure the impedance magnitude and phase as:

$$\text{Impedance magnitude (Ohms)} = V_{\text{actuator}} (\text{amplitude}) / I_{\text{actuator}} (\text{amplitude})$$

$$\text{Impedance phase (degrees)} = V_{\text{actuator}} (\text{phase}) - I_{\text{actuator}} (\text{phase})$$

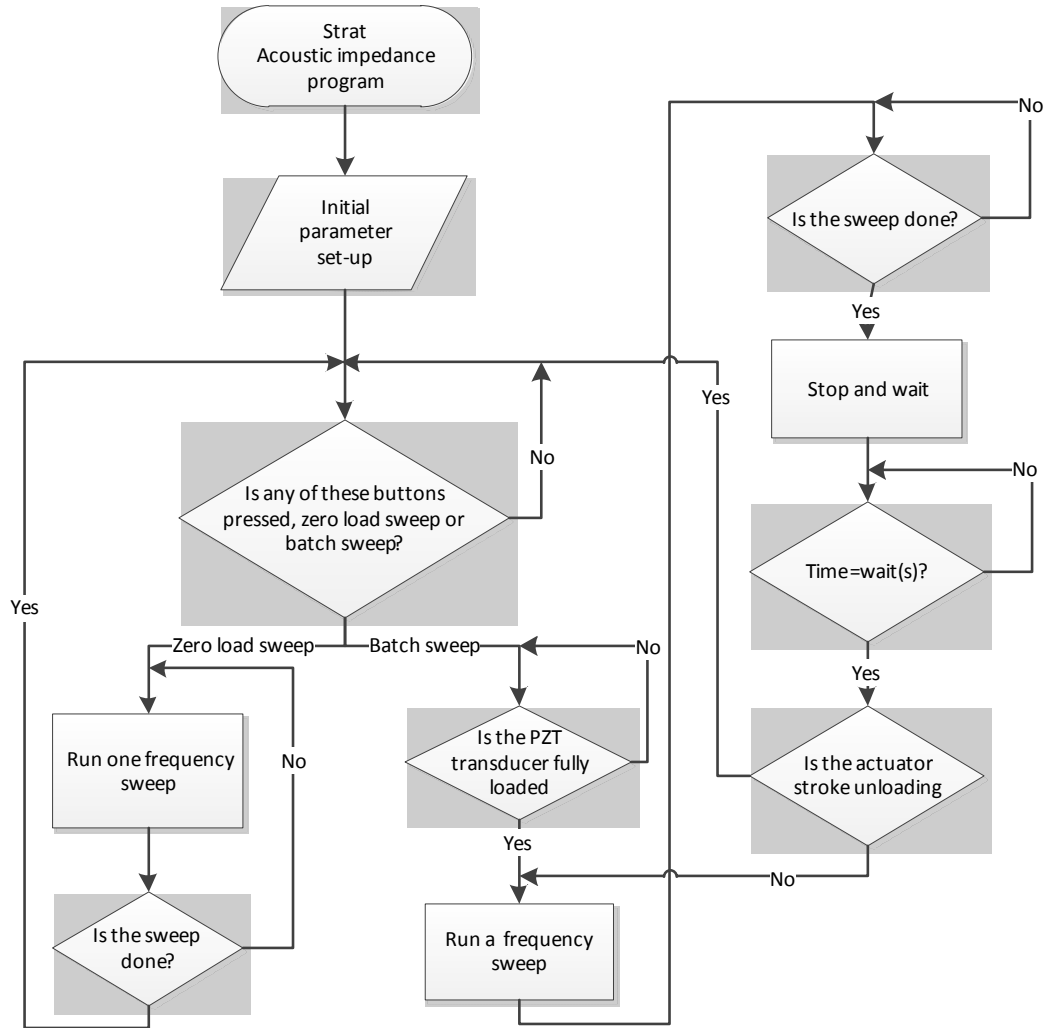


Figure 3-14: Software flowchart adapted for acoustic impedance measurement of the tissue. The flowchart is set in accordance with the testing protocol in Table 3-4

3.4 Mechanical properties measurement

Characterising mechanical and viscoelastic properties of tissue can be performed by applying a mechanical load to the tissue and observing the time dependent viscoelastic decay of stress when the applied strain is held constant for a short/long period of time [50, 74, 95].

A typical indentation process comprises three phases. Once the indenter tip makes contact with the tissue, the *loading phase* begins and the applied strain increases linearly until a peak force is reached. The indenter is then held in this position for 10 s in the *relaxation phase*. Finally, in the *unloading phase* the indenter is retracted back to the start position. The tensile test follows the same steps except instead of indentation; the tissue is stretched and released gradually for *loading* and *unloading phases*. These

three phases are marked as 1-3 in stress versus strain and stress versus time graphs in Figure 3-15-a and b. The short relaxation period of 10 s was selected as a short hold time for loading the tissue based on a study on 31 different surgeons performing 3 surgical tasks involving tool-tissue interaction. The results indicates that all the compression/grasping tasks were performed for duration of 10 s or less [10, 121].

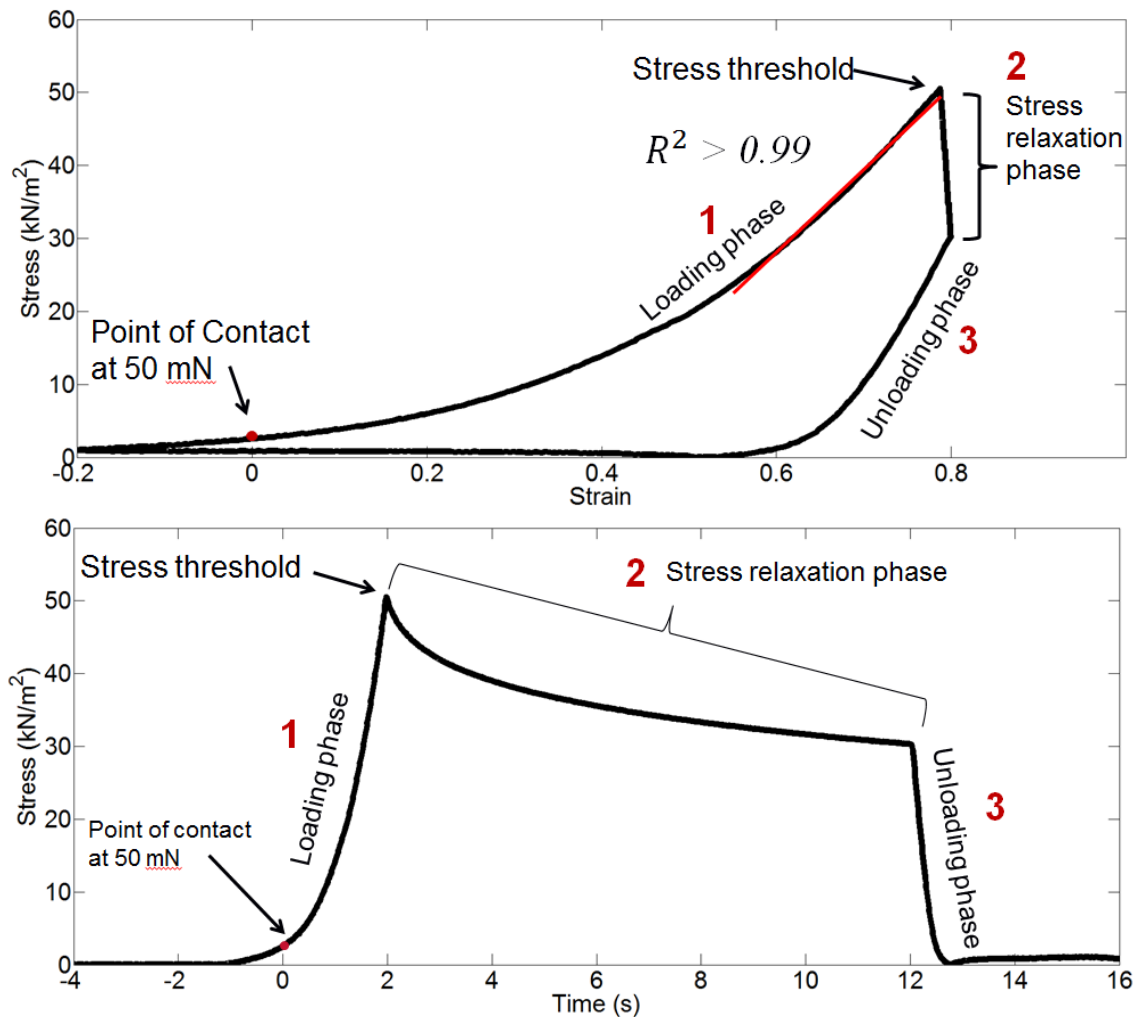


Figure 3-15: Typical a) stress-strain and b) stress-time responses of tissue to indentation/tension in 3 phases. Phases are defined as loading (1), stress relaxation (2), unloading (3). The red line in figure 'a' represents a linear regression fit used to determine the linear modulus. The regression fit starts from the point of maximum stress/strain threshold and a variable start point. The start point is progressively moved back until $R^2 > 0.99$

The indentation and tensile tests are performed in two modes: stress control or strain control. The stress control mode was selected initially for the first set of tests and then it was replaced by strain control mode as it provides a better result comparison between similar studies.

3.5 Experimental protocols

3.5.1 Method I: Indentation characterisation using the MUST rig

To characterise the mechanical properties of rectal tissue a testing methodology was designed firstly to simulate the static single and repeated indentation response, and secondly to observe the biomechanical effect of varying the indentation speeds. In this research the methodology was evaluated using fresh porcine rectal tissue. As explained previously, the stress control mode was employed for the first set of tests. To determine an appropriate peak force for stress control mode, tissue was loaded such that its behaviour remained in the linear-region of strain and any tissue damage is avoided.

To present data, force and displacement were converted to stress and strain, respectively. From preliminary tests a peak load of 1N (=50.9 kN/m² stress) was found to achieve this objective [97]. For strain calculations, the thickness of the tissue was approximated based upon the first point of contact. The initial point of contact was identified as the point at which a 50 mN (=2.5 kN/m² stress) load change occurred from baseline [117].

The experiments were divided into two categories: Intra-rectal tissue variation tests and repeated interaction tests. Also, to examine the effect of indentation speed, the above tests were repeated three times for each strain-rate, low (0.05mm/s), medium (0.2mm/s) and high (0.5mm/s) [8].

- **Intra-rectal tissue variation test:** In this test, the tissue was indented three times at regularly spaced points to give a total of 30 indentations along the full length of rectum as shown in Table 3-2. For simulating a step change in strain, a high strain-rate of 0.5 mm/s was selected for indenting into the rectum. This is equivalent to an average of 1-2 seconds of loading duration (dependent on the tissue thickness and properties). The objective was to investigate how the behaviour of tissue varies along the length of the rectum.
- **Repeated interaction test:** Twenty indentations were made in the same location on each segment, with no delay between cycles. This test was designed to evaluate tissue behaviour under repeated loading.
- **Strain-rate variation test:** In order to examine the effect of indentation speed, the repeated interaction test was repeated three times for each strain-rate, low

(0.05 mm/s), medium (0.2 mm/s) and high (0.5 mm/s) in common with other studies [8].

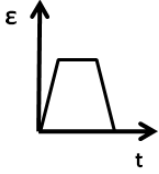
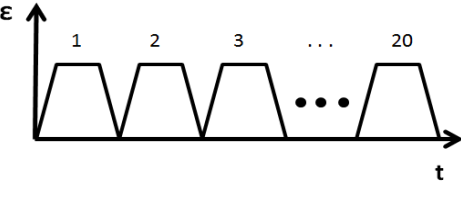
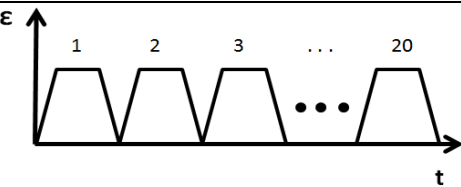
Tests	Location	Protocol illustration	Objectives
Intra-rectal tissue variation test , no preconditioning	Three indentations on each segment		Assess the averaged linear modulus & parameters of the viscoelastic model
Repeated interaction test	One indentation on each segment		Examine the effect of repeated interaction on linear modulus & parameters of viscoelastic model
Strain-rate variation test at 0.05, 0.2 & 0.5mm/s	One indentation on each segment		Examine strain-rate dependency of the tissue

Table 3-2: Testing protocol set for characterising mechanical properties of rectum

3.5.2 Method II: Combined indentation plus tensile characterisation using the MMC rig

The focus of this study was to design a solid methodology to investigate various aspects of the mechanics of the large intestine. The methodology was based on evaluating indentation and tensile properties of the large intestine through examination of time and strain history dependent viscoelastic properties. In addition, the hydration effect on the mechanical behaviour of the tissue was observed along the full length of the large intestine. After a series of trials, a strain-rate of 0.1 mm/s was chosen as used in [40] for all the tests as to avoid the unwanted overshoot, vibration and noise caused by fast strain-rates. This speed allows for studying the tissue under quasi-static status [110].

As shown in Table 3-3 the experiments were divided into three categories: Intra-large intestine variation test, repeated interaction test and stepwise strain test.

- **Intra-large intestine variation test:** This test investigates the variation of mechanical and viscoelastic behaviour of tissue along the full length of large intestine. Each segment was cut into three equally sized sections and a sample from each section was taken, giving 15 samples along the full length of colon.

50% strain was selected to apply to each specimen to allow for relative comparison of the results to other similar studies [122]. The initial five preconditioning cycles (loading and unloading) are performed to stabilise the behaviour of tissue as reported previously in Chapter 4 [50]. A preconditioning cycle is referred to as a two phased loading-unloading cycle. This is followed by a full loading-relaxation-unloading cycle with no recovery period in between as explained previously in Chapter 4.5.3. with this difference that the relaxation duration is extended from 10 s to 300 s in the new protocol. The data obtained from the full indentation cycle performed after the preconditioning cycles was taken for the analysis.

- **Repeated interaction test:** In this test, a specimen cut from the transverse colon was indented 10 times [75] at the same location with a constant strain-rate. This test was designed to evaluate the effect of repeated interaction for various testing modes. The tissue is strained by 50% in each cycle. It is assumed that equilibrium is reached before the next cycle is performed.
- **Stepwise strain test:** Four successive stepwise elongations were applied to a sample cut from the transverse colon. Each step includes a loading phases following a 300 s of stress relaxation period in between each increment. This test aimed to examine the strain history dependent behaviour of tissue. The increments are in order of 20%, 35%, 50% and 65% strains.

As part of the intention of this chapter was to investigate the hydration effect, the repeated interaction test was performed both in hydrated and dehydrated conditions.

One of the challenges in indentation measurements is to find the first point of contact as the force is very small at the beginning of the tissue-indenter contact. A technique was used to estimate this point utilising force feedback control. In this technique prior to each test the initial point of contact was determined by detection of 50 mN load change at 0.05 mm/s indentation speed as set in the literature [117]. Furthermore, to measure the thickness of the tissue the sample holder platform was indented once at the beginning of the test and the distance between the initial point of contact obtained in advance and the sample holder platform was calculated as the thickness measurement for each sample as shown in Figure 3-16.

Tests	Sample Location	Protocol illustration	Data analysis
Intra-large intestine variation test, single indentation cycle with 5x precondition cycles in PBS	Three equal spaced samples from each segments		Averaged linear modulus & parameters of viscoelastic model
Repeated interaction test, 10 consecutive indentation cycles in PBS and in air	One sample from mid transverse colon		The effect of repeated interaction on linear modulus & parameters of viscoelastic model & the hydration effect
Stepwise strain test, 4 strain levels 20%, 35%, 50% and 65% in PBS	One sample from mid transverse colon		Examine strain dependency of tissue using two normalisation techniques

Table 3-3: Testing procedure for characterising indentation/tensile properties of large intestine

Sample holder platform indentation

Initial point of tissue-indenter contact

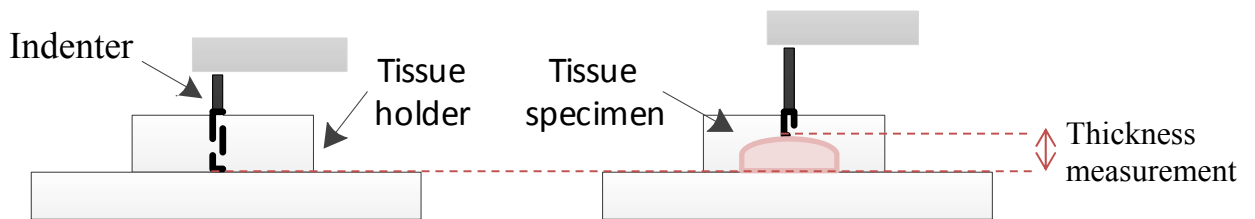


Figure 3-16: Schematic diagram of thickness measurement technique

3.5.3 Method III: Acoustic impedance tissue characterisation

In this method acoustic impedance properties of the large intestine are investigated to achieve in-vivo stiffness properties assessment of the tissue. Preliminary tests were performed on silicon rubbers with various degrees of shore. Since the PZT transducer was mounted at the indenter end of the MMC rig, the linear modulus of each sample was also measured during the tests. This enables comparison of mechanical properties and the acoustic impedance properties of the tissue. The first stage of the experiment began with sweeping the frequency across a fixed frequency range whilst the PZT is in a stationary position kept in air in no contact with the object. Figure 3-17 gives an example of the excitation appearance on the measuring system front panel. As the frequency is swept through the chosen frequency range, the minimum peak

(representing the resonance frequency) or the maximum peak (indicating the anti-resonance frequency) of the impedance magnitude is detected. The sweep time is defined by the number of points in a sweep. Higher the number of points results in lengthier sweep time.

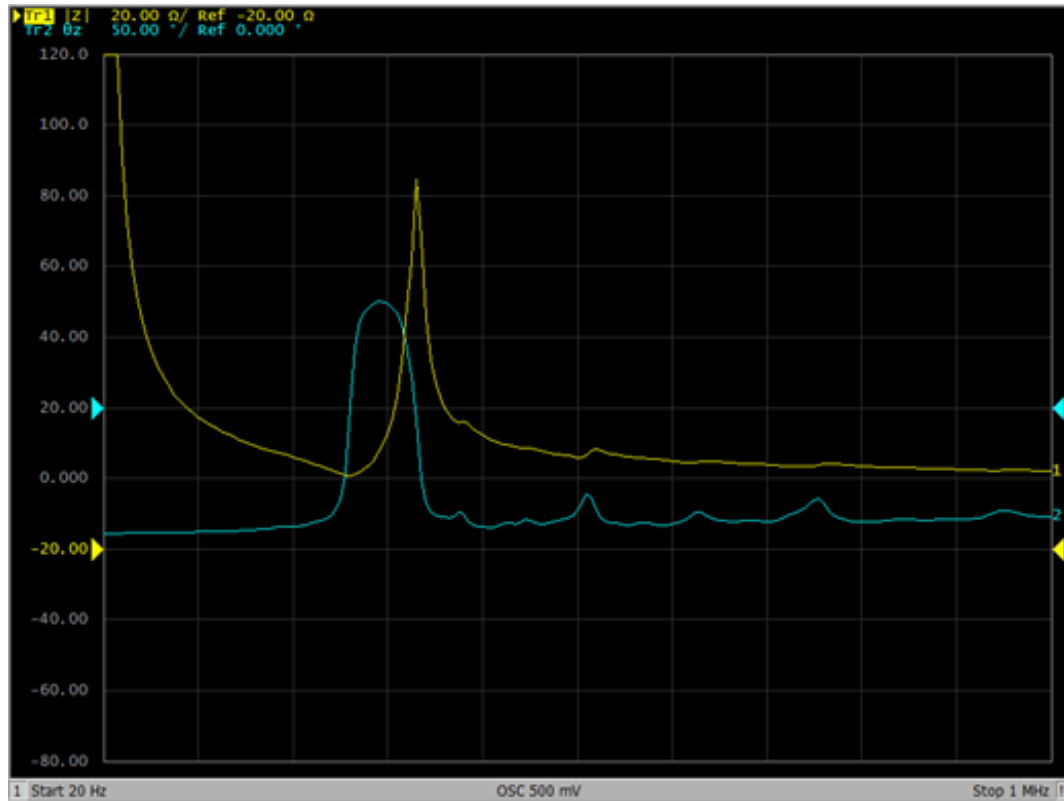


Figure 3-17: An example of frequency sweep starting from 20 Hz to 1 MHz. The yellow and blue signals represent the impedance magnitude and impedance phase respectively

Table 3-4 shows the testing protocols designed for each stages of concept development. The experiments included single indentation and 300 s relaxation tests:

- **Stiffness variation test:** This test was intended to validate the method using the Network Analyser and PZT probe I and PZT probe II. This test assesses the changes in the resonance frequency Δf and impedance magnitude Δz of the excitation upon contact with silicon samples with shore hardness of full 980, 40, 50, 60, 70, 85 and 95. Each sample was indented three times and the frequency and impedance magnitude of the excitation before and after the contact was monitored and then averaged. The contact pressure was set to 4 N.
- **Force and stiffness variation tests:** To investigate the sensitivity of the Δf and Δz to the contact pressure, the tissue samples were indented up to force thresholds of 1 and 4 N. The samples were taken from two different sites on the

large intestine, rectum and transverse colon. Using PZT probe III, each sample was indented five times and the results of Δf and Δz were averaged for each segment and force level.

- **Stress relaxation tests:** This experiment was designed to explore the effect of tissue relaxation on the frequency and impedance responses of the excitation. The stress relaxation duration was set to 300 s. Eight sweeps of frequency were undertaken within this time, long enough to observe possible shift in frequency and impedance magnitude. The test was repeated five times at 1 N on the transverse colon.

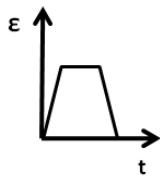
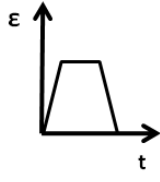
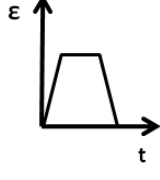
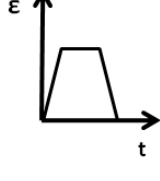
Concept development stages	Test	Samples	Protocol illustration	Objectives
Network analyser Agilent model E5061B, PZT probe I	Stiffness variation test	Silicon samples shores: full 980, 40, 50, 60, 70, 85 and 95		Observe the trend of Δf and Δz as a function of stiffness change
Data acquisition board NI PCI-6110, PZT probe II	Stiffness variation test	Silicon samples shores: full 980, 40, 50, 60, 70, 85 and 95		Observe the trend of Δf and Δz as a function of stiffness change
Data acquisition board NI USB-5133, PZT probe III	Force and stiffness variation	Pig rectum and transverse colon		Detect the load sensitivity of the acoustic impedance response of the tissue
Data acquisition board NI USB-5133, PZT probe III	Stress relaxation tests	Pig transverse colon		Observe the effect of tissue relaxation on the acoustic impedance response of the tissue

Table 3-4: Testing procedure for in-vivo characterisation of impedance properties of tissue

3.6 Data analysis

3.6.1 Linear modulus

Although tissue is non-linear, linear modulus is used in the literature [13, 22, 40, 71, 110] as a measure of deformation resistance or stiffness. The linear modulus of a tissue can vary from location to location and it is influenced by varying loading and boundary conditions [110]. The linear modulus is determined by computing the slope of the

linear-region of the stress-strain curve (region III in Figure 2-1) during the loading phase as shown by a red line in Figure 3-15-a. An approximated 'linear' region was computationally identified through an iterative algorithm implemented in Matlab (Mathworks). This evaluates the linearity (R^2) between the point of maximum stress and a variable start point. The start point is progressively moved back until $R^2 > 0.99$. The 'Polyfit' function is utilised for linear regression fitting [22, 40]. Linear modulus or stiffness is the derivative (slope) of the linear regression fit to the stress versus strain data [111].

Two linear regions are seen on the stress versus strain response of any viscoelastic soft tissues, toe-region I and linear-region II, as shown in Figure 2-1. Since the toe-region is not always detectable when high loads are applied to the tissue calculating the toe modulus has been neglected for mechanical properties characterisation. To determine the linear-region under indentation, nano-indenters have been employed but only to measure the surface mechanical properties rather than the material's bulk properties. Indentation methods are also limited in measuring the mechanical response of tissue due to the influence of the supporting plate/indenter tip, and tissue thickness. In addition, finding the linear-region of the tissue under indentation is challenging since there is no point of rupture to take as a reference similar to the tensile experiments. With regard to the effect of the metal supporting plate on the tissue mechanical response, some studies [117, 123] suggested to keep the peak depth to less than 9% of the specimen thickness to avoid any influence of the sample holder mechanical properties on the tissue response. This means that the tissue can only be strained up to the toe-region. The problem with this technique is that firstly this region cannot represent the level of stress that the tissue undergoes during surgical manipulation; and secondly since measuring the toe-region has always been neglected therefore there is no reference in the literature to compare the toe-region data.

As reported by [13, 22, 71] linear modulus can only yield the true elastic properties if the tissue is stretched under tensile examination and at a very fast strain-rate (to avoid any relaxation during the loading phase) or the tissue is subject to an infinitely low strain-rate (to allow viscoelastic dissipation before the linear region) In both cases the force applied to the tissue has to be large enough to reach its elastic range of strain before rupture. This relates to two facts, firstly performing the step like stretch introduces unwanted overshoot, vibration, and noise caused by fast strain-rates. Moreover, reduction of the speed to reach the ultimately small strain-rate is limited by

the capability of the mechanical testing equipment available in the laboratories. Also, only through using tensile techniques the tissue can this tissue be stretched to rupture. These may be the reasons this parameter has not been used widely as a valid representation of tissue stiffness. Therefore, in this research the validity of linear modulus as a true representation of tissue stiffness under indentation and tensile testing is investigated.

3.6.2 Stress relaxation model fitting

The models investigated in method 1 and 2 are the linear viscoelastic Wiechert 5-element model and the AQLV model explained in detail in Chapter 2.4.

3.6.2.1 Method 1: Wiechert 5-element modelling

In adopting a mechanical relaxation model, an investigation is needed to evaluate if the complex structure of the rectum can be represented as a linear viscoelastic material. Soft tissue is composed of elastic structures containing collagen and elastin fibres. They also comprise proteoglycans, the highly charged molecules which absorb water and keep tissue hydrated [124]. In the literature [22, 50, 95, 96, 125] models comprising a linear combination of springs and dashpots are commonly used to explain the viscoelastic stress-relaxation behaviour of soft tissues. Figure 3-18 shows a range of spring and dashpot combinations, progressively increasing in complexity from a Maxwell-model a to Wiechert 9-element model. The typical fit of models as obtained from the preliminary experiments on rectum tissue is illustrated in Figure 3-19. Observing the trend of model fitting visually, it is clear that the fits improve substantially from Maxwell model to Wiechert 5-element model and keep consistent for the remaining models. For quantitative evaluation of the models, the mean standard errors of the models were calculated as measures of goodness of fit.

From the results in Figure 3-20 it was evident that the Maxwell model presents the largest mean error followed by the Kelvin model, and then the Wiechert models. However, the value of fitting error does not differ much for Wiechert 5-elements to Wiechert 7-element and it increases for Wiechert 9-element. The increase of RMSE for the Wiechert 9-element suggests that the model is moving away from any sensible physical representation of the tissue properties. Maintaining a balance between the fitting error and model complexity, the Wiechert 5-element model was selected as the most appropriate model to represent viscoelastic behaviour of rectum.

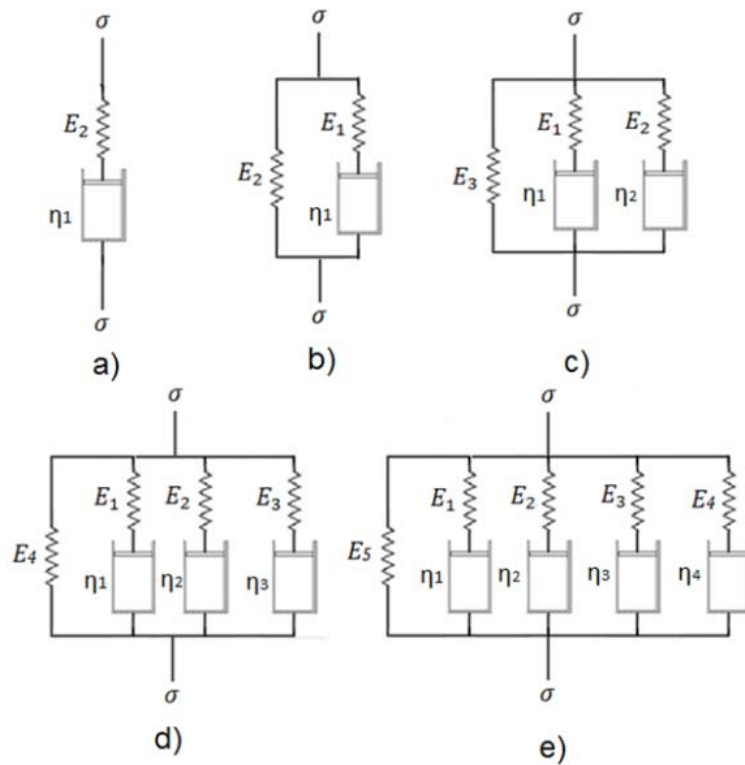


Figure 3-18: Viscoelastic models a) Maxwell, b) Standard Linear (Kelvin model), c) Wiechert 5-element, d) Wiechert 7-element, and e) Wiechert 9-element [12]

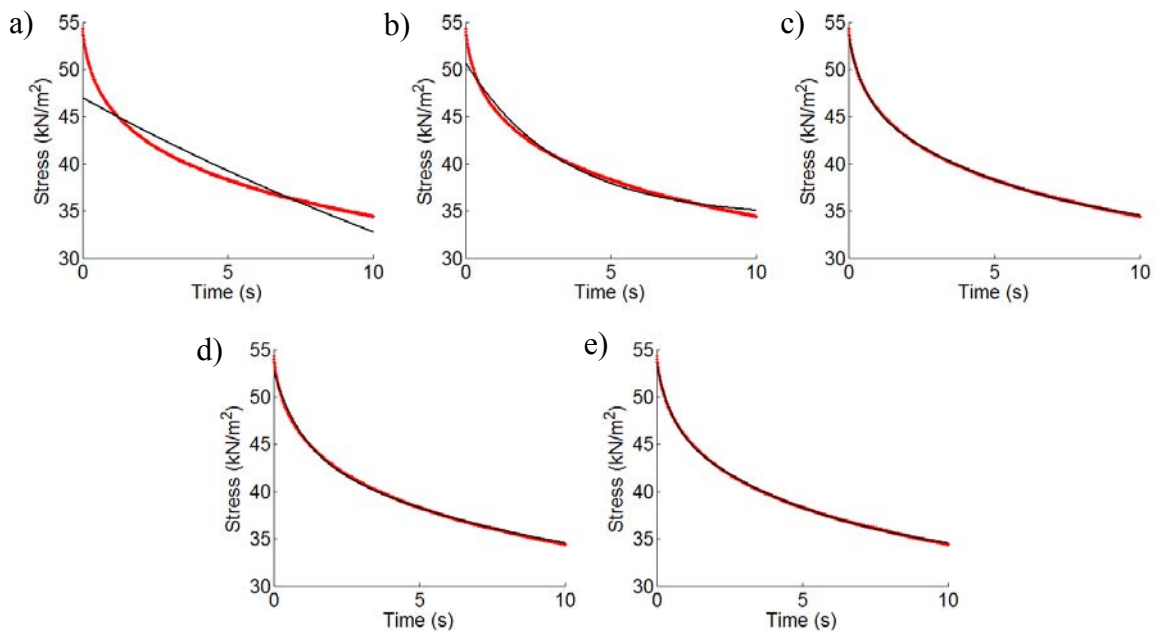


Figure 3-19: Typical stress relaxation response of soft tissue fitted to a series of viscoelastic models presented in Figure 3-18 . The models are a) Maxwell, b) Standard Linear (Kelvin model), c) Wiechert 5-element, d) Wiechert 7-element, and e) Wiechert 9-element.

From the results in Figure 3-20, it was evident that the Maxwell model presents the largest mean error followed by the Kelvin model, and then the Wiechert models.

However, the value of fitting error does not differ much for Wiechert 5-elements to Wiechert 7-element and it increases for Wiechert 9-element. The increase of RMSE for the Wiechert 9-element suggests that the model is moving away from any sensible physical representation of the tissue properties. Maintaining a balance between the fitting error and model complexity, the Wiechert 5-element model was selected as the most appropriate model to represent viscoelastic behaviour of rectum

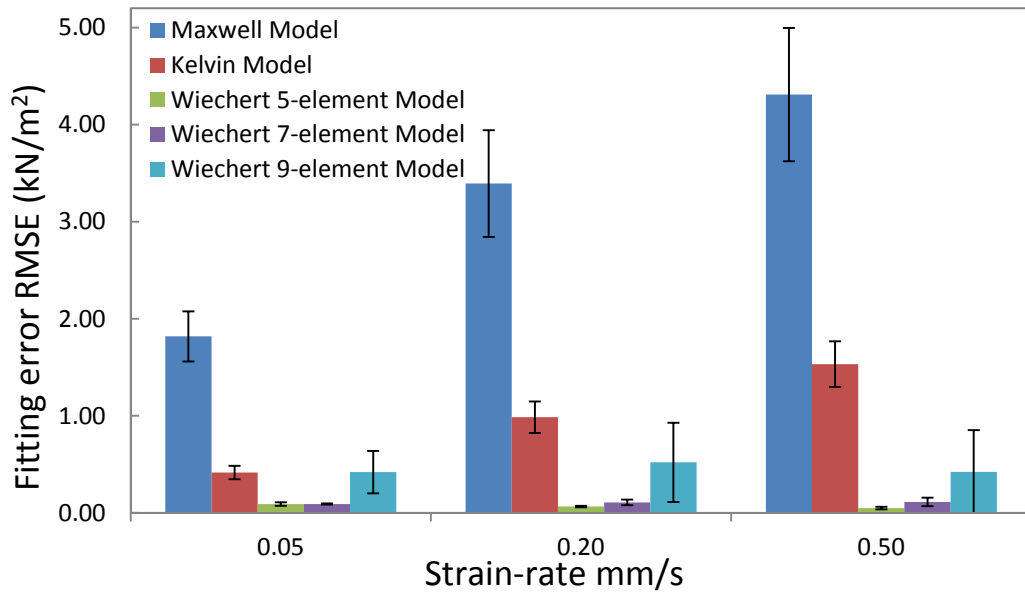


Figure 3-20: Mean error \pm SD of the viscoelastic models. From left to right: Maxwell Model, Kelvin Model, Wiechert Model 5, 7, and 9 elements.

Ideally, the Wiechert 5-element model parameters are determined from an instantaneous step in the strain or an infinitely low strain-rate since the model does not account for the relaxation that occurs during the loading phase. The above statement can be explained better in terms of spring and dashpot representation of the tissue as shown in Figure 2-31. Under unit step stretch only the three springs in parallel are activated whilst the two dashpots are still. This way the linear region is only subjected to the elastic response of the tissue and the stress relaxation phase covers the full viscoelastic response through relaxation of the spring and extension of the dashpot. On the other hand, stretching the tissue at a very slow rate allows to strain both springs and dashpots simultaneously therefore the viscous response dissipates fully before the linear region, and linear modulus yields pure elastic response. The stress relaxation phase then captures the viscoelastic response of the tissue through relaxation of all the spring and dashpots. However, experimentally achieving a step change in the strain or an infinitely

low strain-rate is not feasible. Even if a rapid step-like change in the strain is assumed to represent an instantaneous stress response as mentioned in [126, 127] there are still various challenges including tissue damage, overshoot and vibration [23]. Studies [22, 96, 117] performed 1-2 s of loading duration and modelled the tissue employing the Wiechert model. Hence, in this research 1-2 s of loading was assumed to be a good approximation of a step-like change in the strain.

3.6.2.2 Method 2: AQLV modelling

As mentioned in Chapter 2.4, the adaptive QLV (AQLV) can represent the tissue more sufficiently as it takes into account the influence of strain history on the relaxation response and unlike the linear models it can be used for tissue response prediction for different levels of loading strain. Therefore, in method 2 the experimental data were fitted to this model and compared to the results obtained from the linear Wiechert 5-element model fitting. Here similar to Nekouzadeh *et al.* [23] three Maxwell models were employed for the shape functions $g_i(t) = e^{-t/\tau_i}$.

To identify the optimum time constants which yields the best fit to the relaxation responses the following technique inspired by [99] was used. First, the highest time constant of 300 s was picked as τ_3 . Then using equally spaced logarithmic scaling, the other two time constants are determined as $\tau_2=30$, and $\tau_1=3$. Fixed time constants are identified so to help making the comparison between different samples easier.

3.6.3 Model fitting

Model fitting was conducted using a Least Squares minimisation method (Lsqnonlin) in Matlab software. Lsqnonlin is based on point by point minimisation of the error between the measured stress $\sigma_m(x)$ and the predicted stress $\sigma_p(x)$. The error function is calculated as the root mean square of the residual (i.e. the difference between the measured stresses and the fit):

$$\text{Error} = \sqrt{\sum_p (\sigma_m(x) - \sigma_p(x))^2 / n} \quad 1)$$

3.6.4 Viscoelastic ratio

The ratio of the instantaneous modulus E_0 and equilibrium modulus E_3 is used as the overall extend of relaxation $VR= E_3/ E_0$. $VR=0$ is an indication of a perfectly viscous

material and VR=1 represents a perfectly elastic material and intermediate values specify a viscoelastic solid. [64, 117]

3.6.5 Data normalising

A normalising method has been proposed to examine the strain dependency of the large intestine. In this method first the stress relaxation data are normalised using the reduced relaxation function $R(t)$. This method has been frequently employed in many studies for examining the strain history dependency of soft tissue [74, 101, 114]. The function subtracts the stress by the final stress and divides it by the total amount of relaxation.

$$R(t) = \frac{\sigma(t) - \sigma(\text{end of relaxation})}{\sigma(\text{start of relaxation}) - \sigma(\text{end of relaxation})} \quad 2)$$

3.6.6 Statistical analysis and data representation

An unpaired t-test was performed for each specimen to explore any significant differences between the data at different tissue hydration levels and fiber orientations. Significance was considered for $p \leq 0.05$. The data obtained from repeated interaction tests are all expressed as average \pm SD since the data only represents three samples. For the results which includes more than three samples the data are represented in box plots so to observe the true distribution of dataset.

3.6.7 Acoustic impedance response noise reduction

As explained in Chapter 3.5.3 the minimum or maximum peaks of the detected excitation signal were detected to measure the shift in the impedance magnitude and resonance/anti-resonance frequencies before and after contact. Figure 3-21 demonstrates an example of the unwanted noise in such signal created due to possible vibration introduced from the MMC rig. In order to smooth the signal for detecting the resonance peak a post processing technique was used to smooth the signal. The red line on the curve in Figure 3-21 represents a 10th order polynomial fit providing the best fit for the signal at its minimum peak.

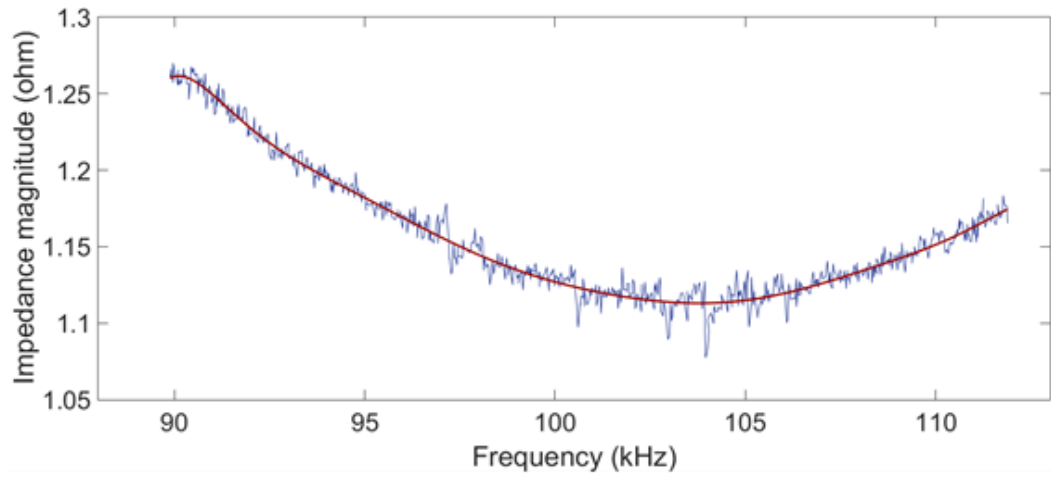


Figure 3-21: An example of the noise in the detected excitation signal (blue lines) and the polynomial fit for peak detection

Chapter 4. Mechanical characterisation of the rectum under indentation using the MUST rig

4.1 Introduction

Table 2-1 in the literature review summarises the existing studies that have been conducted on the mechanical properties of the large intestine, including the rectum. In general, there is a lack of experimental data on the mechanical properties of many segments of human/animal large intestine and in particular rectal tissue. In addition, there is no standardised measurement protocol upon which the existing data has been obtained and analysed.

Several studies have characterised the effect of repeated loading and relaxation on the time-dependent response of other tissues such as collagen or skin [50, 96], yet this effect has not been widely studied for the large intestine. Also, according to Chapter 2.5.4 there is a difference of opinion on the effect of the varying indentation speed on the mechanical and viscoelastic properties of the soft tissue where only one of these studies examined this effect on the stiffness of the large intestine. Therefore, in this regard both the above effects need to be examined to fill gaps in the literature.

4.2 Test objectives

This chapter delivers two novel aspects to address the dearth of knowledge on the rectum tissue properties in the literature: 1- a methodology based on indentation to characterise tissue properties, and 2- quantification of an initial set of rectal tissue mechanical properties acquired using this method. It is aimed to consider the effects of varying interaction speed by varying the applied strain-rate, repeated interaction through multi-cyclic tests and intra-tissue variation tests to determine the variation in behaviour across different regions of the rectum. The data analyses focus on identifying the linear modulus of the rectum which has been used as a simple approximation of the tissue stiffness together with a more detailed mechanical model that can describe the stress relaxation behaviour of the rectum.

4.3 Methods

The full description of tissue preparation and instrumental set-up were given in Chapters 3.2.1 and 3.3.1. Before running each experiment, the desired maximum and minimum force thresholds, the approaching loading and unloading rates, and the

relaxation duration have to be set in the MUST rig. Table 4-1 details these settings for each experiment:

Experiment	Location on the tissue	Max. force N	Strain-rate mm/s	Relaxation Duration s	Cycle iteration	Sampling rate Hz
Repeated interaction test	One indentation on each segment	1	0.5	10	20	100
Strain-rate variation test	One indentation on each segment	1	0.05, 0.2 & 0.5	10	20	100
Intra-rectal tissue variation test	Three indentations on each segment	1	0.5	10	1	100

Table 4-1: Summary of the experimental set-up for each experiment

Figure 4-1 summary indicates where the MUST Tester is placed among all the other devices in terms of the maximum applied stress-strain; thus to help this study understand capability of the MUST Tester for characterising mechanical properties of colon.

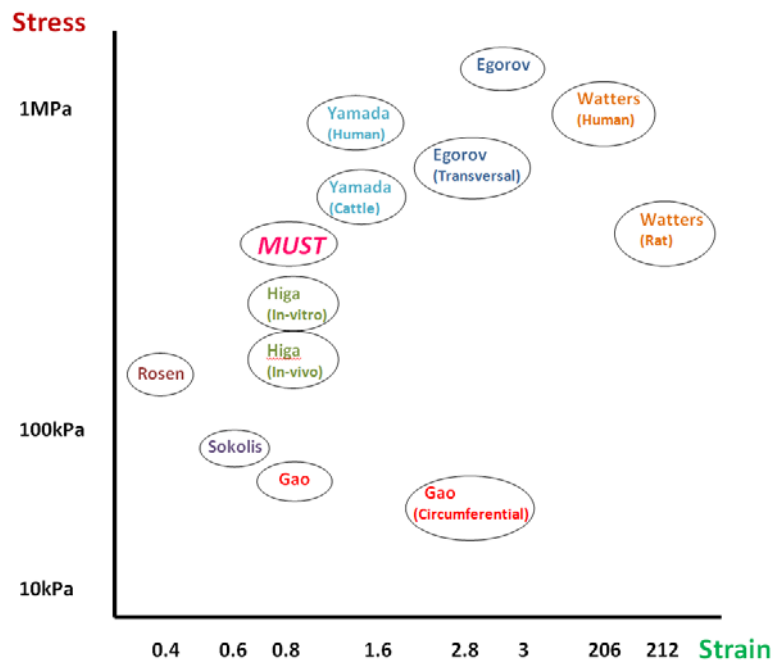


Figure 4-1: MUST Tester stress-strain relationship measurement capability to other colon mechanics studies [7, 8, 10-14, 41]

4.4 Results

4.4.1 Repeated interaction test

The typical pattern of loading and stress relaxation for a sample of porcine rectum during 20 indentations is illustrated in Figure 4-2 and Figure 4-3, respectively. In Figure 4-2, the cycles tend to progressively shift to the left, showing decreased strain at the peak force, followed by a plateau in this effect after the initial five indentations.

However, in some cases from cycles five onward some of the cycles have a small shift to the right instead of left. A similar trend is observed for the stress versus time data in Figure 4-3, where the tissue relaxes less cycle by cycle, with a pronounced effect over the first five cycles and then a plateauing in the remaining cycles (The red arrow indicates the direction of cycle progression).

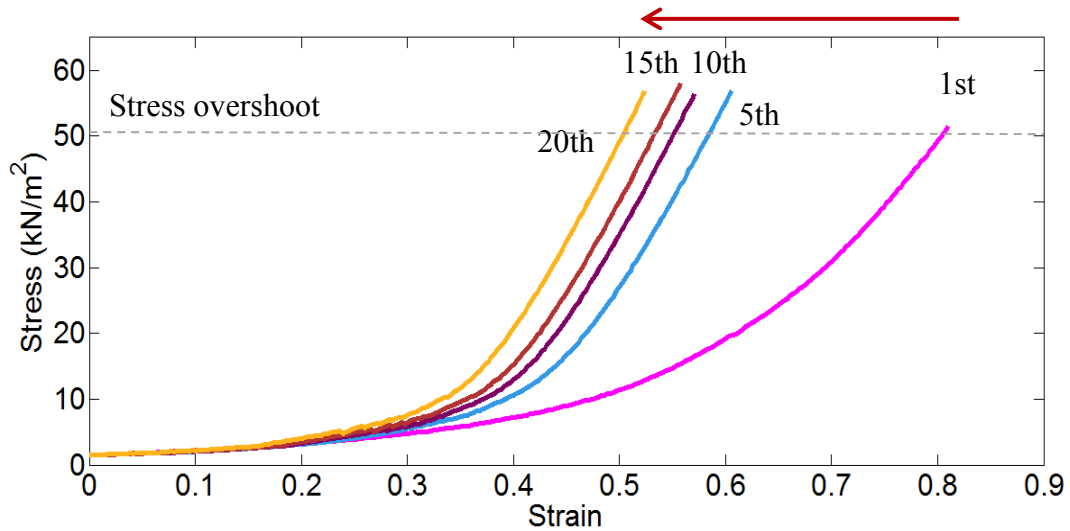


Figure 4-2: Typical loading stress-strain curves of porcine rectum where the value of strain is normalised to the first point of contact. Red arrow shows the direction of cyclic progression.

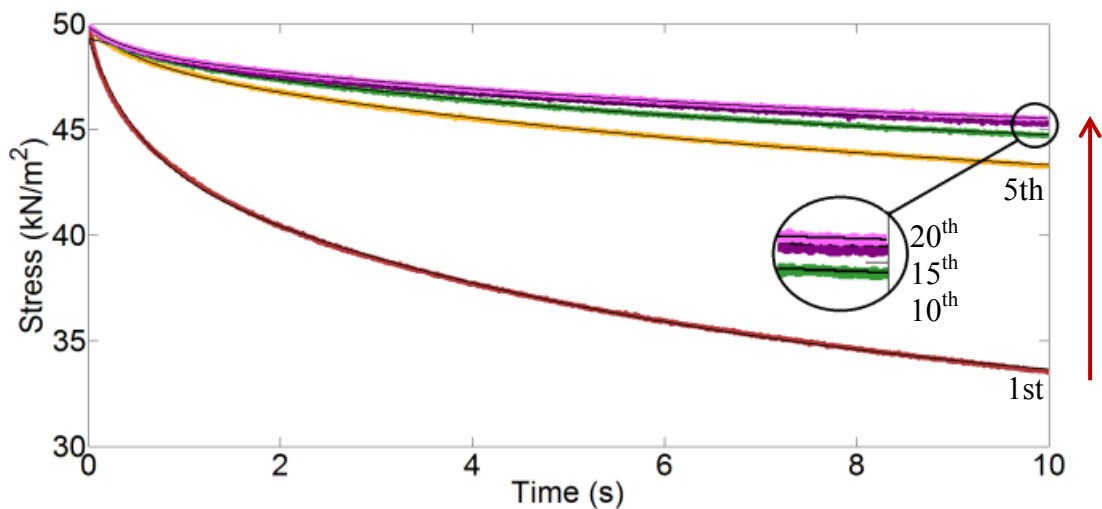


Figure 4-3: Typical stress relaxation curves (coloured lines) and Wiechert 5-element fits (black lines) for 20 consecutive indentations at 0.5mm/s strain-rate in segment E. Red arrow shows the direction of cyclic progression

Evaluating the sensitivity of the linear modulus to the tissue stiffness, the shift of strain at the peak stress for every five consecutive cycles in Figure 4-2 was tabulated against its corresponding linear modulus shift in Table 4-2. It is noticeable that linear modulus is sensitive enough to detect very small strain shifts, for example, the slight increase of linear modulus shift from -8.43 to -6.46 between cycles 5-10 and 10-15 corresponds to a

very small strain shift of 0.03. However, it is evident that the linear modulus is unable to correspond to the shift in strain. An inaccurate judgment of stiffness was made by linear modulus shift between cycles 15-20 and 10- 15 where increase of cycles from 15-20 resulted in lower linear modulus shift for higher strain shift.

The results in Table 4-2 show that the shift of peak strain to the left for the first five cycles is significantly higher than that of the remaining cycles. The responses match much more closely after the fifth cycle and hence despite the very small changes between the remaining cycles it is assumed that the steady state is reached by the fifth cycle.

Cycle numbers	Shift in strain at 50kPa	Linear modulus shift (kN/m ²)
From cycles 1-5	-0.20	87.83
From cycles 5-10	-0.04	8.43
From cycles 10-15	-0.01	6.46
From cycles 15-20	-0.03	1.27

Table 4-2: Typical shift of linear modulus and strain for every five cycles. The negative strain shift means the shift of cycles to the left direction (i.e. lower strain) on the strain-stress graph

The coefficients of the Wiechert model for the data shown in are given in Table 4-3. The time-independent modulus (E_3) increases between cycles 1-5 and then it changes slightly for the remaining cycles. This implies that the tissue becomes stiffer under repeated interaction. Interestingly, the difference between the E_3 values for every five cycles is in the same order as the shift of peak strains in Table 4-2. Unlike E_3 , the time-dependent moduli (E_1 and E_2) decrease with the progression of cycles. This is whilst the time constants τ_1 and τ_2 remain relatively constant.

Cycle No.	E_3 (kN/m ²)	E_1 (kN/m ²)	E_2 (kN/m ²)	τ_1 (s)	τ_2 (s)
1	31.3	5.3	12.6	0.5	5.9
5	41.2	1.6	7.0	0.6	8.5
10	43.5	1.3	5.0	0.5	7.2
15	43.6	1.3	5.0	0.5	7.8
20	44.4	1.2	4.3	0.5	7.6

Table 4-3: The Wiechert coefficients at 0.5 mm/s strain-rate in section E

The results in Figure 4-2 and Figure 4-3 are presented in terms of linear modulus and viscoelastic ratio in Figure 4-4 and Figure 4-5. Figure 4-4, demonstrates the linear modulus (gradient) of the loading portion and its significant rise (by a multiple of ~2.5) from the first to the second cycle. After cycles 5-6, the linear modulus varies marginally from cycle to cycle implying that the behaviour of tissue becomes more consistent.

However, the linear modulus distribution after 5th cycle does not agree with the consistence decrease of strain in Figure 4-2.

The typical trend of the viscoelastic ratio over repeated indentations is shown in Figure 4-5. The graph shows that the tissue becomes more elastic during stress relaxation, as there is a progressive increase in the amount of viscoelastic ratio with each indentation.

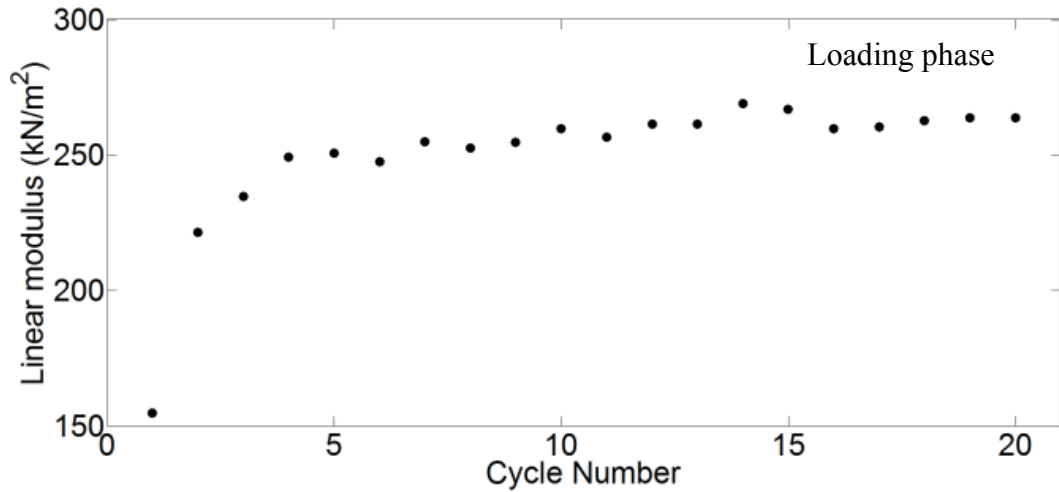


Figure 4-4: Repeatability effect on linear modulus obtained from the loading phase at 0.5mm/s strain-rate in segment E

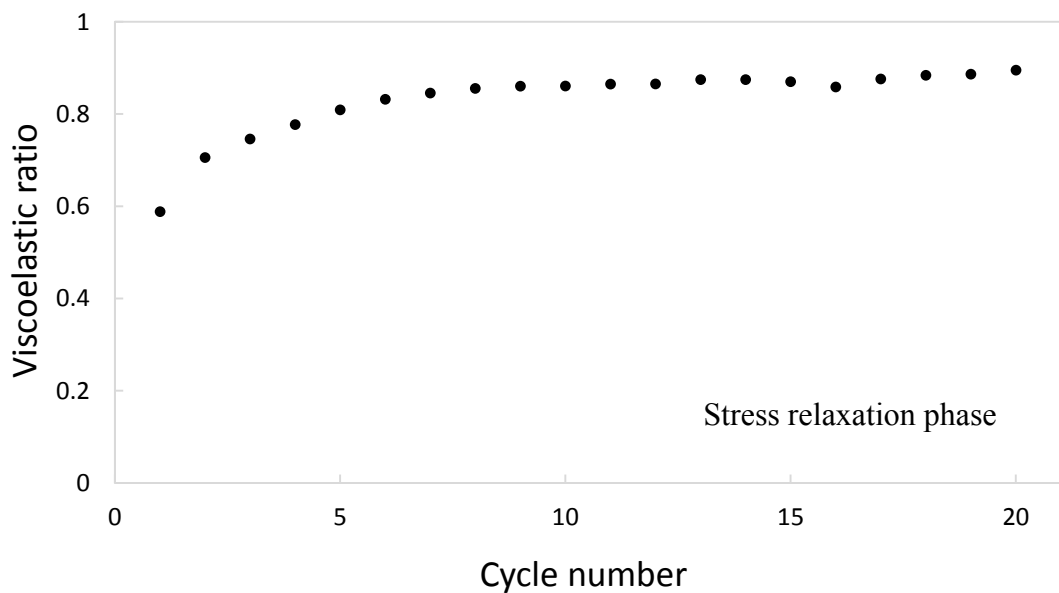


Figure 4-5: Typical trend of viscoelastic ratio obtained from the indentation test

4.4.2 Strain-rate variation test

The effect of varying strain-rate on the stress-strain and stress relaxation responses was investigated. The average \pm SD linear modulus values calculated from the slope of the stress-strain curve were 144 ± 44 kN/m², 139 ± 39 kN/m² and 144 ± 44 kN/m² for strain-rates 0.05, 0.2, and 0.5 mm/s implying that linear modulus is not strain-rate dependent.

Figure 4-6 shows the typical stress versus strain response of tissue under varying strain-rate. The Figure 4-6-a shows that the lower the strain-rate the higher the strain to reach the peak stress. In Figure 4-6-b two regions of interest on the curves are pointed out by dashed circles. The dashed circle 1 illustrates that the higher the strain-rate the more upward curvature within the viscoelastic region of stress-strain response. Dashed line 2 indicates a shift in peak strains to the left as shown by the red arrow. Both observations signify the fact that the tissue response is more elastic under higher loading rate.

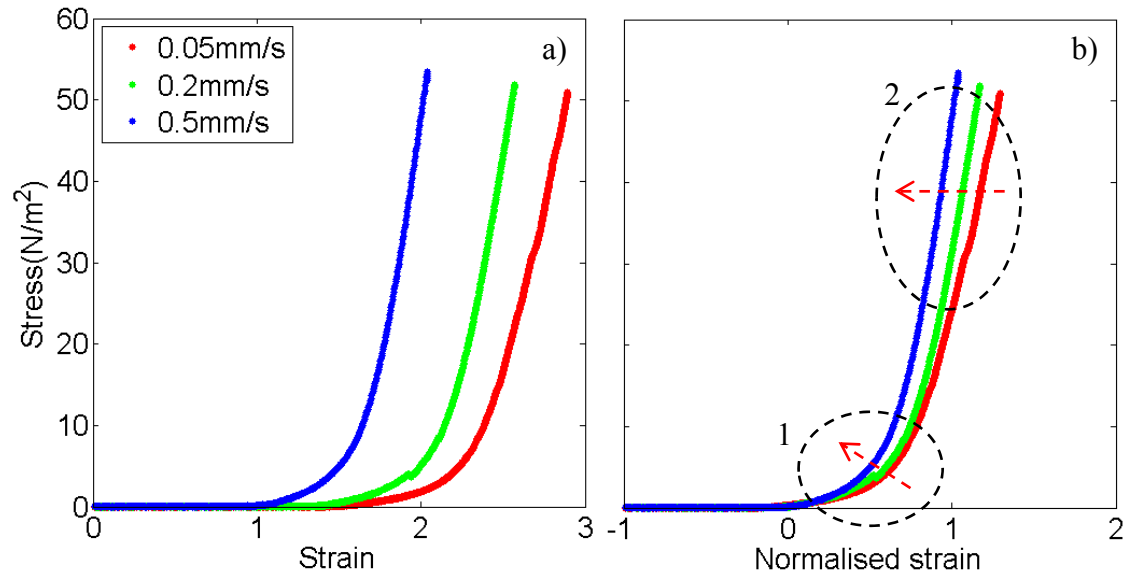


Figure 4-6: Typical a) stress versus strain response of the large intestine at varying strain rate, b) the strain was normalised to compare the gradients of the curves

To get some qualitative insight into the sensitivity of the relaxation response to strain-rate, the percentage of stress drop for the first cycle of the multi-cycles tests for the entire dataset was calculated and averaged. The results show that faster strain allows for greater stress relaxation resulting in 23%, 30% and 36% of relaxation drop for 0.05mm/s, 0.2mm/s & 0.5mm/s strain-rates, respectively.

Figure 4-7 depicts the typical trend of normalised stress relaxation response for the 5th cycle where the tissue response to the indentation has settled after preconditioning. Two phases of relaxation were observed for the high strain-rate of 0.5mm/s. Initially, a rapid fall of stress is seen for the first 1-2 second of relaxation. This is followed by a steady decay of stress for the rest of duration. The low strain-rate of 0.05mm/s, however, shows a steady decay of stress throughout the whole relaxation period whilst the medium strain-rate of 0.2mm/s falls between the two with a tendency towards the trend in the 0.5 mm/s curve. The model coefficients obtained from the Wiechert model fitting

to these responses at the three strain-rates are presented in Table 4-4. Each response shows a drop in time constants τ_1 and τ_2 as strain-rate increases which indicate faster overall relaxation. E_1 increases with the strain-rate for all the segments. This is while the majority of data show a reduction in E_2 as the strain-rate increases. E_3 (which represents the stress at the end of the relaxation process) shows no consistent dependency to the strain-rate which suggests that varying strain-rate does not affect the elastic properties of the tissue. The overall goodness of the model fitting determined by the root mean square error (RMSE) shows better fit for higher strain-rate.

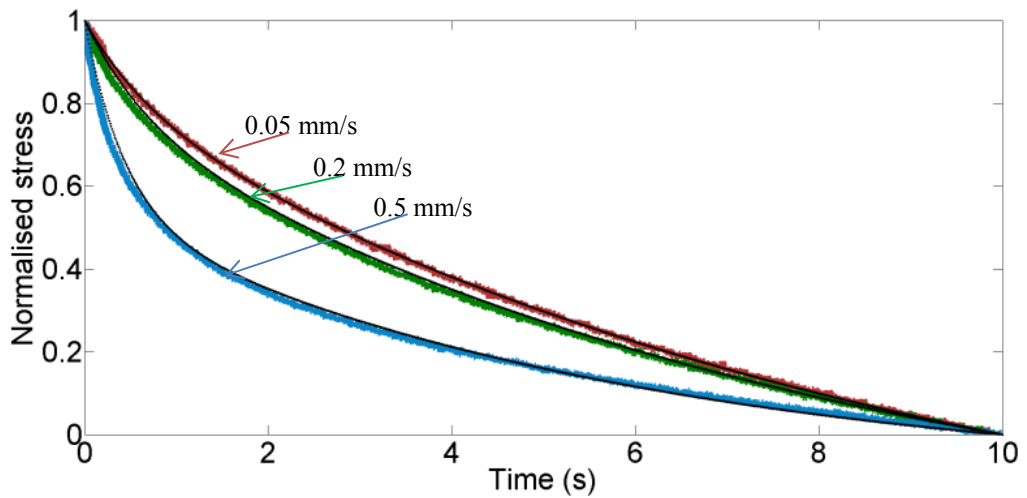


Figure 4-7: The typical trend of normalised stress relaxation response at three strain-rates of 0.05mm/s (red), 0.2mm/s (green) and 0.5mm/s (blue) for the 5th cycle of repeated interaction test in section G. The black line represents the Wiechert fit for the curves

	E_3 (kN/m ²)	E_1 (kN/m ²)	E_2 (kN/m ²)	τ_1 (s)	τ_2 (s)	RMSE
0.05 (mm/s)	42.3	1.1	7.5	0.7	8.8	0.087± 0.009
0.2 (mm/s)	40.9	1.8	7.2	0.6	8.2	0.065± 0.007
0.5 (mm/s)	41.2	4.4	6.2	0.4	5.8	0.049±0.013

Table 4-4: The Wiechert model coefficients of the 5th cycles at three strain-rates from the repeated interaction test in section G

4.4.3 Intra-rectal tissue variation test

The average linear modulus \pm SD of 144 \pm 44 kN/m² is obtained for 0.5 mm/s strain-rate. The linear modulus varies between 77 and 230 kN/m² and shows no spatial dependency on the location along the rectum therefore it is averaged. However, a strong influence of tissue thickness on the linear modulus of the tissue is observed where higher thickness results in an increase of linear modulus value (Figure 4-8).

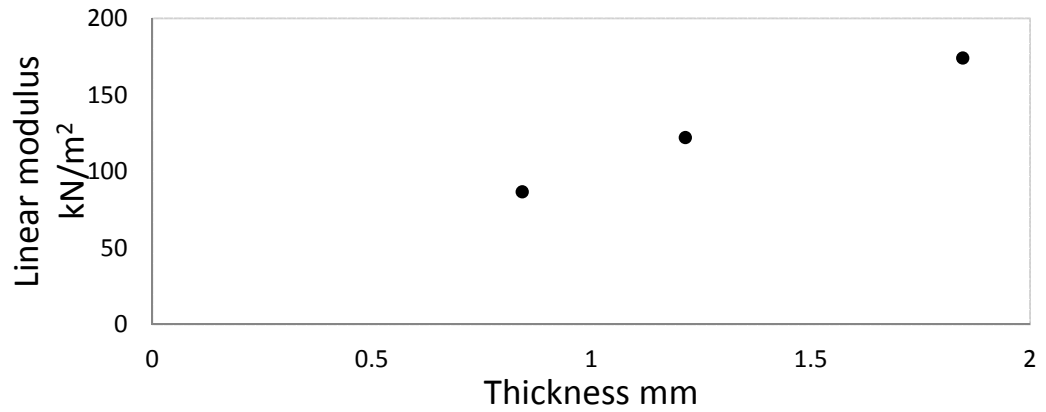


Figure 4-8: Linear modulus versus thickness measurements for three spatial indentations in segments A at 0.5mm/s strain-rate. This pattern is consistent for all the other segments

4.5 Chapter summary

Table 4-5 summarises the key points in this chapter. The three main objectives in this chapter were to investigate:

- The effect of repeated interaction on the tissue response during tool-tissue interference
- The effect of varying speed of interaction
- The anisotropic behaviour of the large intestine.

As well as the specific results obtained for each test, the sufficiency of the designed testing protocol was also evaluated, so the next set of experiments are designed and modulated appropriately.

Objective	Method	Results
Effect of repeated interaction on tissue properties	20 consecutive multi-cyclic indentations on each segment of the rectum	<ul style="list-style-type: none">• Tissue becomes more elastic and stiffer cycle by cycle until it reaches a steady state.• Preconditioning is necessary to stabilise the tissue response similar to the in-vivo condition
Effect of varying strain-rate on tissue properties	Strain-rate variation test on each segment of the rectum at 0.05, 0.2 & 0.5 mm/s	<ul style="list-style-type: none">• Faster the strain-rate, greater the stress relaxation response.• The loading phase should be short and fast to observe the full relaxation response during the relaxation phase
The variation of tissue behaviour along the length of rectum	Single indentation with no preconditioning on each segment of the rectum	<ul style="list-style-type: none">• No spatial dependency of stiffness and stress relaxation responses on the location along the rectum• Linear modulus should not be used as a robust representation of elastic modulus

Table 4-5: An overview of Chapter 4 aims and results

Chapter 5. Mechanical characterisation of the large intestine under indentation

5.1 Introduction

In the previous chapter the mechanical properties of rectal tissue are investigated. Porcine rectums were tested in air and the effect of varying strain-rates, repeatable indentation and intra-rectum variation of tissue response were examined. Tissue samples were kept in air as it replicates open abdomen/prolong surgeries or CO₂ insufflation colonoscopy procedure [116]. However, in order to investigate tissue properties during laparoscopy surgeries where the tissue natural hydration is preserved or hydro-colonoscopy procedures where extra liquid is inserted into the organ, it is important to quantify the effect of varying hydration levels on tissue response to indentation. As explained in the literature review (Chapter 2.3), in addition to varying strain-rate strain history has also been found to influence the response of tissue during stress relaxation [50, 74, 90, 114, 115]. It is essential to observe this effect as it may lead to a better model prediction of the tissue relaxation behaviour.

5.2 Test objectives

In this research a series of indentation tests were conducted using a testing protocol modified based on the results obtained in Chapter 4. These amendments include:

- Performing the tests in hydrated conditions as well as in air so to observe the differences in tissue response
- Preconditioning the tissue for four cycles which allow the tissue response to settle and so the fifth cycle represents the tissue behaviour in the in-vivo state
- Expanding the testing area to cover the whole large intestinal track, so to observe the variation of behaviour along the full length of the tissue
- Increasing the relaxation duration to 300 s in order to observe the full relaxation process where the relaxation response reaches steady state. This allows for a fair assessment of the relaxation constants belonging to the two relaxation processes
- Using a low strain-rate of 0.1 mm/s to avoid unwanted overshoot, vibration and noise to the data

- Adapt a new viscoelastic model for predicting the response of the tissue. This model should be able to incorporate the strain history and strain-rate of the loading to the model prediction.
- Changing the experiment mode to strain control (was originally stress control) as it provides a better result comparison with similar studies.

5.3 Method

A new testing rig was developed to overcome several limitations of the MUST rig such as handling only up to 60s of relaxation time, maximum force threshold of 1N and maximum indentation speed of 0.5 mm/s. The new rig designed with the following design considerations:

- No limitation on the relaxation duration
- Up to 6N force threshold
- Up to 25 mm/s strain-rate
- Run in various modes: Indentation and tensile modes
- Portable and user friendly for in-vivo testing in a theatre

Full details of the tissue preparation and instrumental set-up were provided in 3.2.2 and 3.3.2.

Experiment	Location on the tissue	Condition	Max. % strain	Strain-rate mm/s	Relaxation Duration s	Cycle iteration	Sampling rate Hz
Intra-large intestine variation test	Three indentations on each segment	In PBS solution	50%	0.1	300	1	60
Repeated interaction test	One indentation on transverse colon	In air and PBS solution	50%	0.1	300	10	60
Stepwise strain test	One indentation on transverse colon	In PBS solution	20%, 35%, 50% & 65%	0.1	300	1	60

Table 5-1: Illustration of the main features of the experimental set-up

5.4 Results

5.4.1 Length, circumference and thickness measurements

In addition to investigation the mechanical properties, characterising the geometry of the large intestine for creating tissue-like phantoms with realistic size and dimension is crucial for the evaluation of new surgical tools. Therefore, the length and circumference of each large intestinal segment was measured and the mean \pm SD are given in Table 5-2.

	Rectum	Descending	Transverse	Ascending	Cecum
Length (Mean \pm SD)	59.1	144.4	144.4	144.4	26.9
Circumference(Mean\pm SD)	7.1	8.3	10.8	14.3	26.1

Table 5-2: The average value of length and circumference of 9 porcine large intestines for five segments

The thickness of the large intestines ranged from 0.36 to 2.52 mm as given in Figure 5-1. As shown in the graph, Thickness value varies the most in rectum segment. Likewise, the average thickness for rectum is higher than the rest of the segments. From descending colon to cecum the thickness varies between 0.36 to 1.36 mm whereas in rectum the thickness is ranged between 0.54 to 2.52 mm. This trend was clearly apparent during the experiments. The variation of the tissue thickness is due to the differences in size and age of the pigs. The thickness measurement can also lead to some valuable information regarding the tissue mechanical properties. In a study by Liu *et al.* [128] the influence of tissue thickness on the non-linear stress-strain relationship was investigated and different tissue response at various levels of tissue thickness was found [128]. This effect will be examined in the next section.

5.4.2 Intra-large intestine variation test

The distribution of the linear modulus obtained at various segments of large intestine is given in Figure 5-2. Similar to the thickness pattern, the rectum shows the highest variation of linear modulus ranged from 268 to 642 kN/m^2 , and the highest average linear modulus of 401 kN/m^2 . The upper and lower whiskers overlap each other in the segments, hence no particular trend in the distribution of the linear modulus among the 5 segments is observed. The overall linear modulus response varies largely between 123-643 kN/m^2 . Investigating the effect of tissue thickness condition on the mechanical stress-strain response, the linear modulus of the tissue is plotted against the measured thickness at each segment in Figure 5-3. The data for this plot are taken from the intra-

large intestine variation test. From the plot it is evident the spread of linear modulus values are in a good agreement with the trend of tissue thickness variation along the full length of the large intestine. This implies that thickness of the tissue has significant effect on stress-strain response of the tissue. The same trend was obtained from the indentation data in Chapter 4. This suggests a possible sensitivity of linear modulus to tissue thickness. The only other report supports this finding is by [128] in which the change of tissue thickness condition effects the non-linear stress-strain relationship (except for strains <6%). Zheng *et al.* [129, 130] recommended using an indenter's tip radius not more than 25% of the tissue thickness for the response of tissue to be independent of the thickness.

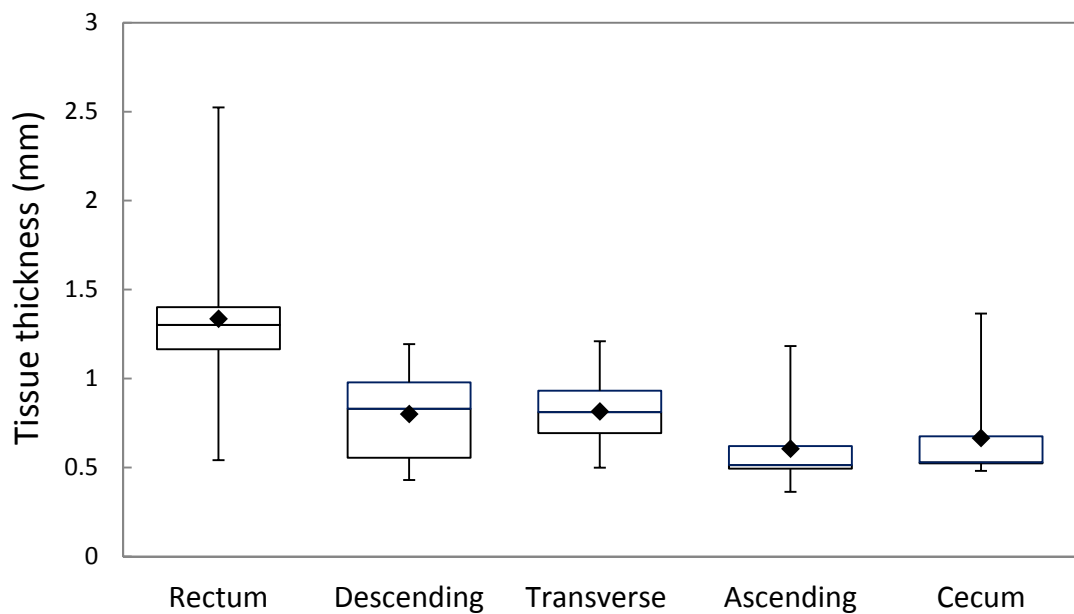


Figure 5-1: Box plot of the tissue thickness obtained in the indentation test for five segments

This may work for many tissue types like brain or liver with large thicknesses, but for the large intestine where the wall thickness can be as small as 0.5 mm at some locations, measuring the bulk properties of the tissue with an indenter's tip radius of less than 1 mm is complicated. Therefore, in the indentation tests here the effect of tissue thickness on the linear modulus is inevitable.

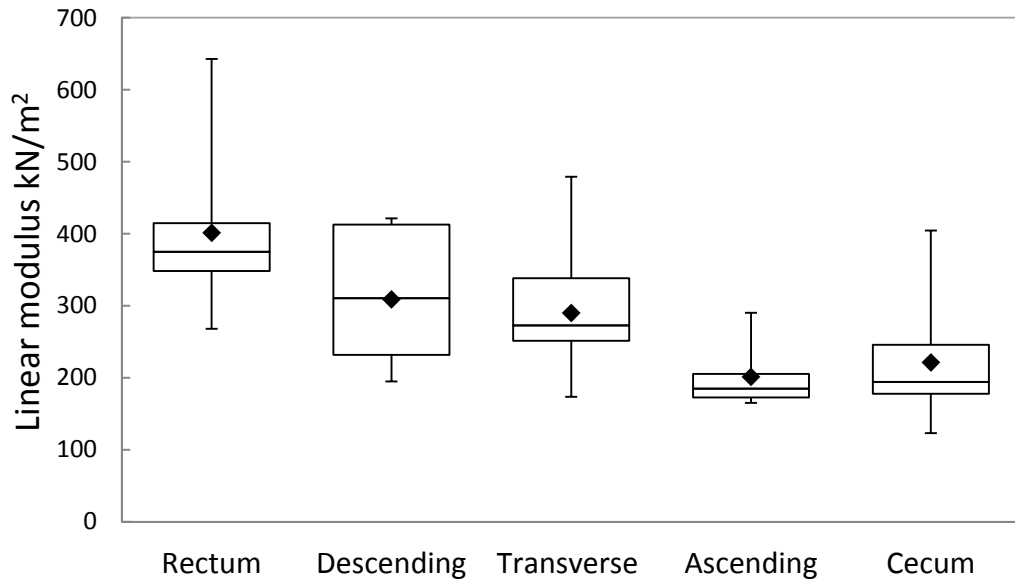


Figure 5-2: Linear modulus variation at five segments

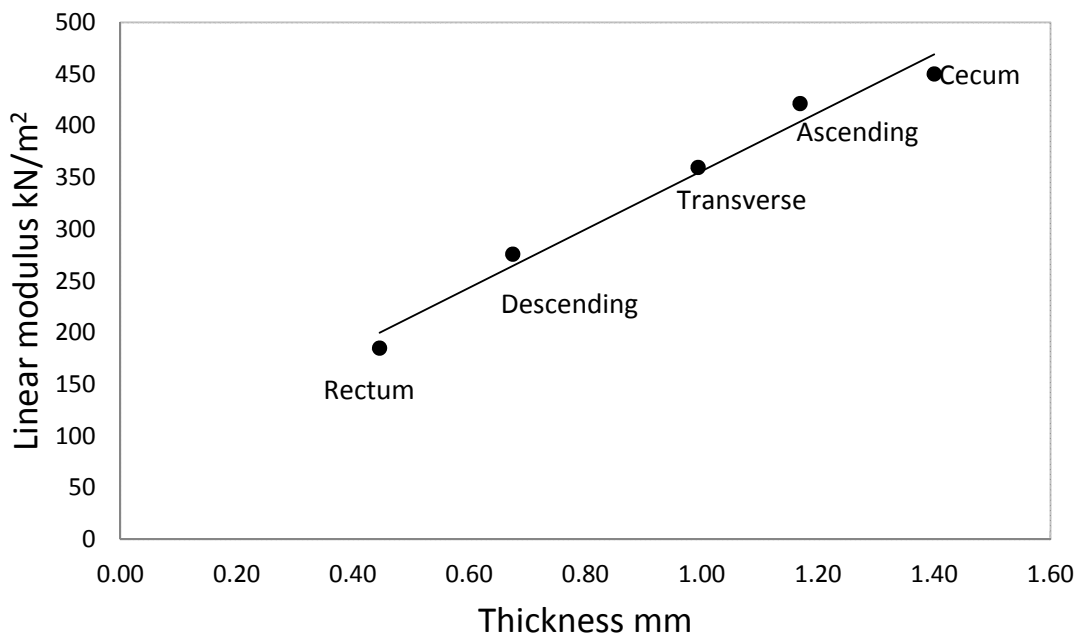


Figure 5-3: The plot of linear modulus versus tissue thickness at various segments of the large intestine. This correlation is consistent across all the data

Considering the variation of relaxation response among the 5 segments of large intestine, Figure 5-4 plots the spread of viscoelastic ratio [25] ranged from 0.00 to 0.27. In general the viscoelastic ratio exhibits low time-dependent deformation during the stress relaxation for all the segments i.e. tissue is largely viscous. The overall trend of viscoelastic ratio demonstrates a consistent distribution of this value among the segments.

Figure 5-5 shows an example of the AQLV model fitting on the experimental data. The average RMSE value was calculated to be 0.16 ± 0.03 . The same data was fit using the Wiechert model which result in an average RMSE value of 0.2 ± 0.05 . Both RMSE values are an order of magnitude higher than the results obtained in Chapter 4, due to the differences in the relaxation time between the two methods (10 s of stress relaxation for method I). Figure 5-5 depicts the relaxation process of two samples taken from different segments on the large intestine. Figure 5-5-a represent a sample of rectum indented to 50% strain. For this sample the loading phase took 2.7 s and the stress reached 120 kN/m^2 .

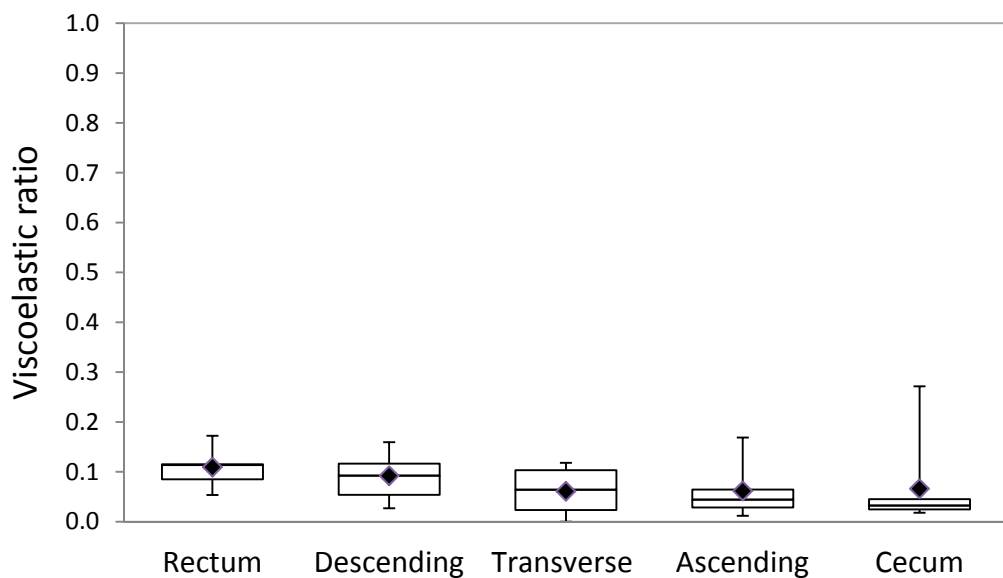


Figure 5-4: Viscoelastic ratio obtained from the indentation test

The second sample shown in Figure 5-5-b is taken from the ascending colon, and took 5.9 s to be fully indented by 50% strain where it reached 37 kN/m^2 . This difference in the loading duration is due to varying tissue mechanical properties and thickness in different locations of the tissue. It is noticed that the ascending sample relaxes very fast at the beginning of the period where the stress drops to over 80% of its initial value by the first 20 s and it reaches steady state after 50 s. This is whilst the rectum sample relaxes in much slower rate and does not seem to reach equilibrium within the relaxation phase (300 s). The graph also shows that rectum samples are stiffer than the ascending sample as the peak stress is three times greater for the rectum sample than the ascending sample. An averaging technique [122] was used to predict the mean of the AQLV parameters for the relaxation response of the three samples at each segment. In this technique each set of data is fitted to the model and the predicted stresses from all

the tests are averaged + SD. Then the averaged stress is plotted against strain and the model is fitted to this curve. The extracted parameters from model fitting are taken and presented in Figure 5-6 and Table 5-4. Each curve represents the mean of nine indentations in total, three indentations at each segments on three samples. As mentioned in Chapter 3.6.2 (Method 2), optimum time constants are deployed for model fitting to simplify the comparison between the segments.

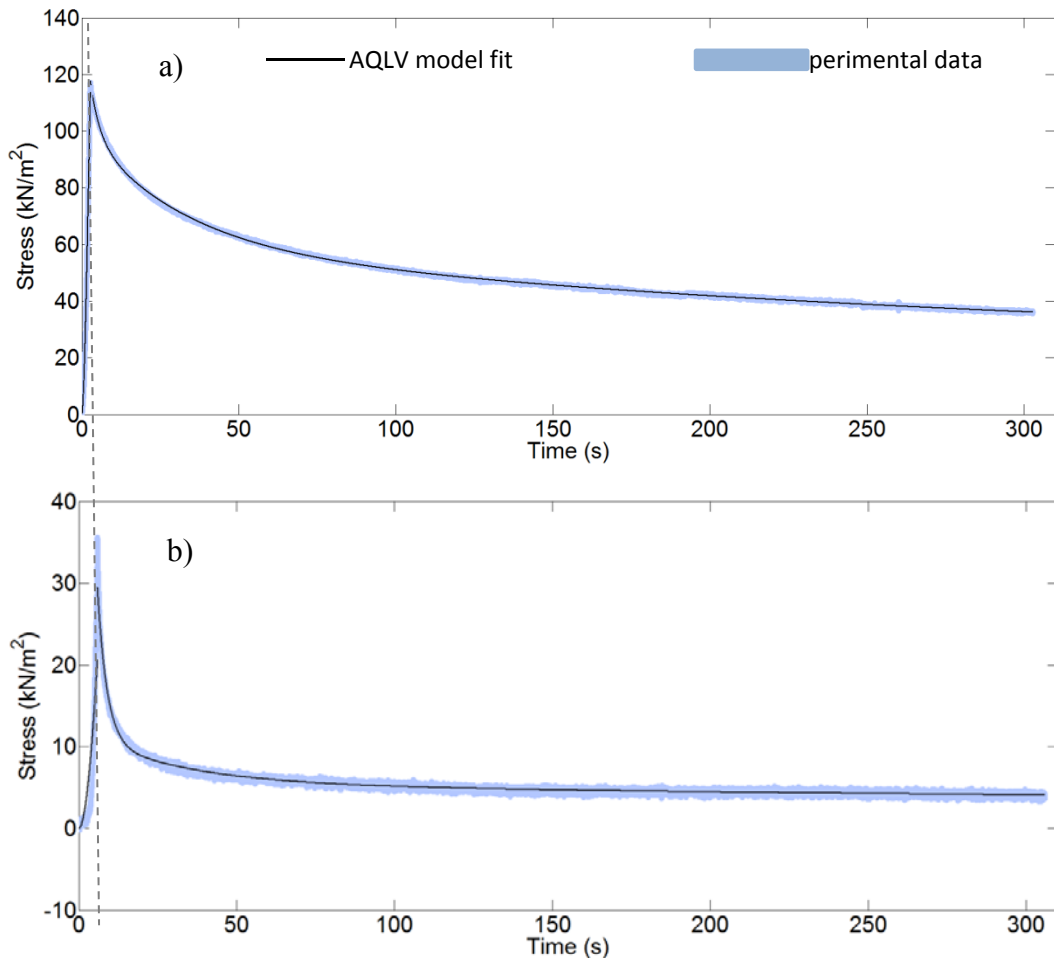


Figure 5-5: Typical AQLV fit to the stress versus time data of a) a rectum sample and b) an ascending sample during intra large intestinal indentation test. The black dash line separates the loading phase from the relaxation phase

AQLV parameters	σ_0 (kN/m ²)	k_1 (kN/m ²)	k_2 (kN/m ²)	k_3 (kN/m ²)	τ_1 (s)	τ_2 (s)	τ_3 (s)
Rectum	44.3	48.2	146.0	150.9	3.0	30.0	300.0
Ascending	0.6	24.2	19.0	8.7	3.0	30.0	300.0

Table 5-3: AQLV parameters of the model fitting to the relaxation data for the two specimens in Figure 5-5

The loading responses could not be averaged as the number of data points varies depending on the tissue thickness. Therefore, the force and displacement data length do not match between the samples.

As the results in Figure 5-6 show, the adjacent segments rectum and descending share very similar viscoelastic response to the hydrated indentation test. The same is observed for ascending and cecum segments. Higher stress was required to achieve 50% strain for rectum and descending followed by transverse compared to ascending and cecum, which suggests that tissue becomes less resistant to indentation force as progressing from rectum towards cecum. The average $\Delta\sigma$ for each segment starting from rectum to cecum are 79, 83, 76, 56 and 55 kN/m². It is noticed that both ascending colon and cecum have lowest values of the linear modulus and relaxation drop.

Similar to E_3 in Table 4-3, Table 5-4 shows that the equilibrium modulus σ_0 can represent the elastic properties of the tissue as it follows the same changes in the peak stress. The table also reveals that the equilibrium modulus σ_0 obtained in rectum is significantly higher than those obtained in cecum. Overall, the values of the equilibrium and elastic moduli σ_0 , k_1 , k_2 and k_3 , decrease segment by segment when moving from rectum to cecum. The coefficients of the AQLV are ordered as $k_1 > k_2 > k_3$ and $\tau_1 < \tau_2 < \tau_3$ where the most rapid stress relaxation modulus k_1 contributes to the fast time response of $\tau_1=3$ s. Likewise, the slowest stress relaxation modulus k_3 corresponds to the slowest time response $\tau_3=300$ s.

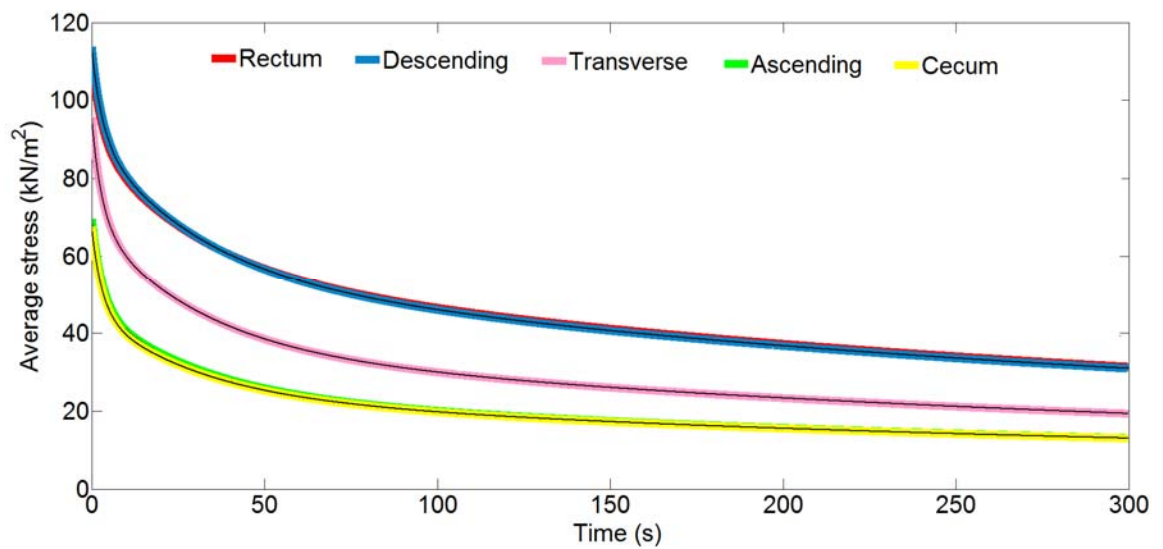


Figure 5-6: Exponential fit of the AQLV model (black lines) to the stress relaxation data. Optimum time constants are 3, 30 and 300 s

AQLV parameters	σ_0 (kN/m ²)	k_1 (kN/m ²)	k_2 (kN/m ²)	k_3 (kN/m ²)	τ_1 (s)	τ_2 (s)	τ_3 (s)
Rectum	33.3	205.8	147.6	161.8	3.0	30.0	300.0
Descending	32.7	139.3	148.0	159.4	3.0	30.0	300.0
Transverse	18.8	179.5	138.5	109.2	3.0	30.0	300.0

Ascending	13.1	162.3	97.6	71.2	3.0	30.0	300.0
Cecum	13.5	167.2	93.0	69.0	3.0	30.0	300.0

Table 5-4: Optimum time constants and coefficients of the AQLV fit to the stress relaxation data for three samples, each sample includes three indentations at each segments

5.4.3 Repeated interaction test

The repeated interaction test was performed at two levels of hydration; in PBS solution and in air on the transverse segment. This test evaluates the effects of hydration and repeated interaction on the large intestine mechanical properties. The stress versus strain response of tissue under 10 cycles for both hydration levels are given in Figure 5-7. As noticed, some of the responses did not reach 50% strain which could be due to a systematic error. Regardless of that, the results in Figure 5-7-a show random arrangement of stress response to 50% strain in the PBS solution. This is assumed to be due to the fact that even though the samples were held from their edges, the surface of tissue floated in the solution which introduced discrepancies in the estimation of the tissue thickness. For the samples kept in air in Figure 5-7- b, however, despite a few irregular responses the overall shift points toward an increase of stress with the progression of cycles. This is similar to the results obtained in Chapter 4 for the rectal tissue kept in air.

The magnitude of stress at peak strain can also indicate the effect of hydration on the stress-strain response of the large intestine. Higher average peak stress is obtained for the samples in air than in PBS solution implying that tissue is generally stiffer in air than in the solution. Also, for the samples in PBS stress varies greater (10-90 kN/m²) compared to the samples in air (90-130 kN/m²).

Table 5-5 shows the shift of linear modulus associated with the change in peak stress between the successive cycles for the samples in PBS. The first thing to notice is that for every positive change in stress there is a positive increase of linear modulus and vice versa, except for the last two cycle. However, the degree in which the linear modulus values shift is not consistent with the amount of stress shift, i.e. for instance, between cycles 6-7 and 8-9 where the linear modulus shift is expected to be larger for cycles 6-7 as it has the bigger stress shift; lower value of linear modulus shift is observed. This trend was also seen in Table 4-2 for the indentation of rectal tissue. For cycles 9-10 a

completely opposite effect was observed in that linear modulus seems to increase with decrease of stress response at the peak strain.

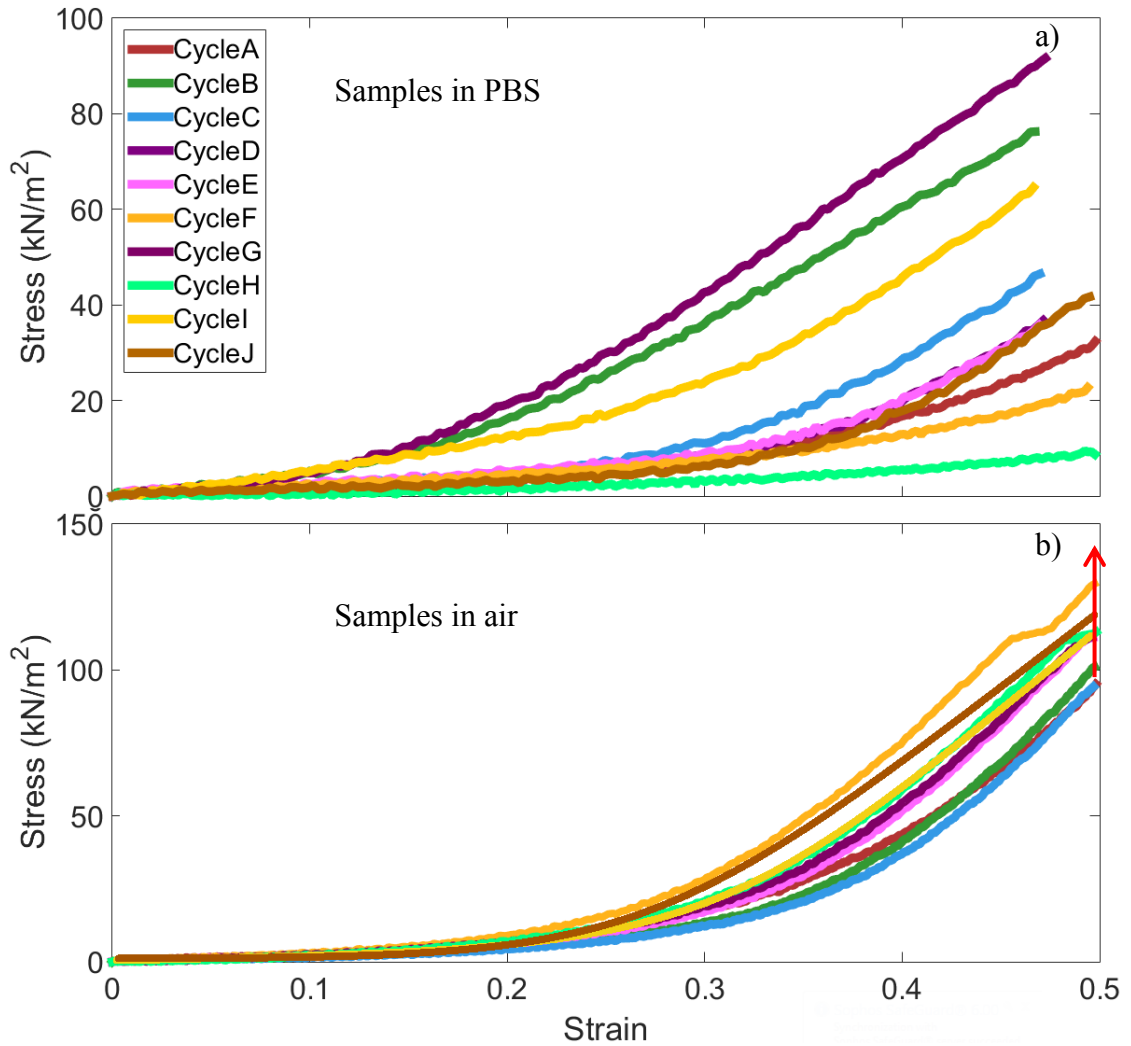


Figure 5-7: Stress versus strain response of transverse colon under 10 repetitive loading in a) PBS and b) air. Red arrow on b) indicates the progression of cycles

Cycle numbers	Stress shift (kN/m ²)	Linear modulus shift (kN/m ²)
From cycles 1-2	43.89	72.22
From cycles 2-3	-29.76	-3.82
From cycles 3-4	-9.76	-10.79
From cycles 4-5	-0.94	-6.18
From cycles 5-6	-13.09	-90.60
From cycles 6-7	68.93	145.48
From cycles 7-8	-82.11	-190.63
From cycles 8-9	55.07	166.05
From cycles 9-10	-22.90	9.04

Table 5-5: The shift of strain and linear modulus between each cycle for the samples in PBS solution corresponding to Figure 5-8-a

The spread of linear modulus along the 10 repeated indentations for both hydration conditions are shown in Figure 5-9. For both hydration conditions, there is a large increase of linear modulus from the first to the second cycle across the three samples. The difference between linear modulus values at different hydration levels are highly significant ($p < .01$) for all the cycles. The samples kept in air demonstrate a steadier pattern where they seem to reach steady state from cycles 2-3 onwards. This is whilst, for the samples in PBS the response of tissue only changes slightly for the first two cycles, and the remaining cycles show more steady responses in comparison with the samples in air. This is directly due to the influence of hydration.

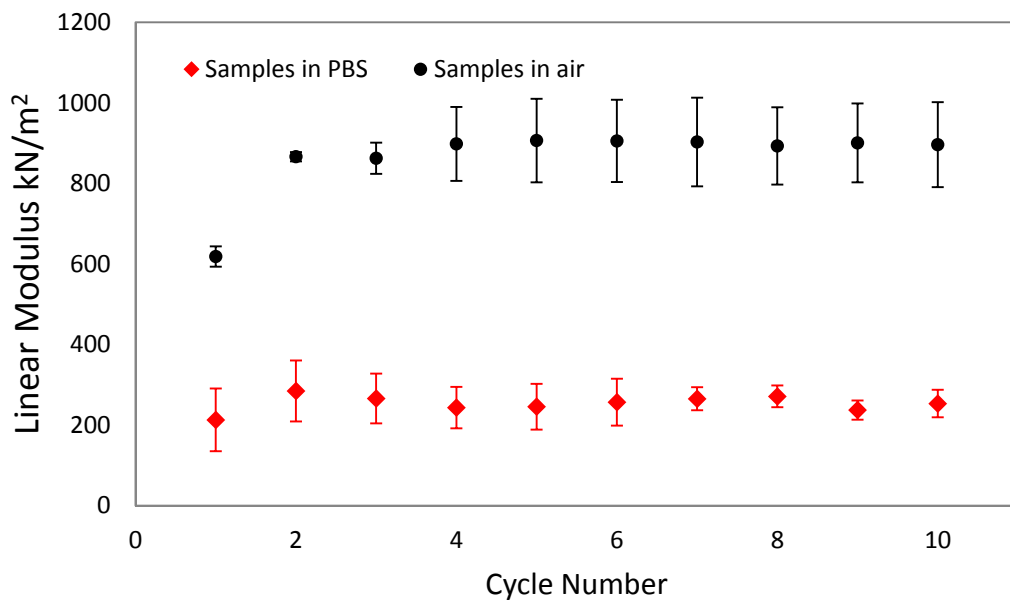


Figure 5-9: Effect of hydration level on linear modulus of transverse colon during the repeated interaction test

The hydration effect was also investigated on the viscoelastic response of the large intestine using AQLV model equation 2.40 in Chapter 2.4. As shown in Figure 5-10, before the preconditioning (cycle one), viscoelastic ratio values for both hydration levels are very similar. However, the tissue elasticity increases in large steps with the progression of cycles for the indentation in air, whilst, for the samples in PBS this trend increases slightly until the fourth cycle where it starts to become inconsistently. The higher overall elasticity of samples in air compared to the samples in PBS with the p value of $< .01$ suggests that the viscoelastic properties of the tissue is better preserved in the PBS solution. It is also worth noticing that within 10 cyclic indentations the tissue properties changes from being a highly viscous to a highly elastic for the samples in air.

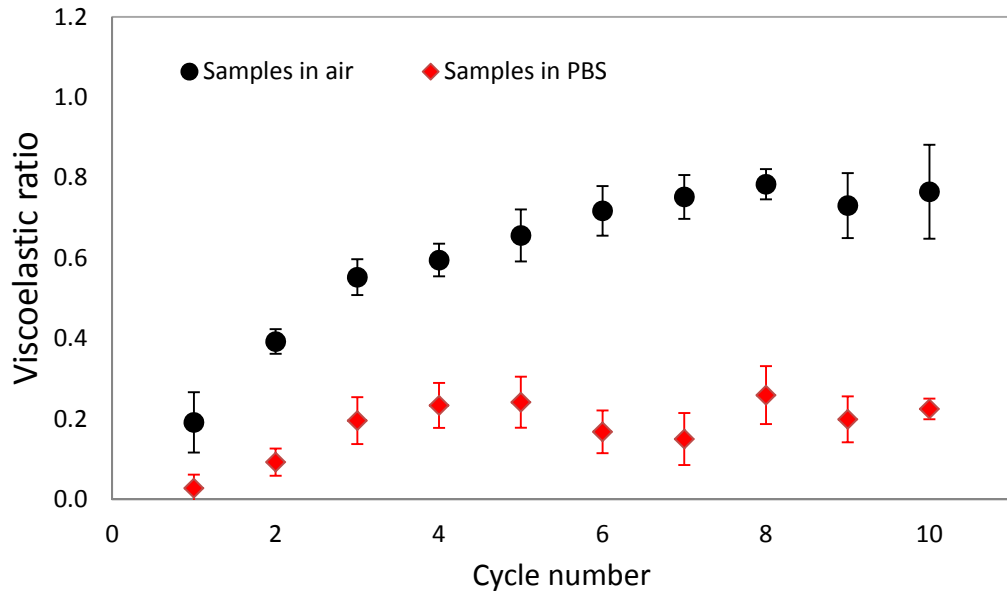
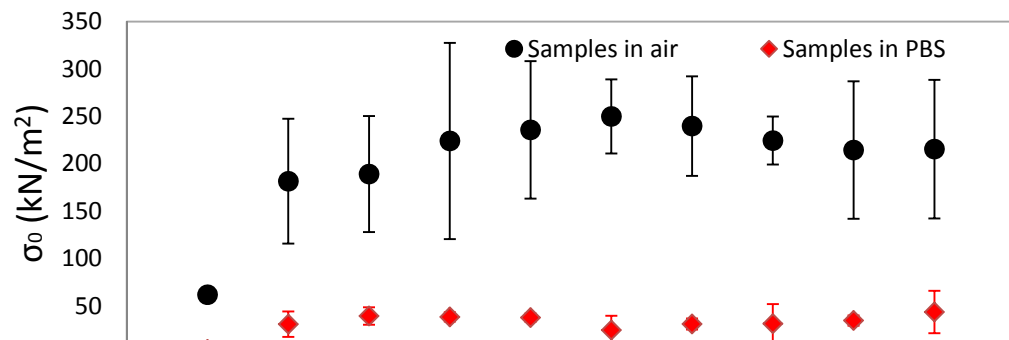


Figure 5-10: Effect of hydration level on viscoelastic ratio of transverse colon during the repeated interaction test

Fitting the stress relaxation data to the AQLV model, Figure 5-11 represents the result of the model parameters under repeated interaction test. For the samples in air, when the relaxation terms ordered starting from highest relaxation time to the smallest one $\tau_1 < \tau_2 < \tau_3$ the elastic moduli are ordered the same, $k_1 < k_2 < k_3$. For the samples in PBS, however, the correlation between the elastic moduli's is inconsistent. As Figure 5-11 shows despite the greater initial relaxation k_1 observed for the hydrated samples, the instantaneous modulus (which is the summation of all the moduli) is higher for the samples in air where p values for both parameters σ_0 and k_1 were found $<.05$. This is whilst there is no significant difference ($p>.05$) between the two hydration levels for moduli k_2 and k_3 among all the cycles.

Furthermore, there is a general increase of σ_0 and decrease of k_1 from the first to the second cycles for all the samples under both hydration conditions. From cycles two/three onwards σ_0 and k_1 seems to reach steady state. Conversely, the AQLV parameters k_2 and k_3 seems to show no dependency to the hydration level. The only consistent pattern is the general decline of both k_2 and k_3 values starting from the second cycle for the remaining cycles.

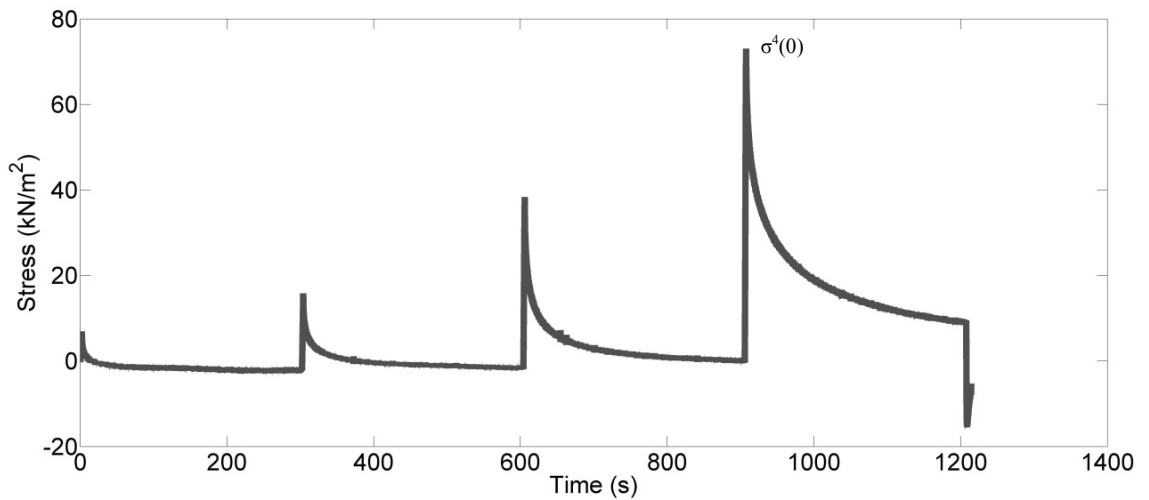
Figure 5-11: Fitted values of σ_0 & k_i for the AQLV model under repeated interaction test for both hydration conditions, in PBS and in air



5.4.4 Varying strain level dependency examination

In order to observe the strain dependency of large intestine the same location on each sample was indented to 20%, 35%, 50%, and 65% strain consecutively and stress relaxation is performed in between each level of strain as shown in Figure 5-12.

The spread of linear modulus obtained from the loading phase of indentation at each strain step for the three porcine samples are shown in Figure 5-13. It is clearly visible



that there is a significant increase of linear modulus value as a function of strain level.

Figure 5-12: Typical curve of stress versus time for 4 incremental strain steps. The peak and final stresses are identified as $\sigma^i(0)$ and $\sigma^i(\text{end})$, respectively.

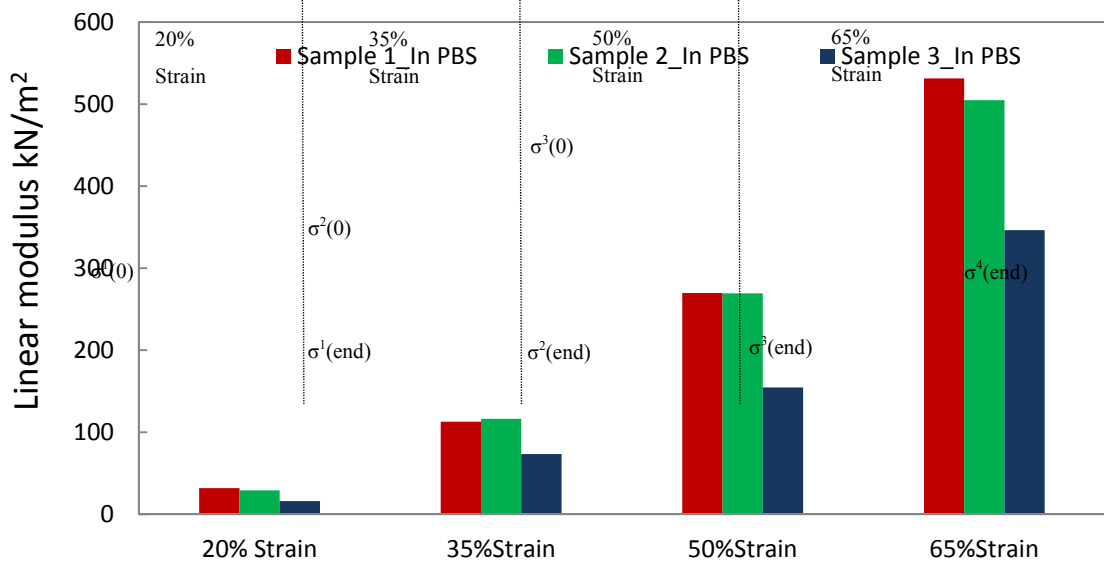


Figure 5-13: Linear modulus distribution at four strain levels 20%, 35%, 50% and 65%.

Also confirmed by Lista *et al.* [115] and Provenzano *et al.* [90] this trend indicates that the stiffness of the large intestine is significantly affected with the strain level. In order to investigate the effect of varying strain level on the stress relaxation response the stress relaxation drop $\Delta\sigma$ at each strain step was obtained. The results show full $\Delta\sigma$ of 100% for both 20% and 35% strain steps, 96% $\Delta\sigma$ for 50% strain step and 74% $\Delta\sigma$ for the highest strain steps 65%, indicating that the average equilibrium value increases with increasing strain level. Also, as shown in Table 5-6, the average stress at 50 s decreases with increasing strain level which signifies that the lower the strain level, the greater the relaxation/decaying rate.

The stress relaxation data were normalised using the reduced relaxation function mentioned in Chapter 3.6.5, then the normalised curves were fitted to the AQLV model and the coefficients of each curve were obtained. Figure 5-14 plots the typical normalised stress as a function of time at various levels of strain. As evident by the plots the curves diverge at the beginning of the relaxation process and meet again at the end of the process. The variation of normalised stress as a function of time (taken at 0, 1, 10, 50, 100, and 300 s) for the three tissue samples is given in Table 5-7. The mean values are obtained by averaging the normalised stresses obtained from the four strain levels at the chosen timestamp and then take the overall average for the three samples. The table demonstrates an increase of standard deviation by time, reaching its highest value at 10s followed by a decrease of this effect for the rest of the relaxation period. This trend shows a dependency of viscoelastic properties of the large intestine to the history of strain. The black dashed line in Figure 5-14 is an example of the location from where the average and \pm SD of the normalised stresses were taken.

To investigate the capability of the AQLV to predict the stress relaxation response of the large intestine the second, third and fourth stretched were calculated using the model parameters calibrated for the first stretch as explained in Chapter 2.4.

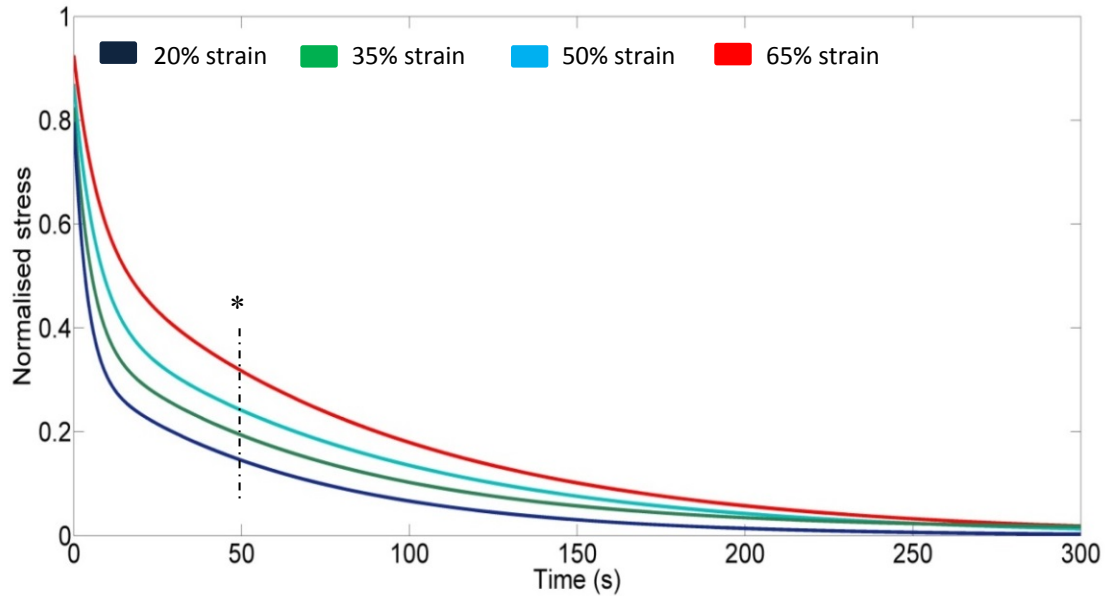


Figure 5-14: Normalised stress versus time for four strain increments. The curves represent the AQLV model fit of the normalised experimental data

Time (s)	Average normalised stress	± SD
0.0	0.82	0.05
1.0	0.71	0.09
10.0	0.35	0.12
50.0 *	0.16	0.07
100.0	0.08	0.04
300.0	0.01	0.01

Table 5-7: Typical mean reduced relaxation function +/- SD for all the four strain levels obtained at several points in time along the relaxation process

Figure 5-15 demonstrates that for the second and third stretches the model predicts both responses with acceptable accuracy, except for the exact initial points. However, for the highest stretch, 65%, the model overestimates the initial point which leads to predicting a greater ‘relaxation process 1’. Also, the experimental data has a greater upward curvature compared to the predicted data. This trend was repeated in all the other specimens. The possible reason for this error can be the difference in the technique used here. The model claims to predict the relaxation history of the tissue under tensile stretch in which manipulates tissue in a totally different manner to tissue indentation.

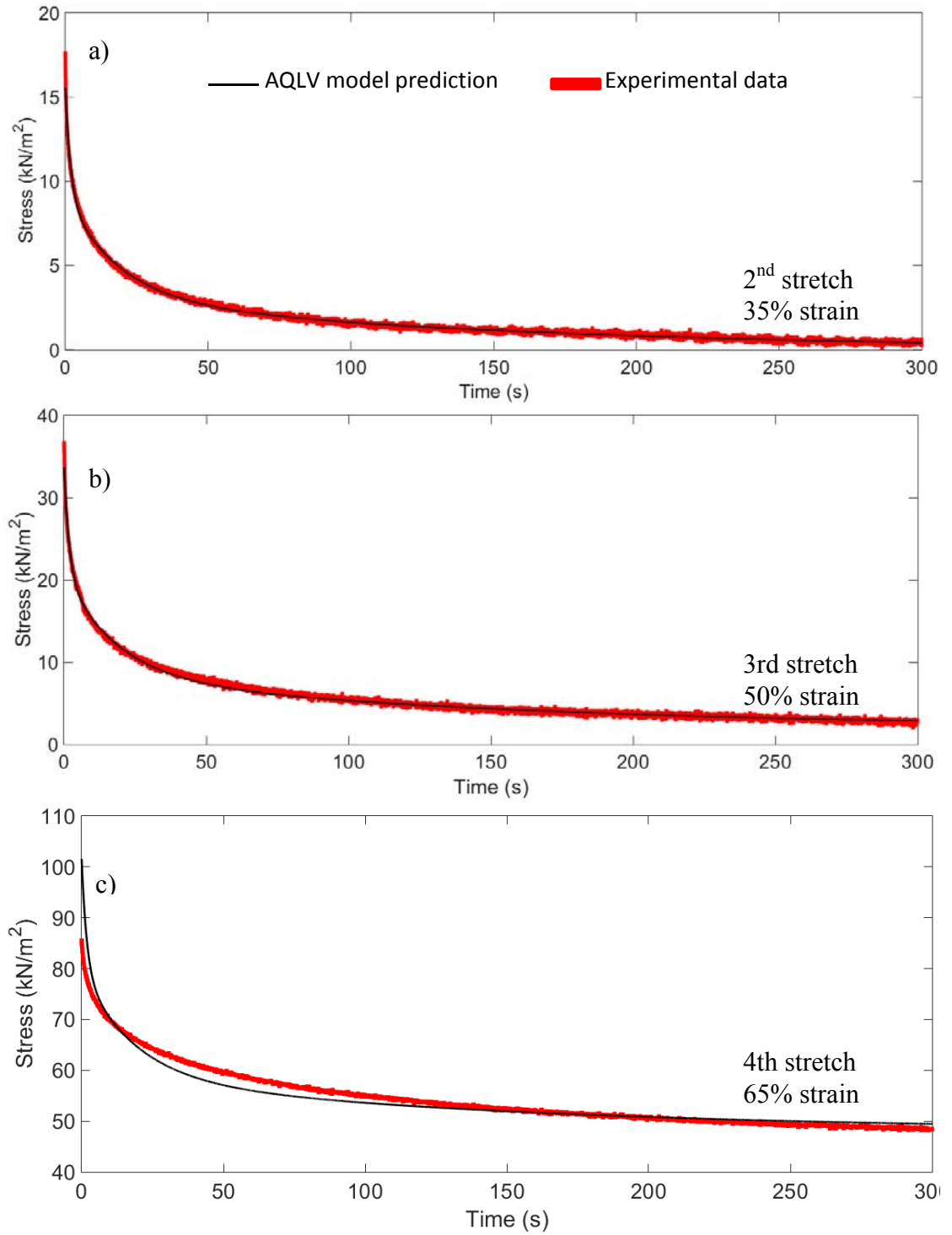


Figure 5-15: Measured (red curves) and predicted (black curves) stress relaxation for the large intestine using the AQLV model under stepwise strain test. The initial strains are a) 35%, b) 50%, & c) 65%

5.5 Chapter summary

The repeatability, time and strain history dependent responses of the tissue were investigated on the large intestine. Also, the influence of hydration on the response of tissue was examined. A more advanced viscoelastic model was employed to fit the experimental data which takes into account the strain history effect. Moreover, the strain history dependency of the large intestine was explored by incrementing strain in four steps. The experimental data obtained from the first increment was used to predict the response of the tissue to the next strain steps using the viscoelastic model. Table 5-7 demonstrates the results drawn from each experiment.

Objective	Method	Results
Effect of repeated interaction on tissue properties	10 consecutive multi-cyclic indentations on transverse colon	<ul style="list-style-type: none"> • Tissue viscoelasticity is directly influenced by the degree of tissue hydration tissue properties change significantly when samples kept in air compare to random but steady changes of properties for the samples in PBS
Effect of varying strain levels on tissue properties	4x stepwise strain test at 20%, 35%, 50% and 65% strain on transverse colon	<ul style="list-style-type: none"> • Viscoelastic properties of the tissue is strain history dependent • The lower the strain level, the greater the relaxation/decaying rate • AQLV model can predict the tissue response more accurately at low strain levels
The variation of tissue behaviour along the length of the large intestine	Preconditioned single indentations on each segments of the large intestine	<ul style="list-style-type: none"> • Tissue thickness has significant effect on stress-strain response of the tissue • Stiffer the tissue, greater the stress relaxation response • Tissue becomes less compliant to indentation force as progressing from rectum towards cecum • The relaxation response of the large intestine is modelled well with the AQLV viscoelastic model

Table 5-8: An overview of the key points in this chapter

Chapter 6. Mechanical characterisation of large intestine under tensile stretch

6.1 Introduction

Traditional indentation tests are commonly conducted to determine the hardness and elastic modulus of a material through measuring the resistance of a material to penetration. In the same context tensile tests are mainly aimed to determine the failure of materials under static stress [131]. Tensile tests are mostly favoured for their simplicity, small sample size, commercially available devices and capturing multi-axial characterisation of tissue properties *ex-vivo*. As mentioned in the literature review Chapter 2.3.2, the viscoelastic properties of the large intestine under multi-axial tensile load has been disregarded in the literature. These data are necessarily to understand the normal response of the large intestine in various conditions and to develop a model to characterise their behaviour under various pulling actions during minimal invasive surgeries and conventional colonoscopy.

6.2 Test objectives

This chapter aims to evaluate the effects of different tensile loading scenarios on the longitudinal and circumferential mechanical and viscoelastic properties of the large intestine. Time and strain history dependency of the anisotropic, inhomogeneous and non-linear material properties of tissue as a function of the loading condition in a fully hydrated environment is investigated through three testing procedures: preconditioned single tensile test along the full length of the large intestine, multi-cyclic tensile test and stepwise strain test. The same testing procedure was used for both fibre orientations to assist the comparison of mechanical and viscoelastic properties.

6.3 Methods

As mentioned previously in Chapter 3.3.2, the MMC rig was employed to perform the tensile test. Stretch to the point of failure could not be achieved due to sample slippage off the tissue holder over certain stretch forces and limited movement range of the linear stage. Therefore, all the tensile tests followed the same protocol as the indentation tests in Chapter 5. Different tissue fixture Figure 3-8-b to that of the indentation test was employed to grasp and stretch the tissue firmly. Samples were cut in longitudinal and circumferential manners and kept hydrated throughout the experiment as detailed in 3.2.2. Table 6-1 summarises the main features of the experimental set-up.

Experiment	Location on the tissue	Fibre orientations	Max. strain %	Strain-rate mm/s	Relaxation Duration s	Cycle iteration	Sampling rate Hz
Intra-large intestine variation test	Three stretches on each segment	longitudinal and transversal	50%	0.1	300	1	60
Repeated interaction test	One stretch on transverse colon	longitudinal and transversal	50%	0.1	300	10	60
Stepwise strain test	One stretch on transverse colon	longitudinal and transversal	20%, 35%, 50% & 65%	0.1	300	1	60

Table 6-1: Summary of the experimental set-up

6.4 Results

6.4.1 Intra-large intestine variation

The distribution of the linear modulus values among the five segments of the large intestine in both fibre orientations (i.e. aligned and transverse) are shown in Figure 6-1. The box plots were obtained from the three preconditioned tensile cycles performed on three different sites on each segment (Table 3-3). The highest and the lowest average linear modulus values for the longitudinal samples were found in cecum and ascending, however, the results are inconclusive as the whiskers of the box plots overlap each other. Furthermore, no statistical significant differences in linear modulus between descending, transverse and cecum were found as for the $p > .05$. Even though for rectum and ascending the p -value is $> .05$, the direction of difference is not consistent. The lowest and highest average linear modulus values for the circumferential samples were found in the rectum and ascending segments. The average linear modulus ranged between 590-2700 kN/m^2 and 320-2600 kN/m^2 for longitudinal and circumferential samples.

Figure 6-2 depicts the variation of the viscoelastic ratio (obtained using AQLV model fitting) corresponding to the experimental data presented in Figure 6-1. The viscoelastic ratio of the samples in both fibre orientations varies between 0.6-0.9. There is a statistically significant difference in viscoelastic ration in different fiber orientation in all segments of the large intestine ($p < .05$).

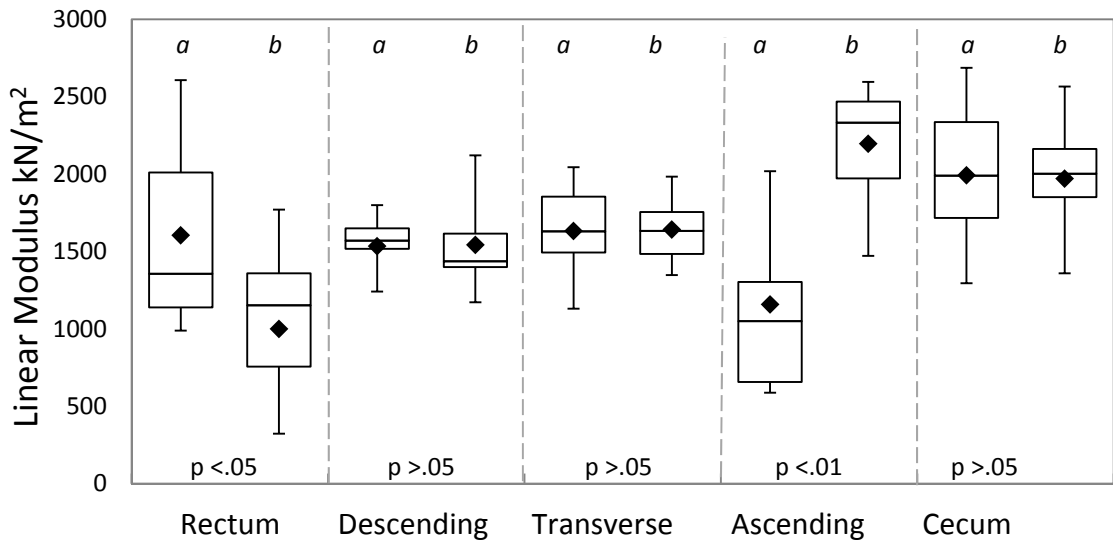


Figure 6-1: The distribution of linear modulus in various segments of the large intestine for a) longitudinal and b) circumferential samples

As mentioned previously, the samples were cut 30 mm in length and the loading rate was set to 0.1 mm/s. Setting the maximum strain threshold to 50% imposes 150 s of loading duration which is half of the stress relaxation duration.

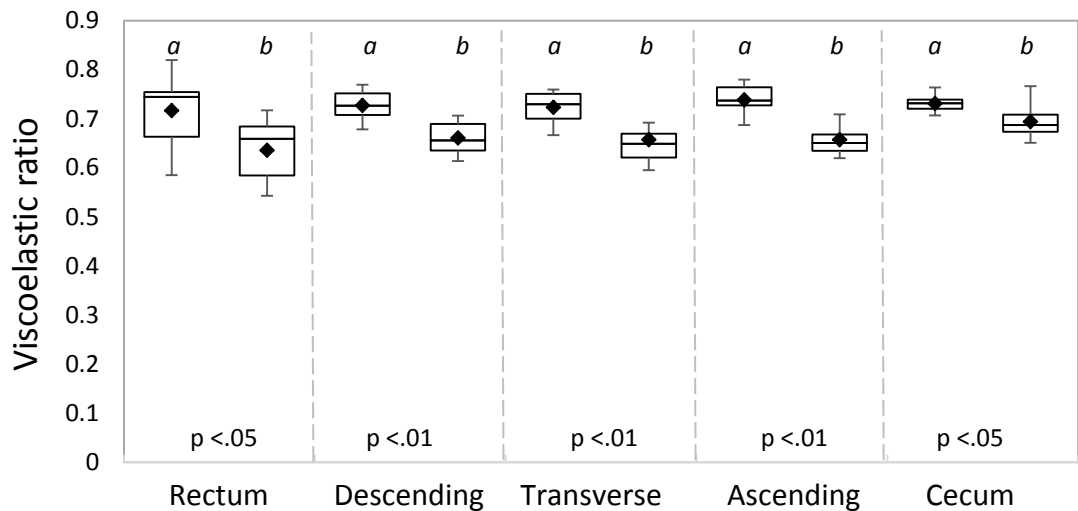


Figure 6-2: The distribution of viscoelastic ratio in various segments of the large intestine for a) longitudinal and b) circumferential samples

This suggests that considerable amount of stress relaxation must have occurred during the loading phase. Figure 6-3 confirms this hypothesis. It shows the typical stress versus time response of the tissue after 5 preconditioning cycles in both fibre alignments during loading and relaxation. Table 6-2 reveals the best fit coefficients of the AQLV

model fitted to the stress relaxation data in Figure 6-3. Zero k_1 infers that no rapid stress relaxation or ‘process 1’ is detected for the two stress relaxation curves at different fibre orientations. Low relaxation modulus k_2 from ‘process 2’ is followed by a large k_3 value associated with the slowest relaxation response. This is due to a longer loading duration (half the duration of the relaxation) which resulted in considerable amount of tissue relaxation during the loading phase prior to the peak strain. This relaxation during the loading phase reduces the amount of relaxation during the stress relaxation phase and consequently leads to inaccurate parameter estimation. Therefore, as opposed to several reports on anisotropic behaviour of soft tissue/large intestine [40, 71-73] no difference in mechanical properties between the longitudinal and circumferential large intestine samples was found here. This pattern also opposes the trend observed for the indentation experiments in Chapter 5 as the loading phase was very short due to using tissue thickness for calculation of the strain threshold.

Fitting the experimental data to the AQLV model, average RMSE values of 0.168 ± 0.03 and 0.171 ± 0.02 were obtained for longitudinal and circumferential samples, very similar to those obtained for indentation tests.

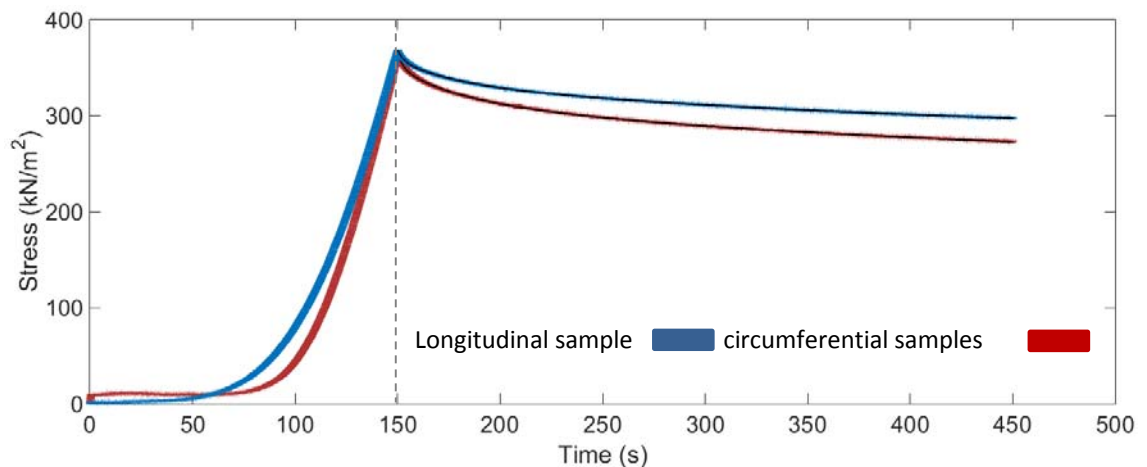


Figure 6-3: Typical AQLV fit (black line) to the stress relaxation data of both longitudinal and circumferential samples. The black dash line separates the loading phase from the relaxation phase

AQLV parameters	σ_0 (kN/m ²)	k_1 (kN/m ²)	k_2 (kN/m ²)	k_3 (kN/m ²)	τ_1 (s)	τ_2 (s)	τ_3 (s)
Transverse colon (Longitudinal sample)	684.4	0.0	4.3	249.4	3.0	30.0	300.0
Transverse colon (Longitudinal sample)	493.9	0.0	4.5	215.3	3.0	30.0	300.0

Table 6-2: AQLV parameters of the model fitting to the relaxation data for the two specimens in Figure 6-3

The same averaging method used in Chapter 5 for indentation data was employed to find the average fit of the AQLV model to the tensile experimental data for each segment. As depicted in Figure 6-4, except for samples from ascending colon all the longitudinal samples reach the same level of stress at 50% strain. This suggests that ascending colon has lower total resistance to the longitudinal stretch. This trend is also evident in the parameters of the AQLV model fitting given in Table 6-3 . According to this table, ascending colon owns the lowest values of the relaxation and equilibrium moduli. The rest of the segments have similar values of the model coefficients. The average $\Delta\sigma$ values for each segment are as follow: rectum=64, descending=65, transverse=62, ascending=46 and cecum=69. Overall, ascending colon shows in average lower linear modulus and relaxation response compare to the rest of segments.

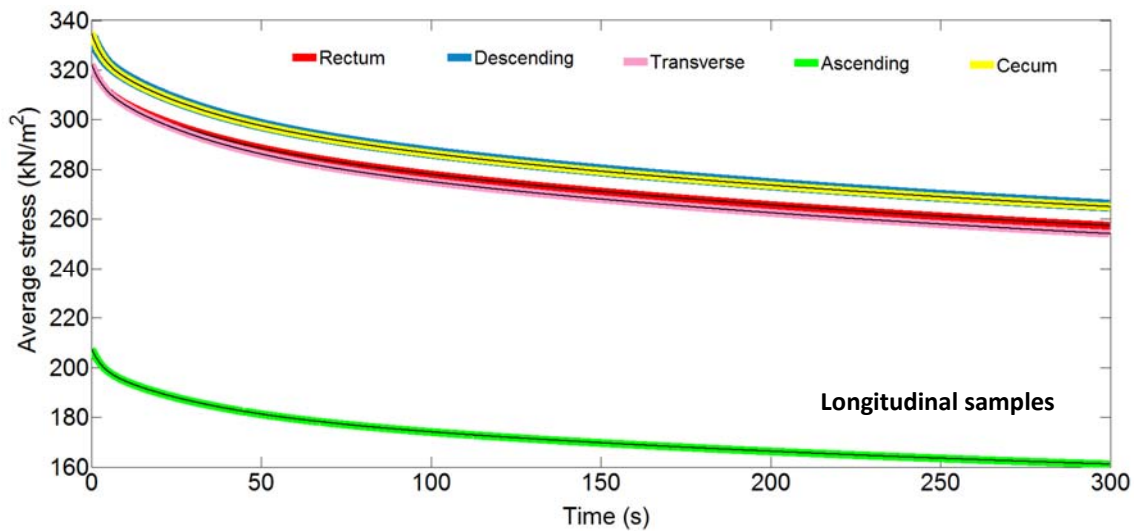


Figure 6-4: Exponential fit of the AQLV model (black lines) to the averaged relaxation data under longitudinal tensile stretch. Optimum time constants are 3, 30 and 300 s

AQLV parameters	σ_0 (kN/m ²)	k_1 (kN/m ²)	k_2 (kN/m ²)	k_3 (kN/m ²)	τ_1 (s)	τ_2 (s)	τ_3 (s)
Rectum	472.73	0.00	2.78	175.97	3.00	30.00	300.00
Descending	487.30	0.00	3.10	182.05	3.00	30.00	300.00
Transverse	465.80	0.00	3.21	177.81	3.00	30.00	300.00
Ascending	296.01	0.00	2.25	109.73	3.00	30.00	300.00
Cecum	486.58	0.00	3.09	181.96	3.00	30.00	300.00

Table 6-3: Optimum time constants and coefficients of the AQLV fit to the stress relaxation data for three samples, each sample includes three longitudinal stretches at each segments

Unlike longitudinal samples, the compliance of the samples to the circumferential stretch is at its lowest value for the rectum and it increases as progressing towards the cecum. As Figure 6-5 shows, descending and transverse segments share similar initial

stress. The same is observed for ascending and cecum segments. Table 6-4 verifies this trend as the equilibrium and relaxation moduli of the AQLV fit increase from rectum to cecum. The drop of stress, $\Delta\sigma$, is 52.0, 70.5, 87.2, 99.2 and 76.0 for the segments rectum, descending, transverse, ascending and cecum, respectively. Again the segment (i.e. rectum) with the lowest linear modulus value owns the lowest relaxation response. This implies that the lower the tissue stiffness the smaller the relaxation response. This trend was also agreed in the indentation results in Chapter 5.

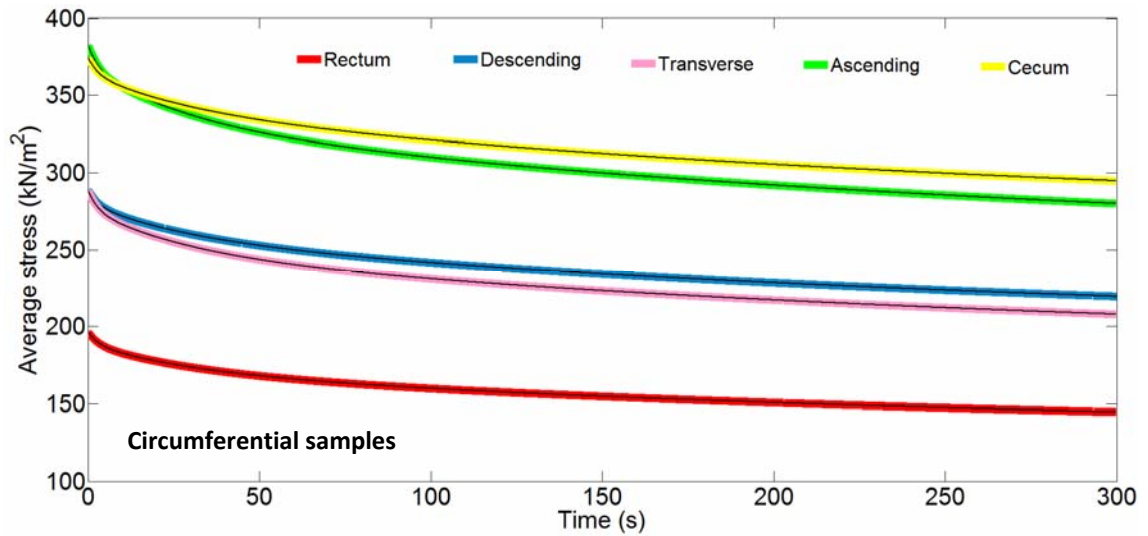


Figure 6-5: Exponential fit of the AQLV model (black lines) to the averaged stress relaxation data under circumferential tensile stretch. Optimum time constants are 3, 30 and 300 s

AQLV parameters	σ_0 (kN/m ²)	k_1 (kN/m ²)	k_2 (kN/m ²)	k_3 (kN/m ²)	τ_1 (s)	τ_2 (s)	τ_3 (s)
Rectum	258.6	0.0	2.4	128.7	3.0	30.0	300.0
Descending	348.9	0.0	3.3	175.9	3.0	30.0	300.0
Transverse	369.2	0.0	3.8	195.3	3.0	30.0	300.0
Ascending	499.8	0.0	4.9	252.6	3.0	30.0	300.0
Cecum	459.8	0.0	4.0	202.7	3.0	30.0	300.0

Table 6-4: Optimum time constants and coefficients of the AQLV fit to the stress relaxation data for three samples, each sample includes three circumferential stretches at each segments

6.4.2 Repeated interaction test

Figure 6-6 illustrate the typical stress versus strain response of the large intestine under repeated interaction test. The mechanical response of cycle one (i.e. the red curve) appears to be very distinctive in that initially the stress almost increases linearly with strain up to 20% strain then there is an exponential growth followed by another linear-region. The same pattern was obtained for all the other experiments. The rest of cycles

follow the standard exponential growth as expected. Since comparing the mechanical properties of the first cycle to the rest can be tricky and misleading, the loading phase of the first cycle has been discarded from the rest of measurements.

As seen in Figure 6-6 there is a major decrease in stress at 50% strain from cycles one to two, followed by the reduction of this effect as the cycles are built up. Overall, there was a 45.5% decrease in the peak stress from 1st to 10th cycles indicates that the tissue samples show some stress relaxation with each stretch-release cycle. This trend is consistent with the results presented in the literature [75, 122]. Table 6-5 reveals the shifts in values for linear modulus and stress between consecutive cycles started from the second cycle. Except in two cases, all the responses show reduction of the linear modulus shifts as a function of stress shift. This is due to the lengthy loading which causes the tissue to lengthen and part of it hangs away from the straight axis between the sample holders. As the length of the tissue does not recover fully during the unloading, this extra length adds up and passes on from one cycle to another and therefore the peak stress decreases with progression of cycles. Yet, similar to the results obtained in the indentation tests the amount of linear modulus shift fails to correctly correlate with the shift in the peak stress. A good example is seen when comparing the shifts between cycles 6-7 and cycles 8-9 where stress shifts of -6.03 and -5.34 associate with linear modulus shifts of 0.02 and -0.24, respectively.

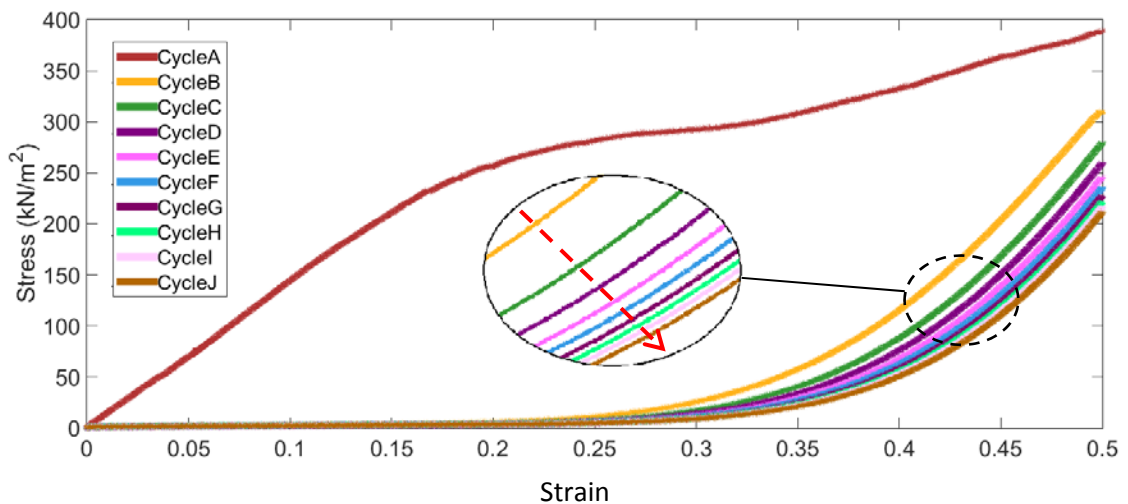


Figure 6-6: Typical stress-strain response of the large intestine to repeated interaction under tensile stretch. Red arrow on the magnified view shows the direction of cyclic progression

Cycle numbers	Stress shift (kN/m ²)	Linear modulus shift (kN/m ²)
From cycles 2-3	-31.57	0.21
From cycles 3-4	-17.20	-0.28
From cycles 4-5	-12.22	-0.29
From cycles 5-6	-9.12	-0.25
From cycles 6-7	-8.05	-0.50
From cycles 7-8	-6.03	0.02
From cycles 8-9	-5.34	-0.24
From cycles 9-10	-4.19	-0.17

Table 6-5: The shift of strain and its corresponding linear modulus shift for every two consecutive cycles under tensile stretch

Figure 6-7 represents the stress versus strain response of longitudinal and circumferential samples during the loading phase under repeated interaction test. The shaded bars demonstrate the spread of stress-strain data for the three longitudinal samples in blue and circumferential samples in red each indented 10 times and coloured in blue. The first cycles are not excluded as explained earlier. Except in two cases which caused the two regions to overlap, all the longitudinal samples exhibited higher stress to reach 50% strain than the circumferential samples, implying that the tissue in the longitudinal direction is stiffer than in the circumferential direction.

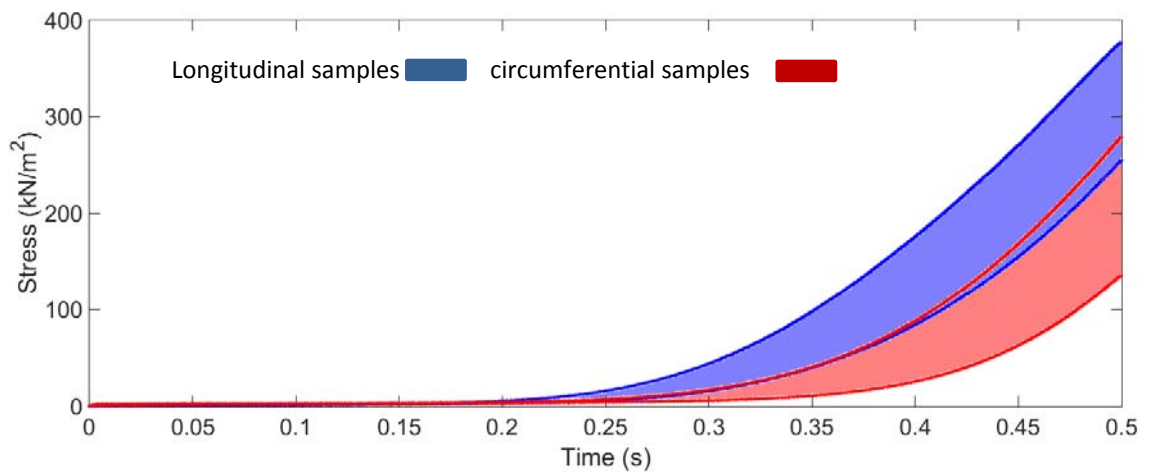


Figure 6-7: The stress-strain response of the large intestine during the loading phase for longitudinal and circumferential samples

In Figure 6-8-a linear modulus values increase rapidly from the first to the second cycle then it settles for the remaining cycles in both fibre orientations. In average, the longitudinal linear modulus values are slightly higher than the circumferential ones, although, there is a major overlap in standard deviations. The data demonstrate no significant difference ($p > .05$) in linear modulus determined for the two fiber

orientations among the 10 repeated cycles. In Figure 6-8-b the average viscoelastic ratio values for the first cycles of both samples coincide where the biggest \pm SD is observed. Then, a big increase is seen from the first to the second cycles for both samples followed by insignificant increase of the viscoelastic ratio thereafter. This implies that the samples become very elastic by the second stretch and maintain their elasticity level for the remaining cycles. Except for the first cycle ($p > .05$), the p value is $< .01$ which suggests that there is a high statistically significant difference between the viscoelastic ratio of the two fiber orientation in all the cycles.

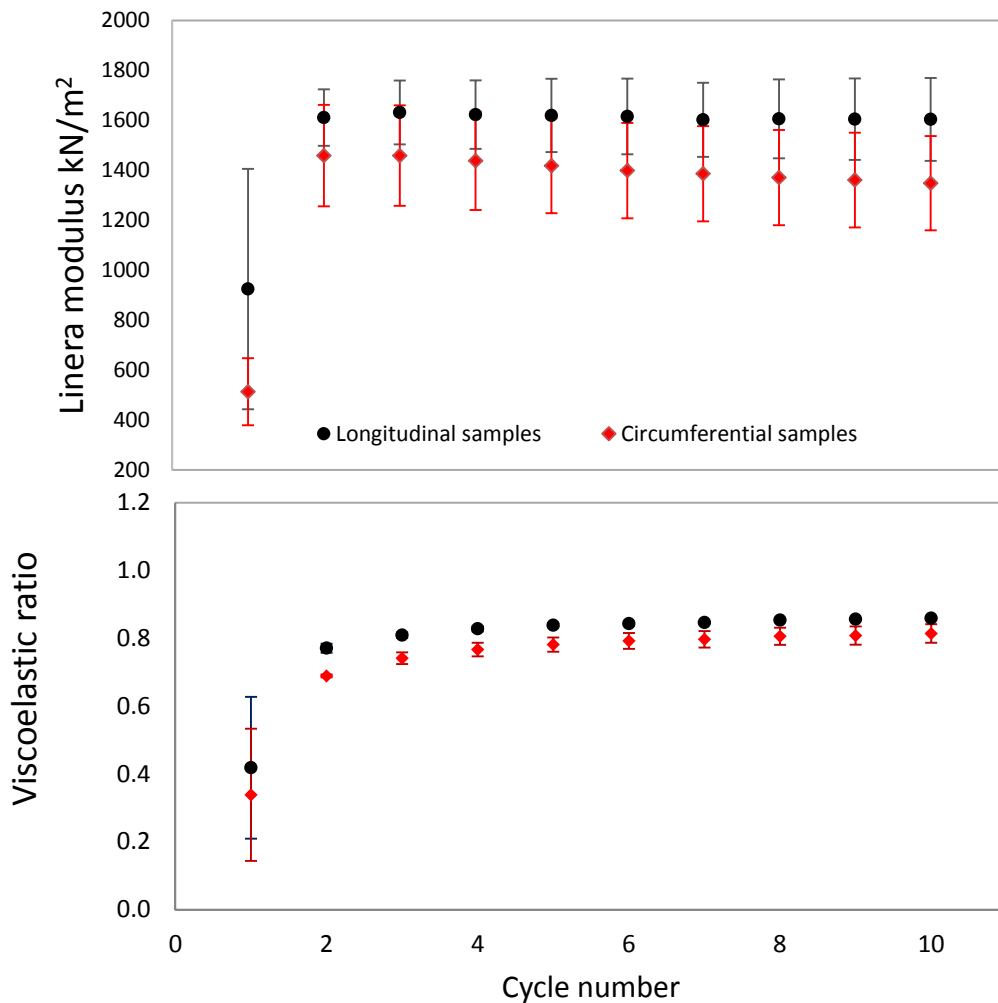


Figure 6-8: Effect of fibre orientation on a) linear modulus and b) viscoelastic ratio of transverse colon during the repeated interaction test

The model coefficients of AQLV model fitting to the experimental data are plotted in Figure 6-9. The equilibrium modulus σ_0 seems to be in average higher in longitudinal direction as compared to the circumferential direction. However the result of the t-test statistical analysis shows that there is no significant difference ($p > .05$) between the two fiber orientations. Likewise, no significant difference was found between the relaxation

moduli (i.e. K_1 , K_2 and K_3) of the two fibre orientations ($p > .05$). Similar to the results obtained for the intra-large intestine variation test, no initial fast relaxation occurs ($k_1 = 0$) since the samples were relaxed during the long loading phase of 150 s. Relaxation moduli k_2 and k_3 show an increase from the first to the second cycles, which is followed by reaching a steady state from the third to the fourth cycles. Since the loading phase contains considerable amount of stress relaxation, investigating the loading responses should reveal some viscoelastic properties missed in the relaxation response.

In order to extract viscoelastic responses in the loading phase, the two linear regions on the stress versus strain response, toe-region and linear-region, were found and the viscoelastic region between the two linear regions was fit to the viscoelastic Wiechert 5-element model. The typical results are presented in Figure 6-10 and Table 6-6. The RMSE values indicate that Wiechert model provides a good fit to the tissue response. The viscoelastic response tends to shift to the right with progression of cycles. Table 6-6 indicates that the longitudinal samples exhibit no pure elastic response σ_0 , and only one relaxation process is needed to describe the tissue relaxation behaviour. The same trend is observed for the circumferential data in Table 6-7.

As for the two relaxation processes, only one of the relaxation processes happen at a time. This is not surprising as in Figure 6-10 the exponential growth which represents the relaxation response is very consistent. In average elastic modulus k_i have higher range in longitudinal samples than the circumferential ones. The viscous modulus η_i , however, is similar in the two fibre directions. In either case, the viscous and elastic moduli values drop gradually with the progression of cycles. Also, it is noticeable that the toe-region lasts longer with every cycle (i.e. the first point of viscoelastic region shifts to the right as indicated by the red arrow) implying that the initial response of the tissue becomes more elastic under repeated interaction. This is whilst the linear-region does not move up after the second cycle. Therefore shorter viscous responses are observed as cycles are built up.

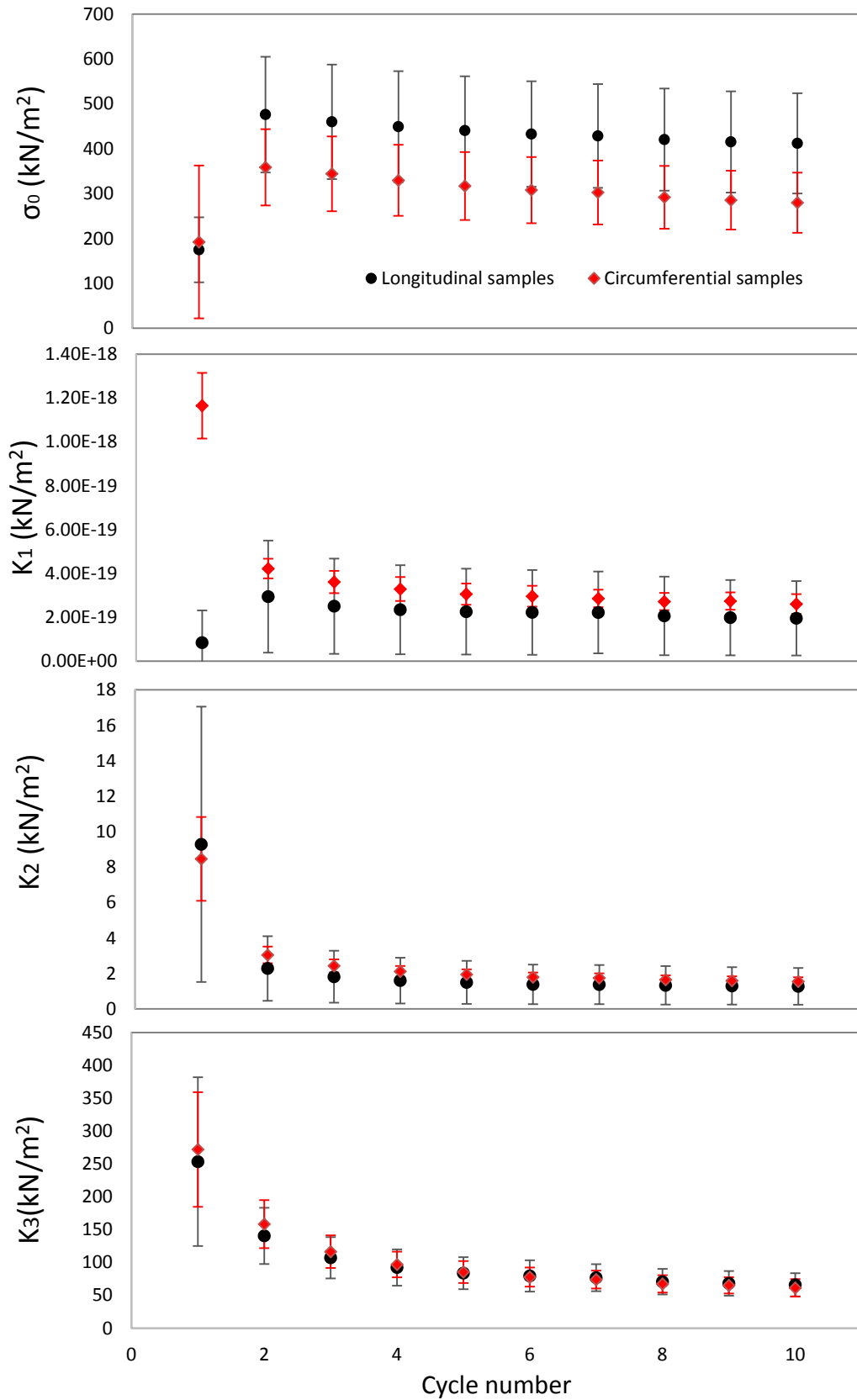


Figure 6-9: Fitted values of σ_0 & k_i for the AQLV model under repeated interaction test for both fibre directions, longitudinal and circumferential alignments

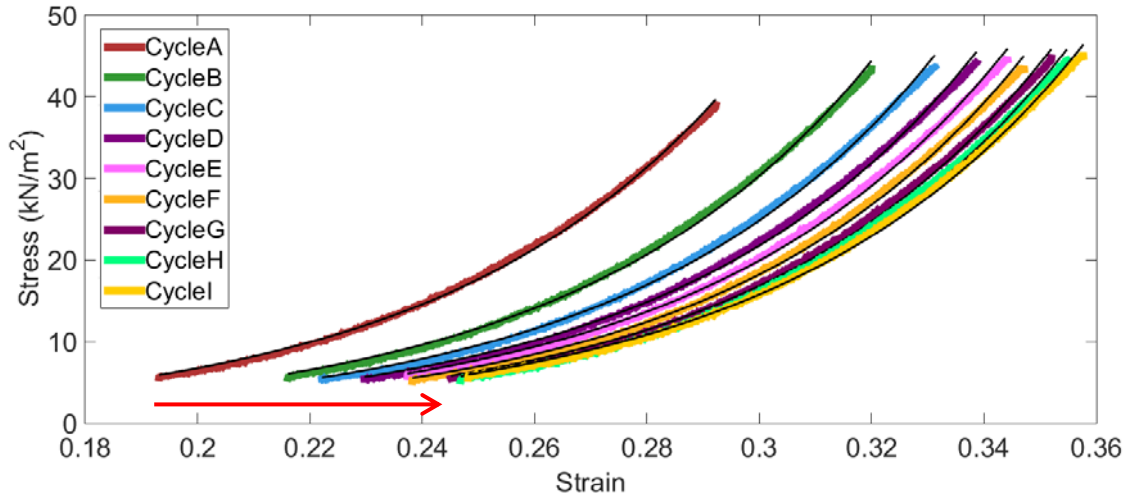


Figure 6-10: An example of the Wiechert fit to the loading viscoelastic region for 10 consecutive cycles

Cycle number	σ_0 (kN/m ²)	k_1 (kN/m ²)	k_2 (kN/m ²)	η_1 (N ^s /m ²)	η_2 (N ^s /m ²)	RMSE (kN/m ²)
2	0.00	0.15	0.00	2.29	0.00	0.05
3	0.00	0.10	0.00	1.53	0.00	0.06
4	0.00	0.08	0.00	1.27	0.00	0.06
5	0.00	0.00	0.07	0.00	1.11	0.07
6	0.00	0.00	0.07	0.00	1.10	0.06
7	0.00	0.00	0.06	0.00	0.90	0.07
8	0.00	0.00	0.05	0.00	0.81	0.07
9	0.00	0.00	0.05	0.00	0.79	0.07
10	0.00	0.00	0.06	0.00	0.92	0.06

Table 6-6: The Wiechert model coefficients of the loading viscoelastic response occurred in viscoelastic region corresponding to the responses in Figure 6-10 under longitudinal stretch.

Cycle number	σ_0 (kN/m ²)	k_1 (kN/m ²)	k_2 (kN/m ²)	η_1 (N ^s /m ²)	η_2 (N ^s /m ²)	RMSE (kN/m ²)
2	0.00	0.00	0.11	0.00	2.07	0.08
3	0.00	0.00	0.11	0.00	2.10	0.61
4	0.00	0.00	0.11	0.00	2.14	0.47
5	0.00	0.00	0.08	0.00	1.52	0.40
6	0.00	0.00	0.06	0.00	1.25	0.34
7	0.00	0.00	0.05	0.00	0.98	0.31
8	0.00	0.00	0.03	0.00	0.57	0.10
9	0.00	0.00	0.04	0.00	0.75	0.25
10	0.00	0.00	0.03	0.00	0.51	0.13

Table 6-7: The Wiechert model coefficients of the loading viscoelastic response occurred in the viscoelastic region corresponding to the responses in Figure 10 under circumferential stretch

6.5 Strain level dependency examination

Figure 6-11 presents the normalised stress relaxation response of the large intestine under four strain steps for both fibre alignments (longitudinal and circumferential). In both cases the curves at different strains coincide with each other well. As Table 6-8 depicts, the mean standard deviations of the normalised stress are 0.01 and 0.02 for longitudinal and circumferential samples, respectively. These all suggest that the stress relaxation response of both samples is independent of the strain history. However, it should be taken into account that the stress relaxation phase does not cover the full relaxation response as a big portion of the relaxation occurred during the lengthy loading phase.

It is noticed from the experimental data that unlike the indentation data, stress values in none of the relaxation steps reach full recovery in the tensile test. The average $\Delta\sigma\%$ values of 52%, 65%, 70%, and 74% for first, second, third and fourth steps suggest that more relaxation is achieved as incrementing the ramp and hold steps. This trend happens in both fibre orientations and opposes the trend found for the indentation test and those in the literature Chapter 2.5.5 where the $\Delta\sigma\%$ decreases as the strain level increases.

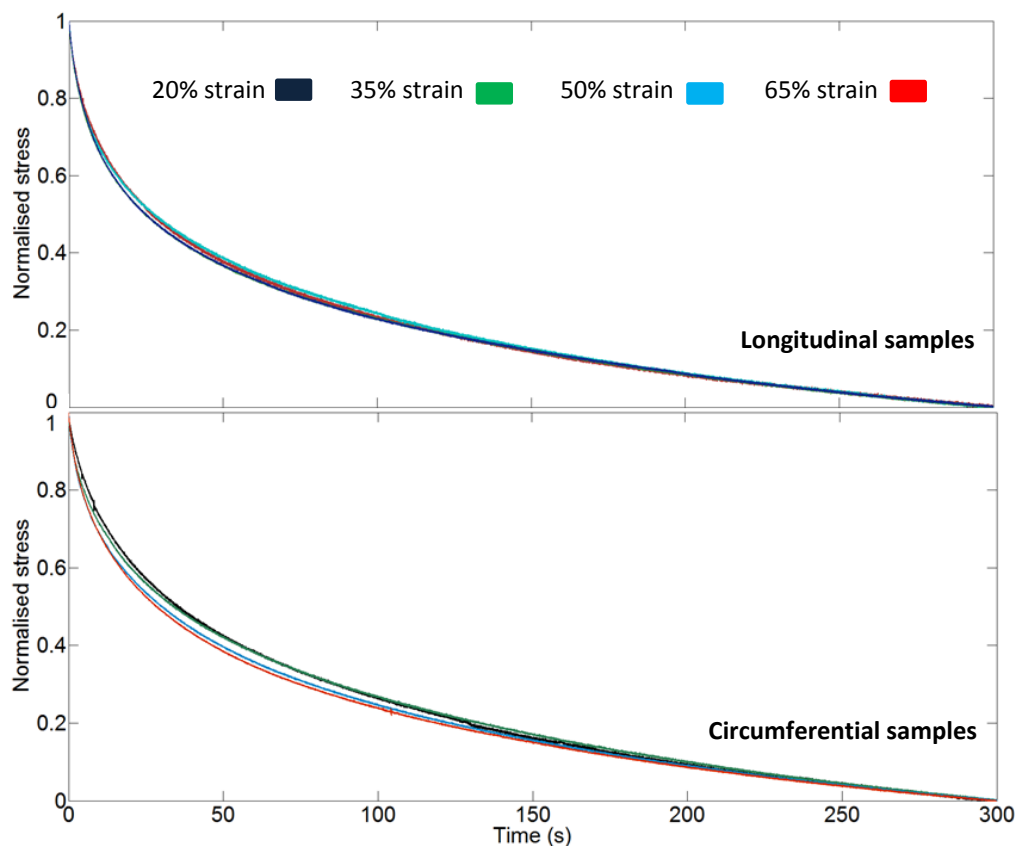


Figure 6-11: Normalised stress versus time for four strain increments for two fibre alignments; longitudinal and circumferential directions

Time (s)	Longitudinal samples		Circumferential samples	
	mean	s.d.	mean	s.d.
0	0.93	0.00	0.97	0.03
1	0.92	0.00	0.93	0.01
10	0.67	0.01	0.71	0.02
50	0.37	0.01	0.41	0.02
100	0.23	0.01	0.25	0.01
300	0.00	0.00	0.00	0.00

Table 6-8: Typical mean reduced relaxation function +/- SD for all the four strain levels obtained at several points in time along the relaxation process

The predicted responses given in Figure 6-12 were calculated based on the AQLV parameters calibrated from the curve fitting of the first stretch as explained previously in Chapter 2.4. Interestingly, the predicted responses show no agreement with the measured experimental data. The peak stress of the experimental data stays around 200 kN/m² whilst the predicted peak stress increases with increasing strain. Lengthy loading phase can be the only reasonable explanation for the poor prediction. Supposedly, if the tissue had been exposed to a reasonably short loading duration similar to the rate introduced in [99, 132, 133] the predicted response obtained in Figure 6-12 would match closely with the experimental data. Compared to the measured data, $\Delta\sigma$ for the predicted data seem to increase in a greater magnitude resulted in a greater curvature of relaxation response for the predicted data. The incorrect estimation is supposed due to the very lengthy loading duration adopted for these experiments. It causes the tissue to greatly relax during the loading therefore by the end of relaxation phase the tissue is loosened extensively and thus hung off the straight axis. On the other hand, knowing that the original tissue length was 30 mm, the MMC rig moves the top sample holder 6 mm away from the bottom sample holder for the first step (20% strain) and 45 mm each for the next three strain increments (35%,50%, and 65%). Thus if part of the tissue is hung off the straight axis between the two sample holders, the tissue is only stretched to the predetermined distance between the sample holders and does not add the extra distance to first straighten the tissue and then apply the set strain. So, in this case the peak strain is hugely underestimated. This is shown in Figure 6-12, where although the

predicted peak stress increases with each strain steps, the experimental data show approximately no change upon the increase of strain.

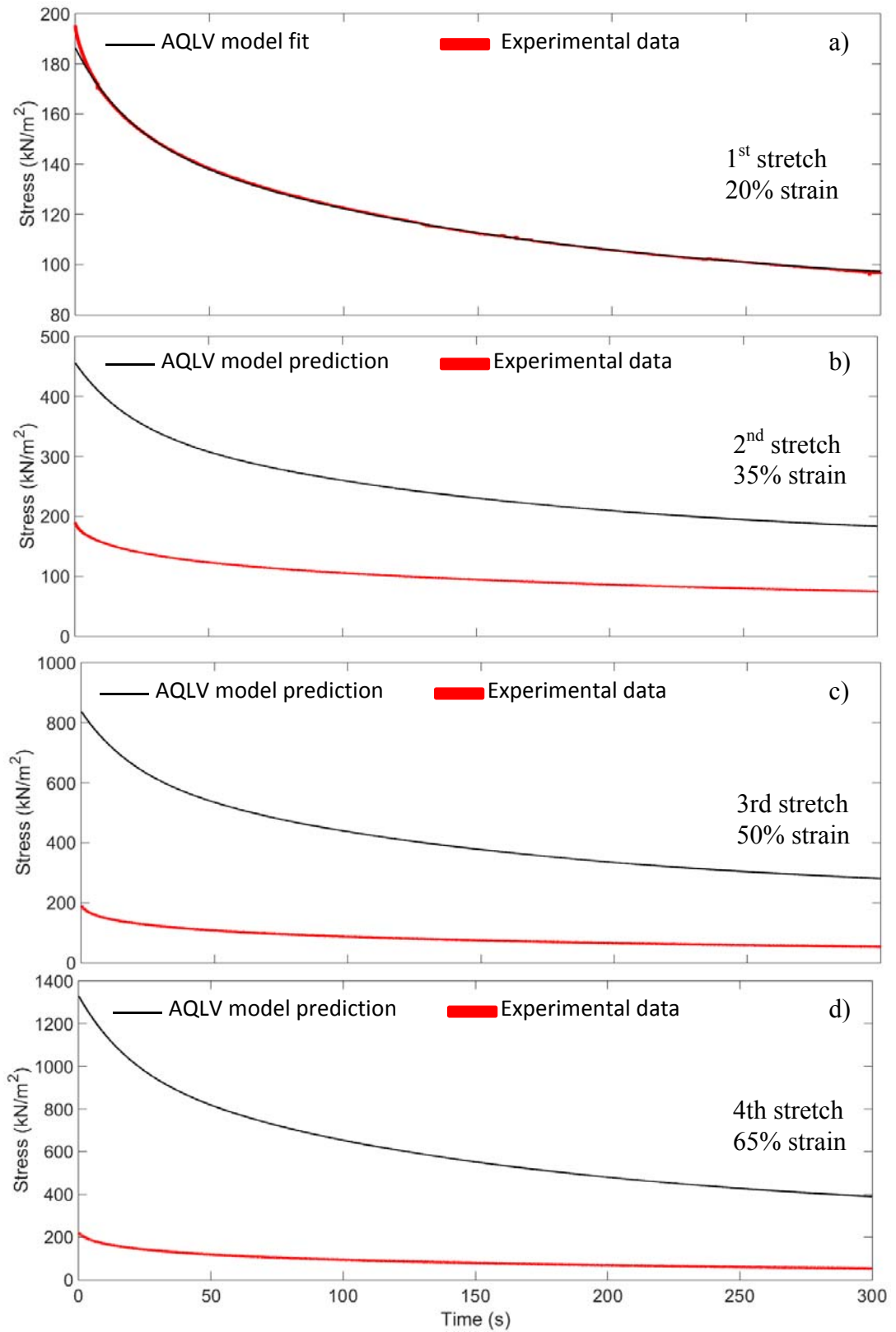


Figure 6-12: Measured (red curves), fitted/predicted (black curves) stress relaxation for the large intestine using the AQLV model under stepwise strain tensile test. The initial strains are a) 20%, b) 35%, c) 50%, & d) 65%. The AQLV model parameter from a) 20% strain level is used to predict the response of tissue for the rest of steps

6.6 Chapter summary

A summary of the main points in this chapter is given in Table 5-2. The effect of fibre orientation on the tissue mechanical behaviour under tensile examination was the main focus of this chapter. The testing protocol followed the one used in Chapter 5 for indentation examination. The mechanical properties assessment included intra-large intestine variation in behaviour, repeated interaction and strain level variation tests. The AQLV viscoelastic model was adopted to fit and predict the relaxation response of the large intestine under tensile stretch. The results are briefed in the table and discussed in the discussion section.

Objective	Method	Results
Multi-axial repeated interaction effect on tissue properties	10 consecutive multi-cyclic indentations on transverse colon in both longitudinal and transversal fibre alignment	<ul style="list-style-type: none"> • Tissue along its longitudinal direct exhibits higher overall stiffness and viscoelastic response. • The mechanical response of both fibre oriented samples settles after 2-3 cycles
Multi-axial strain level variation effect on tissue properties	4× stepwise strain test at 20%, 35%, 50% and 65% strain on transverse colon	<ul style="list-style-type: none"> • The loading phase should be short and fast to observe the full relaxation response during the relaxation phase. • For lengthy loading, tissue relaxation response prediction fails due to unwanted tissue lengthening effect
Multi-axial intra-large intestine tissue variation in behaviour	Preconditioned single indentations on each segments of the large intestine	<ul style="list-style-type: none"> • Stiffer the tissue, greater the stress relaxation response • Due to lengthy loading a lot of unwanted relaxation occurs during the loading phase therefore true relaxation response could not be captured • The relaxation response of the large intestine is modelled well with the AQLV viscoelastic model

Table 6-9: The outline of the objectives addressed in Chapter 5

Chapter 7. Acoustic impedance characterisation of large intestine

7.1 Introduction

So far in this research, ex-vivo mechanical properties of the large intestine were investigated using indentation and tensile techniques. Both techniques have some limitations in terms of the environment in which they can be utilised. In general, tensile tests are only used for tissue characterisation under ex-vivo conditions as the tissue needs to be accessed and held from both ends. On the other hand, although the indentation techniques can perform ex-vivo as well as in-vivo tissue characterisations, they are more difficult to miniaturise and also that it is difficult to control the environment, e.g. what is behind the tissue being indented. The technology deployed for such measurements must be compact so it can efficiently adapt with the design requirements of conventional colonoscopy tubes or the new coming robotic colonoscopy system such as stability, scalability and accuracy. This will enable the practitioner to assess any suspicious area and avoid unnecessary biopsy. Therefore, in this chapter an investigation is presented on a potential technique to characterise tissue properties in-vivo.

As discussed in the literature review Chapter 2.3.2.3 several studies have been successfully investigated the stiffness properties of the objects/tissue based on the acoustic impedance measuring technique. In this technique, the small size of the piezoelectric transducers employed to excite/sense the tissue properties are the key features and makes this a promising candidate method to evaluate here.

7.2 Method

Porcine colon tissue samples were prepared as detailed in Chapter 3.2.2. For these tests, all samples were cut into 20 mm × 20 mm slices. The tissue samples were kept hydrated by brushing saline solution to the samples' surfaces throughout the experiment. The concept development and instrumental set-up was illustrated in Chapter 3.3.3. Table 7-1 summarises the experiments undertaken for each stage of the concept development in this chapter. These tests are selected to link back to the mechanical tests performed in previous chapters. Stiffness variation test is designed to characterise the tissue acoustic impedance properties at peak stress. Force and stiffness variation test determines the effect of varying pressure on tissue's acoustic properties at peak stress and the stress

relaxation tests is conducted to monitor any changes in acoustic impedance properties whilst tissue is relaxing.

Development stages	Sample type	Set-up	Loading force N	Strain-rate mm/s	Relaxation Duration s	Repeat
Stiffness variation test	Silicon shores: full 980, 40, 50, 60, 70, 85 & 95	PZT probe II	4	0.1	40	3
Force and stiffness variation test	Pig rectum and transverse colon	PZT probe II	1 & 4	0.1	40	5
Stress relaxation tests	Pig transverse colon	PZT probe II	1 & 4	0.1	300	5

Table 7-1: Summary of the experimental set-up for each stage of the concept development

7.3 Results

7.3.1 Validation of the method

Figure 7-1 reveals the result of frequency shift and impedance magnitude change as a function of the silicon sample shore using PZT probe I as explained in Chapter 3.3.3. As mentioned in Chapter 3.5.3, the linear modulus values of the silicon samples were also measured during the test. Each data point represents the average of three consecutive shifts on the same location on the tissue (no contact–contact loop, refer to Chapter 3.5.3). The positive frequency shift decrease with the increase of sample hardness. In contrast, the impedance magnitude increases as a function of samples hardness. The positive values of the frequency shift imply that the frequency increases from the no load to the fully loaded states. This is whilst the impedance magnitude seems to drop after transducer-sample contact.

To assess the consistency of the trend, the distribution of the frequency and impedance magnitude shifts across the three samples are shown as box plots in Figure 7-2. Both shifts have high spread of data suggesting that the measuring range changes experiment to experiment. This is because of observing different values of resonance frequency under no load condition every time the experiment was repeated which is due to the experimental error. However, as seen in Figure 7-1 the change of Δf and Δz as a

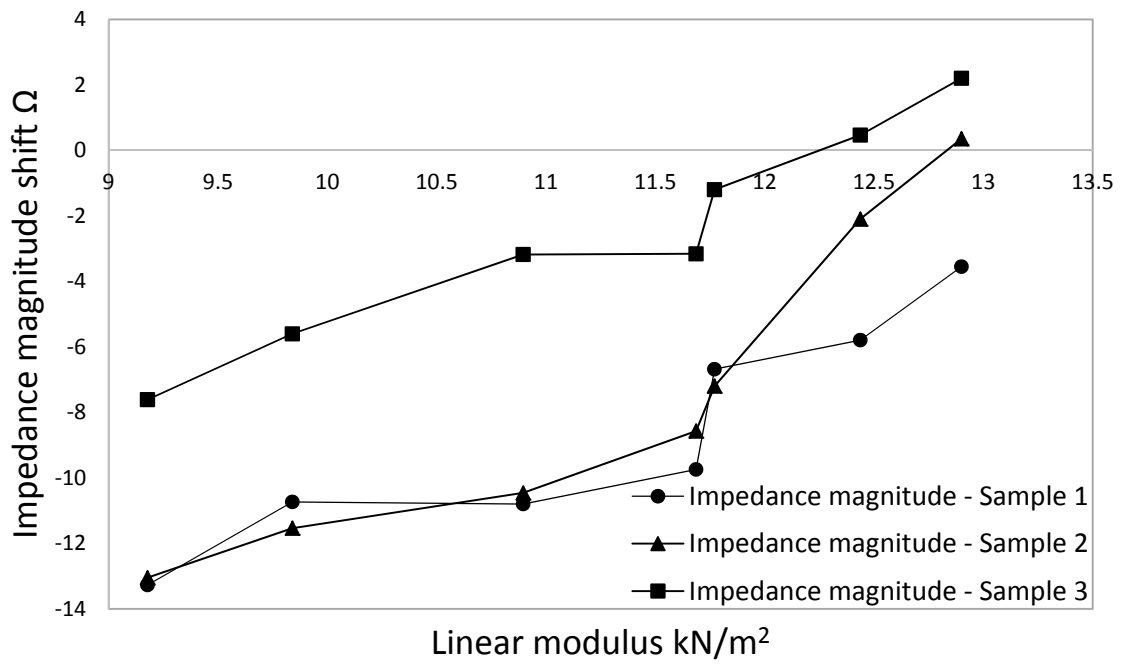
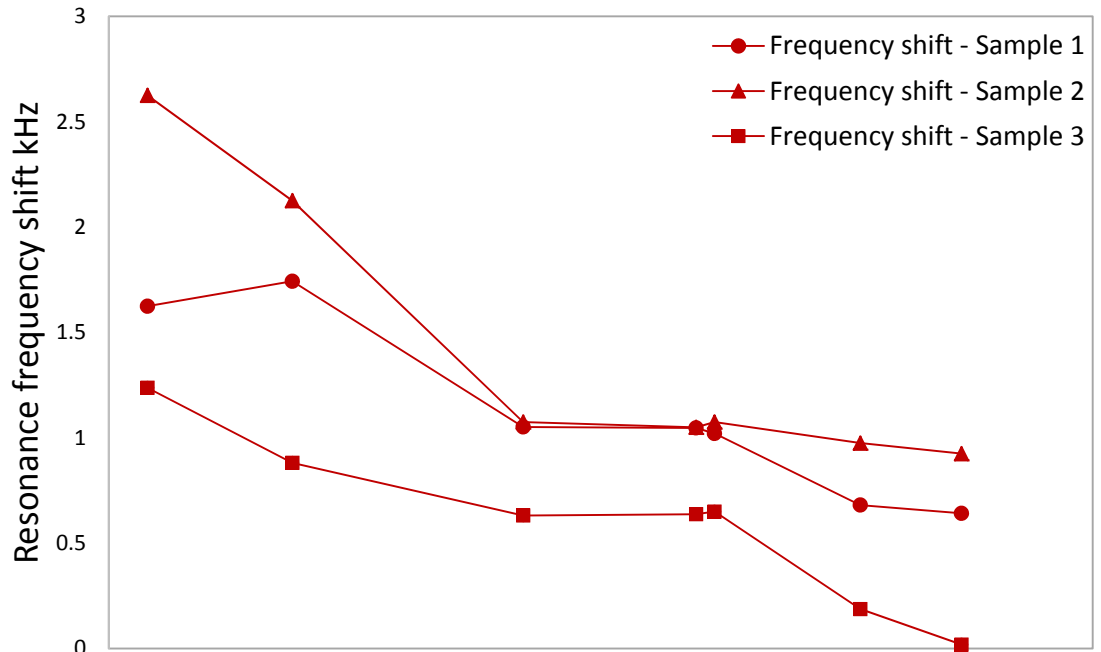


Figure 7-1: Change in resonance frequency and impedance magnitude upon contact on silicon samples with different hardness

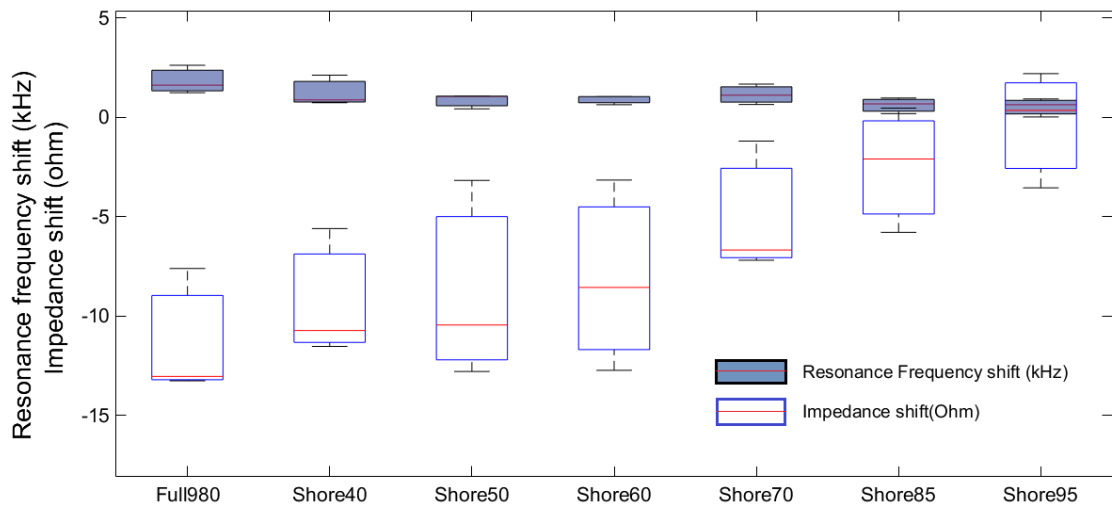


Figure 7-2: The spread of frequency and impedance magnitude shifts

function of tissue hardness is consistent in all the experiments. Hence, method shows efficacy in being able to qualitatively compare between the relative stiffness of the silicon samples as opposed to quantitatively assigning a range of Δf or Δz values to the material stiffness.

Figure 7-3 and Figure 7-4 demonstrate the results of characterising acoustic impedance properties of silicon using a bespoke system PZT probe II comprises an NI data acquisition board PCI-6110 and the stationary PC as explained in Chapter 3.3.3. Figure 7-3 demonstrates a decline in the average frequency shift as the stiffness of the silicon samples increases. Conversely, impedance magnitude increases as a function of stiffness. Both trends agree with the previous finding using the commercial Network analyser in Figure 7-1. However, there is a difference in the results between the two methods in that the range of values for Δf and Δz does not match. Δf greater drops from the softest to the hardest silicon when tested with the PZT probe I (approx. 3 kHz in Figure 7-2) than Network Analyser (1.7 kHz maximum drop from sample 1 in Figure 7-3). Similarly, using the Network Analyser Δz increases significantly, in average 10 Ω , between the softest to the stiffest silicon samples as oppose to the rise of 1.4 Ω obtained by the PZT probe I.

7.3.2 Ex-vivo tissue testing

Utilising the PZT probe III for all the ex-vivo tissue tests, the acoustic impedance response of the large intestine to the excitation under varying applied load was measured and shown in Figure 7-5. The first thing to notice from Figure 7-5-a are the

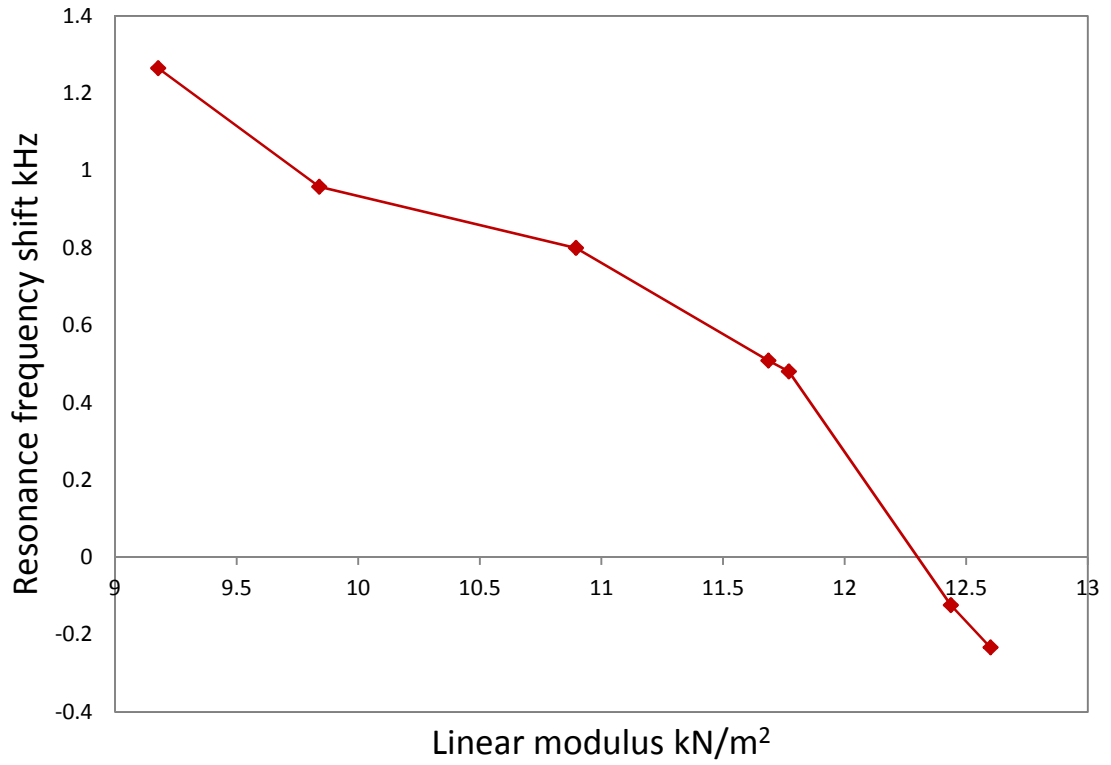


Figure 7-3: Change in resonance frequency upon contact on silicon samples with different hardness

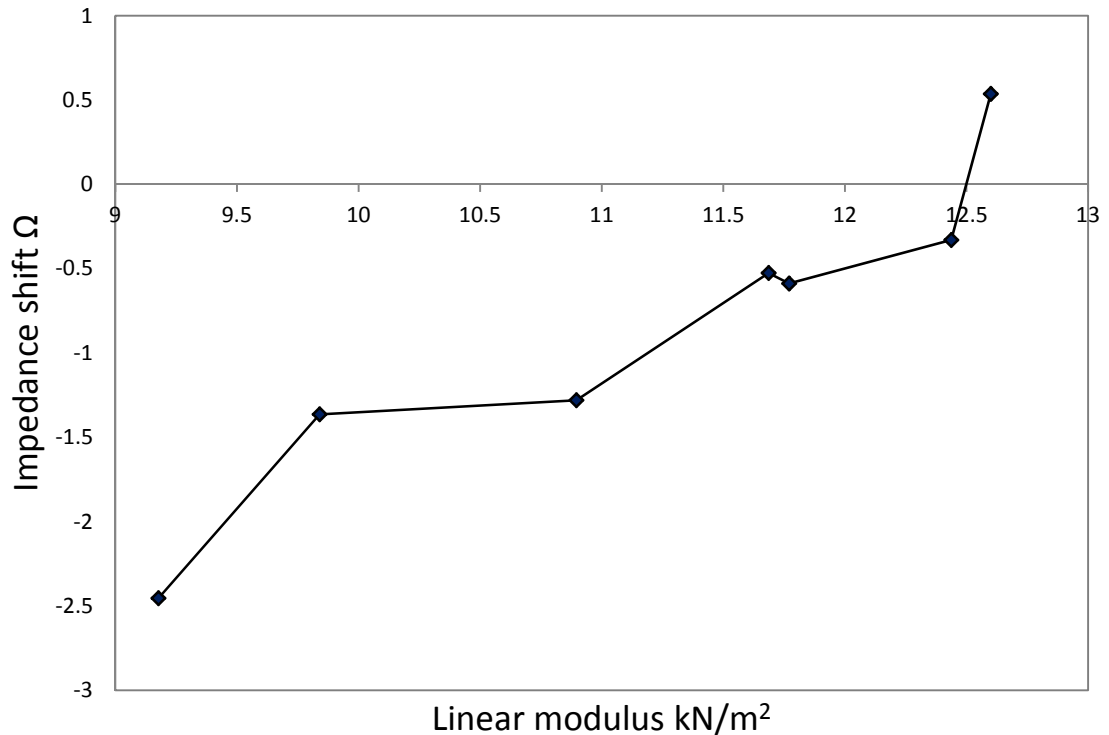


Figure 7-4: Change in impedance magnitude upon contact on silicon samples with different hardness

negative shifts of frequency for the large intestinal samples which implies that the frequency was damped after coming in touch with the tissue. Also, greater negative Δf is observed for the transverse colon compared to the rectum. Based on the results obtained in the literature [76, 79, 84, 86, 134], this pattern of Δf indicates that transverse colon is softer than rectum. This observation is due to the increase of contact area between the transducer and the tissue for the softer tissue which in turn damps the frequency more and results in higher negative Δf . This result is in full agreement with the literature as explained in Chapter 2.3.2.3 [82, 84, 86]. The Δz of the excitation signal in Figure 7-5-b is positive and noticeably small when compared with the results obtained from the silicon samples. Also, the softer tissue samples causes in average higher impedance shift. An opposing observation was obtained in the literature [76] where higher stiffness resulted in higher Δz . The possible explanation for this observation was mentioned in the literature review Chapter 2.3.2.3. It was found that some studies [79, 80] represent Δz as a product of the damping/viscous properties of the tissue. In Chapter 5.4.2 the transverse colon was found to be more viscous than the rectum, therefore here greater Δz was observed for the transverse colon compared to the rectum.

As shown in the measurements results in Figure 7-5-a, the negative frequency shift with increasing contact pressure is obtained by the PZT probe II. Increase of contact pressure from 1 N to 4 N doubles the negative Δf for rectum sample and increase Δf by 1.5 in transverse colon. This is whilst, in Figure 7-5-b positive Δz increases by 1.3 for both samples. This proves considerable sensitivity of Δf and Δz to the varying contact pressure. As discussed in the literature review Chapter 2.3.2.3 several other studies [78, 82, 84] have also found the same trend for Δf under varying contact pressure. No report was found on the trend of impedance magnitude change with varying load in the literature.

The next set of experiment was conducted to investigate the effect of stress relaxation on the acoustic impedance response of the tissue. Figure 7-5 demonstrates this response under 1 N contact pressure. The unloaded response in red is located distinguishably underneath all the other responses. As magnified in the graph the resonance frequency peaks are positioned towards top left in reference to the unloaded responses. This indicates a negative shift of Δf and a positive shift of Δz similar to the results obtained in the previous experiment shown in Figure 7-5 .

Figure 7-6 shows the results of Δf and Δz obtained from four sweeps of frequency captured during the tissue relaxation. The frequency sweeps were performed every minute within 300 s relaxation phase. In Figure 7-7-a all the negative Δf 's decrease with time during the tissue relaxation. This trend is explained by the change in contact area in the course of the stress relaxation. As the tissue relaxes the contact area

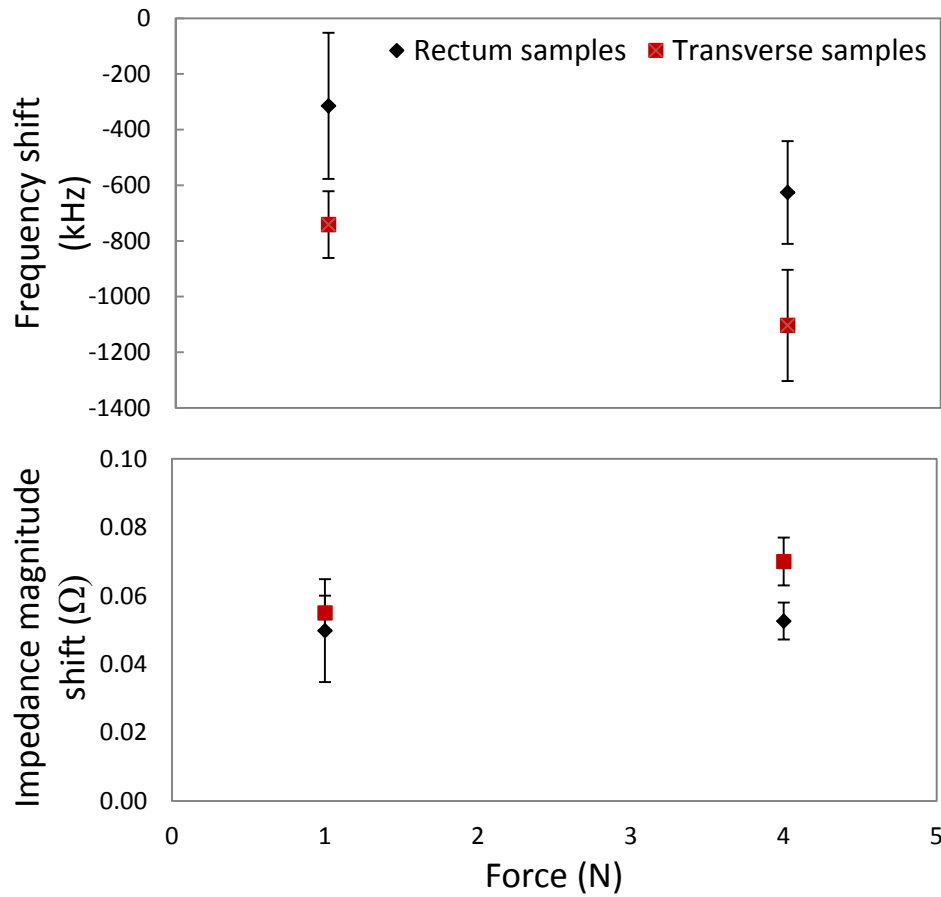


Figure 7-5: The change of a) frequency and b) impedance amplitude for two segments of the large intestine under varying applied load

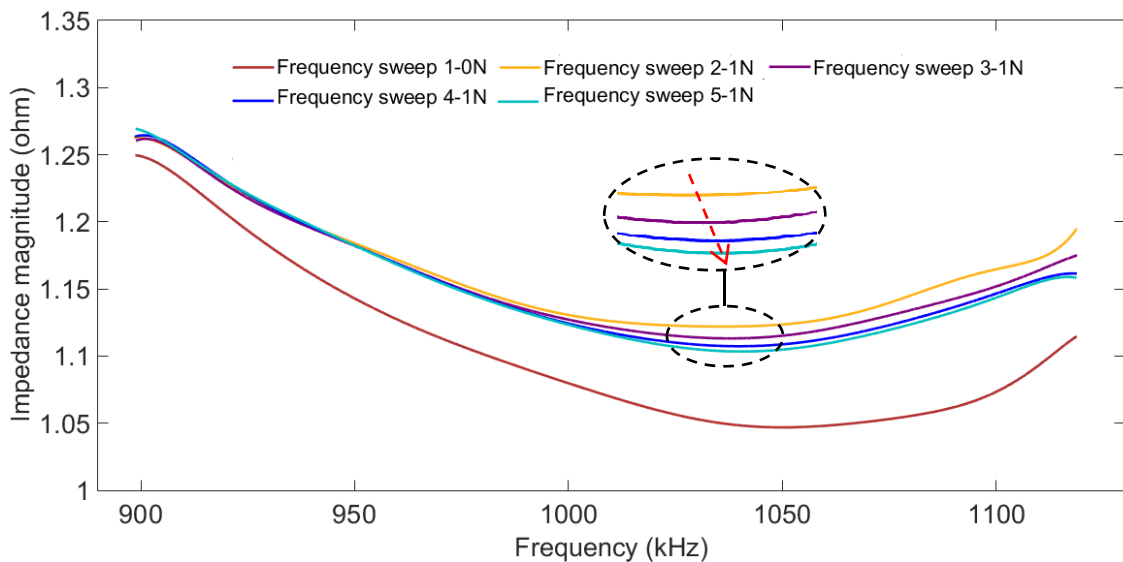


Figure 7-6: Acoustic impedance response of the tissue during stress relaxation. The red curve parted from the rest represents the frequency sweep under no load and all the other curves demonstrate the frequency sweep at 1 N loaded tissue

between the tissue and the PZT probe II decreases and hence frequency is damped less. The impedance magnitude response shown in Figure 7-7-b indicates that, except in one case, the rest of positive Δz responses decline with time. As explained before Δz

corresponds to a viscous response of the tissue therefore the trend shows the loss of viscosity with time as the tissue relaxes.

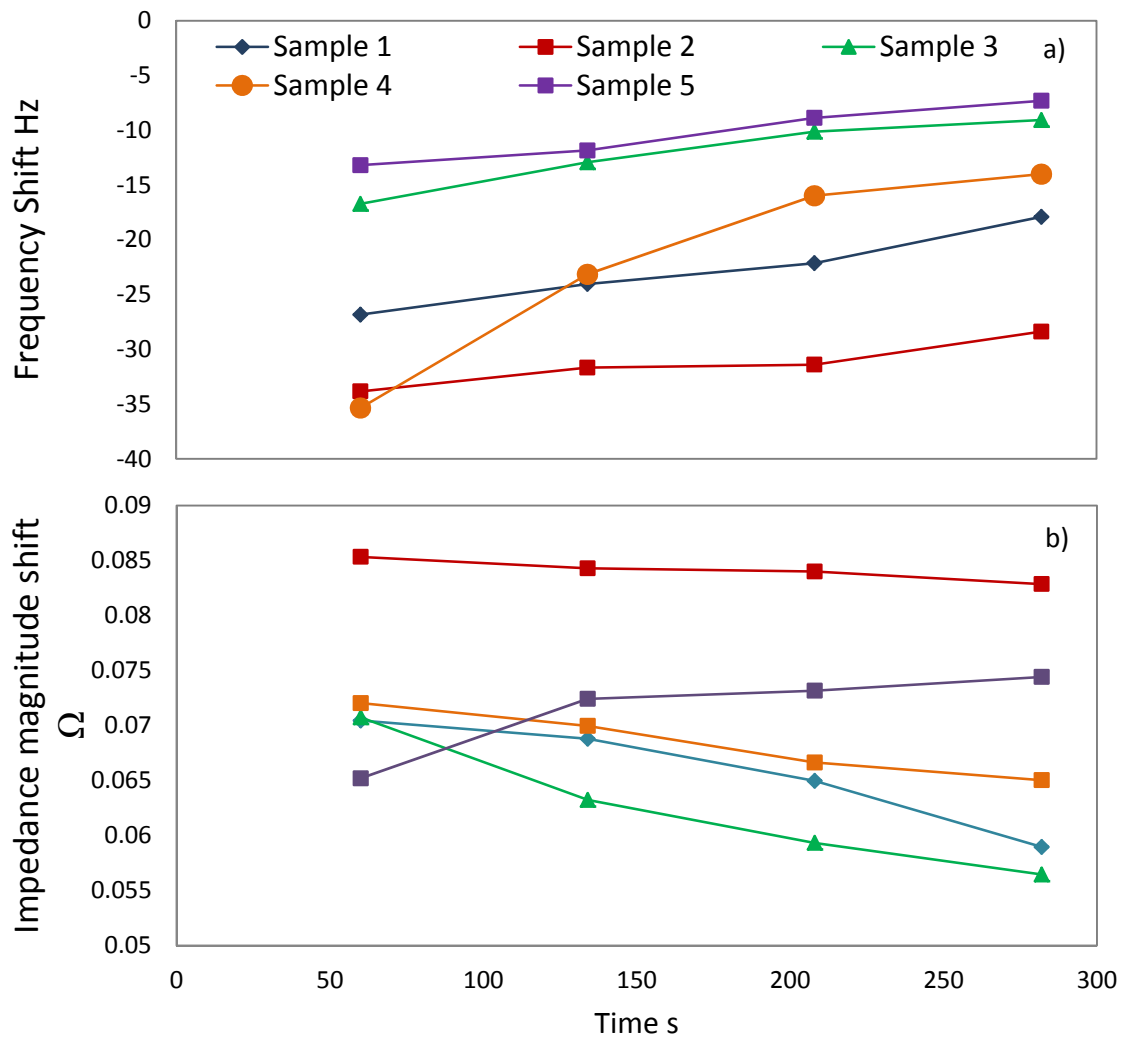


Figure 7-7: a) Frequency shifts and b) impedance magnitude shifts of the tissue to the PZT probe II oscillation under 1 N contact pressure during 300 s relaxation phase.

7.4 Chapter summary

This chapter explored the feasibility of a new technique to characterise tissue properties of the large intestine which has a possible application for in-vivo characterisation of the tissue. A commercial machine was employed to validate the technique and the bespoke devices built in house to conduct the measurements. Silicon samples as well as the large intestine samples were tested under various experimental modes. The experiments were designed to measure the sensitivity of the devices to measure the stiffness change of the samples, and to measure the effect of varying contact pressure, and tissue relaxation on

the acoustic impedance properties of the samples. Valuable results were obtained and compared with the literature. The results are summarised in Table 7-2.

Objective	Method	Results
Stiffness property variation test	3×Single indentations at 4 N	<ul style="list-style-type: none"> •The shifts of frequency and impedance magnitude are consistent with the change of material hardness •The technique is accurate enough to qualitatively detect the relative stiffness of the silicon samples using •The bespoke PZT probe I is as accurate as the commercialise Network analyser
Force and stiffness variation	5×Single indentations at 1&4 N	<ul style="list-style-type: none"> •Δf and Δz are sensitive to the applied pressure where increase of contact pressure results in higher -ve Δf and +ve Δz
Stress relaxation tests	5×Single indentations at 1 N	<ul style="list-style-type: none"> •The shift of Δf during tissue relaxation indicates a consistent decrease of contact area between the indenter and the tissue •Decrease of Δz during stress relaxation shows the decline of tissue viscosity

Table 7-2: An overview of the key points in this chapter

Chapter 8. Discussion

This chapter aims to bring together a comprehensive discussion which covers various features of characterisation of the large intestine properties investigated in this research. It begins with examining the effects of repeated loading, varying strain-rate and strain history on tissue properties are discussed which consequently helps to develop guidelines for designing an appropriate testing protocol for assessing mechanical properties of the large intestine. Then, it evaluates the linear and non-linear tissue modelling employed to extract various tissue properties under testing conditions considered in this research. Finally, the potential use of the acoustic impedance technique for in-vivo tissue characterisation is assessed and the future implication of this technique for medical use is discussed. The following bullet points outline the main discussion in this chapter:

- Mechanical characterisation of the large intestine - In this section it is illustrated that optimising protocols for data collection are critical in evaluating the mechanical properties of soft tissue.
- Tissue modelling - This section defined how describing tissue from the point of view of mechanical properties is complex. It is shown that non-linear modelling is by far superior to a simple linear modulus modelling.
- Acoustic impedance tissue characterisation - This technique was found to be an effective method to evaluate softness/hardness of soft tissue and has the potential to be used for in-vivo assessment of tissue during colonoscopy/robotic hydro-colonoscopy procedures.

For each of these areas the contribution to this field made in this field are outlined.

8.1 Mechanical characterisation of the large intestine

The major concern in this research was to design an appropriate testing protocol which could consider the requirements and the limitations of measuring mechanical properties of the large intestine. The large degree of variability associated with strain-rate dependency, preconditioning, stress relaxation duration and tissue sample condition were found to extensively influence the mechanical response of the large intestine. These variables are the common reasons that make comparisons between existing

studies very challenging. The influence of these effects on the large intestine is discussed as follows.

8.1.1 Repeated interaction effect

According to several studies, under repeated interaction the viscoelastic properties of the soft tissue change due to the structure composition of biological tissue and the movement of fluid within the tissue [10, 22, 50, 96]. The stress/strain history of the soft tissue is eliminated by mechanical preconditioning to obtain a consistent mechanical response. Linear and non-linear models were employed to identify the effect of repeated interaction on the large intestine.

8.1.1.1 Stress- strain response

Figure 8-1 demonstrates a correlation between tissue hydration and preconditioning on the linear modulus response of tissue. The results of repeated interaction tests for the sample in air show that tissue becomes stiffer with preconditioning. According to the MUST and MMC results five repeated cycles were enough to reach stable results. A similar trend was also observed by Meghezi et al. [22] study on collagen fibres. This pattern occurs because of residual strain (the deformation left in the tissue from the previous state). Under cyclic or lengthy loading, deformation recovery happens slowly and imperfectly. The viscous and plastic properties of the tissue are responsible for the partial recovery of the tissue to its original length. Once strain is applied to the tissue the fluid that surrounds the collagen chains are squeezed into the porous network. This realigns the tissue chains [95]. By repeating the indentation, the movement of fluid through the chain reduces and the chains stiffen. The collagen network is responsible for the elastic and plastic characteristics of the tissue whilst the fluid provides the viscous characteristics [95]. This type of behaviour agrees with the findings from other studies, for instance, Rosen *et al.* [10] suggested seven to nine loading cycles for stabilising the stiffness properties of the in-vivo large intestine under indentation loading, and Liu *et al.* [50] captured repeatable strain-stain response of the skin tissue from the fourth-sixth cycles onwards.

Considering the MMC-indentation results in Figure 8-1, insignificant change of linear modulus due to preconditioning is observed for the samples in PBS compared to the samples in air. This is because the water content in the tissue collagen chains is

preserved in PBS solution and this prevents the tissue from stiffening. This is also why the peak stress is ranged lower for the hydrated tissue than the tissue sample in air. This is confirmed by [64, 104] where the biological tissue were found more compliant when hydrated.

The multi-axial tensile tests in PBS, demonstrates a slight decrease of the peak stress as it is preconditioned. This was due to the lengthy loading and the consequent tissue lengthening effect as explained previously. When comparing the stress-strain response of the tissue in different fibre orientations, a higher peak stress is observed for the longitudinal stress implying to the stiffer properties of tissue in this orientation compared to the circumferential sample. Studies such as [6, 71, 72] also agreed with this trend, as explained in Chapter 2.3.2.2.

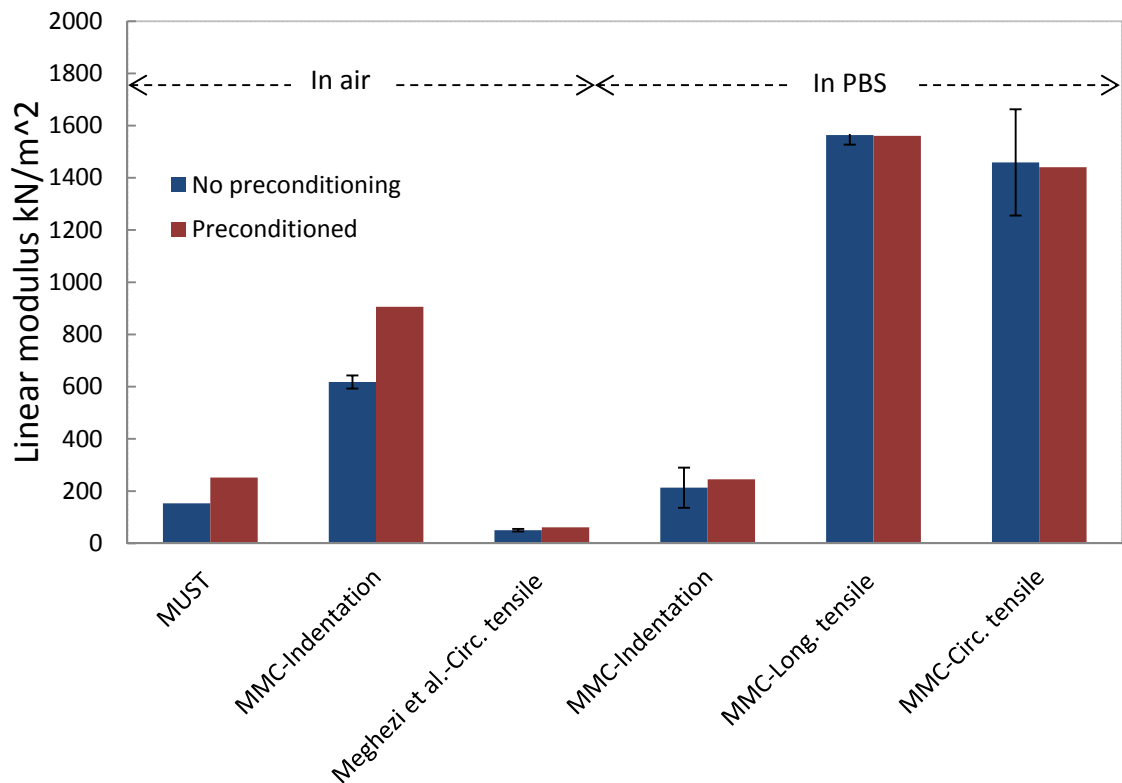


Figure 8-1: The effect preconditioning and hydration on the linear modulus values in this study and the literature. All the samples are obtained from pig large intestine except Meghezi et al. study on collagen gel

8.1.1.2 Stress relaxation response

Viscoelastic ratio VR, which is the ratio of the instantaneous modulus E_0 and equilibrium modulus E_3 , is used to compare between the overall extend of relaxation of the tissue. The general trend of viscoelastic ratio shows that the tissue becomes more

elastic and less viscous with each successive indentation, as there is a progressive increase in the viscoelastic ratio with each indentation. The decrease of viscosity can be explained by the fact that after preconditioning the collagen fibres are aligned in the direction of the force and the chain motion is enhanced by disrupting some molecular interactions [22]. In comparison to other tissues, the average viscoelastic ratio of porcine large intestine obtained in this research (VR=0.63) shows less elasticity to that of PS-4 polymer (VR= 0.89) and calf bone (VR=0.75), but more elastic than that of calf patella cartilage (VR=0.1) [64].

In Figure 8-2, with lower initial VR, the viscoelastic ratio response of transverse colon in air follows the same pattern as that of rectum. However, there is a big difference between the VR in air and in PBS under indentation in that the samples in PBS show more viscosity from the beginning of repeated interaction test and the VR in PBS does not change as drastically as the VR in air with increase of cycles (Figure 5-10). These both demonstrate that the natural state of the tissue is best preserved in the PBS solution, and tissue manipulation in a hydrated state does not change the properties of the tissue as much as when the tissue is kept in air. In the multi-axial tensile test, both fibre orientations have very similar VR throughout the whole process. There is no data in the literature to compare these results with.

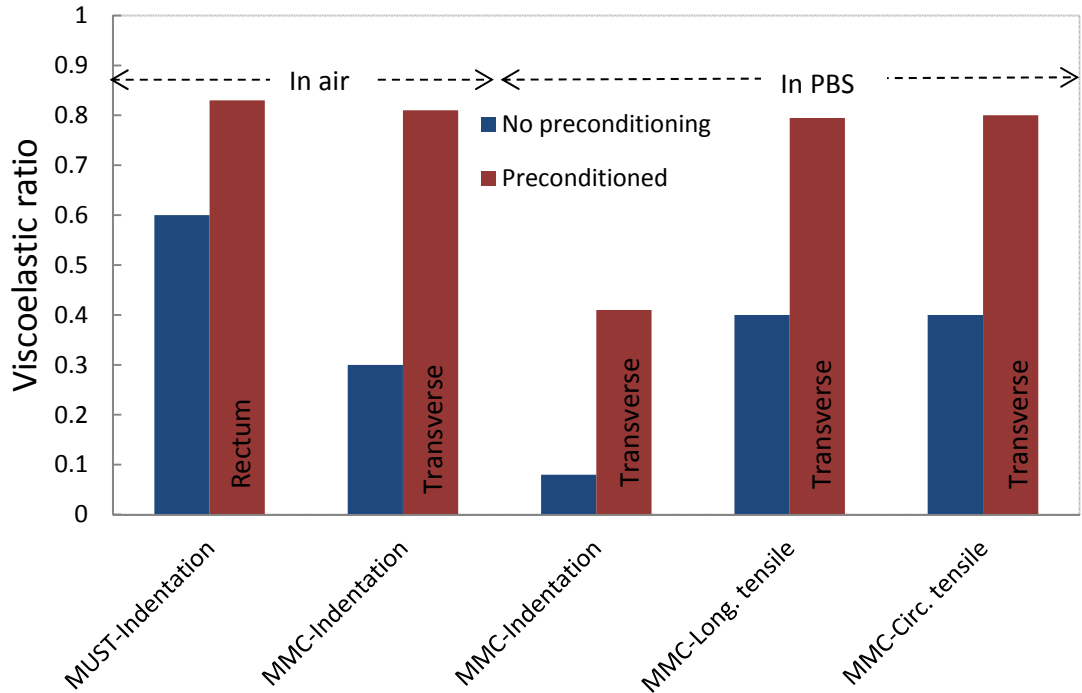


Figure 8-2: The effect of preconditioning and hydration on viscoelastic ratio of the large intestine. Rectum samples were used for the MUST-Indentation whilst transverse colon samples were obtained for all the other of data

The increase of equilibrium modulus, E_3 in Wiechert model or σ_0 in AQLV model, with progression of cycles suggest that the collagen fibre structure of the rectum becomes stiffer cycle by cycle as plastic deformation occurs in the direction of the applied load. This plastic deformation is more permanent for the first cycle as the most significant deformation to the tissue occurs during the first indentation. As in Figure 8-3, the samples in the PBS exhibit much lower σ_0 values and therefore lower stiffness properties than the samples in air. The variation of σ_0 values for the PBS samples had a much smaller range throughout the repeated interaction process compared to the σ_0 values for the samples in air which shows that the elastic properties are kept more consistent under manipulation in PBS. The average σ_0 is marginally higher in longitudinal than circumferential directions, however due to the experimental error caused by tissue lengthening effect during the loading phase the results of tensile examination is inconclusive as explained in Chapter 6.4.2. Analysis of the stress relaxation in [71, 135] showed that tissues such as cortical bone and tendon are strongly anisotropic where the mechanical properties of the longitudinal samples significantly greater than the circumferential samples.

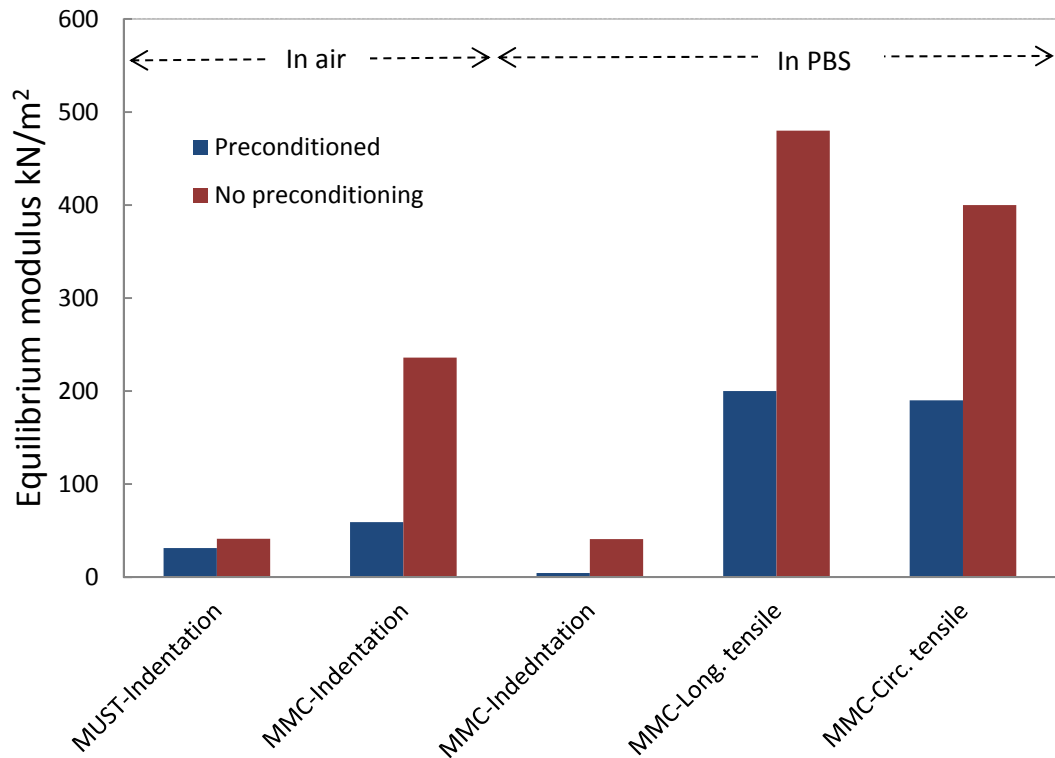


Figure 8-3: The effect of preconditioning and hydration on the equilibrium modulus of Wiechert model (MUST-Indentation) and AQLV model (MMC-Indentation/Tensile). Rectum samples were used for the MUST-Indentation whilst transverse colon samples were obtained for the rest of data

8.1.2 Strain-rate variation effect

The effect of varying strain-rate on two mechanical responses of the large intestine, stress-strain response and the stress relaxation, were investigated. In the literature review Chapter 2.5.4, it was mentioned that soft tissues respond differently to varying strain-rate. In one study [8] the loading stress-strain response of large intestine in-vitro was identified as strain-rate dependent with higher stiffness obtained for higher strain-rates. In this section, linear and non-linear modelling tools were utilised to determine the influence of varying loading rate on tissue properties.

8.1.2.1 Stress-strain response

The results of varying strain-rate shows that where the elastic response of tissue (Figure 4-6- b) demonstrates small strain-rate dependency, the linear modulus values are left almost unaffected with change of strain-rate (between 0.01, 0.2, 0.5 mm/s strain-rates). In the literature, the only example of such data obtained for the large intestine is by Higa *et al.* [8]. For the samples in-vitro the stress versus strain response showed very little dependency to strain-rate under compression. This backs up the trend of elastic

response obtained in this study. However, the low strain-rate dependency in the Higa *et al.* [8] experiments was mainly pronounced between the fast strain-rates (i.e. between 0.5 and 5 mm/s). It would not be known here to what extent the strain-rate dependency of the large intestine changes if the range of strain-rate increases. Other studies in the literature have reported contrary results. Where the linear modulus of pig liver (with strain-rates of 1.27, 2.54, 25.5 mm/s) [110] and sheep tendon (0.002 and 0.2 mm/s) [71] were found rate dependent (i.e. higher strain-rates resulted in lower resistance to deformation), the linear modulus of mice tendon (0.05 and 5 mm/s) [111] and canine collateral ligament (0.001, 0.01 and 0.1 mm/s) [136] did not show any rate dependency. The difference in the reported results is understandable due to the variety of factors which could affect the mechanical properties of the tissue such as experimental protocols/conditions, the species, and the range of strain-rate.

8.1.2.2 Stress relaxation response

Stress relaxation behaviour of the rectum demonstrated a great dependency on strain-rate where higher strain-rate resulted in greater tissue relaxation and faster overall relaxation. This is believed to be due to the amount of tissue relaxation that occurs during the loading phase prior to the peak strain. On average, 1.5 s, 5 s and 15 s of loading duration was observed for the strain-rates of 0.5, 0.2, and 0.05 mm/s respectively. Lengthier loading allows for higher tissue relaxation during the loading phase and therefore reduces the amount of relaxation during the stress relaxation phase. By increasing the strain-rate, as demonstrated by the pattern of elastic moduli in Table 4-4, E_1 increases, E_2 decreases and E_3 is not affected. In the literature, there is no study on the large intestine that has evaluated the effect of strain-rate on non-linear properties. Similar to this work, [137] uses a series of non-linear models to investigate this effect on aortic valve tissue and found that different models result in observing different strain-rate sensitivity of the model parameters. For two of the models investigated in this study, the QLV model and Kwan and Woo [138], strong correlations were found between the model parameters, where relaxation rate slows down with increasing strain-rate. Whilst parameters of the direct-fit method proposed by this study [137] were not significantly affected by the strain-rate.

8.1.3 Strain history dependency

The mechanical properties of the large intestine tissue under indentation were found to be strongly dependent on the level of strain in Chapter 5. The increase of linear modulus and stress at equilibrium σ_0 as a function of strain level indicates that tissue becomes stiffer as it is indented further. Also, it was interesting to observe that the tissue relaxation proceeded faster with decrease of strain level. This is in complete agreement with the response of human and rat collateral ligament reported in Lista *et al.* [115] and Provenzano *et al.* [90]. Conversely, the multi-axial tensile viscoelastic response of tissue in Chapter 6 showed no dependency to the history of strain as a result of lengthy loading as explained previously; therefore the results from the tensile tests are inconclusive. The performance of the AQLV model in predicting the response of tissue at different strain levels will be discussed in Chapter 8.2.2.2. It was concluded that the loading strain-rate and loading duration should be set appropriately for the AQLV model to accurately predict the tissue response.

8.1.4 Testing protocol design for tissue characterisation experiments

Based on the above investigations guidelines are proposed to set suitable testing protocols for tissue mechanical characterisation of soft tissue as follows:

- To observe pure elastic response during the loading phase and full relaxation response during the relaxation phase, any relaxation of tissue prior to the relaxation phase should be avoided. This is possible through selecting a rapid change in the strain whilst taking into account the errors such as vibration, noise and overshoot which are introduced to the data due to the rapid loading. Strain rate of 0.5 mm/s was the highest speed used for indentation in this research and found to be still too slow to serve the purpose. In the literature, up to 5 mm/s for indentation [8] and 300 mm/s for tensile stretch [12, 13] were used to keep the loading under 1 s for characterising properties of the large intestine, as shown in Table 2-1. Therefore, to set an appropriate strain-rate it is suggested to run some preliminary tests using the highest speed that the apparatus allows and reduce the speed until the system reaches the desired signal to noise ratio.
- The stress relaxation should be long enough to observe the full tissue relaxation. According to [22, 135, 139, 140] 300 s is long enough to reach steady state. However, as seen in Chapter 5 and Chapter 6, the majority of the tissue

responses did not achieve equilibrium at this duration. As a result, it is suggested to run preliminary tests prior to the main tests to find the suitable duration for relaxation phase.

- It is crucial to keep the tissue hydrated from the moment it is excised to ensure the mechanical properties are preserved
- The necessity of tissue preconditioning depends on the end application and the tissue condition. For example, under constant hydration (in PBS) preconditioning is not necessary. On the other hand, preconditioning is essential to stabilise the tissue response if the tissue is kept in air as to replicate open abdomen/prolonged surgeries or CO₂ insufflation colonoscopy procedures.

One of the main fields which can truly benefit from accurate definition of the mechanical properties is design and development of colonoscopy tools, robotic endoscopy, or laparoscopic instruments for minimally invasive surgery. As mentioned previously, as part of the essential requirements for designing these tools the behaviour of tissue under manipulation by these devices needs to be understood. Whether it be a colonoscopy or a robotic endoscopy device manoeuvring inside the lumen or a laparoscopic tool palpating/compressing the tissue for detecting tumours and abnormalities, it is important to understanding the effects of any possible physical interaction (i.e. collision), varying manipulation speed and repeated interaction on the tissue response. Also, in robotic endoscopy it is essential to be fully aware of the robot's surrounding environment for an effective and safe procedure.

8.2 Tissue modelling

As presented in the literature review Chapter 2.4, tissue modelling is essential to extract valuable information that the raw experimental data cannot identify. In this research a range of phenomenological models were examined to identify various characteristics of the large intestine. The main characteristics of any soft tissue are manifested itself in the relationship between the applied stress and resultant strain. Linear modulus modelling using the linear regression fit to the stress versus strain data is one of many methods to estimate a quantitative elastic response or stiffness of the tissue. However, for soft tissues with non-linear mechanical properties estimating linear modulus can be challenging. The other way of characterising soft tissue properties is through analysing the stress response of tissue to a constant strain during the stress relaxation phase.

Various viscoelastic models were utilised to analyse the elastic and viscous properties of the soft tissues. Whilst linear modulus values are used in development of medical instruments and tissue engineering for quantitatively identifying the elastic behaviour/stiffness of soft tissues, some viscoelastic models can be used as predictive tools for analysing non-linear viscoelastic response of the soft tissue.

8.2.1 Linear modulus

The accuracy of the linear modulus for assessing the large intestine stiffness was found inconsistent for detecting changes in stiffness under indentation examination. As the results in Chapters 4 to 6 reveal, the mechanical response of tissue is highly non-linear, strain-rate and history dependent, these make the linear modulus an approximation that should only be used under certain conditions (as discussed in Chapter 3.6.1), as to eliminate the viscous behaviour to incorporate with linear modulus [22]. The most practical testing condition for measurement of linear modulus according to the literature [13, 22, 71] is stretching the tissue at a very fast strain-rate to the point of rupture. The highest loading speed achieved from the MUST rig was limited to 0.5 mm/s and that was under indentation examination. For the MMC rig, the strain-rate was kept low, 0.1 mm/s, to avoid the stage actuator introducing vibration and noise to the data for both indentation and tensile examinations. As Figure 8-4 illustrates, the average linear modulus value of rectum obtained from the MUST rig is lower than that of the MMC rig which is as a result of the difference in the peak stress ($115 \pm 11 \text{ kN/m}^2$ for the MMC rig as opposed to 50 kN/m^2 for the MUST rig) and the strain-rates. The MMC linear modulus is suggested to be a better representation of indentation response of the rectum compared to that of the MUST rig, since firstly greater elastic response is observed at higher peak stress and secondly because of its slower strain-rate greater dissipation of viscoelastic response is achieved before the linear region.

For the tensile examinations, the average linear modulus of the rectal wall in longitudinal and circumferential orientations obtained using MMC rig are an order of magnitude greater than the Young's Modulus reported by Watters *et al.* and Qiao *et al.* [13, 40]. The same pattern is observed for the linear modulus of the colorectal wall. As well as the several differences in the testing protocols such as higher strain-rate, both studies managed to stretch the tissue to the point of rupture to identify the correct linear region for linear modulus calculations. Therefore, the linear modulus values reported

here under tensile tests are unable to represent the true stiffness values of the large intestine at different segments.

The indentation results are much closer to the reported tensile data in the literature, although the relationship between the two techniques has not been determined. Several studies have compared the two techniques for alloy materials in order to find a correlation between the tensile yield strength and the indentation hardness [118, 131, 141]. In [141] the hardness value obtained from indentation test was found overestimating the measured strength, whilst in [118, 131] good correlations between indentation-tensile creep, and hardness-yield strength was obtained. In the present study, due to experimental discrepancies the tensile data were found unreliable for a direct comparison with the indentation results. But besides that, there are factors that differentiate the response of tissue to the two techniques. In the indentation technique, the deformation is localised around one point and so particle fracture is suppressed [141]. The particles fracture under tensile testing develops during the stretch under a uniform deformation. In contrast, as the tissue is indented further the plastic deformation is concentrated in the localised region and so the density of particle under the indentation increases which leads to tissue hardening. This is whilst outside the region the tissue is highly elastic [141]. Therefore, the hardness obtained from the indentation test tends to overestimate tensile strength. This also can be seen in the data obtained in this research. The linear modulus values of colon and rectum associated with indentation are two to three times greater than the tensile linear modulus values obtained in the literature as shown in Figure 8-4.

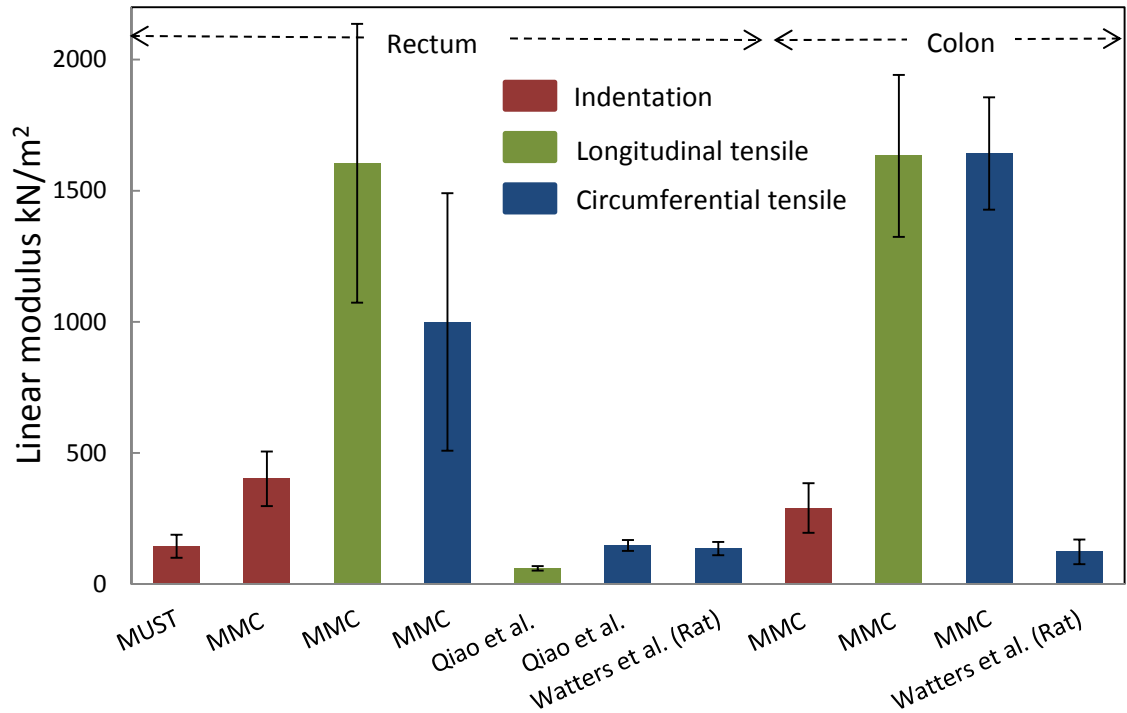


Figure 8-4: Comparison of linear modulus values between different techniques used in this study and the literature on the large intestine. All the reported studies were performed on pig samples except stated otherwise

8.2.2 Non-linear modelling

The response of tissue under the stress relaxation phase can be used as an alternative to linear modulus obtained from the loading phase with regard to estimation of the elastic properties. Several viscoelastic models have been proposed in Chapter 2.4 to analyse the stress relaxation response of soft tissues. The two models investigated in this research were the Wiechert 5-element model and AQLV model.

8.2.2.1 Wiechert 5-element model

The Wiechert 5-element model, Equation 2.23, was initially chosen and found to be well suited to the relaxation response of the rectum under indentation. Observing the values in Table 4-3, it is evident that when one of the elastic modulus is higher than the other its corresponding time constant is also greater, i.e. if $E_1 > E_2$ then $\tau_1 > \tau_2$ and vice versa. This implies that, the first relaxation process allows for greater stress decay within a longer relaxation time than the second process. This is in accordance with results obtained by Shahmirzadi et al. [142] on bovine aortic tissue. In his report each relaxation process is associated with microstructural components in the tissue, elastin and collagen [142] where the higher elastic and viscous coefficients are contributed

from collagen fibres (which are responsible for the strength of the tissue) and the lower constants belong mainly to elastin fibres [142]. However, in other studies the relation between the relaxation constants were found as $E_1 > E_2$ and $\tau_1 < \tau_2$, suggesting that the first relaxation process is more elastic and the second one is rather viscous [22, 135, 139]. Yet, all the above studies used very high loading strain-rates and long periods of stress relaxation ≥ 300 s where the stress almost reaches steady state. In Table 4-4 the increase of the strain-rate results in the magnitude of E_1 and E_2 approaching one another, suggesting that by increasing the strain-rate further the two values may converge, and eventually become $E_1 > E_2$ and $\tau_1 < \tau_2$ as found in [22, 135, 139]. The lower fitting errors RMSE for the higher strain-rates indicate improved suitability of the Wiechert model at greater strain-rates. When compared with the literature [128], the fitting error obtained from the high strain-rate of 0.5 mm/s lies within the acceptable range. This confirms that to describe the tissue response using Wiechert model the best result is achieved by loading the tissue at high strain-rates approaching a step input (whilst considering the drawbacks such as tissue damage and vibration) as the relaxation response is sensitive to the loading strain-rate.

Moreover, choosing a short relaxation time of 10 s was aimed to simulate the viscoelastic effects under compression/grasping tasks as explained in chapter 3.4 [10, 121]. It was then concluded that there are three issues with these measurements which may compromise the results. Firstly, the low strain-rate allows some stress relaxation during the loading phase which the Wiechert model does not take into account. Also, the 10 second relaxation does not seem to relax the tissue to the equilibrium state meaning that the calculated E_3 is not the true long-term elastic response. Secondly, tissue was tested in air implying that the tissue dryness can also influence the elastic response.

Besides these limitations in the methodology, the model has no predictive value as it does not take into account the strain history. According to the strain-rate and strain-level variation experiments conducted in this study (Chapters 4.4.2, 5.4.4, 6.5) the large intestine relaxation response is strain-rate and strain history dependent. This means under any normal loading rates (i.e. not extremely fast or ultimately slow) the tissue's stress relaxation response depends on the selected strain-rate and peak strain. The Wiechert 5-element model provided a good fit for the viscoelastic response of tissue; nonetheless, it is unable to simulate the non-linear tissues response to generic

elongation. Hence, a suitable viscoelastic model adopted to predict the large intestine should consider the speed of loading as well as the level of strain during the tissue loading.

8.2.2.2 Adaptive Quasi-Linear Viscoelastic (AQLV) model

Proposed by Nekouzadeh *et al.* [23], AQLV has been used to predict the mechanical response of the soft tissue depends on its strain history and strain-rate. The model, equation 2.41, includes terms to consider strain history ($n\Delta\varepsilon$) and an element of strain-rate ($\frac{\Delta\varepsilon}{T}$) which satisfy the prediction of the large intestine relaxation response.

The equilibrium modulus (E_3 in Wiechert model or σ_0 in AQLV model), which represents the parallel single spring in Figure 2-31, has been used in the literature [22] as an estimation of the tissue elastic modulus. In [22] it was argued that this value is a better indication of the elastic response of the tissue as oppose to linear modulus, due to the fact that the linear modulus value incorporates both elastic and viscous responses and therefore, it overestimates the degree of elasticity. The results of indentation and tensile examination in this study also show a good agreement of this parameter with the changes in peak strain/stress. As shown in Figure 8-5, the equilibrium modulus values obtained from the Wiechert 5-element and AQLV model fitting to rectum data are in good agreement. Comparing to the literature, Wang *et al.* [140] observed lower modulus for liver and spleen employing a similar method as in this study. The main difference between the studies is the low stress threshold 0.5 N (as opposed to 50 N and 115 N used here) up to which was used to indent the tissue, therefore liver and spleen tissues show an order of magnitude lower modulus values. Due to the similar reason, greater modulus was found for the rectum than the collagen gel and achilles tendon.

Two different types of relaxation responses were observed for the indentation of the large intestine using the MMC rig where ascending colon sample relaxes to a steady state the rectum samples does not. This is investigated further by considering the parameters of the AQLV model for the two responses. The equilibrium modulus σ_0 obtained for the ascending sample is two orders of magnitudes less than that of the rectum sample. For the rectum sample, when the relaxation parameters are ordered starting from the highest time constant to the smallest one as $\tau_1 < \tau_2 < \tau_3$, the elastic moduli

are ordered in the same way $E_1 < E_2 < E_3$, which is similar to the results of Wiechert model.

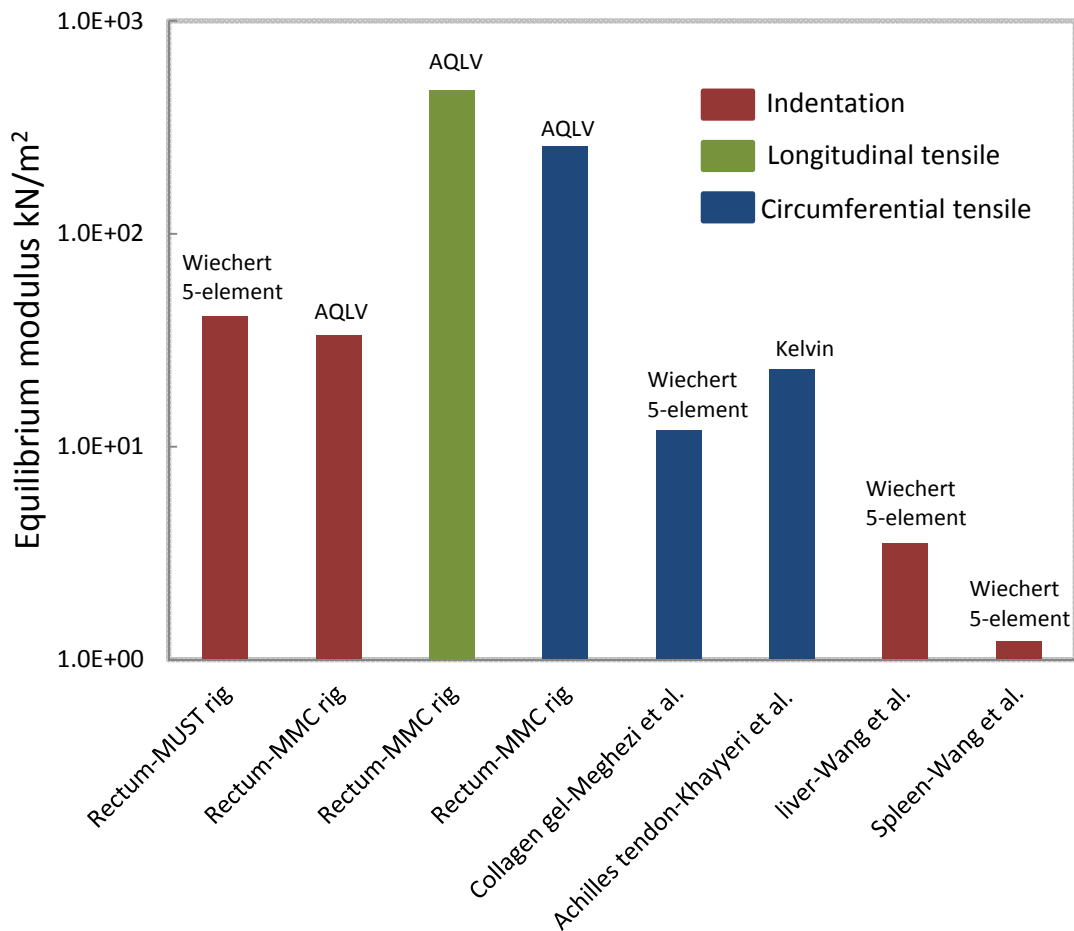


Figure 8-5: The equilibrium modulus obtained from different viscoelastic model to indentation and tensile experimental data

However, the full relaxation of the ascending sample showed that the ‘relaxation process 1’ occurs the fastest but had the greatest stress drop and the ‘relaxation process 3’ contains the longest but smallest stress drop i.e. $\tau_1 < \tau_2 < \tau_3$ when $E_1 > E_2 > E_3$. This is consistent with the molecular mechanism explained in Chapter 2.1, Figure 2-1. Other studies such as [22, 96, 135] have obtained the same trend.

The AQLV model fitted to the experimental data was slightly lower than the RMSE obtained for the Wiechert 5-element model. In Chapter 6, the RMSE values of the Kelvin model fit is the highest as found in this study and by Khayyeri et al. Other studies such as Liu et al. and Yang et al. observed much lower RMS value. Overall, AQLV model shows a reasonable fit to the large intestine behaviour for both indentation and tensile data.

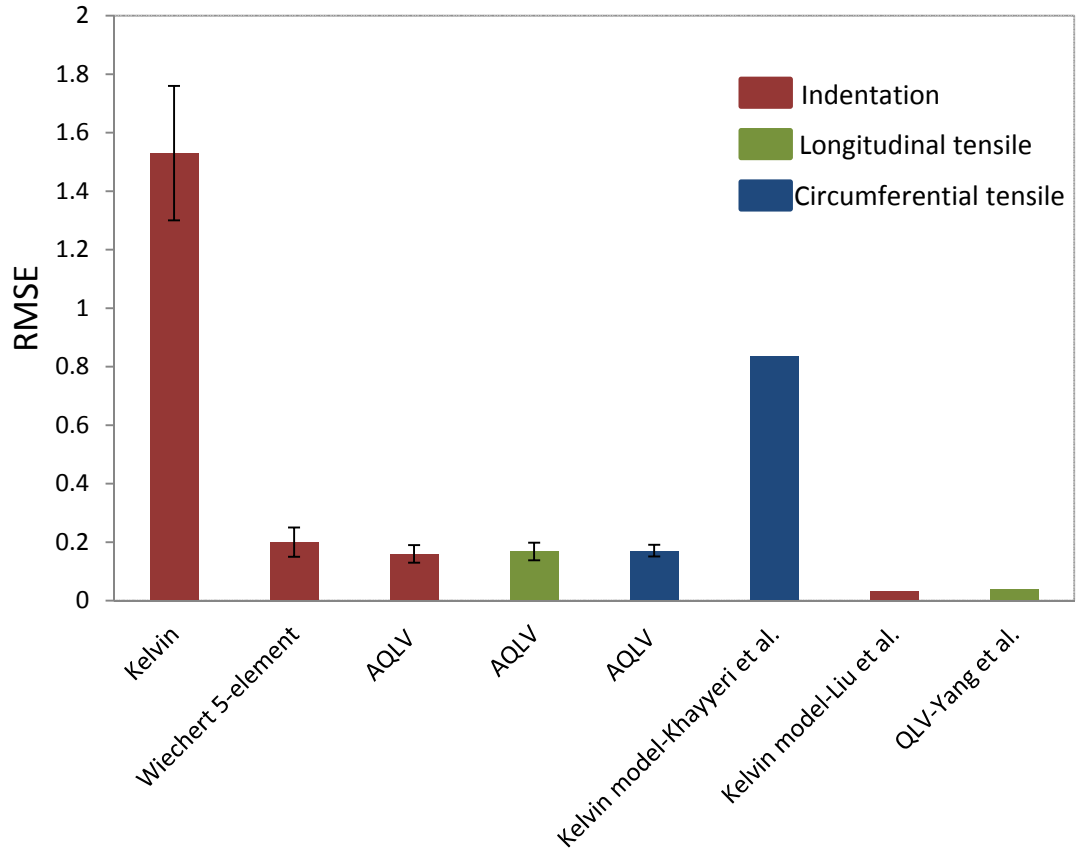


Figure 8-6: Comparison between the RMSE values obtained from different models used in this research and in the literature

In the indentation tests presented in Chapter 5, the AQLV model was found to be accurate in predicting the relaxation response of the 35% and 50% strains under the incremental strain experiment. However, at 65% strain the model overestimates the initial peak stress and the stress relaxation of the ‘relaxation process 1’. This trend was seen for all the other samples. This is assumed to be due to the different relaxation response caused by indenting at high strains of 65%. On the other hand, under tensile incremental stretch the AQLV model fails to predict the pattern on account of lengthy loading which introduced extra tissue relaxation during the loading phase. This disagrees with the behaviour seen in Chapter 5 and the tensile data found in the literature; where, for example, in [114] Figure 2-35 the stretch of vocalis muscle from 13% to 33% in four increments resulted in an increase of maximum stress from 12 kPa to 19 kPa. In his experiments, Nekuzadeh induced maximum 20 s of loading duration to stretch the synthetic collagen specimens. According to several studies the model proved to be a very good predictive tool for estimating the response of soft tissues at varying strain levels.

In both linear and non-linear tissue modelling presented above, there are various limitations that need to be considered to avoid poor estimation of the tissue properties. The linear modulus should be used on the stress-strain response of soft tissue under tensile testing. The elastic response of tissue is best observed at the most linear region of the stress-strain response of tissue just before rupture loaded at a fast or infinitely low strain-rates. Obtaining the linear modulus of the tissue this way can allow for direct comparison between the elastic responses of various soft tissues.

Therefore, AQLV model is found to be a better representation of the non-linear behaviour of the large intestine when compared to Wiechert 5-element model as it accounts for the strain-rate and strain history of tissue loading. However, the use of the model is limited by several factors. As the results show, employing AQLV model to predict the response of tissue under indentation is not appropriate as the prediction fails after passing certain strain levels. For tensile experiments, it is important that the loading phase is not extended for too long since the model prediction cannot account for high volume of tissue relaxation in the loading response.

8.3 Acoustic impedance tissue characterisation

Acoustic impedance technique is an alternative method to obtain mechanical properties of biological tissue. Since the technique can be miniaturised it can be used for non-invasive in-vivo tissue characterisation. In this research the large intestine samples were obtained to characterise the true response of tissue under acoustic impedance technique. The results of ex-vivo tissue tests showed that the pattern of frequency shift Δf can be used to differentiate between the softness/hardness of two different sites of the large intestine. The pattern of Δf demonstrated that rectum is on average stiffer than transverse colon, confirmed by studies performed on silicon [76, 84, 86, 134], saline concentration [79] and muscle contraction [76]. This finding agrees with the results of indentation test in Chapter 5.4.2, where higher linear modulus was found for the rectum compared to the transverse colon. This suggests that the acoustic impedance technique can successfully identify relative stiffness and replace palpation/indentation techniques for mapping stiffness during in-vivo tissue assessment. Δz was also found to be a good indication of the relative viscous response of tissue as a results of impedance measurement agreed with the indentation results. Transverse colon was found to be slightly more viscous than rectum in both indentation and impedance measurements.

This trend is also in agreement with the literature such as [79] where higher viscous concentration of saline solution resulted in greater Δz .

A high correlation was found between the impedance properties and applied force as shown in Figure 7-5 which is supported by the findings in [78, 82, 84]. The most interesting trend was found during the stress relaxation of the tissue. As tissue relaxes Δf increases since the contact area between the tissue/probe decrease. This agrees with the Δf -force relationship in Figure 7-5-a. Decrease of Δz (viscosity) with time during the stress relaxation confirms the fact that tissue viscoelasticity dissipates with time, a trend that agrees with the non-linear tissue relaxation represented by spring and dashpot under both indentation and tensile examinations. Unfortunately, the impedance response of tissue during relaxation has not been examined anywhere else in the literature, so there is little to compare to but results do show agreement with those of the viscoelastic AQLV model obtained in Chapter 5.

Chapter 9. Conclusions

9.1 Summary

This study investigated mechanical and viscoelastic properties of porcine large intestine through various indentation and tensile tests. Several gaps in the literature regarding the existing knowledge on mechanical properties of the large intestine were highlighted including the anisotropic behaviour, hydration, preconditioning, strain-rate, and strain history effects on the mechanical behaviour of the large intestine. One of the main steps to conduct an investigation to address this is to design a suitable testing protocol; however, due to the lack of appropriate guidelines in the literature, various different testing protocols were developed to extract these properties. Consequently, a special interest was paid to develop a robust guideline for characterising the large intestine properties in future work. For in-vivo tissue assessment, a technique based on acoustic impedance characterisation of tissue was developed and evaluated. The key findings and novel aspects of this work were:

- The preconditioning effect on tissue properties was assessed for the large intestine under repeated interaction test using both indentation and tensile examinations. From the results it was concluded that five preconditioning cycles are needed to observe repeatable behaviour for the tissue kept in air. This is important during mechanical characterisation testing as it eliminates the strain history effect. Therefore, the uniform mechanical response which was obtained from cycle 4-5 onwards suggests that no particular plastic deformation or damage occurs to the tissue if the tool/tissue interaction is kept consistent. However, preconditioning did not improve the reproducibility of the tissue response in PBS. Therefore, hydration is necessary as keeping the tissue hydrated preserves the water content in the soft tissue and avoids major tissue deterioration by time and keeps the ex-vivo tissue in conditions similar to the in-vivo state.
- Strain-rate was found to be a key element in the large intestine mechanical characterisation. Firstly it was observed that the tissue elastic response and rate of relaxation increases with higher strain-rates. Secondly, slow strain-rate causes some tissue relaxation during the loading phase. To observe the full relaxation behaviour during the relaxation phase, which is desirable for mechanical properties characterisations, strain-rate has to be high enough to avoid tissue

relaxation during the loading but low enough to eliminate the chance of introducing discrepancies such as noise and vibration to the data. The fact that the large intestine is strongly strain-rate dependent implies that the tissue resistance during surgical tool manipulation is altered with varying strain-rate during the tissue loading/holding.

- Strain history was found to strongly influence the mechanical properties of the large intestine. Greater stiffness and slower relaxation results from an increase of strain level. Preconditioning is one way to eliminate this effect. However, by choosing a suitable viscoelastic model which takes into account the level of strain this effect can be characterised and predicted.
- Tissue modelling was found to be the essence of any mechanical properties characterisation study. Despite all the limitations of using linear modulus, it remains one of the only metrics that can compare between the elastic properties of different tissue. The results of various non-linear models showed that even though Wiechert viscoelastic model can provide good fit to the response of the large intestine it has no predictive value. Among all the non-linear models, Adaptive QLV was found the one model that can take into account the strain-rate and strain history effects on the mechanical properties of the tissue and the results showed that if the testing protocol was designed appropriately, the AQLV can produce suitable coefficients for characterising the stress relaxation behaviour. These data can be employed for modelling and simulation of the large intestine.
- As mentioned above the accuracy of tissue modelling in observing generic mechanical characterisation of the large intestine depends directly on appointing an appropriate testing protocol. For linear modulus modelling, the testing protocol should include a series of tensile stretches to the point of rupture at a very fast strain-rate. For capturing the viscoelastic response of tissue the main factors to consider are the stress relaxation duration and loading strain-rate. 10 s stress relaxation, which was chosen initially based on the surgical experience during compression/grasping, was found not long enough to reveal the full relaxation response of tissue. Even a duration of 300 s selected for the second set of experiment was not long enough in all cases. Preliminary tests should be

performed to specifically investigate the most suitable strain-rate and stress relaxation duration for the soft tissue under examination.

- The following points should be considered for setting a suitable 'standard operating procedure' for assessing soft tissue mechanical properties:
 1. For linear modulus measurements tensile testing must be performed where the tissue is stretch to its rupture point. The strain rate has to be set high to avoid tissue relaxation during loading (<1 s). Also, the testing platform must be stable enough to avoid introducing any vibration and noise to the experimental data.
 2. For viscoelastic properties measurements, the testing protocol should include five repeats of preconditioning followed by a single cycle of loading-relaxation-unloading. The maximum force should be limited to avoid any tissue damage. Tissue relaxation should be long enough (>300 s) for observing the full relaxation response. Strain-rate should achieve a <1 s loading duration to avoid tissue relaxation within this phase. Finally, since strain-rate and strain history appear to effect the mechanical response of soft tissue, a model which takes both factors into account should be selected.
- The acoustic impedance technique has a great potential to be miniaturised for applications such as colonoscopy/robotic colonoscopy. The technique showed consistent sensitivity to impedance properties of the large intestine. Relative stiffness of the large intestine samples was clearly detected. The viscoelastic properties of the tissue identified by the acoustic impedance technique correlated well with the mechanical and viscoelastic properties of the tissue under indentation, which implies that it can replace the indentation technique for stiffness mapping and stress relaxation analysis of tissue response under in-vivo tissue assessment.

It is believed that the developed methodology and the results presented here provide an initial contribution to a database of rectum tissue properties in order to enhance the development of the emerging technologies and clinical tools such as robotic laparoscopy and tissue simulation and can lead further expansion on the mechanical properties of the large intestine in general.

9.2 Future work

For future studies, the following points were suggested:

- For characterising mechanical properties of the large intestine the testing protocol used in this study has to be modified as follows. Using the same testing rig i.e. MMC rig and chapter 5 and 6 testing protocol, the strain rate should be increased to the actuator's maximum speed of 20 mm/s. This will allow for the stress relaxation response to be fully observed both for indentation and tensile experiments. However, in case the data are too noisy as a result of system vibration, the strain rate should be reduced until the noise level is acceptable. Following that the predictive value of the AQLV model should be evaluated again for the strain level dependency examination of tissue under tensile test. Secondly, the sample size under the tensile examination should be reduced so that together with the strain rate the loading phase takes under 1 s. This means the sample holder for the tensile test has to be scaled down. For tensile test some rupture test should be performed to find the tensile strength and Young's Modulus of the large intestine.
- Since the MMC rig is portable, some human cadaver study is suggested to be performed to study the properties of the human large intestine and observe the difference between the pig and the human large intestine. The test should include stress relaxation, strain rate variation, and repeated interaction tests on the entire large intestine under indentation modality.
- For in-vivo tissue assessment, the acoustic impedance technique developed here needs to be miniaturised. Smaller transducer should be outsourced. In terms of software design, the resonance system should be closed loop so that as the resonance frequency of the oscillation shifts (as a result of the contact with the tissue), the transducer is oscillated at its new resonance frequency at all time.

References

- [1] Cotton PB, Williams CB. *Practical Gastroenterological Endoscopy*. 2009:133 & 604.
- [2] Destounis S, Arieno A, Skolny M. The role of elasticity imaging (EI) in a large community-based breast imaging center. 95th Scientific Assembly and Annual Meeting of the Radiological Society of North America (RSNA) LL-BR4059-B04: Nov2009.
- [3] Papadoukakis S, Kusche D, Truss M. *History of laparoscopy, endoscopic, extraperitoneal radical prostatectomy and robotic Surgery*. Springer. 2007;XVI.
- [4] Jones DB, Wu JS, Soper NJ, Rege RV. *Laparoscopic surgery: principles and procedures*. Journal of the American College of Surgeons. 1998;186:377.
- [5] Bharucha A. Viscoelastic properties of the human colon. *Am J Physiol Gastrointest Liver Physiol* 2001;281:G459–G66.
- [6] Egorov V, Schastlivtsev I, Prut E. Mechanical properties of the human gastrointestinal tract. *Journal of Biomechanics*. 2002;35:1417–25.
- [7] Gao C, Gregersen H. Biomechanical and morphological properties in rat large intestine. *Journal of Biomechanics*. 2000;33:1089-97.
- [8] Higa M, Luo Y, Okuyama T, Takagi T, Shiraishi Y, Yambe T. Passive mechanical properties of large intestine under in vivo and in vitro compression. *Medical Engineering & Physics*. 2006;29:840–4.
- [9] Itasaka S, Shiratori K, Takahashi T, Ishikawa M, Kaneko K, Suzuki Y. Stimulation of intramural secretory reflex by luminal distension pressure in rat distal colon. *Yamagata University School of Medicine, Yamagata*. 1992;263:G108-G14.
- [10] Rosen J, Brown JD, De S, Sinanan M, Hannaford B. Biomechanical properties of abdominal organs in vivo and post-mortem under compression loads. *Journal of Biomechanical Engineering* 2008;021020 (1-021020):17.
- [11] Sokolis D, Orfanidis I, Peroulis M. Biomechanical testing and material characterization for the rat large intestine: regional dependence of material parameters. *Physiol Meas*. 2011;32:1969-76.
- [12] Watters D, Smith A, Eastwood M. Mechanical properties of the colon; comparison of the features of the African and European colon in vitro. *Gut*. 1985;26:384-92.
- [13] Watters D, Smith A, Eastwood M. Mechanical properties of the rat colon: the effect of age, sex and different conditions of storage. *Quarterly Journal of Experimental Physiology*. 1985;70:151-62.
- [14] Yamada H. *Strength of Biological Materials*. The Williams and Wilkins company, Baltimore. 1970.
- [15] Barton M, Harris R, Fletcher S. Does This Patient Have Breast Cancer?: The Screening Clinical Breast Examination: Should It Be Done? How? . *JAMA*. 1999;282:1270–80.
- [16] Gao L, Parker K, Lerner R, Levinson S. Imaging of the elastic properties of tissue—A review. *Ultrasound in Medicine & Biology*. 1996;22:959-77.
- [17] Greenleaf J, Fatemi M, Insana M. Selected methods for imaging elastic properties of biological tissues. *Annual Review of Biomedical Engineering*. 2003;5:57-78.
- [18] Fung Y.C. *Mechanical Properties of Living Tissues*. Springer. 1993.
- [19] Holzapfel G. Biomechanics of soft tissue. In *Handbook of Materials Behavior Models* 2001.
- [20] Brown I.A. A scanning electron microscope study of the effects of uniaxial tension on human skin. *British Journal of Dermatology* 1973;89:383.
- [21] Holzapfel G. Biomechanics of soft tissue. In *Handbook of Materials Behavior Models* 2001.
- [22] Meghezi S, Couet F, Chevallier P, Mantovani D. Effects of a Pseudophysiological Environment on the Elastic and Viscoelastic Properties of Collagen Gels. *International Journal of Biomaterials*. 2012.
- [23] Nekouzadeh A, Genin GM. Adaptive quasi-linear viscoelastic modeling. *Computational Modeling in Tissue Engineering*: Springer; 2013. p. 47-83.

- [24] Watters D, SAN, Eastwood M.A. Mechanical properties of the rat colon: the effect of age, sex and different conditions of storage. *Quarterly Journal of Experimental Physiology*. 1985;70:151-62.
- [25] Johnson M, Beatty M. The Mullins effect in uniaxial extension and its influence on the transverse vibration of a rubber string. *Continuum Mech Thermodyn*. 1993;5, 83:115.
- [26] Gregersen H, Emery J, McCulloch A. History-Dependent Mechanical Behavior of Guinea-Pig Small Intestine. *Annals of Biomedical Engineering*. 1998;26:850-8.
- [27] Rosen J. BJD, De S., Sinanan M., Hannaford B. Biomechanical properties of abdominal organs in vivo and post-mortem under compression loads. *Journal of Biomechanical Engineering* 2008;021020 (1-021020):17.
- [28] Natali A, Pavan P, Carniel E, Dario P, Izzo I. Characterization of soft tissue mechanics with aging. *Engineering in Medicine and Biology Magazine, IEEE*. 2008;27:15-22.
- [29] Carniel EL, Gramigna V, Fontanella CG, Stefanini C, Natali AN. Constitutive formulations for the mechanical investigation of colonic tissues. *Journal of Biomedical Materials Research Part A*. 2014;102:1243-54.
- [30] Structure of colon picture. Medline Plus.
- [31] Dall F, Jørgensen C, Djurhuus J, Gregersen H. Biomechanical wall properties of the porcine rectum: a study using impedance planimetry. *Digestive Diseases*. 1991;9:347-53.
- [32] Dall F, Jørgensen C, Houe D, Gregersen H, Djurhuus J. Biomechanical wall properties of the human rectum. A study with impedance planimetry. *Gut*. 1993;34:1581-6.
- [33] Lundby L, Dall F, Gregersen H, Overgaard J, Laurberg S. Distensibility of the mouse rectum: application of impedance planimetry for studying age-related changes. *Colorectal Disease*. 1999;1:34-41.
- [34] Petersen P, Gao C, Rössel P, Qvist P, Arendt-Nielsen L, Gregersen H, et al. Sensory and biomechanical responses to distension of the normal human rectum and sigmoid colon. *Digestion*. 2000;64:191-9.
- [35] Kern MK, Jaradeh S, Arndorfer RC, Jesmanowicz A, Hyde J, Shaker R. Gender differences in cortical representation of rectal distension in healthy humans. *American Journal of Physiology-Gastrointestinal and Liver Physiology*. 2001;281:G1512-G23.
- [36] Drewes AM, Petersen P, Rössel P, Gao C, Hansen J, Arendt-Nielsen L. Sensitivity and distensibility of the rectum and sigmoid colon in patients with irritable bowel syndrome. *Scandinavian journal of gastroenterology*. 2001;36:827-32.
- [37] Petersen P, Gao C, Arendt-Nielsen L, Gregersen H, Drewes AM. Pain intensity and biomechanical responses during ramp-controlled distension of the human rectum. *Digestive diseases and sciences*. 2003;48:1310-6.
- [38] Frøkjær JB, Liao D, Bergmann A, McMahon B, Steffensen E, Drewes AM, et al. Three-dimensional biomechanical properties of the human rectum evaluated with magnetic resonance imaging. *Neurogastroenterology & Motility*. 2005;17:531-40.
- [39] Drewes AM, Frøkjær JB, Larsen E, Reddy H, Arendt-Nielsen L, Gregersen H. Pain and mechanical properties of the rectum in patients with active ulcerative colitis. *Inflammatory bowel diseases*. 2006;12:294-303.
- [40] Qiao Y, Pan E, Chakravarthula S, Han F, Liang J, Gudlavalleti S. Measurement of mechanical properties of rectal wall. *Journal of Materials Science: Materials in Medicine*. 2005;16:183-8.
- [41] Egorov V, Ayrapetyan S, Sarvazyan A. Prostate mechanical imaging: 3-D image composition and feature calculations. *Medical Imaging, IEEE Transactions on*. 2006;25:1329-40.
- [42] Harris J, Therkelsen EE, Zinner NR. Electrical measurements of ureteral flow. *Urodynamics: hydrodynamics of the ureter and renal pelvis*. 1971:465.
- [43] Gregersen H, Stodkilde-Jørgensen H, Djurhuus J, Mortensen S. The four-electrode impedance technique: a method for investigation of compliance in luminal organs. *Clinical Physics and Physiological Measurement*. 1988;9:61.

- [44] Mariappan YK, Glaser KJ, Ehman RL. Magnetic resonance elastography: a review. *Clinical anatomy*. 2010;23:497–511
- [45] Kerdok AE. Characterizing the nonlinear mechanical response of liver to surgical manipulation: Harvard University Cambridge, MA; 2006.
- [46] von Gierke HE, Oestreicher HL, Franke EK, Parrack HO, von Wittern WW. Physics of vibrations in living tissues. *Journal of Applied Physiology*. 1952;4:886-900.
- [47] Fercher AF, Drexler W, Hitzenberger CK, Lasser T. Optical coherence tomography—principles and applications. *Reports on progress in physics*. 2003;66:239-303.
- [48] Kennedy BF, Hillman TR, McLaughlin RA, Quirk BC, Sampson DD. In vivo dynamic optical coherence elastography using a ring actuator. *Optics express*. 2009;17:21762–72.
- [49] Sarvazyan A. Mechanical imaging - a new technology for medical diagnostics. *International Journal of Medical Informatics*. 1998;49:195–216.
- [50] Liu Z, Yeung K. The Preconditioning and Stress Relaxation of Skin Tissue. *Journal of Biomedical & Pharmaceutical Engineering*. 2008;2:1:22-8.
- [51] Elastic imaging. [Online][Cited: 20/06/2012]. <http://www.artannlabs.com/elasticity-imaging.html>.
- [52] Ophir J, Cl, Ponnekanti H., Yazdi Y., Li X. Elastography: a quantitative method for imaging the elasticity of biological tissues. *Ultrason Imaging*. 1991;13:111–34.
- [53] Catheline S, Wu F, Fink M. A solution to diffraction biases in sonoelasticity: The acoustic impulse technique. *The Journal of the Acoustical Society of America*. 1999;105:2941–50.
- [54] Krouskop T, Dougherty D, Vinson F. A pulsed Doppler ultrasonic system for making noninvasive measurements of the mechanical properties of soft tissue. *Journal of Rehabilitation Research and Development*. 1987;24:1-8.
- [55] Lerner RM, Huang S, Parker KJ. “Sonoelasticity” images derived from ultrasound signals in mechanically vibrated tissues. *Ultrasound in medicine & biology*. 1989;16:231-9.
- [56] Yamakoshi Y, Sato J, Sato T. Ultrasonic Imaging of Internal Vibration of Soft Tissue under Forced Vibration. *Ultrasonics, Ferroelectrics, and Frequency Control, IEEE Transactions on*. 1990;37:45-53.
- [57] Taylor L. PB, Rubens D., Parker K. Three-dimensional sonoelastography: Principles and practices. *Phys Med Biol*. 2000;45:1477–94.
- [58] Jia M. ZJW, Hariri A. A new tissue resonator indenter device and reliability study. *Sensors*. 2011;11:1212-28.
- [59] Ottensmeyer M.P. Minimally invasive instrument for in vivo measurement of solid organ mechanical impedance. Massachusetts Institute of Technology. 2001.
- [60] Carter FJ, Frank TG, Davies PJ, McLean D, Cuschieri A. Measurements and modelling of the compliance of human and porcine organs. *Medical Image Analysis*. 2001;5:231–6.
- [61] Vuskovic V. Device for in-vivo measurement of mechanical properties of internal human soft tissues. PhD Dissertation. 2001; ETH No. 14222.
- [62] Mazza E. NA, Hahnloser D., Bauer M., Winter R., Bajka M., Holzapfel G.A. . Mechanical properties of the human uterine cervix: An in vivo study. *Medical Image Analysis*. 2006;10:125–36.
- [63] Araghi MH, Salisbury SP. Improved Evaluation of Dynamic Mechanical Properties of Soft Materials With Applications to Minimally Invasive Surgery. *Mechatronics, IEEE/ASME Transactions on*. 2012:1-8.
- [64] Oyen ML, Shean TA, Strange DG, Galli M. Size effects in indentation of hydrated biological tissues. *Journal of Materials Research*. 2012;27:245-55.
- [65] Kerdok A.E. Characterizing the Nonlinear Mechanical Response of Liver to Surgical Manipulation. The Division of Engineering and Applied Sciences, Harvard University. 2006.
- [66] Rosen J. HB, MacFarlane M.P., Sinanan M.N. Force Controlled and Teleoperated Endoscopic Grasper for Minimally Invasive Surgery—Experimental Performance Evaluation. *International Congress*. 1999;Series 1281:713– 8.

- [67] Miller K. CK, Orssengo G., Bednarz P. Mechanical properties of brain tissue in-vivo: experiment and computer simulation. *Journal of Biomechanics*. 2000;33:1369-76.
- [68] Brown J.D. RJ, Kim Y.S., Chang L., Sinana M.N. , Hannaford B. In-Vivo and In-Situ Compressive Properties of Porcine Abdominal Soft Tissues. *Medicine Meets Virtual Reality*. 2003.
- [69] Samur E. SM, Basdogana C., Avtanb L., Duzgunc O. A robotic indenter for minimally invasive characterization of soft tissues. *International Congress*. 2005;1281:713– 8.
- [70] Scanlan P, Hammer SJ, Good DW, Phipps S, Stewart GD, McNeill SA, et al. Development of a novel actuator for the dynamic palpation of soft tissue for use in the assessment of prostate tissue quality. *Sensors and Actuators A: Physical*.
- [71] Lynch HA, Johannessen W, Wu JP, Jawa A, Elliott DM. Effect of fiber orientation and strain rate on the nonlinear uniaxial tensile material properties of tendon. *Journal of biomechanical engineering*. 2003;125:726-31.
- [72] Quapp K, Weiss J. Material characterization of human medial collateral ligament. *Journal of biomechanical engineering*. 1998;120:757-63.
- [73] Lee M, Boughner DR. Tissue mechanics of canine pericardium in different test environments. Evidence for time-dependent accommodation, absence of plasticity, and new roles for collagen and elastin. *Circ Res*. 1981;49:533–44.
- [74] Yang W, Chian K, Chong C, Fung T. Viscoelasticity of esophageal tissue and application of a QLV model. *Journal of biomechanical engineering*. 2006;128:909-16.
- [75] Taylor D, Dalton J, Seaber A, Garrett W. Viscoelastic properties of muscle-tendon units. *The American Journal of Sports Medicine*. 1990:300-9.
- [76] Han H, Kim J. Active muscle stiffness sensor based on piezoelectric resonance for muscle contraction estimation. *Sensors and Actuators A: Physical*. 2013;194:212-9.
- [77] Hensel T, Stroop R, Uribe DO, Wallaschek J. Resonant vibrating sensors for tactile tissue differentiation. *Journal of Sound and Vibration*. 2007;308:441-6.
- [78] Jalkanen V, Andersson BM, Bergh A, Ljungberg B, Lindahl OA. Explanatory models for a tactile resonance sensor system—elastic and density-related variations of prostate tissue in vitro. *Physiological measurement*. 2008;29:729.
- [79] Li T, Gianchandani YB. An empirical model for a piezoelectric tissue contrast sensor embedded in a biopsy tool. *Proceedings of the 10th International Conference on Miniaturized Systems for Chemistry and Life Sciences (mTAS2006), Tokyo2006*. p. 837-9.
- [80] Lin C, Huang Y, Tsai M. Detection of tissue properties using a piezoelectric vibration-based syringe. *IOP Conference Series: Materials Science and Engineering: IOP Publishing; 2012*. p. 012002.
- [81] Omata S. New type transducer for measuring contact compliances of a soft body. *The Journal of the Acoustical Society of America*. 1985;78:1-5.
- [82] Omata S, Murayama Y, Constantinou CE. Real time robotic tactile sensor system for the determination of the physical properties of biomaterials. *Sensors and Actuators A: Physical*. 2004;112:278-85.
- [83] Krishna GM, Rajanna K. Tactile sensor based on piezoelectric resonance. *Sensors Journal, IEEE*. 2004;4:691-7.
- [84] Murayama Y, Haruta M, Hatakeyama Y, Shiina T, Sakuma H, Takenoshita S, et al. Development of a new instrument for examination of stiffness in the breast using haptic sensor technology. *Sensors and Actuators A: Physical*. 2008;143:430-8.
- [85] Kusaka K, Harihara Y, Torzilli G, Kubota K, Takayama T, Makuuchi M, et al. Objective evaluation of liver consistency to estimate hepatic fibrosis and functional reserve for hepatectomy. *Journal of the American College of Surgeons*. 2000;191:47-53.
- [86] Omata S, Terunuma Y. New tactile sensor like the human hand and its applications. *Sensors and Actuators A: Physical*. 1992;35:9-15.

- [87] Caplain E, Despaux G, Ferrandis J-Y, Attal J. Wide-range viscoelastic measurement using resonating sensors. *Ultrasonics*. 2004;42:569-72.
- [88] Rubin M.B. BSR. A three-dimensional nonlinear model for dissipative response of soft tissue. *International Journal of Solids and Structures* 2002;39:5081–99
- [89] Lakes R, Vanderby R. Interrelation of creep and relaxation: a modeling approach for ligaments. *Journal of biomechanical engineering*. 1999;121:612-5.
- [90] Provenzano P, Lakes R, Keenan T, Vanderby Jr R. Nonlinear ligament viscoelasticity. *Annals of biomedical engineering*. 2001;29:908-14.
- [91] Taylor D.C. DJD, Seaber A.V., Garrett W.E. Viscoelastic properties of muscle-tendon units. *The American Journal of Sports Medicine*. 1990:300-9.
- [92] Van der Vegt A.K. *From Polymers to Plastics*. 2006:115-23.
- [93] Zhang G. Evaluating the viscoelastic properties of biological tissues in a new way. *J Musculoskelet Neuronal Interact*. 2005;5:85-90.
- [94] Ahn B.M. Characterization of Viscoelastic Properties of Intra-Abdominal Organs from In vitro Indentation Experiments and Inverse Finite Element Parameter Optimization. Korea Advanced Institute of Science and Technology. 2007.
- [95] Ahearne M, Siamantouras E, Yang Y, Liu K-K. Mechanical characterization of biomimetic membranes by micro-shaft poking. *Journal of The Royal Society Interface*. 2008:rsif.2008.0317.
- [96] Shen Z, Kahn H, Ballarini R, Eppell S. Viscoelastic Properties of Isolated Collagen Fibrils. *Biophysical Journal*. 2011;100:3008–15.
- [97] Barrie J, Ehteshami Z, Culmer P, Jayne D, Neville A. Relaxation and Recovery of Colon After Application of a Mechanical Stress. *ACTA Press*. 2013;791-048.
- [98] Arezzo A, Menciassi A, Valdastris P, Ciuti G, Lucarini G, Salerno M, et al. Experimental assessment of a novel robotically-driven endoscopic capsule compared to traditional colonoscopy. *Digestive and Liver Disease*. 2013;45:657-62.
- [99] Quaia C, Ying HS, Optican LM. The viscoelastic properties of passive eye muscle in primates. II: testing the quasi-linear theory. *PloS one*. 2009;4:e6480.
- [100] Pryse KM, Nekouzadeh A, Genin GM, Elson EL, Zahalak GI. Incremental mechanics of collagen gels: new experiments and a new viscoelastic model. *Annals of biomedical engineering*. 2003;31:1287-96.
- [101] Sarver JJ, Robinson PS, Elliott DM. Methods for quasi-linear viscoelastic modeling of soft tissue: application to incremental stress-relaxation experiments. *Journal of biomechanical engineering*. 2003;125:754-8.
- [102] Nekouzadeh A, Pryse KM, Elson EL, Genin GM. A simplified approach to quasi-linear viscoelastic modeling. *Journal of biomechanics*. 2007;40:3070-8.
- [103] Ottensmeyer MP, Kerdok AE, Howe RD, Dawson SL. The effects of testing environment on the viscoelastic properties of soft tissues. *Medical Simulation: Springer*; 2004. p. 9-18.
- [104] Jiroušek O. *Nanoindentation of Human Trabecular Bone—Tissue Mechanical Properties Compared to Standard Engineering Test Methods*. ISBN. 2012:978-53.
- [105] Ferrara TL, Boughton P, Slavich E, Wroe S. A Novel Method for Single Sample Multi-Axial Nanoindentation of Hydrated Heterogeneous Tissues Based on Testing Great White Shark Jaws. *PloS one*. 2013;8:e81196.
- [106] Miller K, Chinzei K, Orssengo G, Bednarsz P. Mechanical properties of brain tissue in-vivo: experiment and computer simulation. *Journal of Biomechanics*. 2000;33:1369-76.
- [107] Bembey A, Oyen M, Bushby A, Boyde A. Viscoelastic properties of bone as a function of hydration state determined by nanoindentation. *Philosophical Magazine*. 2006;86:5691-703.
- [108] Broz J, Simske S, Greenberg A, Luttgies M. Effects of rehydration state on the flexural properties of whole mouse long bones. *Journal of biomechanical engineering*. 1993;115:447-9.
- [109] Mazza E, Nava A, Bauer M, Winter R, Bajka M, Holzapfel GA. Mechanical properties of the human uterine cervix: an in vivo study. *Medical image analysis*. 2006;10:125-36.

- [110] Hu T, Desai JP. Soft-tissue material properties under large deformation: Strain rate effect. Engineering in Medicine and Biology Society, 2004 IEMBS'04 26th Annual International Conference of the IEEE: IEEE; 2004. p. 2758-61.
- [111] Robinson PS, Lin TW, Reynolds PR, Derwin KA, Iozzo RV, Soslowky LJ. Strain-rate sensitive mechanical properties of tendon fascicles from mice with genetically engineered alterations in collagen and decorin. Journal of biomechanical engineering. 2004;126:252-7.
- [112] Pal S. Mechanical Properties of Biological Materials. Design of Artificial Human Joints & Organs: Springer; 2014. p. 23-40.
- [113] Vogel H, Hilgner W. The "step phenomenon" as observed in animal skin. Journal of biomechanics. 1979;12:75-81.
- [114] Alipour-Haghighi F, Titze IR. Viscoelastic modeling of canine vocalis muscle in relaxation. The Journal of the Acoustical Society of America. 1985;78:1939-43.
- [115] Bonifasi-Lista C, Lakez SP, Small MS, Weiss JA. Viscoelastic properties of the human medial collateral ligament under longitudinal, transverse and shear loading. Journal of Orthopaedic Research. 2005;23:67-76.
- [116] Pismensky SV, Kalzhanov ZR, Eliseeva MY, Kosmas IP, Mynbaev OA. Severe inflammatory reaction induced by peritoneal trauma is the key driving mechanism of postoperative adhesion formation. BMC surgery. 2011;11:30.
- [117] Mattice JM, Lau AG, Oyen ML, Kent RW. Spherical indentation load-relaxation of soft biological tissues. Journal of Materials Research. 2006;21:2003-10.
- [118] Dorner D, Röller K, Skrotzki B, Stöckhert B, Eggeler G. Creep of a TiAl alloy: a comparison of indentation and tensile testing. Materials Science and Engineering: A. 2003;357:346-54.
- [119] Sherit S, Jones CM, Aldrich JB, Blodget C, Bao X, Badescu M, et al. Multilayer piezoelectric stack actuator characterization. The 15th International Symposium on: Smart Structures and Materials & Nondestructive Evaluation and Health Monitoring: International Society for Optics and Photonics; 2008. p. 692909--12.
- [120] Technologies A. Impedance measurement with E5061B LF-RF Network analyser. 2012.
- [121] Brown JD, Rosen J, Chang L, Sinanan MN, Hannaford B. Quantifying surgeon grasping mechanics in laparoscopy using the blue DRAGON system. Studies in health technology and informatics. 2004:34-6.
- [122] Hunter EJ, Titze IR. Refinements in modeling the passive properties of laryngeal soft tissue. Journal of Applied Physiology. 2007;103:206-19.
- [123] Oliver WC, Pharr GM. An improved technique for determining hardness and elastic modulus using load and displacement sensing indentation experiments. Journal of Materials Research. 1992;7:1564-83.
- [124] Suki B, Bates J. Lung tissue mechanics as an emergent phenomenon. Journal of Appl Physiol. 2011;110:1111-8.
- [125] Taylor L, Lerner A, Rubens D, Parker K. A Kelvin-Voight fractional derivative model for viscoelastic characterization of liver tissue. in ASME 2002 International Mechanical Engineering Congress and Exposition. 2002:447-8.
- [126] Dortmans L, Sauren A, Rousseau E. Parameter estimation using the quasi-linear viscoelastic model proposed by Fung. Journal of biomechanical engineering. 1984;106:198-203.
- [127] Abramowitch SD, Woo SL-Y. An improved method to analyze the stress relaxation of ligaments following a finite ramp time based on the quasi-linear viscoelastic theory. Journal of biomechanical engineering. 2004;126:92-7.
- [128] Liu H, Noonan DP, Zweiri YH, Althoefer K, Seneviratne LD. The development of nonlinear viscoelastic model for the application of soft tissue identification. Intelligent Robots and Systems, 2007 IROS 2007 IEEE/RSJ International Conference on: IEEE; 2007. p. 208-13.

- [129] Zheng Y-P, Mak AF, Lue B. Objective assessment of limb tissue elasticity: development of a manual indentation procedure. *Journal of rehabilitation research and development*. 1999;36:71-85.
- [130] Gefen A, Margulies SS. Are in vivo and in situ brain tissues mechanically similar? *Journal of biomechanics*. 2004;37:1339-52.
- [131] Leroux P. An Indentation Test That Measures Yield Strength. *ADVANCED MATERIALS & PROCESSES*2011. p. 34-5.
- [132] Smith DB, Komaragiri U, Tanov R. Calibration of nonlinear viscoelastic materials in Abaqus using the adaptive quasi-linear viscoelastic model. *SIMULIA Customer Conf*2010. p. 1-10.
- [133] Quiaia C, Ying HS, Nichols AM, Optican LM. The viscoelastic properties of passive eye muscle in primates. I: static forces and step responses. *PloS one*. 2009;4:e4850.
- [134] Jalkanen V, Andersson BM, Bergh A, Ljungberg B, Lindahl OA. Prostate tissue stiffness as measured with a resonance sensor system: a study on silicone and human prostate tissue in vitro. *Medical and Biological Engineering and Computing*. 2006;44:593-603.
- [135] Iyo T. MY, Sasaki N., Nakata M. Anisotropic viscoelastic properties of cortical bone. *Journal of Biomechanics*. 2004;37:1433-7.
- [136] Woo S-Y, Gomez M, Akeson W. The time and history-dependent viscoelastic properties of the canine medial collateral ligament. *Journal of biomechanical engineering*. 1981;103:293-8.
- [137] Doehring TC, Carew EO, Vesely I. The effect of strain rate on the viscoelastic response of aortic valve tissue: a direct-fit approach. *Annals of biomedical engineering*. 2004;32:223-32.
- [138] Kwan MK, Lin TH, Woo SL. On the viscoelastic properties of the anteromedial bundle of the anterior cruciate ligament. *Journal of biomechanics*. 1993;26:447-52.
- [139] Forgacs G, Foty RA, Shafrir Y, Steinberg MS. Viscoelastic properties of living embryonic tissues: a quantitative study. *Biophysical journal*. 1998;74:2227-34.
- [140] Wang X, Schoen JA, Rentschler ME. A quantitative comparison of soft tissue compressive viscoelastic model accuracy. *Journal of the mechanical behavior of biomedical materials*. 2013;20:126-36.
- [141] Shen Y-L, Chawla N. On the correlation between hardness and tensile strength in particle reinforced metal matrix composites. *Materials Science and Engineering: A*. 2001;297:44-7.
- [142] Shahmirzadi D, Bruck H, Hsieh A. Measurement of mechanical properties of soft tissues in vitro under controlled tissue hydration. *Experimental Mechanics*. 2013;53:405-14.